The L-band Ocean Salinity Airborne Campaign, LOSAC

Sten Schmidl Søbjærg, Jesper Rotbøll, and Niels Skou
Ørsted•DTU, Technical University of Denmark,
DK-2800 Kgs. Lyngby, Denmark (e-mail: sss@oersted.dtu.dk)

This report describes the scientific measurements of wind driven ocean surface azimuth signatures using the EMIRAD L-band radiometer. A short description of the experiment setup is given, and the flight plans for the six flights are presented. The data processing and data correction is described in details for one of the flights, and finally results from all flights are presented. A discussion of the results from the flights follows, and possible theories for the nature of the observed signals are presented.

Wind driven polarimetric signatures from the ocean surface have been studied by several scientific groups, using airborne radiometers. However, these studies have been concentrated at higher frequencies, typically Ku- and Ka-band. At these frequencies, the Stokes parameters show some Kelvin dependence on the azimuth look angle, when the wind speed exceeds a few meters per second. At L-band, there is only very little knowledge about eventual signatures, and this paper will describe the LOSAC, L-band Ocean Salinity Airborne Campaign, aiming at filling the void using the EMIRAD L-band radiometer. The campaign is a part of the preparation for the ESA/SMOS mission, and the overall interest is to understand the nature of the wind driven signatures in order to evaluate, if corrections are necessary prior to salinity estimations based on the radiometer signals.

1. The EMIRAD aircraft installation

The EMIRAD radiometer was specially designed for the LOSAC campaign, and details concerning the instrument are found in [1]. The instrument is fully polarimetric, thus measuring the full Stokes vector simultaneously. The integration time is programmable down to 8 msec., providing a sensitivity of 1.0 K. For a typical integration time of 1 sec., the sensitivity is thus 90 mK, which is acceptable for the measurements within the LOSAC campaign. The absolute accuracy is determined by the two built-in calibration targets (a matched load and a noise diode), and experiments in the laboratory show, that an absolute accuracy of less than 1 K is realistic. For a 15 minutes period, the drift is found to be less than 50 mK, without intermediate calibration, and this feature is important for the LOSAC measurements, which focus on relative changes, rather than measurement of absolute levels.

The system, used for the LOSAC campaign, consists of the EMIRAD L-band radiometer itself, along with a 90x90x200 cm horn antenna. The antenna is designed to fit into the parachute door of a C-130 transport aircraft, and using two legs on the antenna structure, it can be stored during take-off, transit and landing. During measurements it can be locked at a fixed depression angle of 23°, with an option for 40°. Figure 1.1 shows the setup.

The antenna is mounted on the cargo rail of the aircraft, aligning the antenna to a side-looking position. At a straight flight, the antenna will describe a profile of the ocean surface at a constant incidence angle, given by $\alpha_i = 90° - d$, where α_i is the actual incidence angle

and d the depression angle, respectively. If the aircraft rolls and the antenna looks to the right side, relative to the flight direction, the nominal incidence angle change with the roll angle, φ, is given by

$$\alpha_i = 90° - d - \varphi \qquad (1.1)$$

For the present experiment, it is of great interest to measure the azimuth signatures at different incidence angles, as the SMOS field of view covers incidence angles from about 20° to 65°. Using 1.1, the range of desired bank angles is found to be the range from 2° to 47°, which is almost realistic in the C-130.

The operator console is located on a freight pallet, positioned in the middle of the aircraft. It holds the system control computer, including the data formatting unit, Local, the storage media and the display features. It also holds the EGI, Embedded GPS (Global Positioning System) / INU (Inertial Navigation Unit), unit, providing the control computer with actual information about aircraft heading, attitude and position. The unit is a Honeywell H-764, which provides heading and attitude better than 0.05°. The EGI is mounted directly on the pallet surface, and the pallet is locked to the aircraft cargo tracks near the antenna when mounted in the aircraft. This mounting is selected to minimize the eventual effects of stiffness problems between the INU co-ordinate system and the antenna.
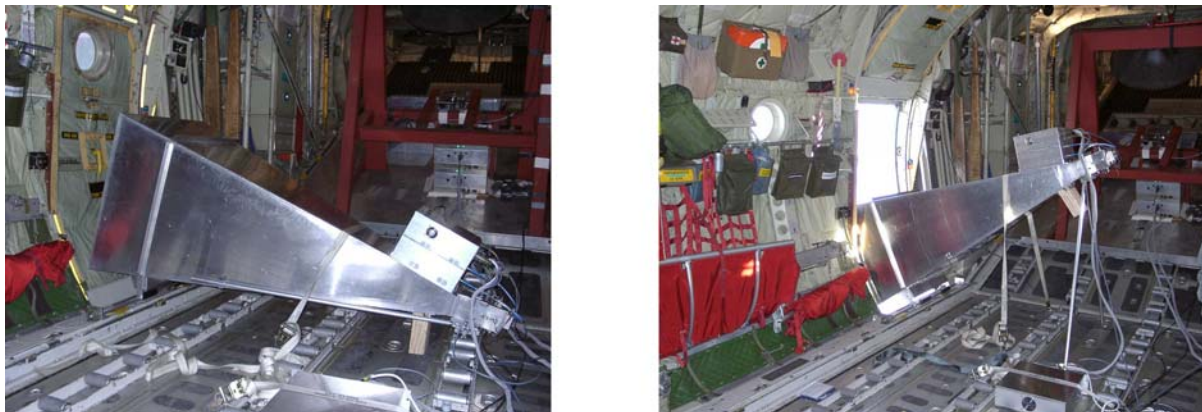

Figure 1.1. The EMIRAD L-band radiometer mounted side looking in the C-130 aircraft. A) Position during take-off and landing. B) The antenna in measurement position at 23° depression angle.

The flight pattern is a full circle, defined by the desire to measure the full azimuth variation of the Stokes vector within the shortest possible time. The ideal situation for the measurements would be instant observation of the same point on the sea surface, from all view directions, but with the circle flight pattern, the realistic observation time is from about 30 seconds to 15 minutes. A major advantage of the circle flight is the opportunity to vary the incidence angle by changing the aircraft roll angle. Due to the aircraft dynamics, the circle radius will change according to the selected roll angle, thus moving the central point of the antenna beam in a circle shape on the surface.

The aircraft navigation and control system can be operated in different modes, depending on the flight purpose. For the circle flights, the navigator can set up the system to maintain a constant roll and pitch angle rather than a perfect circle pattern. This is advantageous in the present campaign, as the aircraft roll will change with the wind direction, when trying to perform perfect circles. By keeping the roll angle constant the corrections for incidence angle changes are significantly smaller, and the influence from uncertainties in the correction algorithm will be smaller.

2. The LOSAC flights

To cover the SMOS range of incidence angles, circles are measured in the full possible range of the C-130, i.e. from 5° to 45°. For the 23° depression angle, equation 1.1 gives an angular range from 22° to 62°, almost covering the desired range. Figure 2.1 shows a typical flight pattern, where it is seen, that the central point of observation is a circle shape, defined by the antenna depression, the flight circle radius, the flight altitude, and the roll angle.
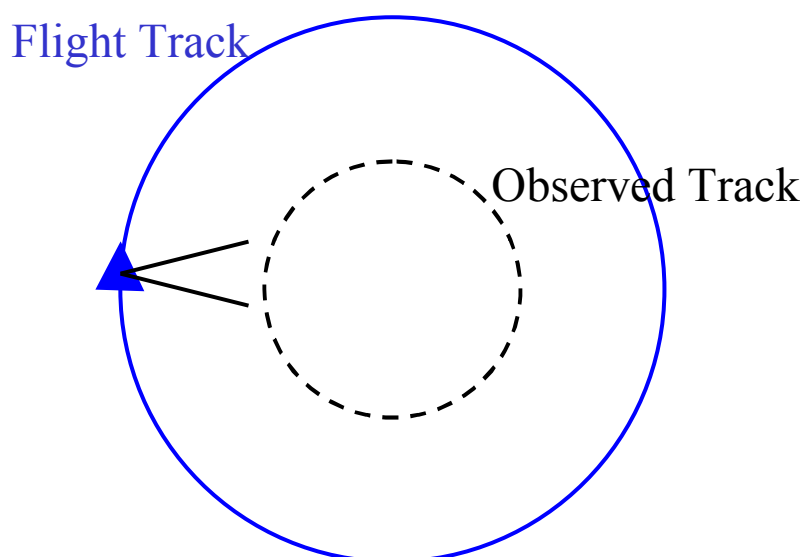

Figure 2.1. Typical circle flight pattern for the EMIRAD L-band radiometer, using the side-looking antenna installation. The observed track changes with flight altitude and roll angle.

The ideal observation situation would be a 360° measurement of a single point, but this will require adjustment of the flight altitude for each selected roll angle, as the observed circle radius changes with roll angle and flight circle radius. This will influence on the footprint size, however, and as this is not wanted, it is decided to keep the altitude constant, while the point of observation moves over the sea surface as indicated in figure 2.1. It is assumed that the surface is homogenous over the observed area, and it is likewise assumed, that the surface remains constant during the total acquisition time for a circle.

A series of test sites have been considered for the experiment, each having a number of advantages and drawbacks. One test site, which has been used in earlier campaigns at higher

frequencies, is located on the North Sea, Denmark, (55.68°N, 4.70°E), between the Tyra and Gorm oilrigs, which are equipped with meteorological instruments. Advantages of this site are the possible access to ground measurements of wind and sea temperature, and the relatively large sea surface area, giving good conditions for the forming of a homogenous wind and wave field. Drawbacks are the transit flight (approximately one hour each way) from Airbase Værløse, and the relatively poor water depth at the site, 25 m to 50 m. This site was chosen as the primary site, and it was used for the technical test flight January 16th 2001, and for the science flights March 15th 2001, October 25th 2001, and October 20th 2003.

As an alternative site can be mentioned Kattegat, Denmark, (57.04°N, 11.07°E), between the islands Læsø and Anholt. The transit time is about 15 minutes, but as the site is located near to land at all sides, the wind field may be less homogenous. Like the North Sea site, also Kattegat has poor water depth, 7 - 8 m. Ground truth data is available from two meteorological stations on land. Due to icing conditions, the March 23rd 2001 flight was carried out at this site, instead of at the originally selected North Sea site.

A test site between the Faeroe Islands and Norway (61.51°N, 1.27°E) was used for the March 6th 2003 flight, due to strong wind and large water depth, more than 1000 m, in open ocean conditions, which is more realistic for SMOS. Data acquisition at this site, however, required a two-hour transit flight each way. For the final flight, October 20th 2003, a secondary target was chosen, as flight time was remaining after the coverage of the North Sea site. A location, to the south of Lista, Norway (57.86°N, 5.47°E), was selected, as the meteorological conditions on the day of the flight caused this area to be in the middle of a low-pressure front, providing a test area with no wind.

The map in figure 2.2 shows the location of the flights, as well as points of meteorological stations, and table 2.1 shows the details of each of the six flights.
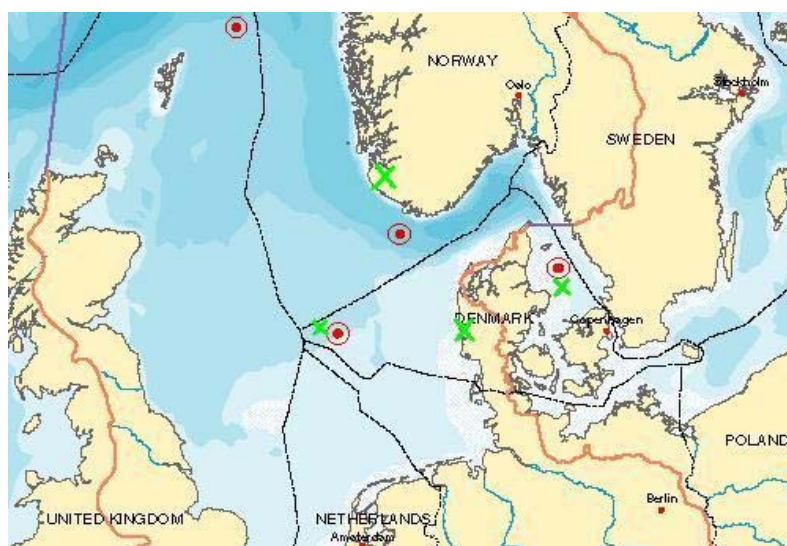

Figure 2.2. Map showing the locations of the airborne EMIRAD L-band radiometer measurements. The red circles show the four sites of data acquisition, and the green crosses show the positions of meteorological stations (Faeroe islands not shown), providing ground truth data for wind speed, wind direction, sea surface temperature, and sea surface salinity.

Position: Time: Flight Pattern: INU:	North Sea (55.68°N, 4.70°E) 16.01.2001 / 12:15 UTC - 12:45 UTC Circle flights, Technical Test OK	No meteorological data

Position:
Time:
Aircraft:
 	
Flight Altitude:
Flight Pattern:
 	
INU:
GPS:
RTP:
	North Sea (55.68°N, 4.70°E)
	15.03.2001 / 18:20 UTC - 19:20 UTC
	C-130, id: B-678
	Updated recently with new
	auto-pilot. Can maintain
	stable attitude within ±0.5°
	for roll < 32.0°
	2000 m
	Circle flights
	  52° incidence angle (3 circles)
	  42° incidence angle (3 circles)
	  35° incidence angle (3 circles)
	  22° incidence angle (3 circles)
	OK
	No
	No
		Meteorological station at oilrigs
		out of order => Ground truth data
		from Hvide Sande at the Danish
		west coast.
		
		Wind Speed: 3.6 m/sec.
		Wind Direction: 300 – changing!
		
		Weather: Partly clouded

Position:
Time:
Aircraft:
 	
Flight Altitude:
Flight Pattern:
 	
INU:
GPS:
RTP:
	Kattegat (57.04°N, 11.07°E)
	23.03.2001 / 17:30 UTC - 18:40 UTC
	C-130, id: B-680
	No updated auto pilot and
	navigation instruments.
	Manual control during data
	acquisition.
	1000 m
	Circle flights
	  62° incidence angle (2 circles)
	  57° incidence angle (3 circles)
	  47° incidence angle (3 circles)
	  37° incidence angle (4 circles)
	  25° incidence angle (3 circles)
	OK
	No
	No
		Icing conditions over the North Sea site
		=> flight impossible in the area
		
		Meteorological stations only
		available on land at the Danish
		east coast and on the island Anholt.
		
		Wind Speed: 5.1 m/sec.
		Wind Direction: 140°
		
		Weather: Clouded

Position:
Time:
Aircraft:
 	
Flight Pattern:
 	
Flight Pattern:
 	
Flight Pattern:
INU:
GPS:
RTP:
	North Sea (55.68°N, 4.70°E)
	25.10.2001 / 17:00 UTC - 18:45 UTC
	C-130, id: B-679
	New auto pilot. Attitude
	within ±0.5° for roll < 32.0°
	Circle flights (2000 m altitude)
	  55° incidence angle (3 circles)
	  45° incidence angle (3 circles)
	  35° incidence angle (3 circles)
	  27° incidence angle (3 circles)
	Circle flights (45° incidence angle)
	  1000 m flight altitude (3 circles)
	  2000 m flight altitude (3 circles)
	  3000 m flight altitude (3 circles)
	±45° Wing Wags, ±5° Nose Wags
	OK
	Yes – Some problems with receiver
	No
		Meteorological station at oil rigs.
		
		Wind Speed: 11.0 m/sec.
		Wind Direction: 190°
		
		Sea Temperature: 13.4° C
		Wave Height: 1.2 m
		
		Weather: Almost clear sky

Position:	Atlantic Ocean (61.51°N, 1.27°E)	Meteorological stations on the Norwegian west coast and at Faeroe islands. Interpolated wind map available from the Danish Meteorological Institute.	
Time:	06.03.2003 / 18:20 UTC - 20:50 UTC		
Aircraft:	C-130, id: B-678		
	New auto pilot. Attitude within ±0.5° for roll < 32.0°	Wind Speed: 20 m/sec.	
Flight Altitude:	2000 m	Wind Direction: 0°	
Flight Pattern:	Circle flights		
	45° incidence angle (14 circles)	Weather: Clouded	
	35° incidence angle (16 circles)		
Flight Pattern:	Level flights (minimum 2 min. legs)		
	50° incidence angle (8 legs)		
Flight Pattern:	±45° Wing Wags, ±5° Nose Wags		
INU:	OK		
GPS:	OK		
RTP:	Yes – Minor problems with processor		
Position:	North Sea (57.86°N, 5.47°E)	Meteorological station at the Norwegian west coast. Interpolated wind map available from the Danish Meteorological Institute.	
Time:	20.10.2003 / 17:10 UTC - 17:45 UTC		
Aircraft:	C-130, id: B-678		
	New auto pilot. Attitude within ±0.5° for roll < 32.0°	Wind Speed: 0 – 1 m/sec.	
Flight Altitude:	1750 m	Wind Direction: changing!	
Flight Pattern:	Circle flights		
	45° incidence angle (16 circles)	Weather: Clouded. In the center of a low pressure, causing very low instantaneous wind speed.	
INU:	OK		
GPS:	OK		
RTP:	OK		
Position:	North Sea (55.68°N, 4.70°E)	Ground truth data from Hvide Sande at the Danish west coast.	
Time:	20.10.2003 / 18:30 UTC - 20:20 UTC		
Aircraft:	C-130, id: B-678		
	New auto pilot. Attitude within ±0.5° for roll < 32.0°	Wind Speed: 9.8 m/sec.	
Flight Altitude:	1750 m	Wind Direction: 40°	
Flight Pattern:	Circle flights		
	45° incidence angle (16 circles)	Weather: Clouded	
	35° incidence angle (16 circles)		
Flight Pattern:	Level flights (minimum 2 min. legs)		
	50° incidence angle (8 legs)		
Flight Pattern:	±45° Wing Wags, ±5° Nose Wags		
INU:	OK		
GPS:	OK		
RTP:	OK		

Table 2.1. Details for each of the six (one flight covered two targets) LOSAC flights, carried out with the EMIRAD L-band polarimetric radiometer.

3. Data calibration and preprocessing

The first step in the processing is alignment of the radiometer data, the housekeeping data, and the navigation data, followed by digital integration of the data from the acquired 8 msec. to a suitable period length. Integration can be time controlled, creating a data file with constant period length, and hence equal sensitivity. The integration can also be navigation controlled, giving data files with equal angular spacing. This will cause small variations in the sensitivity, but it may be easier to compare circles with different incidence angles, when

the angular sample interval is constant. Generally the final integration periods are longer than 1 sec., keeping the sensitivity below 90 mK.

The calibration step of the processing involves a series of operations, intended for correction of instrument specific effects. One of these effects is the inphase/quadrature adjustment of the sampling circuit, causing a potential mixing of the 3rd and 4th Stokes parameters. The major adjustment is done by the digital circuitry itself on startup, but drifts in the sampling delays are not adjusted during the data acquisition. Residual delays are calculated and adjusted in the software off-line, using the data from the observation of the built-in noise diode, injecting correlated noise into the two parallel receiver channels.

Calibration of gain and noise temperature is the next correction, and it is done in two parts. The first part is the internal calibration, using the built-in load and the noise diode, determining the calibration constants at the radiometer input terminals. The step requires presence of data from the load as well as from the load with addition of noise from the noise diode. Alternatively, data from the load and data from the antenna with addition of noise from the diode may be used, as the measurement of antenna and noise along with the pure antenna data enables the gain calibration, while the load data gives the noise temperature. The latter method, however, will suffer from eventual variations in the antenna data during the calibration sequence, and the absolute calibration may deviate by several Kelvin.

An option in the calibration software is to interpolate between calibration points, and thus correct for eventual slow drifts. This method can help to remove small drift errors, but it should be used with caution, as variations may origin from quicker variations, undersampled by the calibration sequence. Moreover the method is useless without the full calibration sequence, as the uncertainty in the absolute calibration level, mentioned above, may introduce a drift over the circle track. In this situation a constant, averaged calibration may be calculated for the whole circle, or a constant calibration set can be applied in a separate file before the processing. This enables averaging of different circles, as they are referenced to the same calibration, but it will not correct a possible drift.

The second step in the data calibration includes correction for the external components, antenna, orthomode transducer, and cables. Physical temperatures of front-end components are continuously measured by the radiometer, and they are included in the data structures. The losses have been estimated in laboratory experiments, and they are corrected for by reversal of equation 3.1, where T_M is the measured brightness temperature, T_L the physical temperature of the component causing the loss, T_A the antenna brightness temperature, and η the attenuation.

$$T_M = \eta \cdot T_L + (1 - \eta)T_A \tag{3.1}$$

All flight data have been calibrated using the same steps. Data from the January 16th 2001 technical test flight turned out to be invalid due to a feedback problem in the radiometer front-end, and due to a software problem in the control computer, data from the March 15th 2001 and the March 23rd 2001 do not include the full calibration data. Observation of the reference load with addition of noise from the noise diode is missing, and thus the absolute calibration level of these data is limited as mentioned above. Data sets from October 25th

2001, and from both flights in 2003 include all desired data, and the full calibration sequence, illustrated in figure 3.1a was carried out. For level flights, i.e. straight flights over a homogenous area, where holes in the data flow are less important, the calibration sequence, illustrated in figure 3.1b, can be used. The length of the observation of each target is fully programmable.
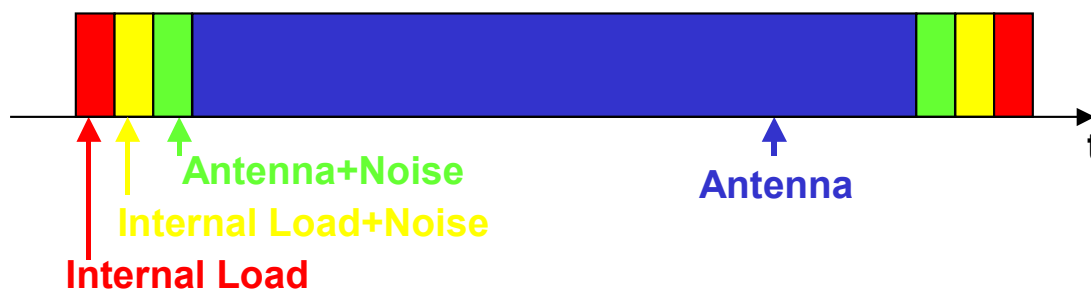

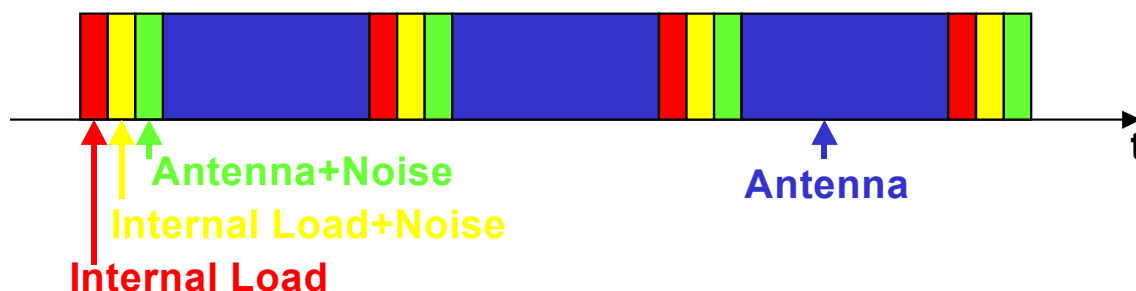*Figure 3.1a. Calibration sequence for the EMIRAD L-band radiometer circle flights.*

Figure 3.1b. Calibration sequence for the EMIRAD L-band radiometer level flights.

For all circles a limited drift is essential, and as described in section 1, tests were carried out in the laboratory prior to the flight campaigns. To validate the field data, however, data from the reference load before and after each data take was analyzed. The data was calibrated using a constant gain and noise temperature setting, and differences, $\Delta = T_{cal,start} - T_{cal,end}$, were calculated. As the circles have different radius, the time interval between calibrations varies, and table 3.1 illustrates the results for the 25th October flight.

Track length [sec]	H-pol. channel $|\Delta|$ [K]	V-pol. channel $|\Delta|$ [K]	3rd St. parameter $|\Delta|$ [K]	4th St. parameter $|\Delta|$ [K]
84	0.12	0.01	0.1	0.05
96	0.08	0.11	0.15	0.06
135	0.17	0.11	0.21	0.15
258	0.09	0.03	0.25	0.31
Mean of all	0.12	0.07	0.18	0.14
Radiometric ΔT	0.10	0.10	0.14	0.14

Table 3.1. Radiometer drift in the radiometer channels during data takes. The table shows the difference in radiometer output from the first to the last calibration sequence at different track lengths, the mean difference value, and the radiometric ΔT .

Some variations are observed in the table, but no systematic deviation may be identified. The mean deviation is found for each channel, and for comparison the radiometric sensitivity, ∆T, for the channels has been calculated for the observation time of the reference load. The typical deviations are of the order of 100 mK, and comparing to the ∆T values, no indication for larger drifts during field operation is identified.

4. Platform attitude and motion compensation

An important issue in polarimetric measurements is the orientation of the antenna relative to the object being measured. The first Stokes parameter, I, is the total power, and for the measurement of this value two antennas with orthogonal polarizations are needed. The other parameters also demand two orthogonal polarizations, but requirements are also related to the orientation of the antennas. The linear polarizations, Q and U, use similar antennas, and only a rotation of the antenna system defines the difference between the two parameters. The circular polarization, V, is independent from rotation, and only the polarization purity of the antenna limits the isolation from the other parameters.

The rotation, and thus the possible mixing of Q and U, is described in several papers and in [2]. For a clockwise rotation, illustrated in figure 4.1, the measured Stokes vector, $\underline{T}_B$', is given by equation 4.1, where I, Q, U, and V is the true Stokes vector, and θ is the rotation angle.
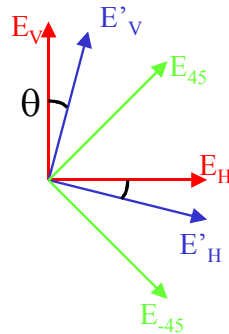
Figure 4.1. Relation between true and measured Stokes parameters, when the antenna plane is rotated clockwise by the angle θ.

$$\underline{T}_B^{'} = \begin{pmatrix} I' \\ Q' \\ U' \\ V' \end{pmatrix} = \begin{pmatrix} 1 & 0 & 0 & 0 \\ 0 & \cos(2\theta) & \sin(2\theta) & 0 \\ 0 & -\sin(2\theta) & \cos(2\theta) & 0 \\ 0 & 0 & 0 & 1 \end{pmatrix} \begin{pmatrix} I \\ Q \\ U \\ V \end{pmatrix} = \begin{pmatrix} I \\ Q*\cos(2\theta)+U\sin(2\theta) \\ -Q*\sin(2\theta)+U\cos(2\theta) \\ V \end{pmatrix} \qquad (4.1)$$

For the EMIRAD radiometer, installed for measurements over the ocean, the influence from an eventual rotation can be estimated with a simple example. Assume typical values for the Stokes parameters, Q = 50 K, and U = 1 K, and assume a rotation angle from –2° to 2°. The

resulting errors, i.e. $\Delta Q = Q' - Q$, and $\Delta U = U' - U$, are shown in figure 4.2, and for $\theta = -0.5°$, the errors are $\Delta Q = 25$ mK, and $\Delta U = 872$ mK.
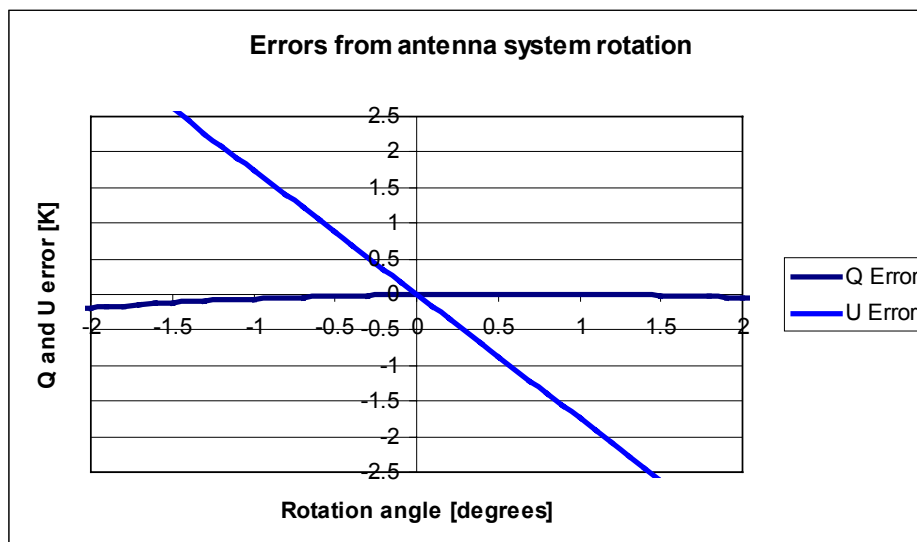
Figure 4.2. Errors in the 2nd (Q) and 3rd (U) Stokes parameters at typical values, Q = 50 K, U = 1 K, and rotation (θ) ranging from –2° to 2°.

Targeting a sensitivity of 100 mK, the rotation must be monitored continuously during radiometer operation, and it must be determined with a precision of down to 0.05° in order to enable corrections to the desired level. In an airborne campaign, the monitoring can be carried out using an inertial navigation unit, INU, which can give a precision of 0.05°, and corrections may be applied to the measured parameters by inversion of equation 4.1.

The antenna installation determines the connection between the aircraft attitude and the eventual rotation. Generally the aircraft attitude will be measured as heading, pitch and roll in the specified order [3], and a vector in the fixed Earth coordinate system will thus be described in the aircraft coordinate system by a series of rotations around the different axis. Likewise the transformation from the aircraft coordinate system to the fixed coordinate system is done by the reverse series of inversions, removing roll, pitch and heading in the specified order.

The aircraft coordinate system is defined as a standard rectangular right-handed coordinate system, with the x-axis pointing from tail to nose, the y-axis from the left to the right wing, and the z-axis hence pointing down. With this definition, and with the Honeywell definition of the aircraft attitude, roll will be a positive rotation around the x-axis, while pitch will describe a positive rotation around the y-axis. The transformation of a vector in the aircraft coordinate system, $\underline{v_a} = (x',y',z')$, to its coordinates in the fixed coordinate system, $\underline{v_f} = (x,y,z)$, is given by the transformation matrix $\underline{A}$ in the relation $\underline{v_f} = \underline{A}\ \underline{v_a}$, where ϕ is the pitch angle and φ is roll. The matrix is shown in equation 4.2.

$$A = \begin{pmatrix} \cos(\phi) & 0 & \sin(\phi) \\ 0 & 1 & 0 \\ -\sin(\phi) & 0 & \cos(\phi) \end{pmatrix} \begin{pmatrix} 1 & 0 & 0 \\ 0 & \cos(\varphi) & -\sin(\varphi) \\ 0 & \sin(\varphi) & \cos(\varphi) \end{pmatrix} = \begin{pmatrix} \cos(\varphi) & \sin(\phi)\sin(\varphi) & \sin(\phi)\cos(\varphi) \\ 0 & \cos(\varphi) & -\sin(\varphi) \\ -\sin(\phi) & \cos(\phi)\sin(\varphi) & \cos(\phi)\cos(\varphi) \end{pmatrix} \quad (4.2)$$

In the present situation, the antenna will be mounted side-looking with a fixed depression, and the rotation angle may be found by evaluating the angle, β, between the horizontal polarization unity vector, x_{ha}=(x',y',z') = (-1,0,0), of the antenna and the fixed vertical unity vector, z_{vf}=(x,y,z) = (0,0,-1). Subtracting 90°, the nominal difference between the horizontal and vertical polarizations, will give the rotation angle, θ. Equation 4.3 gives the results, using 2.16 to transform the coordinates.

$$\theta = \beta - 90° = \phi \quad (4.3)$$

The true incidence angle at the sea surface may be found using the same procedure. The direction of the antenna beam (into the antenna) will be described by the unity vector x_{aa}=(0, -cos(d), -sin(d)), where d is the depression angle, and the vector must be transformed to the fixed Earth coordinate system. The incidence angle, α, is the angle between the antenna beam and the vertical unity vector at the sea surface, given by z_{vf}=(x,y,z) = (0,0,-1). It is found by equation 4.4.

$$\cos(\alpha) = \cos(\phi)\sin(\varphi + d) = \cos(\phi)\cos(\varphi + d - 90°) \quad (4.4)$$

For small pitch angles, a good approximation to the equation is 1.1, which may be used to determine the desired roll angles during the airborne campaign.

$$\alpha = 90° - d - \varphi \quad (1.1)$$

The last parameter of interest for the airborne measurements is the look direction relative to the aircraft heading. As the heading is given by the unity vector x_{nf}=(1,0,0) in the fixed coordinate system, and as the antenna pointing will be the projection, x_{apf}, of x_{af} to the fixed (x,y)-plane, the angle between these two vectors will define the desired angle, ξ, resulting in the relation, given by 4.5.

$$\cos(\xi) = \frac{\sin(\phi)\sin(d + \varphi)}{\sqrt{1 - \cos^2(\phi)\sin^2(d + \varphi)}} \quad (4.5)$$

Knowing the look direction relative to the aircraft heading, hdg, the antenna look direction relative to Earth north will be given by equation 4.6.

$$\psi = hdg + \xi \quad (4.6)$$

As the results show, the three primary parameters, antenna rotation, antenna look direction, and incidence angle, may vary as a result of the aircraft motion. The look direction may be added to the attitude parameters for plotting and analysis of results, and antenna rotation may be corrected using the reverse equation 4.1. Incidence angle variations, however, will cause

the incident brightness temperature to vary as described by the Klein-Swift model [4]. For a typical situation, frequency = 1.4135 GHz, sea surface temperature = 10.0° C, and sea surface salinity = 35 psu, the modeled sea surface brightness temperature as well as the 2nd Stokes parameter, Q, can be seen in figure 4.3 as a function of the incidence angle.
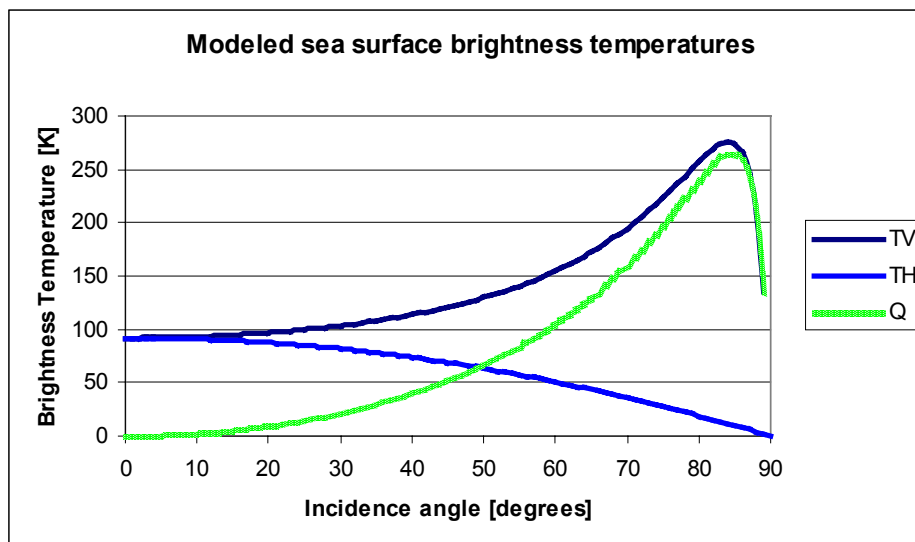
Figure 4.3. Klein-Swift model of sea surface brightness temperature and second Stokes parameter as a function of the incidence angle, when frequency = 1.4135 GHz, sea surface temperature = 10.0°C, and sea surface salinity = 35 psu.

In the range of interest, between 20° and 65° incidence angle, the typical variations for T_V are about 1.5 K/° and about -1 K/° for T_H. $Q = T_V - T_H$, will thus vary about 2.5 K/°, rising need for knowledge about the incidence angle in the order of 0.05°, when a sensitivity of 100 mK is targeted.

When looking for an azimuth signature, the nominal roll angle must be absolutely constant, and eventual variations must be corrected for. The Klein-Swift model can be used for this purpose, as an integration of the model within the antenna pattern will provide the theoretical input to the radiometer for a given incidence angle. The error, i.e. the modeled brightness temperature at the actual incidence angle, T(inc.), minus the modeled brightness temperature at the nominal incidence angle, T(nom.), may be calculated using equation 4.7, and the contribution can be subtracted from the measured values.

$$\delta T = T(inc.) - T(nom.) \tag{4.7}$$

An alternative approach to the theoretical corrections, described in this section, is a simple statistical correction, where it may be assumed, that each of the four Stokes parameters can be described as a linear function of the two attitude parameters, roll and pitch, when variations are small. For a single parameter, e.g. the first Stokes parameter, I, the dependence on the incidence angle, α, is determined by equation 4.8.

$$a_{I\alpha} = \frac{\langle I\alpha \rangle - \langle I \rangle \langle \alpha \rangle}{\langle \alpha^2 \rangle - \langle \alpha \rangle^2} \qquad\qquad (4.8)$$

Corrections can follow, as the error signal will be given by equation 4.9, which can be subtracted from the measured brightness temperatures.

$$\Delta I = a_{I\alpha} \cdot (\alpha_{inc.} - \alpha_{nom.}) \qquad\qquad (4.9)$$

Likewise the dependence on pitch may be determined, and the same determination is used for the other Stokes parameters.

It may be expected that the methods would lead to approximately the same result, but due to the influence from noise and uncertainties in the calibration, some differences may be noticed. The theoretical approach should lead directly to the desired result, but it is limited by the performance of the model and the knowledge of sea surface parameters. In this case the Klein-Swift [4] model is used to correct for incidence angle deviations, while the geometric vector rotation, equation 4.1, is used for polarization mixing. As the real antenna pattern has a certain beam width and some side-lobes, the Klein-Swift model may not provide a precise result for each incidence angle, and there is a small potential risk, that corrections may not be exact. The vector rotation is a simple geometrical problem, and the model is just a mathematical reversal of the rotation. In both cases the calibration of the Stokes parameters is essential, as calibration errors will cause a scaling problem between the parameters and the corrections, eventually over- or underestimating the correction.

The regression analysis is based on real observations, and thus it gives the true, observed correction. Noise may be a problem here, however, as the regression line will be determined with a standard deviation depending on the number of observations. The linear approach may also be too simple for larger errors, causing risk for an over- or underestimation of the correction. The regression method also includes a potential danger. Assuming that the aircraft roll and pitch will change with the aircraft heading, an eventual real signal in the measured data, depending on the azimuth look angle and hence on the aircraft heading, will also be rejected, as it will be regarded as roll or pitch dependent. Roll and pitch variations as functions of the aircraft heading is a realistic situation, as the wind may change the aircraft attitude. The problem is minimized, however, when the aircraft navigation system is set up for constant attitude, rather than for a perfect circle. The result is that the aircraft will drift with the wind in its own coordinate system, where the wind influence is negligible.

A method between the two above mentioned could be the determination of a model function, based on measured values. Large-scale variations must be available, e.g. a ±45° roll leg, and a curve can be obtained and stored. The curve may be stored as a look-up table, and to reduce the influence from noise, it may be low pass filtered, or eventually modeled as a high order polynomial. This correction will be less noise sensitive than the regression method, and it may take into account an eventual deviation from the theoretical model function, e.g. due to unknown sea surface parameters or antenna side-lobes.

A combination of the three correction methods could be an alternative solution. Modeled deviation calculation can be the basic correction, while the regression method can be used to remove eventual residuals. The best method is not easily found from an analysis of advantages and drawback of the different motion compensation methods, as the importance of each potential problem depends on the actual measurement situation. The developed processing software is thus able to perform all three corrections independently, and from a number of test cases, the final correction type can be chosen.

For determination of the influence from large-scale variations and for test of the correction algorithms, two special tracks were recorded on the latest three flights, a ±45°roll, repeated two times, and a ±5° pitch, also repeated two times. The two tracks, referred to as wing wags and nose wags, respectively, were preprocessed and calibrated using the standard preprocessing and calibration steps, and the results from the October 25th 2001 flight are illustrated in figure 4.4 and figure 4.5. As shown in the figures, the two tracks are not ideal, as they both contain some roll and pitch variation. It is obvious, however, that the 1st and 2nd Stokes parameters depend strongly on the roll angle, while changes in the aircraft pitch influence on the 3rd Stokes parameter. It must be noticed, that the wing wags are ±45° roll
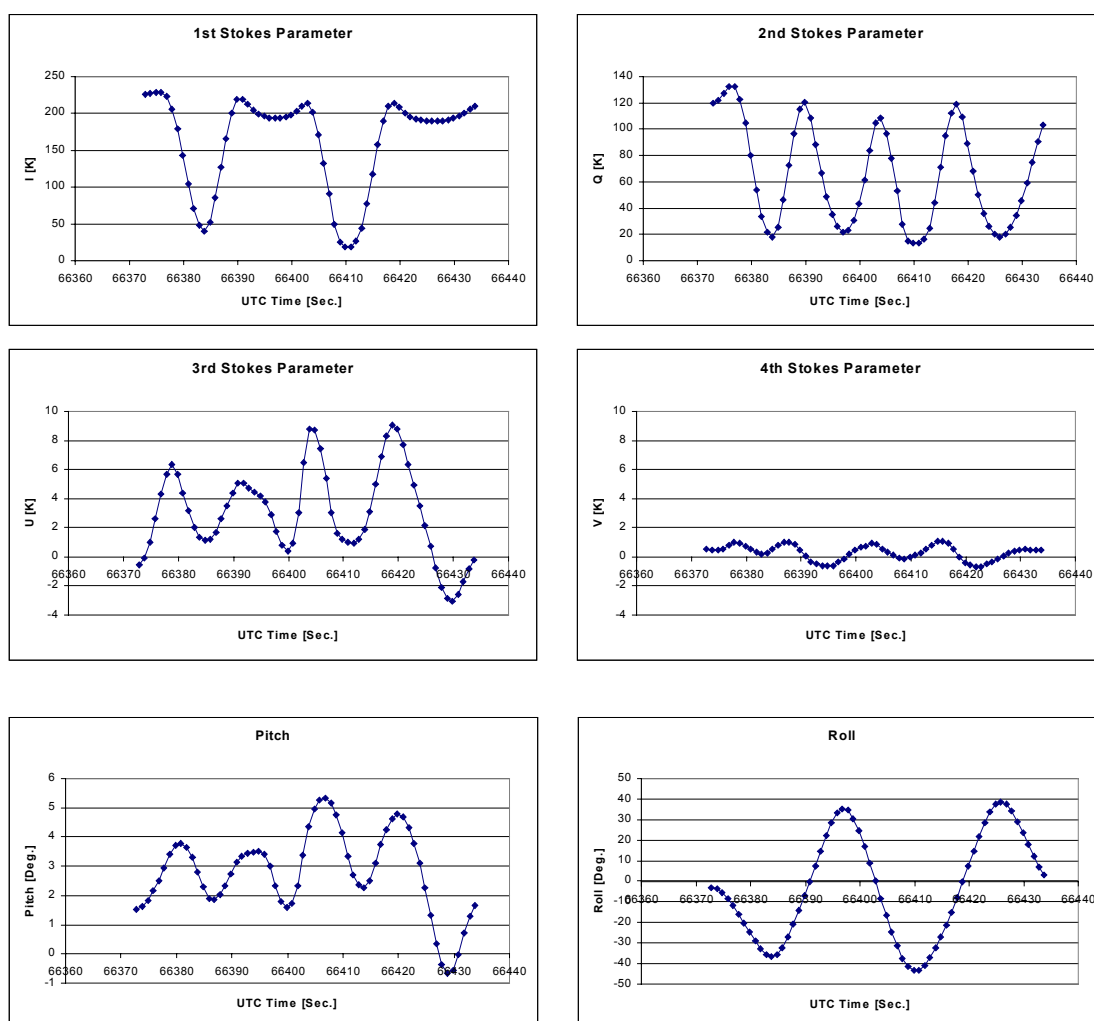
Figure 4.4. Raw data from ±45° wing wags, including the four Stokes parameters (Kelvin) as well as pitch and roll data (°).

variations, causing the antenna to look slightly above the horizon for the negative roll situation. The results are thus used and corrected only for the UTC time ranges from t = 66391 sec. to t = 66403 sec. and from t = 66419 sec. to t = 66433 sec, equal to incidence angles below 70°.

The 1st and 2nd Stokes parameter variations are illustrated in figure 4.6a, where the horizontal and the vertical brightness temperatures are plotted against the incidence angle (red curve). The Klein-Swift model is shown in blue color, and the green curve illustrates the mean of the measured brightness temperatures in the interval from 22° to 62° incidence angle after low pass filtering, i.e. the model function useable for later corrections. Generally it is noticed, that it follows the theoretical model quite well, but for higher incidence angles, above 55°, some deviation is found, and it might be a potential problem for the Klein-Swift model based correction method.
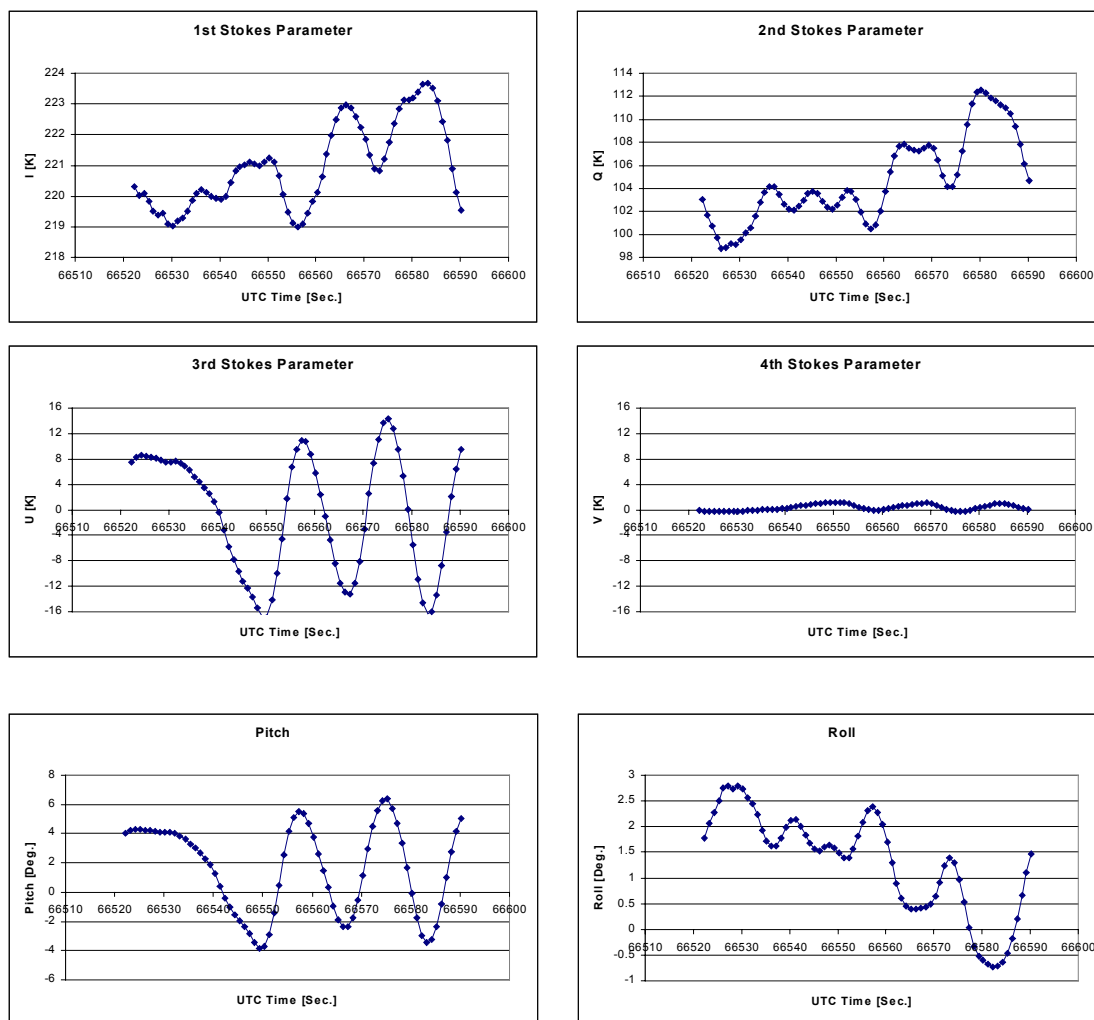
Figure 4.5. Raw data from ±5° nose wags, including the four Stokes parameters as well as pitch and roll data.

Figure 4.6b illustrates the 3rd Stokes parameter as a function of the antenna rotation angle, pitch, and it is seen that the relation is almost linear. An offset, probably due to the installation of the antenna and the inertial navigation unit in the aircraft, is noticed, but it may

be easily determined from the figure, and included in the model. As for the incidence angle the curves may be averaged and low pass filtered, providing a model function for later antenna rotation corrections.
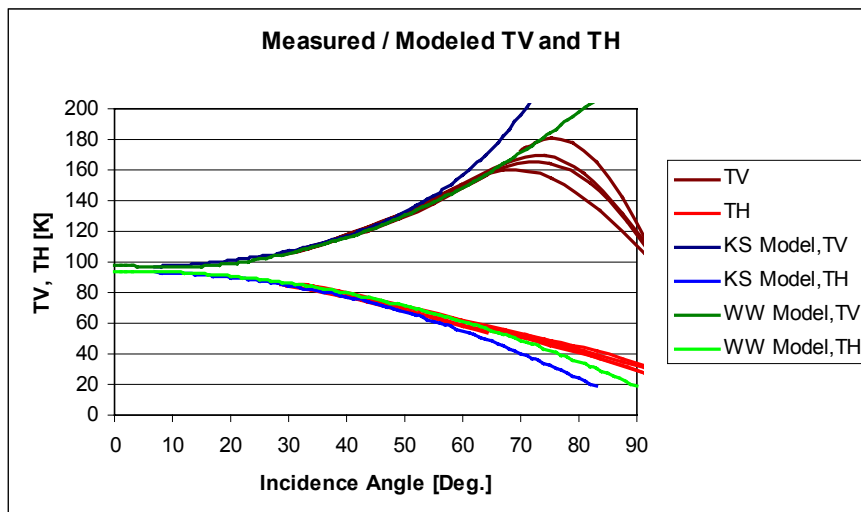
Figure 4.6a. Measured horizontal and vertical brightness temperatures (red curves) as functions of the incidence angle. Each polarization results in four measured curves, representing the increasing and decreasing roll for each of the two wags. The blue curves show the Klein-Swift model for the sea surface state, and the green curves show the average of the measured results after low pass filtering, intended for later incidence angle corrections.
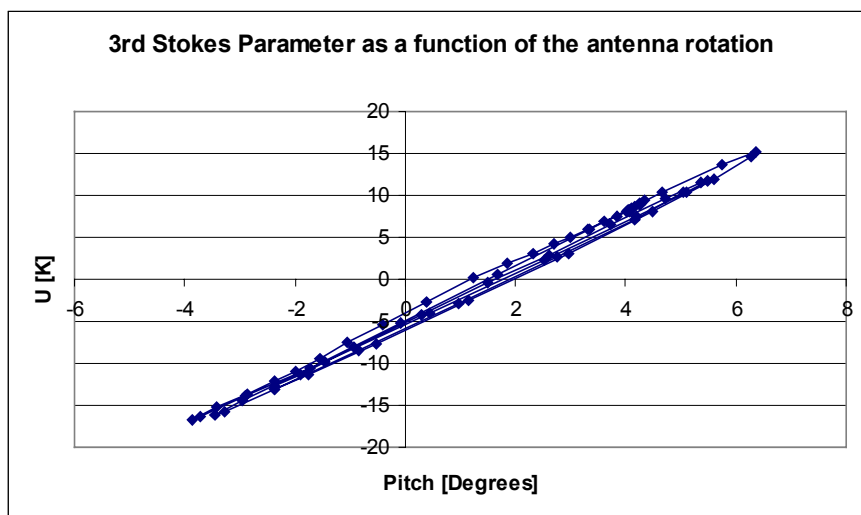
Figure 4.6b. Measured 3rd Stokes parameter as a function of the antenna rotation, pitch. The offset may origin from a mechanical offset between the antenna mounting and the inertial navigation unit.

The different correction types are carried out on the wing wags and the nose wags tracks, and the results are illustrated in the figures 4.7 to 4.16. As the wing wags are corrected only for incidence angles below 70°, a break in the curves, showing the 1st and 2nd Stokes parameters is seen for all corrections.
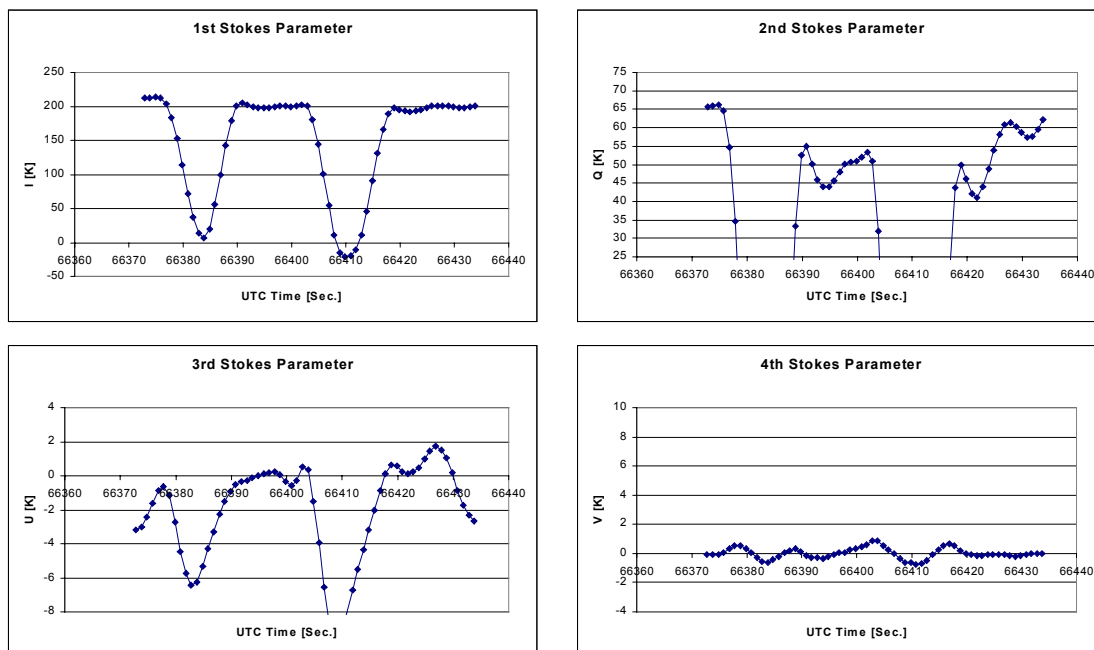
Figure 4.7. The four Stokes parameters from the ±45° wing wags, corrected using the linear regression method. Each parameter's linear dependence on the incidence angle and the antenna rotation is calculated, and corrections are applied according to equation 4.9.
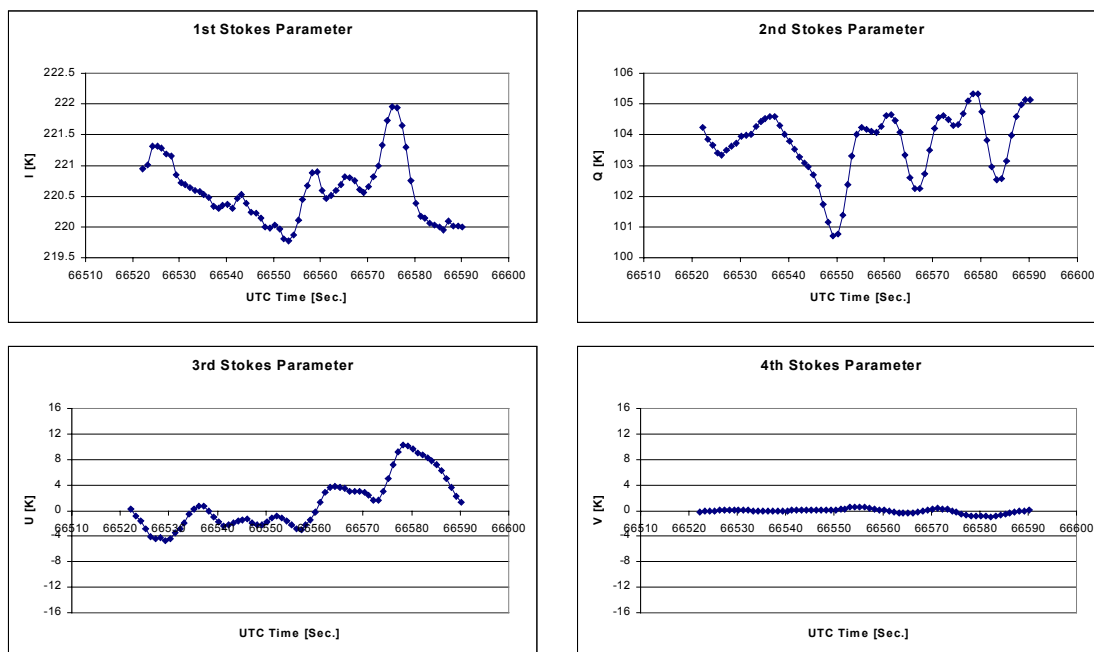
Figure 4.8. The four Stokes parameters from the ±5° nose wags, corrected using the linear regression method. Each parameter's linear dependence on the incidence angle and the antenna rotation is calculated, and corrections are applied according to equation 4.9.
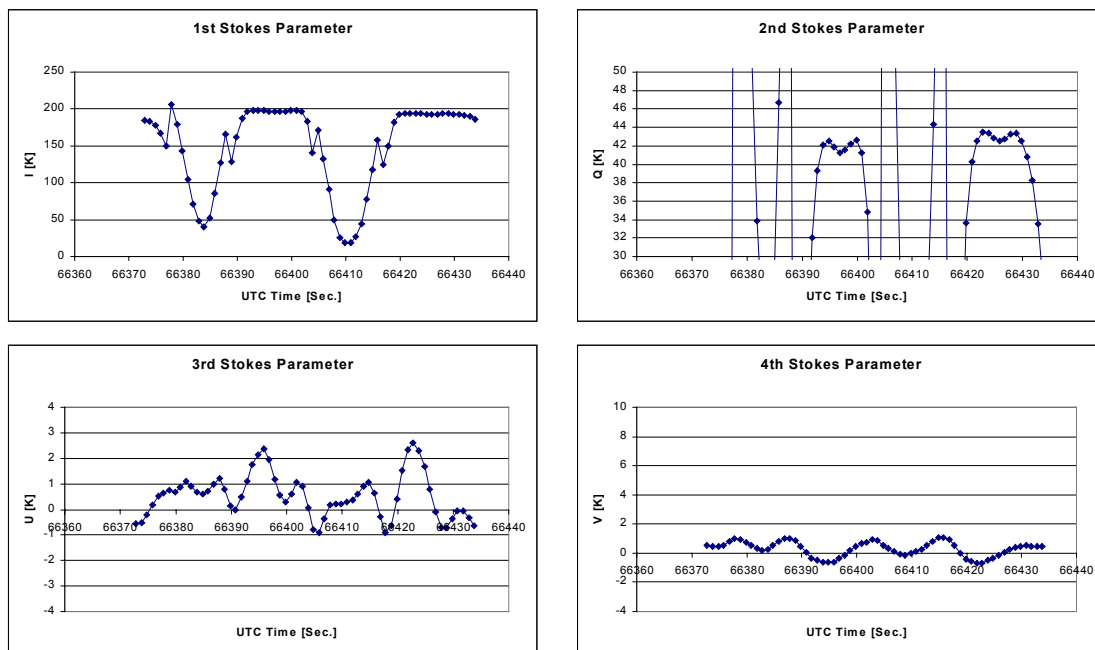
Figure 4.9. The four Stokes parameters from the ±45° wing wags, corrected using the Klein-Swift model and the antenna rotation matrix, equation 4.1. The theoretical error in each parameter is calculated, and the error is subtracted, using equation 4.7.
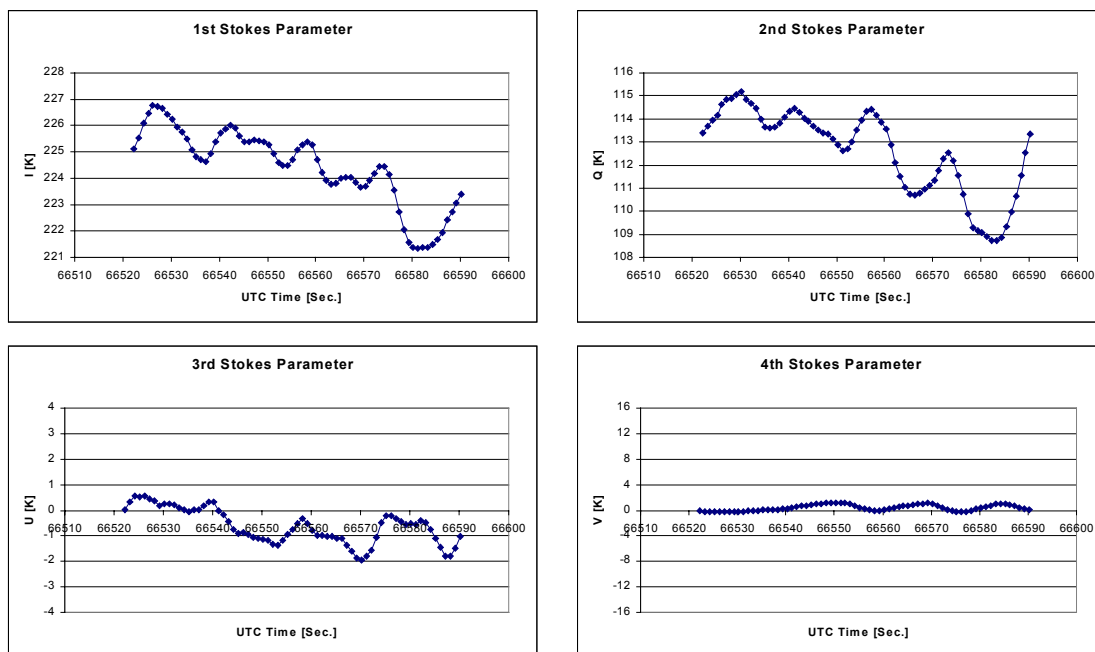
Figure 4.10. The four Stokes parameters from the ±5° nose wags, corrected using the Klein-Swift model and the antenna rotation matrix, equation 4.1. The theoretical error in each parameter is calculated, and the error is subtracted, using equation 4.7.
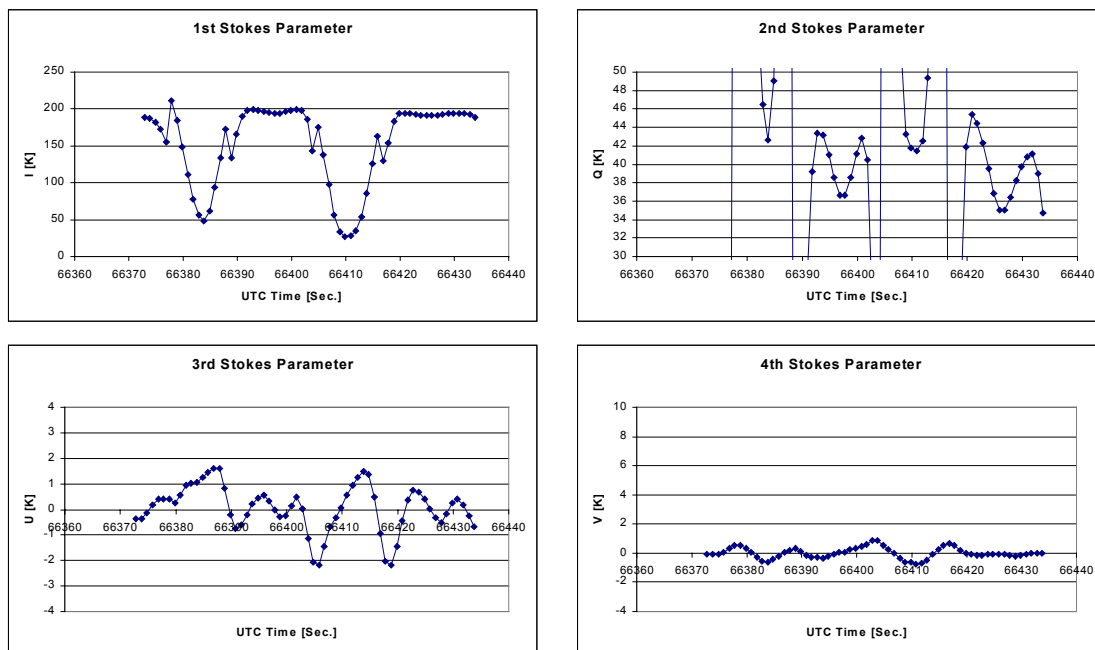
Figure 4.11. The four Stokes parameters from the ±45° degrees wing wags, corrected using the Klein-Swift model and the antenna rotation matrix, equation 4.1. Subsequently the parameters are corrected using the linear regression method.
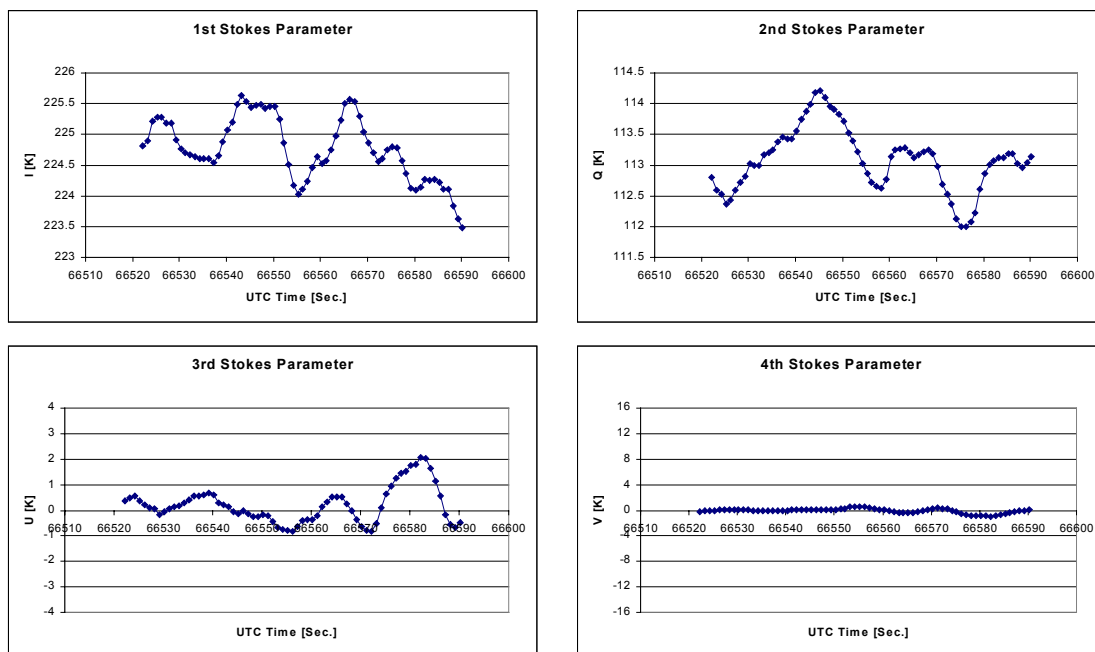
Figure 4.12. The four Stokes parameters from the ±5° nose wags, corrected using the Klein-Swift model and the antenna rotation matrix, equation 4.1. Subsequently the parameters are corrected using the linear regression method.
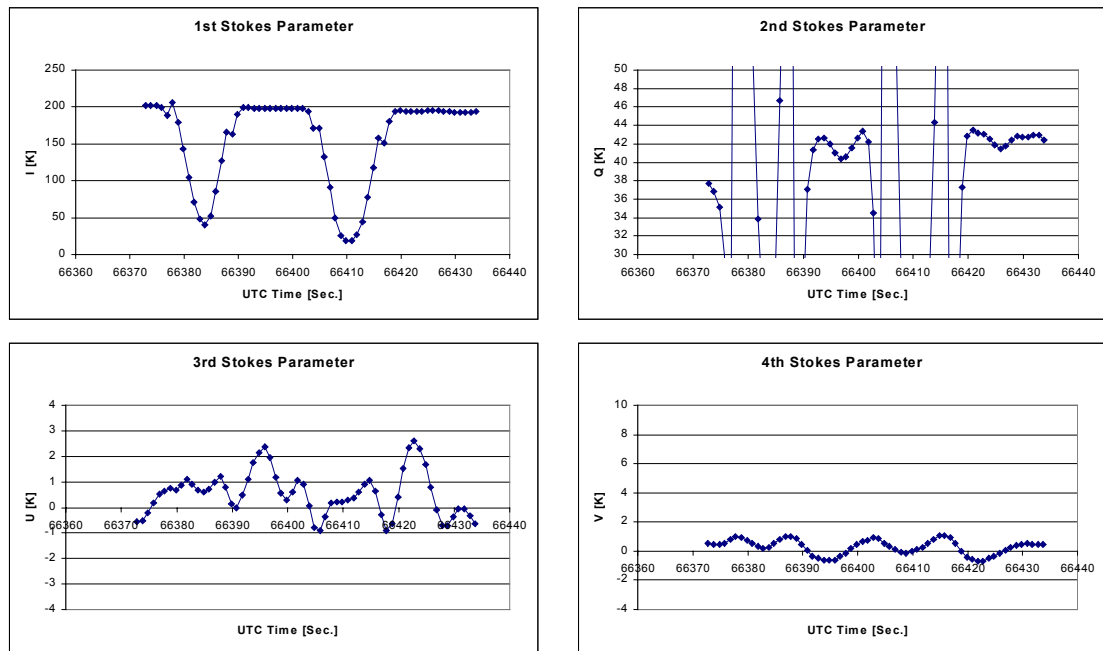
Figure 4.13. The four Stokes parameters from the ±45° wing wags, corrected using the model based on the low-pass filtered mean from the wing wags and the nose wags.
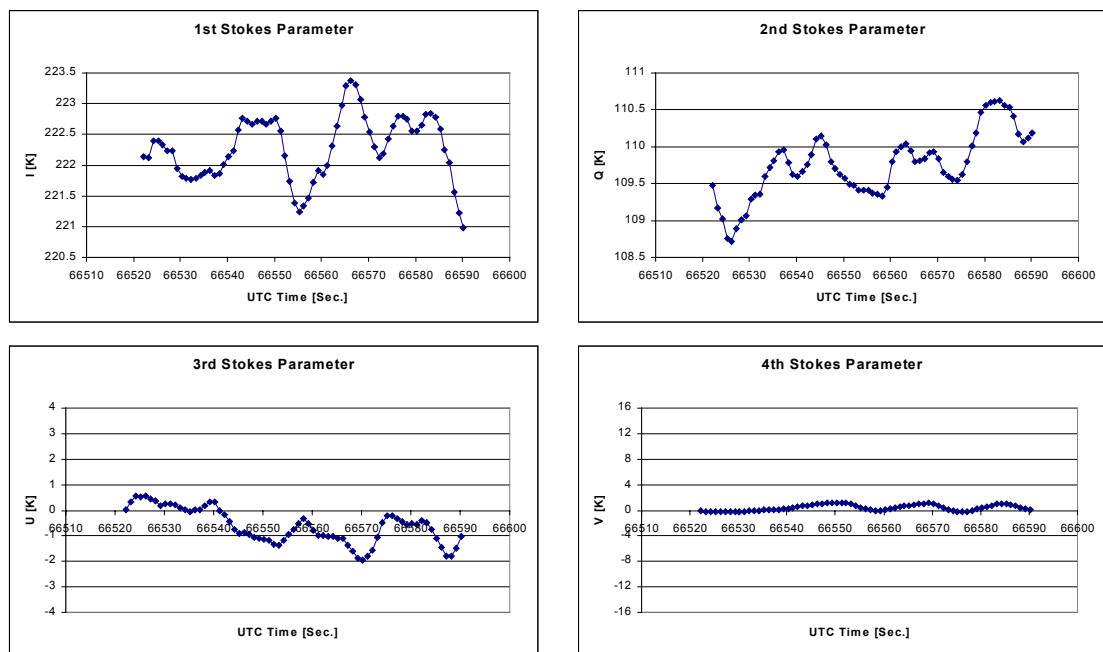
Figure 4.14. The four Stokes parameters from the ±5° nose wags, corrected using the model based on the low-pass filtered mean from the wing wags and the nose wags.
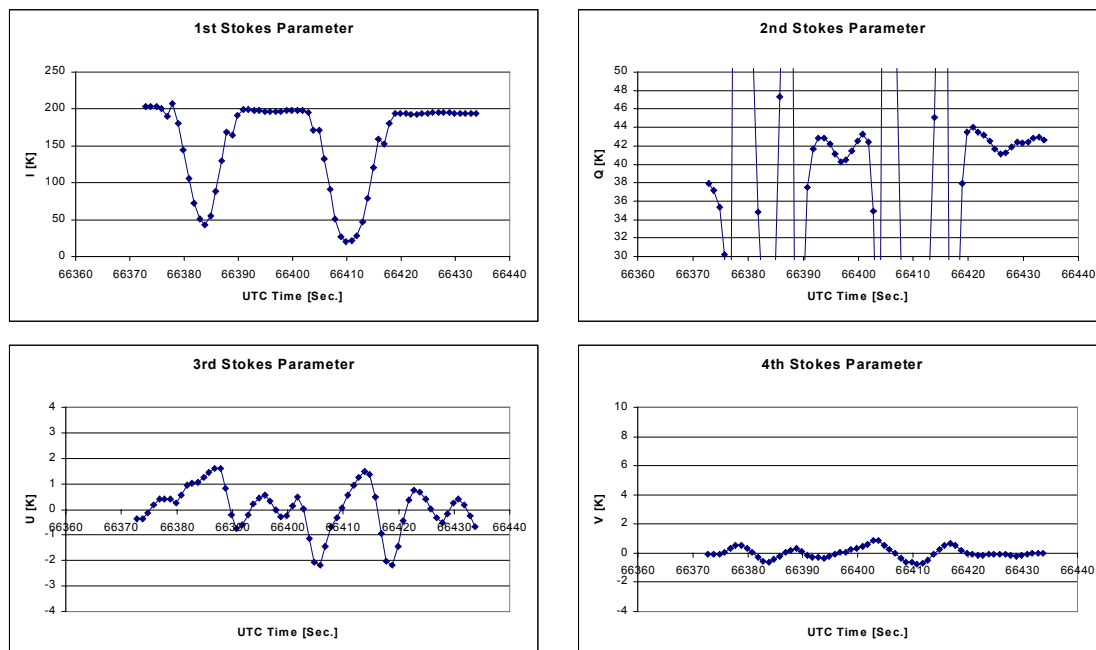
Figure 4.15. The four Stokes parameters from the ±45° wing wags, corrected using the model based on the low-pass filtered mean from the wing wags and the nose wags. Subsequently the parameters are corrected using the linear regression method.
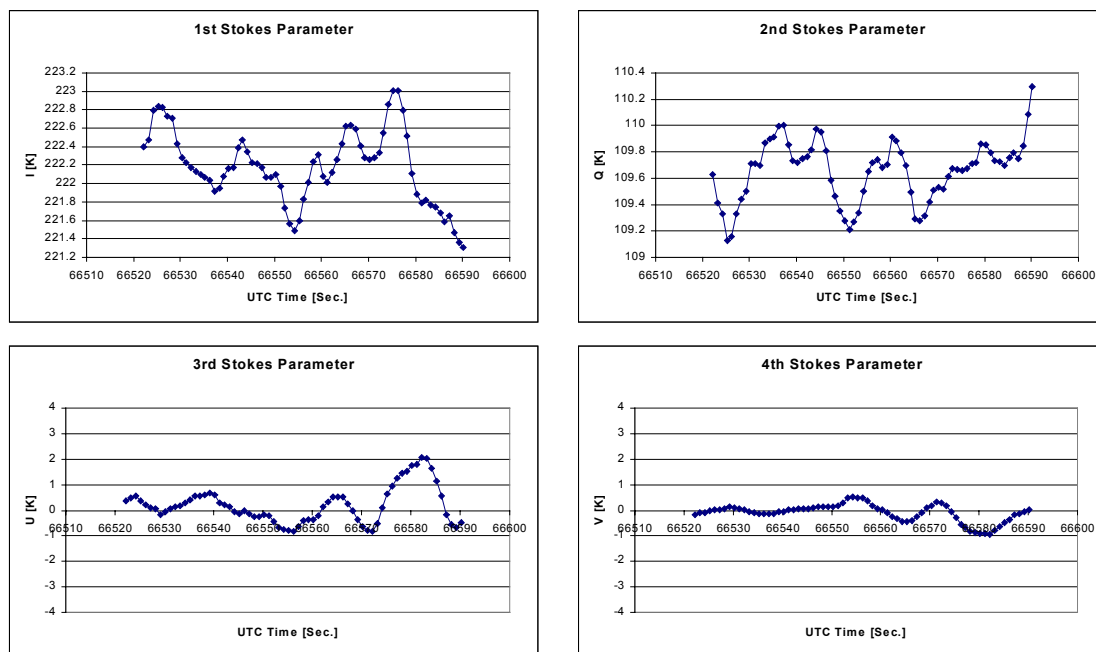
Figure 4.16. The four Stokes parameters from the ±5° nose wags, corrected using the model based on the low-pass filtered mean from the wing wags and the nose wags. Subsequently the parameters are corrected using the linear regression method.

The model-based corrections are seen to provide quite similar results, but it is noticed, that the Klein-Swift model has problems for low roll angles, where the returned brightness temperature is too low, corresponding to figure 4.6a. The result is thus an M-shaped pattern for positive roll angles. The fitted model causes the same basic shape, but the M-shape is wider, and the deviations for lower roll angles are smaller.

The additional linear regression has very small influence on the fitted model, indicating that almost no residual roll dependence, which can be fitted with a linear approximation, is left. For the Klein-Swift model, the regression corrects the edges, but meanwhile it leaves the middle of the pattern deeper. The same happens for the pure regression correction, and the basic problem is, that a linear fit to an M-shaped curve will trade deviations on the edges with deviation in the central part, but it will be unable to remove the ripple.

The result is a total M-shape in all five cases, but the ripple is different, and some methods will thus provide a better correction for the total track. As the overall purpose of the corrections is to get a flat pattern for the full pitch range and for the 0° to +45° roll range, the Stokes parameters dependence on roll, $dT/d\varphi$, and pitch, $dT/d\theta$, may be used to evaluate the methods. The pure regression and the Klein-Swift with regression both provide a peak-to-peak variation of 8 K in the 2nd Stokes parameter, resulting in a slope equal to 0.23 K/°. With typical roll variations within a track in the order of 1°, up to 0.23 K error is to expect, and for the scientific tracks, this is not acceptable. The Klein-Swift model alone, the fitted model, and the fitted model with regression provide smaller deviations, 2 K peak-to-peak, resulting in a maximum slope of only 0.08 K/°.

The additional regression may be able to provide better results for smaller local ranges, as the reason for its problems in the example above is the M-shape, causing problems for the linear model. This is illustrated for the nose wags, where the fitted model along with linear regression provides the lowest variation over the full range. It is thus to expect, that corrections of the scientific tracks can be done to a precision not worse than the above 0.08 K/°. Figure 4.17 shows the wing wags data after correction, where a nominal roll angle of 25° has been selected.

For the nose wags, and the 3rd Stokes parameter correction, the basic impression is the same. The variations are too large to provide good results for the pure regression, while the other methods provide slopes of about 0.15 K/°. If only the first half on the track is regarded, the slope is down to 0.1 K/°. A possible explanation for this behavior may simply be noise, and this theory is supported by figure 4.6b, where some deviation from the average track is observed. As realistic pitch variations are of the order of 1° over long time, the problem will not influence the scientific tracks, and it is believed that the slope can be kept below 0.1 K/°.

To demonstrate the correction technique on a normal flight track, the track, shown in figure 4.18 is selected. The track is a typical track with normal sized variations in pitch and roll, and the oscillations in the roll in the first part of the track makes it a good test case. The track is acquired on the October 25th 2001 flight with a nominal incidence angle of 45°. The different correction methods are applied to the track, and generally the impression is like for the wing wags and the nose wags, that the methods lead to quite similar curves. The results for the Klein-Swift model correction with regression and for the fitted model with regression are
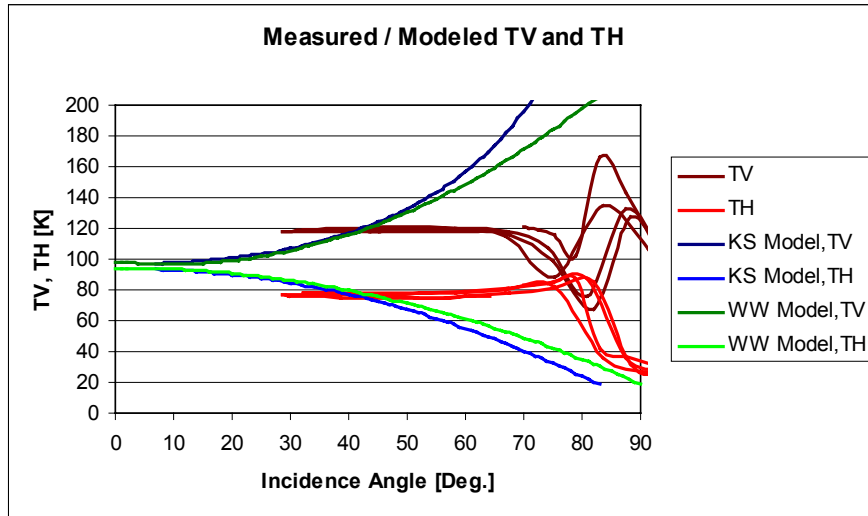
Figure 4.17. Corrected horizontal and vertical brightness temperatures (red curves) as functions of the incidence angle. The blue and green curves show the model functions.
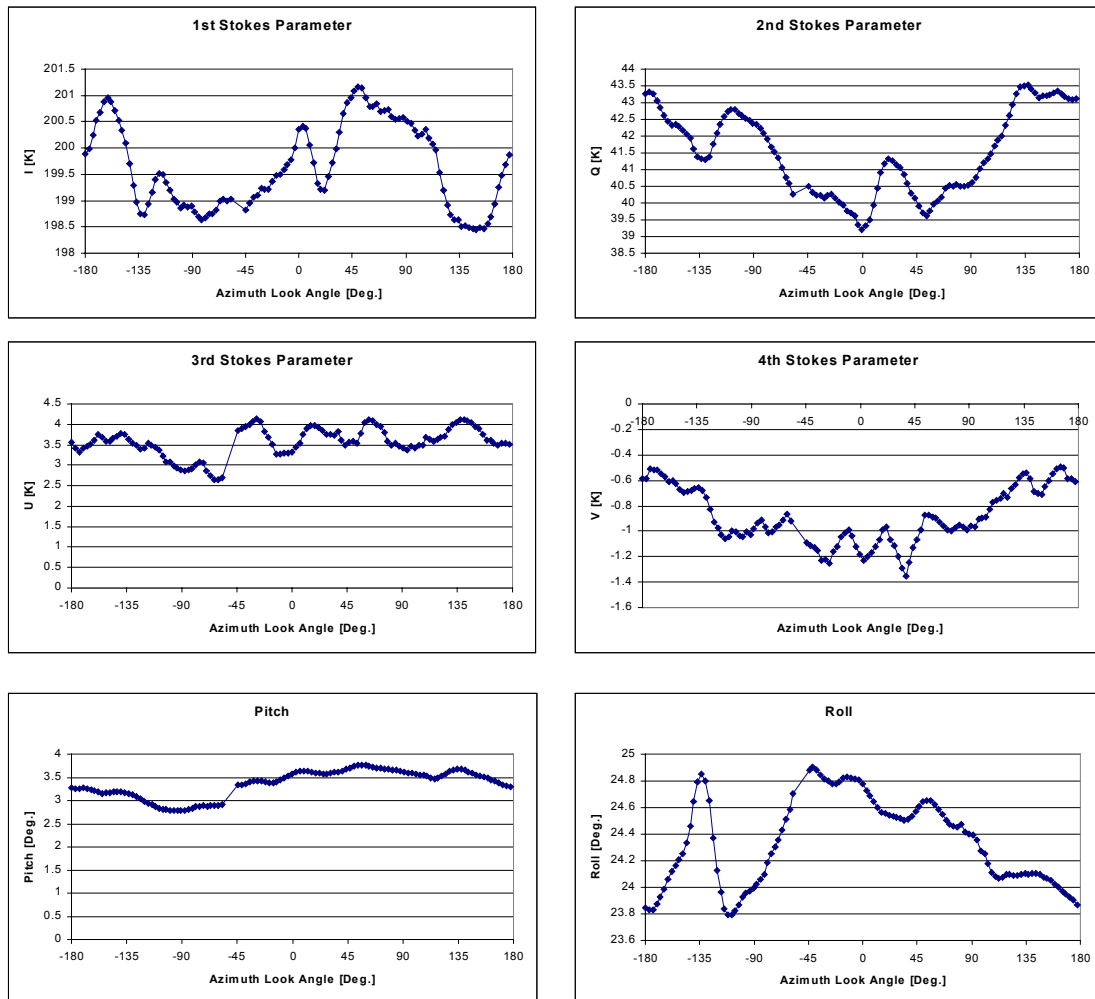

Figure 4.18. The raw four Stokes parameters from a circle flight track from the October 25th 2001 flight. The track is acquired with a nominal incidence angle of 45°.
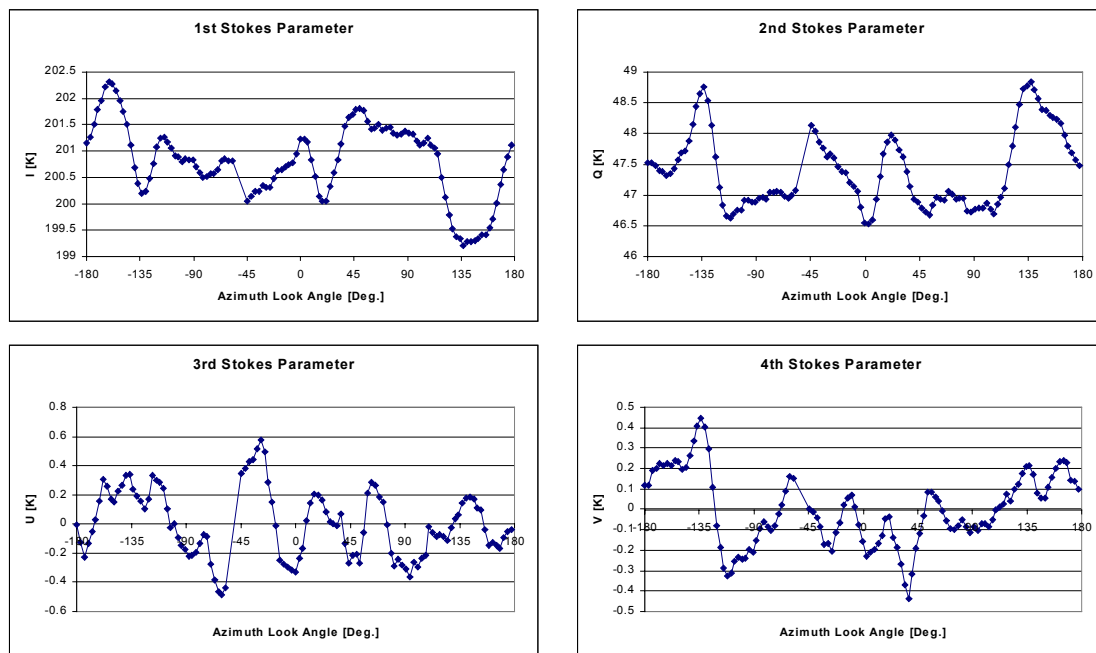
Figure 4.19. The four Stokes parameters from the circle flight track with 45° incidence angle from the October 25ᵗʰ 2001 flight. The track is corrected using the Klein-Swift model, and residual errors are removed with a linear regression.
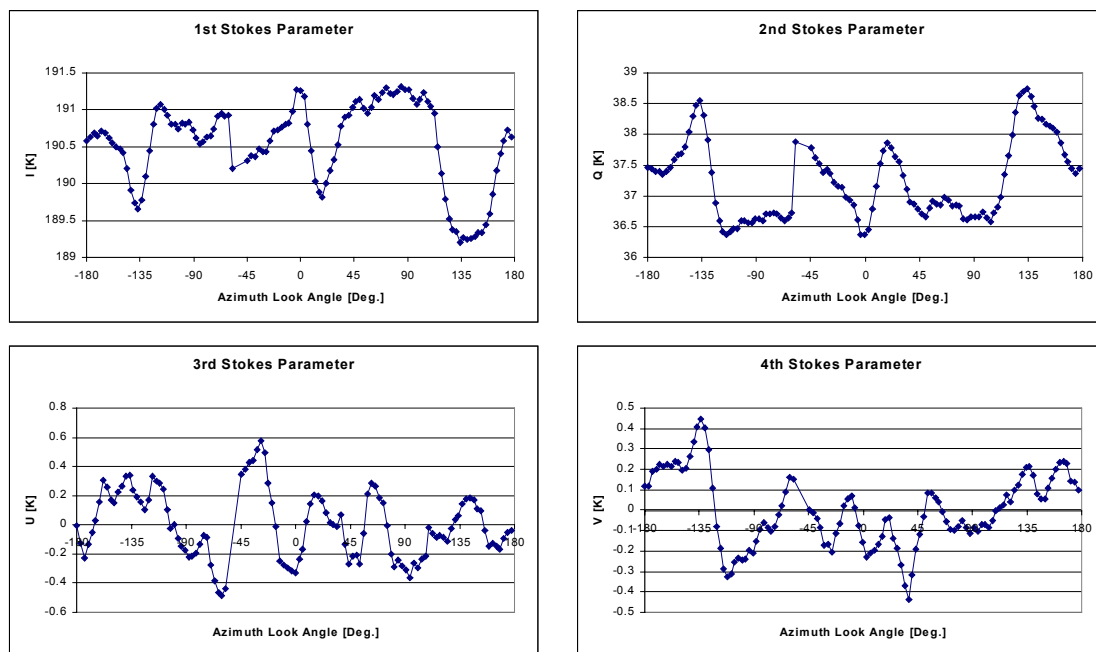
Figure 4.20. The four Stokes parameters from the circle flight track with 45° incidence angle from the October 25ᵗʰ 2001 flight. The track is corrected using the fitted model based on the wing wags, and residual errors are removed with a linear regression.

shown in figure 4.19 and 4.20, respectively. It is seen that the two sets of curves are very similar, and an evaluation of the standard deviation of the difference between them shows values less than 10 mK for the 1st Stokes parameter and 35 mK for the 2nd. The small offset between the two sets is a result of the different model functions behind the corrections, but as the absolute level is not important to the azimuth signature evaluation, it has no influence on the further data processing.

The examples of correction with the different methods and the combinations of them show some differences regarding the large-scale corrections, and it is concluded that a model in combination with a linear regression to remove the residual error is a good solution. Two models, the theoretical Klein-Swift model as well as a fitted model based on the wing wags, have been tested. The fitted model is the response of the full, installed system including antenna side-lobes etc., and as expected, it provides the best results for the large-scale variations. For smaller scale variations, the models turn out to give very similar results, and it may be concluded, that the choice of correction method is of minor influence to the final results. For the present flights, having typical variations of pitch and roll within 1°, it is believed that corrections can be done to a 100 mK level, which is satisfactory for the scientific campaign.

5. Results from the March 15th 2001 flight

The flight on March 15th 2001 was the first scientific measurements, and although the weather forecast predicted relatively low wind, approximately 5 m/sec. the flight was carried out, as a low wind case belongs to the total data set. Meteorological data was ordered from the oilrigs in the North sea, near the target area, but due to a data recorder fail, a standard data set from The Danish Meteorological Institute, DMI, is used as replacement. The data is measured at Hvide Sande at the Danish West Coast, and the data points for wind speed and wind direction are shown in figure 5.1 along with two vertical lines, indicating the time of flight over the target area.
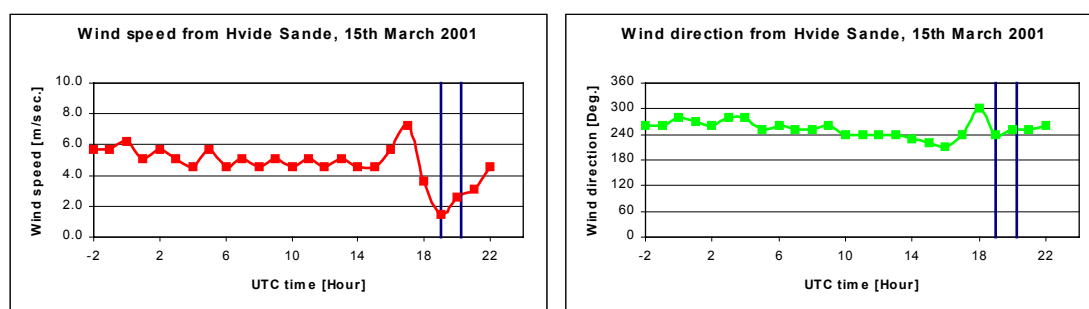
Figure 5.1. Wind speed and wind direction for March 15th 2001, measured at Hvide Sande at the Danish West Coast. The blue lines indicate the flight time.

As seen in the figure, the wind decreased rapidly right before the measurements and the direction changed between 230° and 300°. A risk thus exists, that the wind driven sea surface field was in an intermediate state, and that no homogenous pattern was established.

As indicated in table 2.1, four different incidence angles were covered during the flight, and to compare the stability of eventual signatures, it was decided to measure each circle three times. The data was pre-analyzed during the flight, and the standard deviation between data samples was evaluated for each circle. Some variation was noticed, but as no attitude correction was applied at this point, nothing unusual was seen, and indications for RF-interference were not found at this time.

After the flight, data was processed as described in sections 3, and motion compensation was done according to section 4. It should be noticed, that the full absolute calibration precision is not available for this flight due to a control computer problem, leaving out the combined observation of the calibration load with the noise diode. Several Kelvin of absolute uncertainty is thus the result, but as the stability evaluation, illustrated in table 3.1, shows drifts in the order of 100 mK maximum, the data is useful for determination of azimuth signatures anyway. The full data set is presented in the figures 5.2 to 5.13, where the data is aligned to the azimuth look direction.

For all data a quite large peak-to-peak signal is noticed, typically more than 1 K. The large extremes, however, are in some signatures caused by narrow peaks (point target like signatures), raising from the basic signal during 30° to 45° of scan. It is seen that the peaks do not generally appear in the same position for different circles, and no system can be identified visually. The basic signal, i.e. the slower variations, are in some circles almost without variation, and in figure 5.11 for the 52° incidence angle, no clear 1st or 2nd harmonic variation is present. In figure 5.12, likewise from the 52° incidence angle measurements and obtained between the circles in 5.11 and 5.13, 1st and 2nd harmonics seem to be present in all Stokes parameters.

The two above observations may indicate that some random signal is present, and in this case, averaging could help to reduce the influence. As the three circles in the above example are obtained subsequently in identical conditions, averaging of the curves is possible. As they are not sampled at identical angles, however, the averaging can not be done data point by data point. The circles are thus re-sampled using an interpolation filter, and the figures 5.14 to 5.17 show the results for each of the four incidence angles. For 20° incidence, the 2nd circle is left out, as figure 5.3 indicate the presence on single point RF-interference, while the other averaged curves are based on all three basic circles.

The result from the averaged curves show smaller peak-to-peak variations, almost all below 1 K, and the obvious presence of point target like signatures is reduced, although they are still present in all curves. To reduce the influence from the small peaks additionally, a harmonic analysis of the averaged Stokes parameters can be carried out, focusing on identification of 1st and 2nd harmonics, which are the components in the wind driven sea surface structures at higher frequencies [5]. This analysis is shown in table 5.1, where the magnitude and phase, i.e. the azimuth direction, for the first four harmonics are calculated for each Stokes parameter and for each incidence angle.

The table shows typical values between 50 mK and 200 mK for the magnitudes for all Stokes parameters, but no systematic behavior is observed. For the vertical polarization, the 1st order component is three times larger than the 2nd order component for 20°, while almost equal
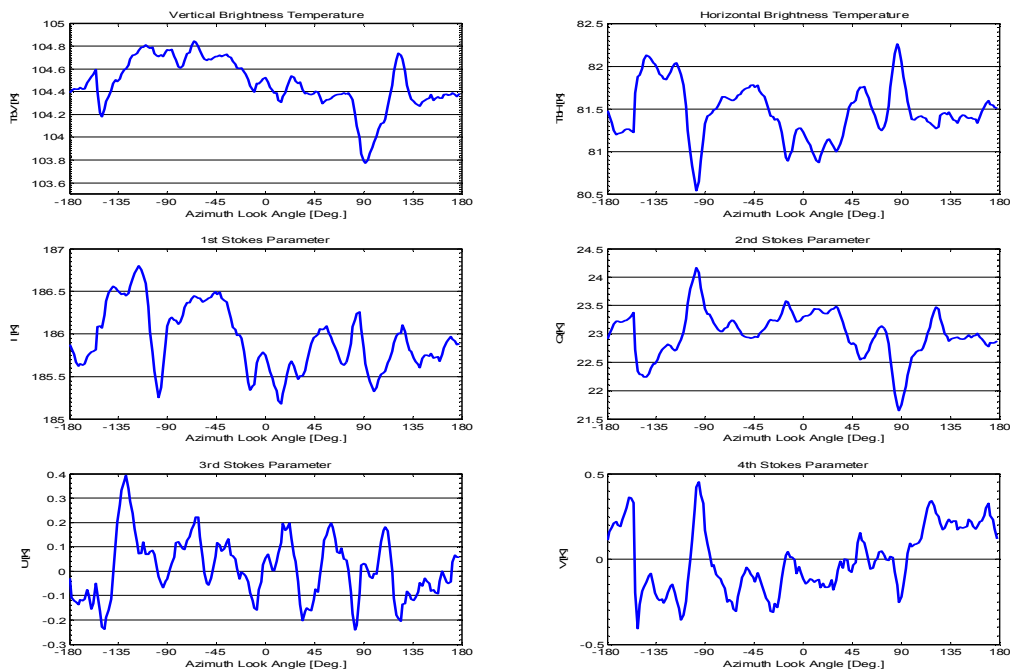
Figure 5.2. The Stokes parameters from the 1st circle flight track with 20° incidence angle from the March 15th 2001 flight.
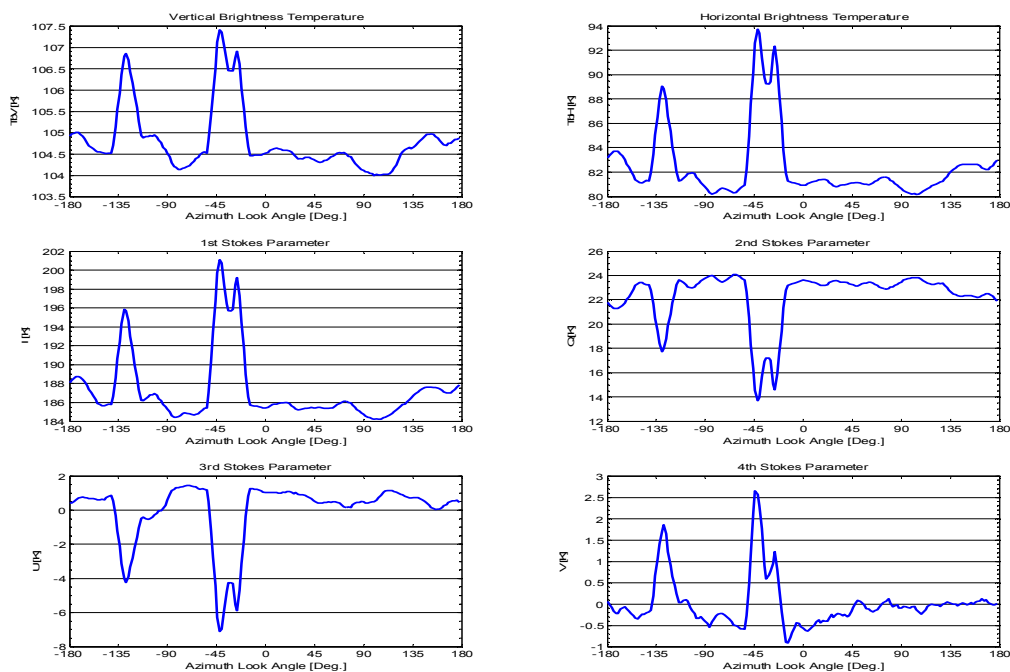

Figure 5.3. The Stokes parameters from the 2nd circle flight track with 20° incidence angle from the March 15th 2001 flight.
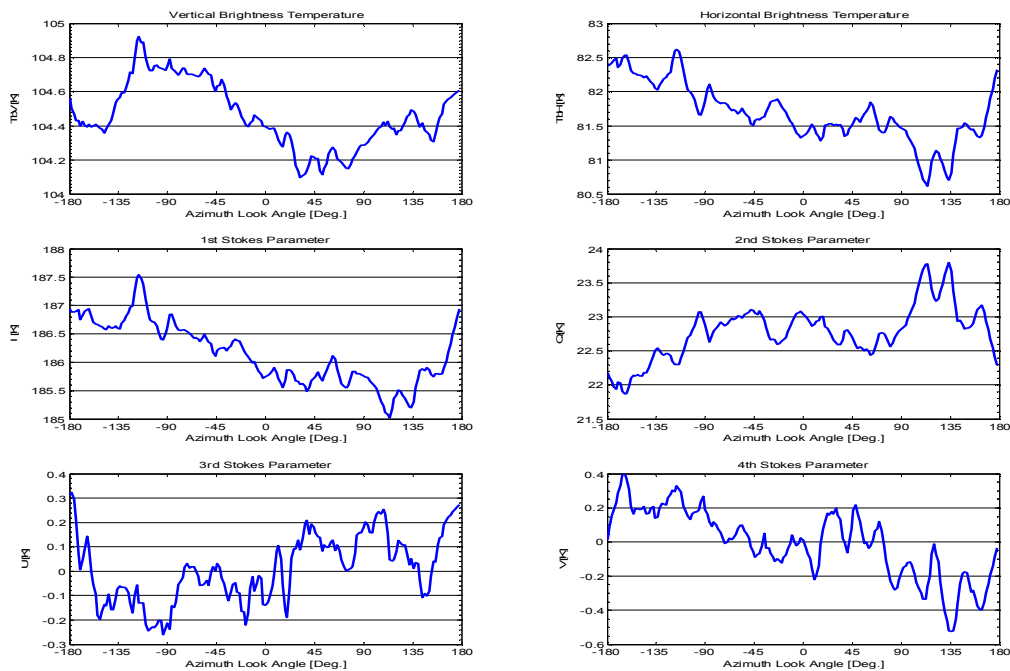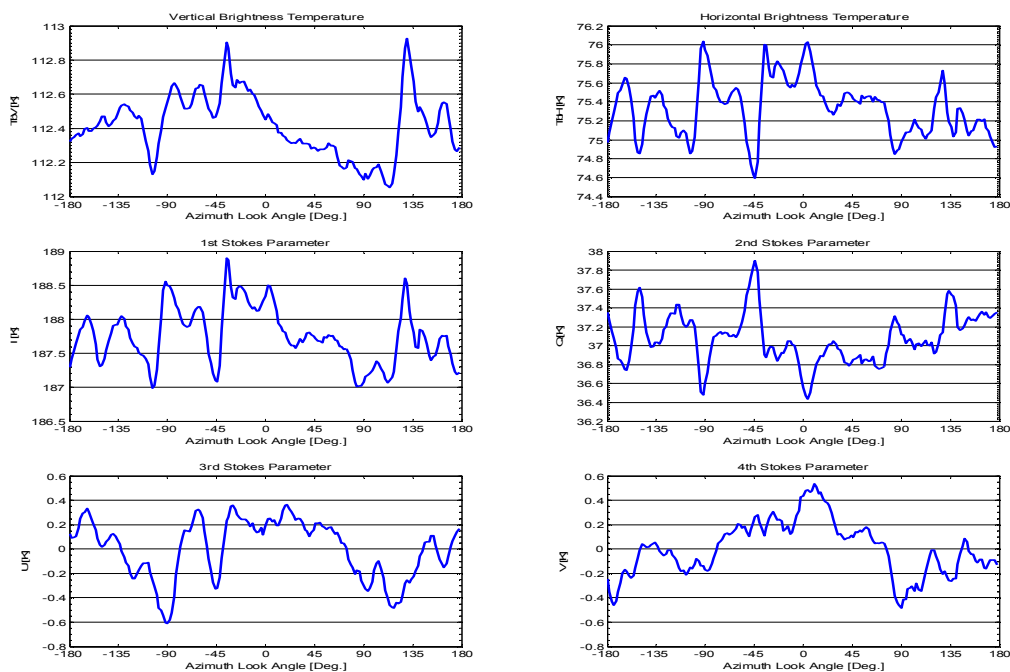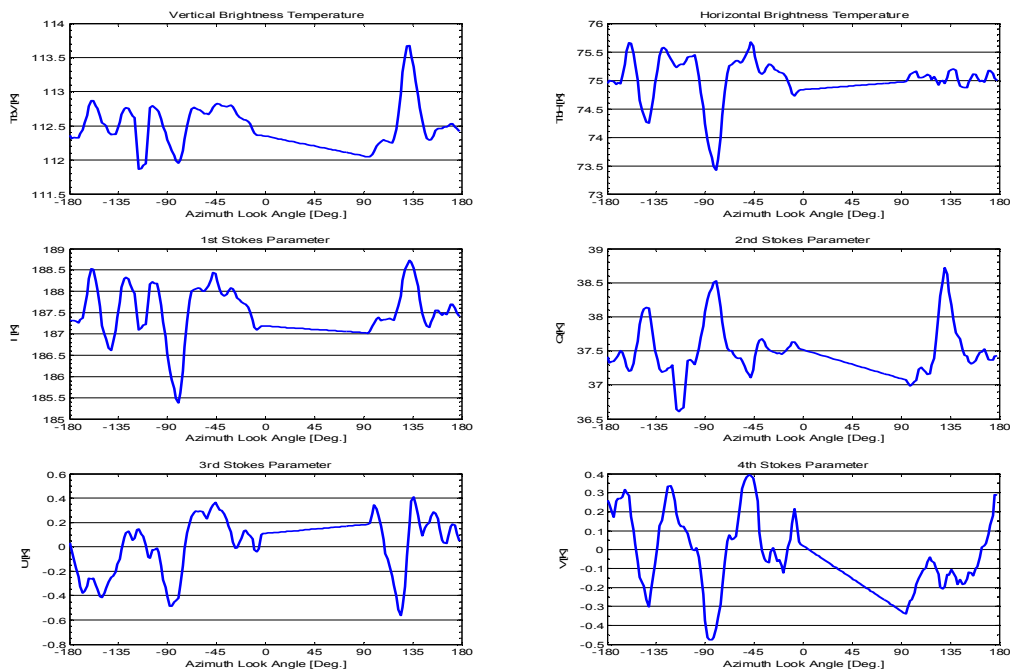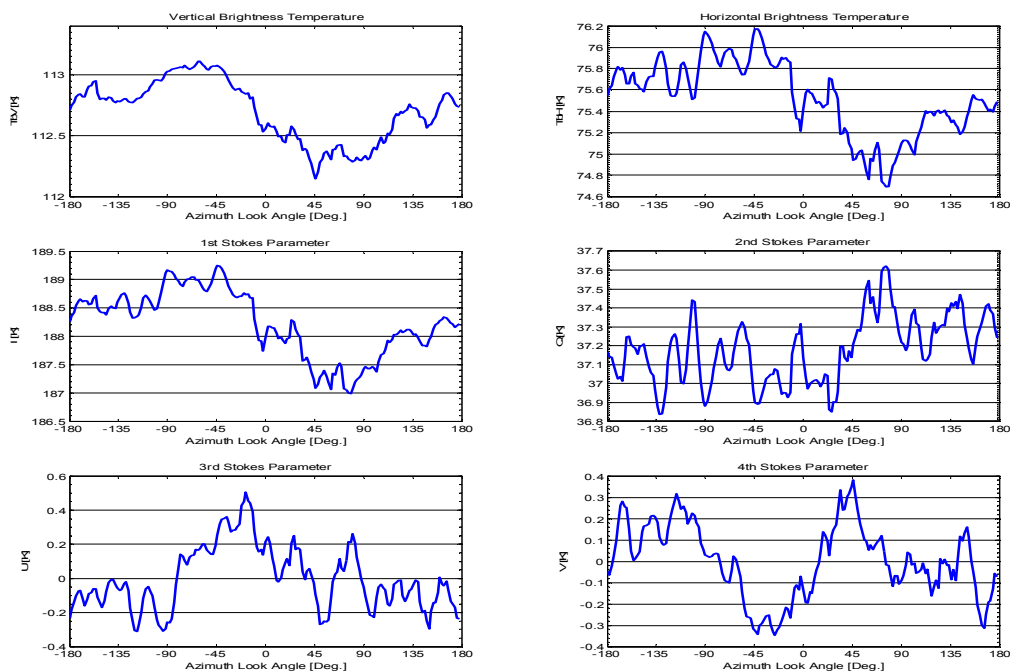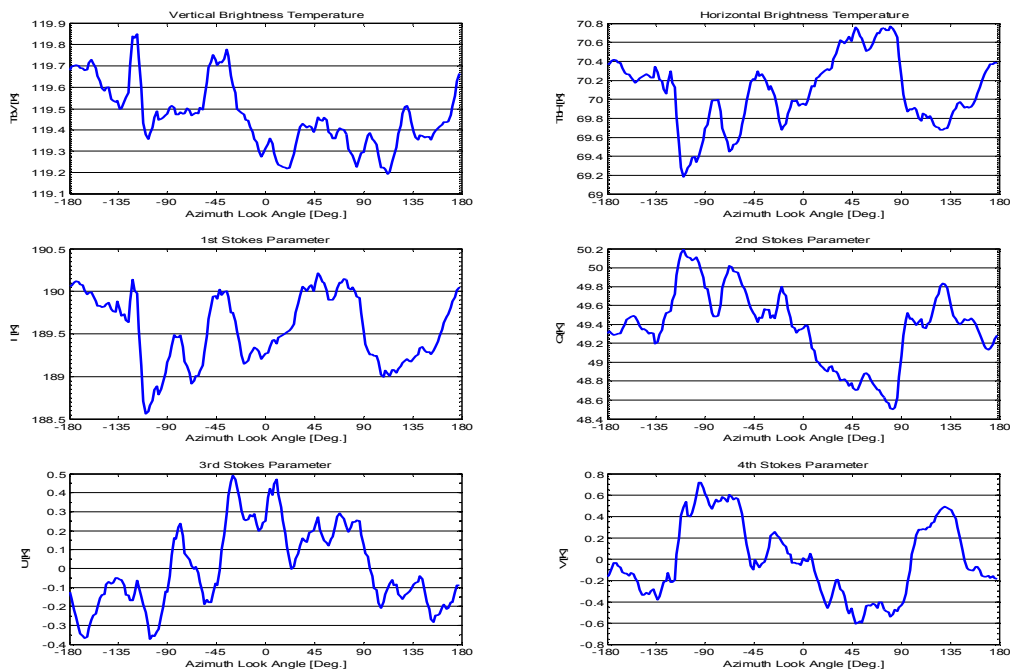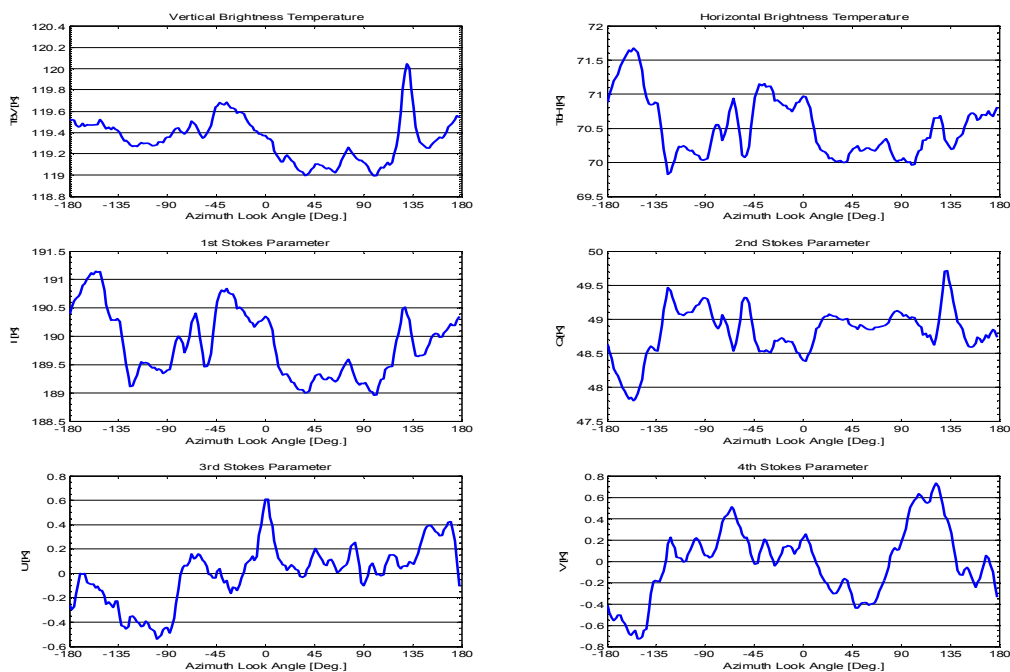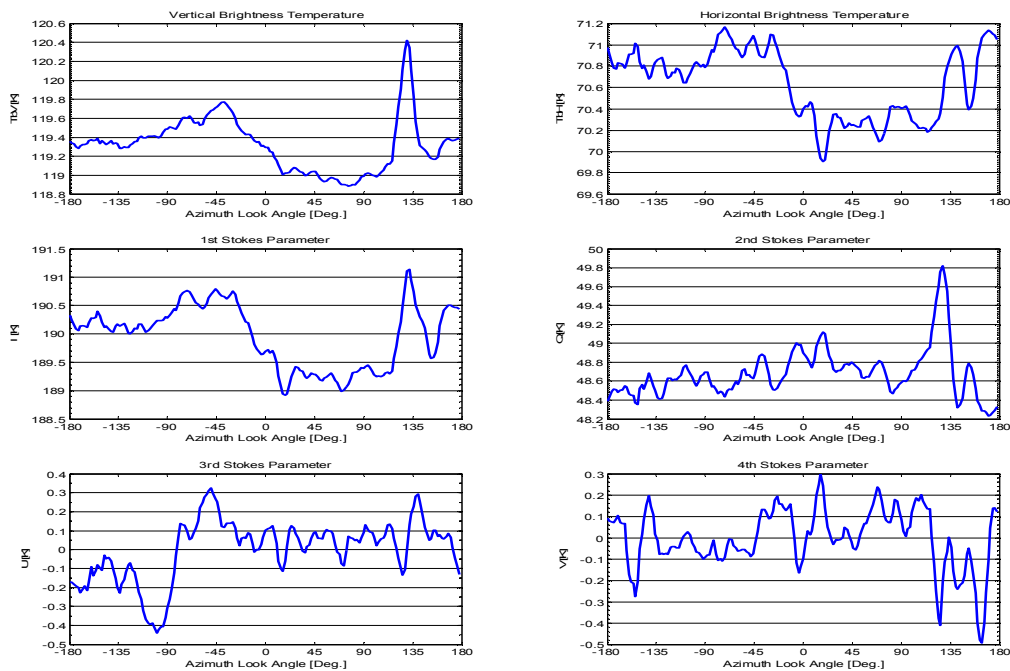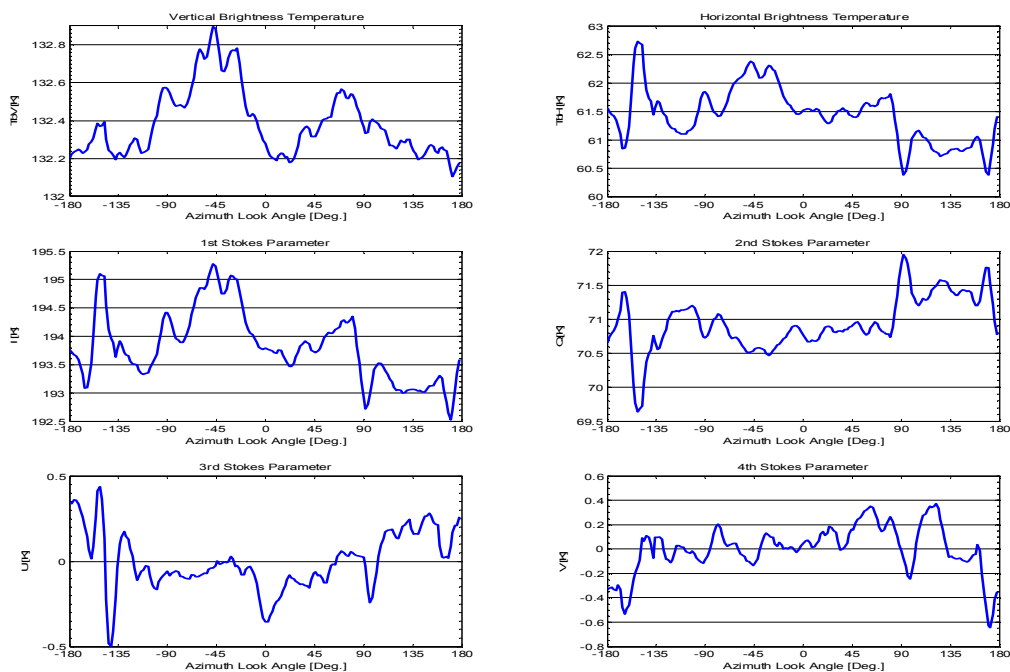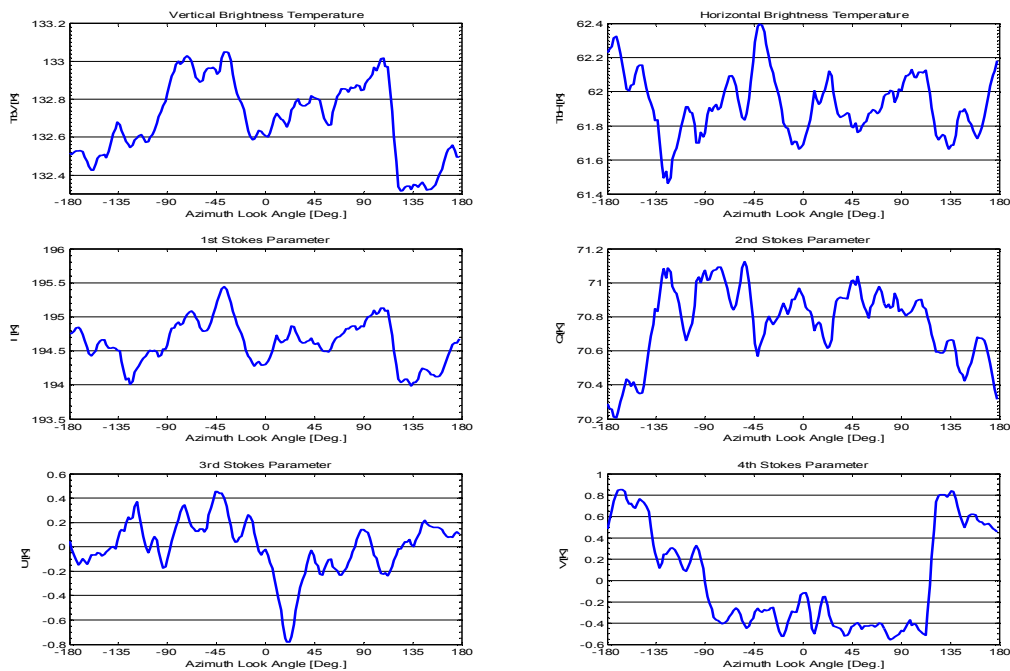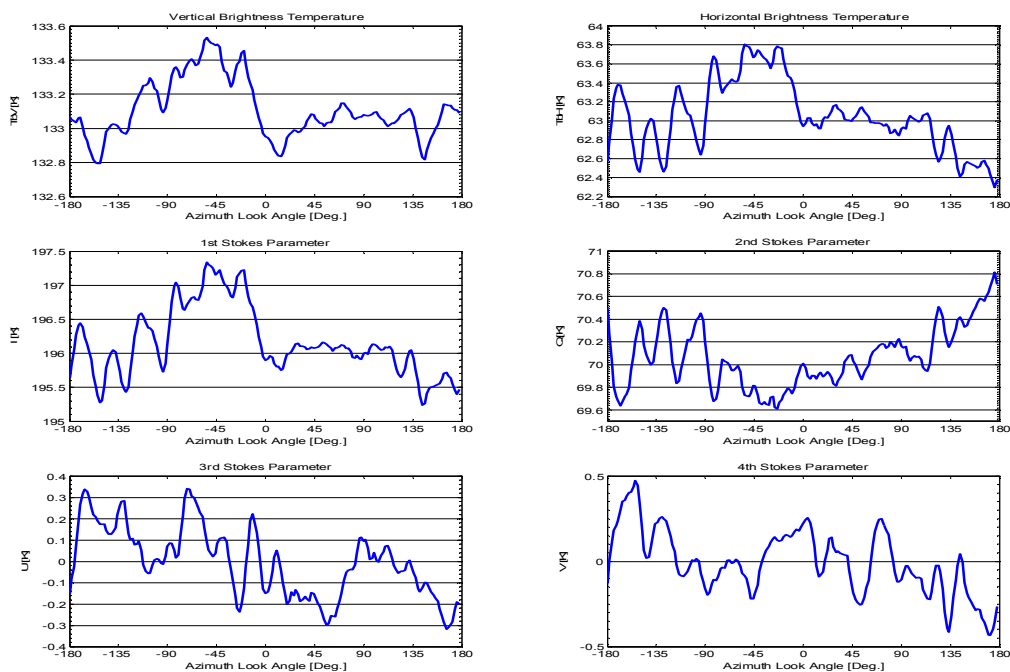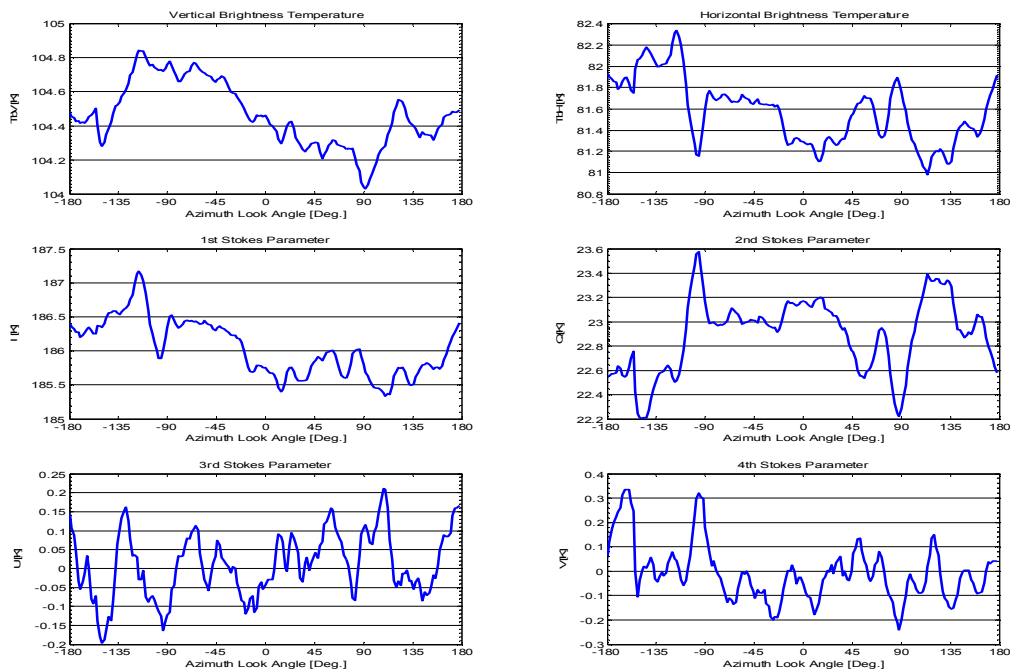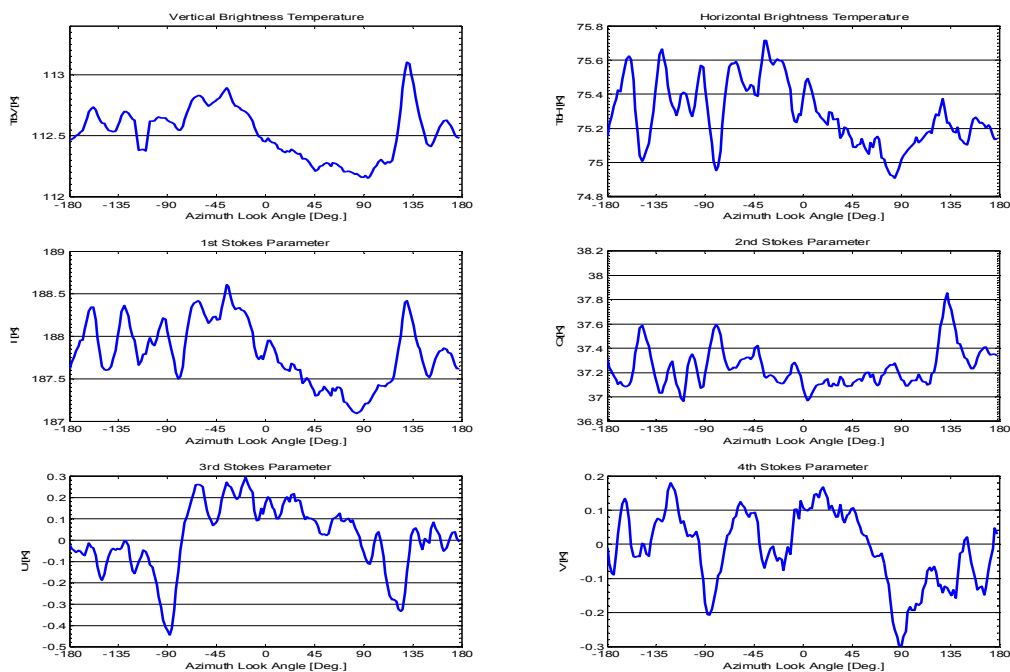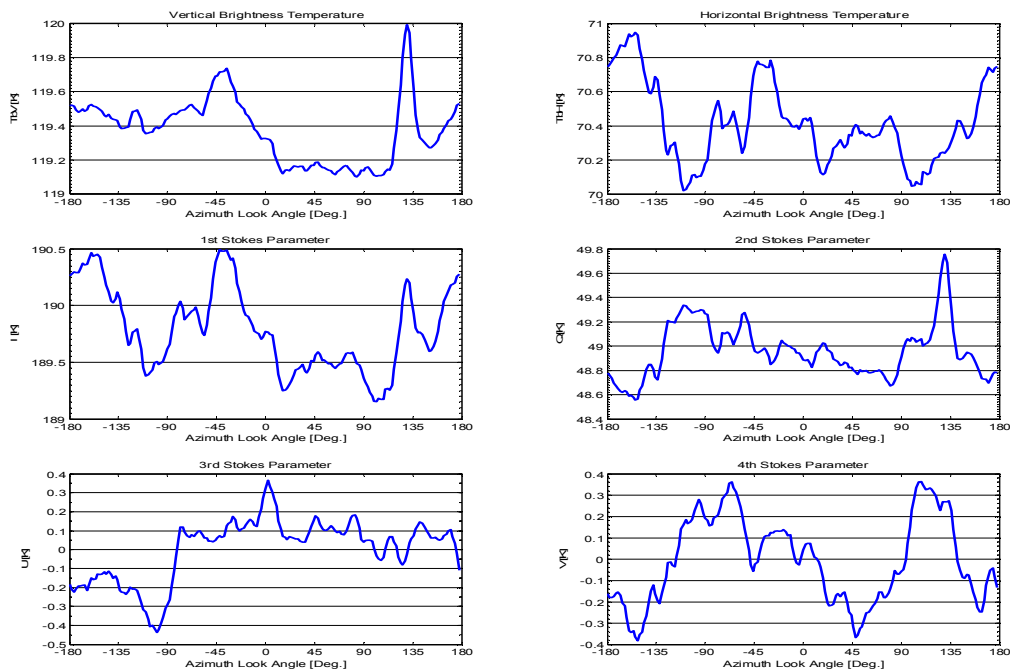
Figure 5.4. The Stokes parameters from the 3rd circle flight track with 20° incidence angle from the March 15th 2001 flight.
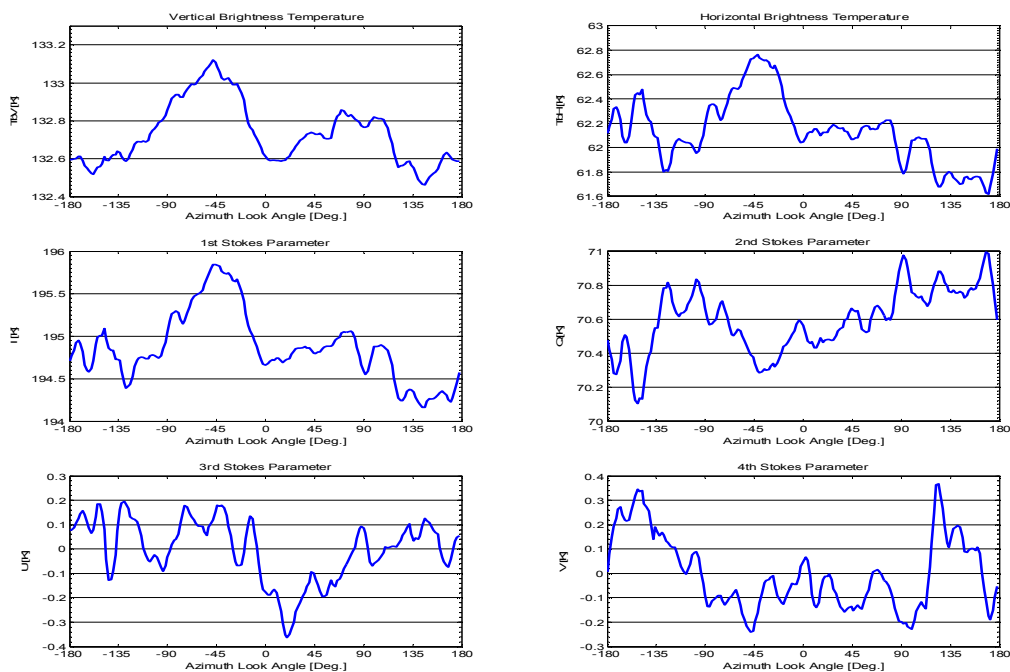

Figure 5.5. The Stokes parameters from the 1st circle flight track with 35° incidence angle from the March 15th 2001 flight.

Figure 5.6. The Stokes parameters from the 2nd circle flight track with 35° incidence angle from the March 15th 2001 flight.

Figure 5.7. The Stokes parameters from the 3rd circle flight track with 35° incidence angle from the March 15th 2001 flight.

Figure 5.8. The Stokes parameters from the 1st circle flight track with 42° incidence angle from the March 15th 2001 flight.

Figure 5.9. The Stokes parameters from the 2nd circle flight track with 42° incidence angle from the March 15th 2001 flight.

Figure 5.10. The Stokes parameters from the 3rd circle flight track with 42° incidence angle from the March 15th 2001 flight.

Figure 5.11. The Stokes parameters from the 1st circle flight track with 52° incidence angle from the March 15th 2001 flight.

Figure 5.12. The Stokes parameters from the 2nd circle flight track with 52° incidence angle from the March 15th 2001 flight.

Figure 5.13. The Stokes parameters from the 3rd circle flight track with 52° incidence angle from the March 15th 2001 flight.

Figure 5.14. The averaged Stokes parameters from the 1st and 3rd circle flight tracks with 20° incidence angle from the March 15th 2001 flight. The 2nd track is left out due to heavy interference.

Figure 5.15. The averaged Stokes parameters from the three circle flight tracks with 35° incidence angle from the March 15th 2001 flight.

Figure 5.16. The averaged Stokes parameters from the three circle flight tracks with 42° incidence angle from the March 15th 2001 flight.

Figure 5.17. The averaged Stokes parameters from the three circle flight tracks with 52° incidence angle from the March 15th 2001 flight.

results are observed for 52° incidence. The phases for the vertical and horizontal polarizations tend to agree within 50°, around 90°, but this does not agree with the wind direction, which from figure 5.1 is found to be approximately 240°.

Inc.	Harm.	TV, M.	TV, Ph.	TH, M.	TH, Ph.	U, Mag.	U, Ph.	V, Mag.	V, Ph.
20°	1	0.23	90.29	0.27	122.50	0.04	-86.65	0.07	150.71
	2	0.07	125.16	0.17	-98.59	0.01	-169.43	0.06	-85.83
	3	0.05	-73.78	0.19	128.66	0.03	179.33	0.03	-140.22
	4	0.03	138.90	0.08	132.01	0.01	-85.41	0.03	-42.99
35°	1	0.19	102.49	0.17	75.34	0.14	-6.13	0.07	50.18
	2	0.16	67.76	0.09	35.09	0.09	12.02	0.08	-44.41
	3	0.02	0.31	0.05	45.83	0.06	146.44	0.03	-77.35
	4	0.09	-173.43	0.04	179.33	0.04	140.81	0.05	-166.46
42°	1	0.16	111.42	0.12	132.74	0.17	-41.21	0.07	56.83
	2	0.13	68.19	0.19	-0.19	0.10	50.60	0.22	124.05
	3	0.03	102.05	0.21	138.58	0.03	163.63	0.11	-16.07
	4	0.07	-178.22	0.02	-178.09	0.01	167.06	0.07	-44.22
52°	1	0.15	31.25	0.28	40.37	0.11	139.78	0.13	169.70
	2	0.13	143.30	0.03	76.68	0.08	107.95	0.07	-33.80
	3	0.10	143.28	0.21	127.29	0.06	108.59	0.06	10.00
	4	0.01	136.15	0.08	-129.67	0.02	157.46	0.05	-166.06
35°, 45° and 52°	1	0.14	85.91	0.16	68.41	0.06	-17.25	0.05	107.25
	2	0.12	89.18	0.09	17.29	0.07	51.94	0.03	96.63
	3	0.04	127.87	0.14	125.83	0.05	135.36	0.06	-14.80
	4	0.06	-177.01	0.04	-152.59	0.03	150.14	0.03	-124.90

Table 5.1. 1st, 2nd, 3rd, and 4th harmonic components in the averaged modified Stokes parameters from the circle flights from March 15th 2001.

For the 3rd and 4th Stokes parameters, no systematic signal seems to be present, and the phases cover a large range of look directions. Some modulation might be expected with the changing incidence angle, but no systematic variation can be identified. The magnitudes for these three parameters are between 10 mK and 200 mK, typically, and generally the 1st harmonic tends to be dominant.

Noise and eventually some very small drifts may influence the results below 100 mK, and as the meteorological situation was a very low wind case with changing wind direction, the results may reflect these conditions. A 1st to 4th harmonic analysis of an average from all circles from 35° to 52° incidence angles, ignoring the changing angle, provides the last row in the table, reducing the magnitude of the signature further.

Using [5] and applying the wind direction $\psi = 240°$, the expected phases will be $\theta = +120°$ and $\theta = -120°$ for the 1st and 2nd harmonics of the 2nd Stokes parameter, $\theta = -150°$ and $\theta = -30°$ for the harmonics of the 3rd Stokes parameter, and $\theta = +150°$ for the 2nd harmonic of the 4th. No clear indication points to a result of this kind, however, and no alternative signature may be identified.

6. Results from the March 23rd 2001 flight

The 2nd scientific flight took place over the Kattegat target area due to icing conditions over the North Sea target site. The meteorological data is again a standard data set from The Danish Meteorological Institute, DMI, recorded at the island Anholt, and it is shown in figure 6.1. The data shows a slightly higher wind, and no changes right before the flight.

Five incidence angles were covered during this flight. All incidence angles, except 62° which needs about 15 minutes for a full circle, were measured three times, and the corrected data can be seen in the figures 6.2 to 6.15. The absolute calibration problem due to the missing observation of the calibration load and the noise diode was present also on this fight, and the absolute level may thus deviate several Kelvin from the expected level. As for the March 15th flight, however, the problem does not influence on the radiometer stability, and the azimuth signatures will be useable for analysis with respect to the wind direction.
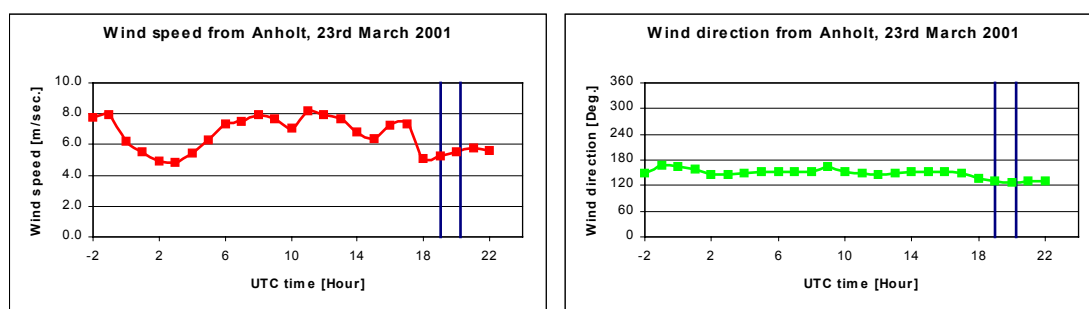
Figure 6.1. Wind speed and wind direction for March 23rd 2001, measured at the island Anholt in Kattegat. The blue lines indicate the flight time.

The basic large peak to peak variation, observed on the previous flight, is repeated in the March 23rd data, but the angular size of the peaks seems to be more varying. The two signatures with 62° incidence angle, figure 6.14 and 6.15, were recorded with only 5° roll, and the acquisition time was long compared to the circles with lower incidence angles. The sample density is thus larger, and it is noticed, that some peaks are shorter than the antenna beam width, excluding point targets at first view. Due to the low roll angle, however, the circle radius is about 6.5 km, and as the distance to the footprint is only 2.1 km from the flight track for the 1000 m flight altitude, point targets are flown by in a fraction of the circle, only equal to 4.9°. Point targets will thus appear as objects down to the size of 4.9°, still possibly able to explain some of the small peaks in the two circles.

Variations of the sea surface may be another origin for the peaks observed, and as for the March 15th flight, averaging of circles with equal incidence angle is applied to reduce the noise. The averaged circles are shown in figures 6.16 to 6.20, and generally it is noticed, that the small peaks reduce again, but the overall variations are seen to be larger than for the March 15th flight. An analysis of the 1st to 4th harmonic components is carried out and presented in table 6.1. The results confirm the larger signals, and some magnitudes for the horizontal polarization are larger than 500 mK. The behavior in magnitude is not systematic, however, and no natural function of the incidence angle is observed. Most phases are again distributed over the azimuth angles, and the random nature from the low wind case on March 15th is repeated.
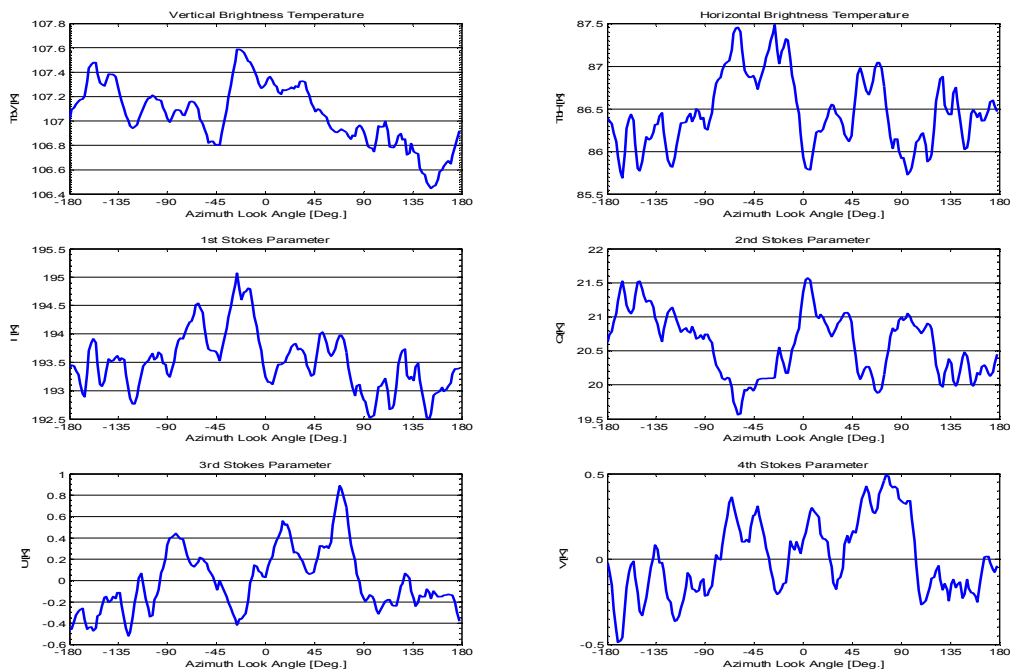
Figure 6.2. The Stokes parameters from the 1ˢᵗ circle flight track with 20° incidence angle from the March 23ʳᵈ 2001 flight.
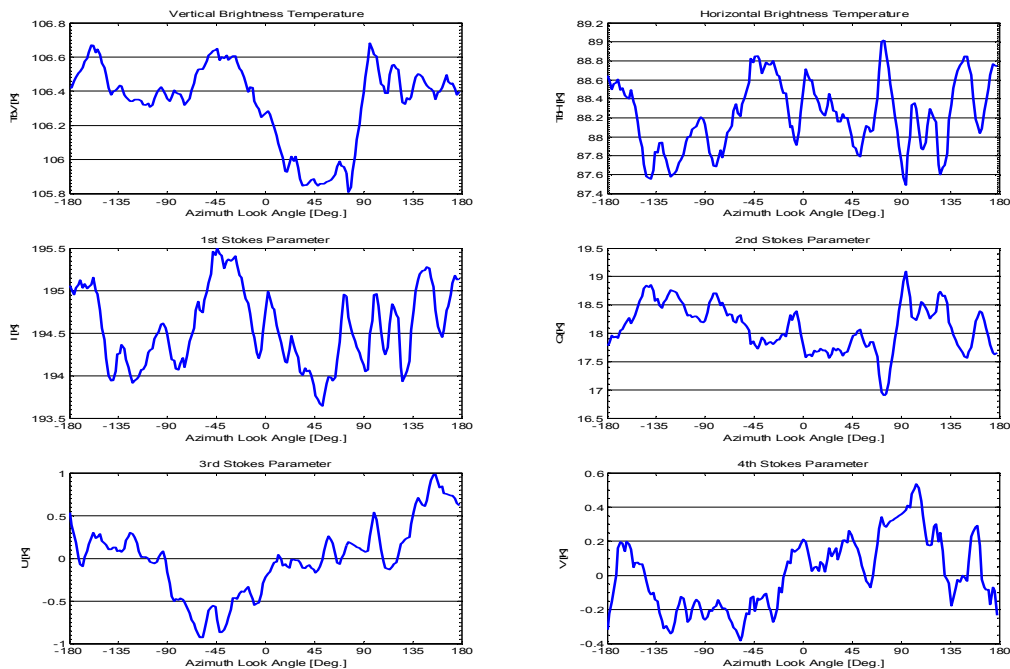

Figure 6.3. The Stokes parameters from the 2ⁿᵈ circle flight track with 20° incidence angle from the March 23ʳᵈ 2001 flight.
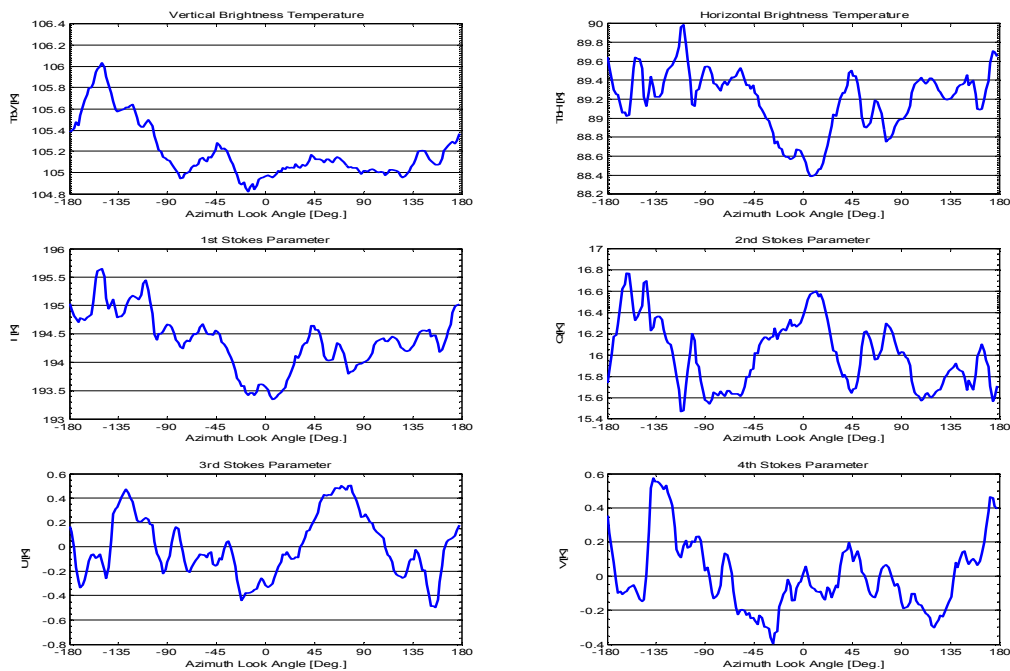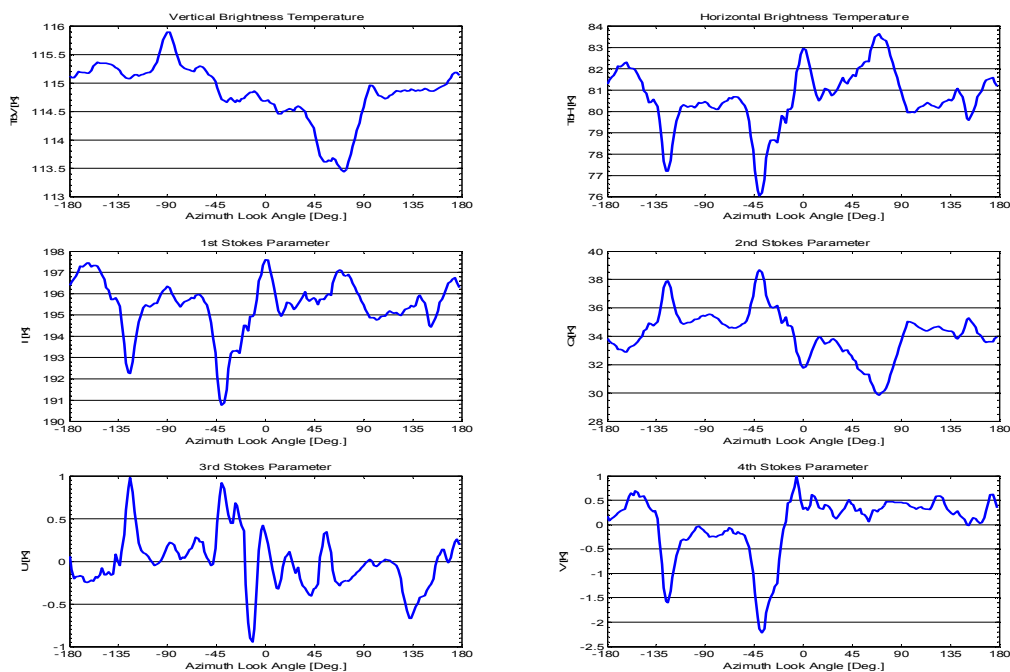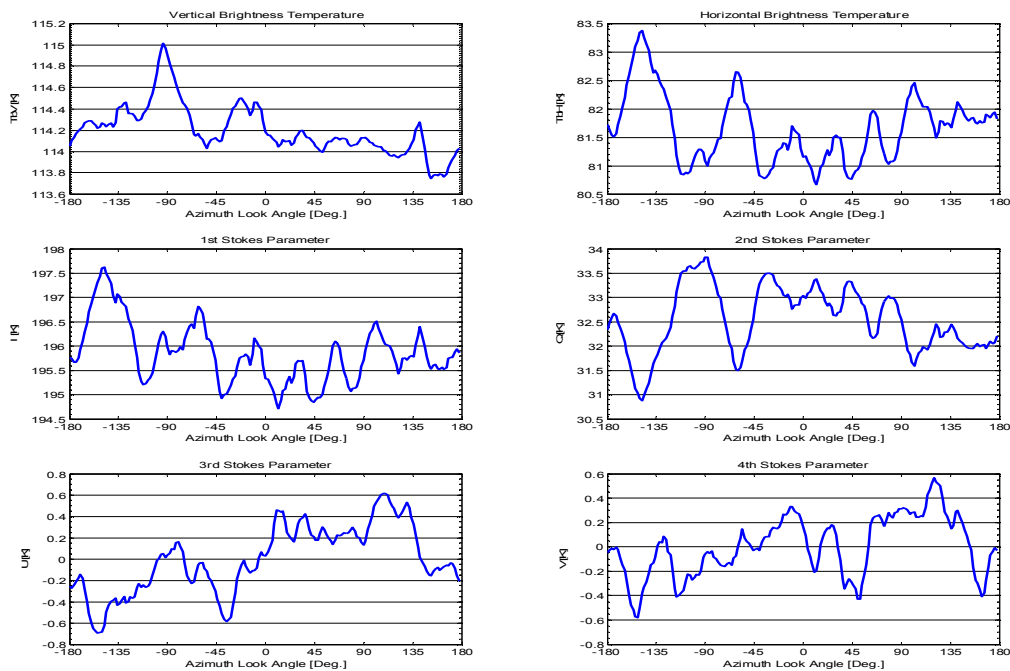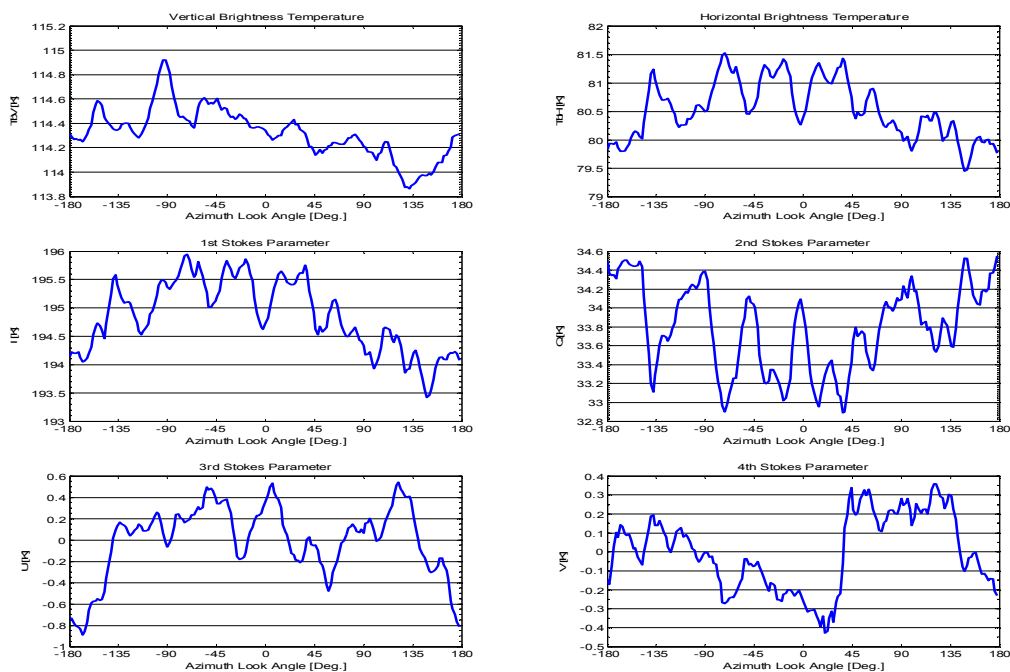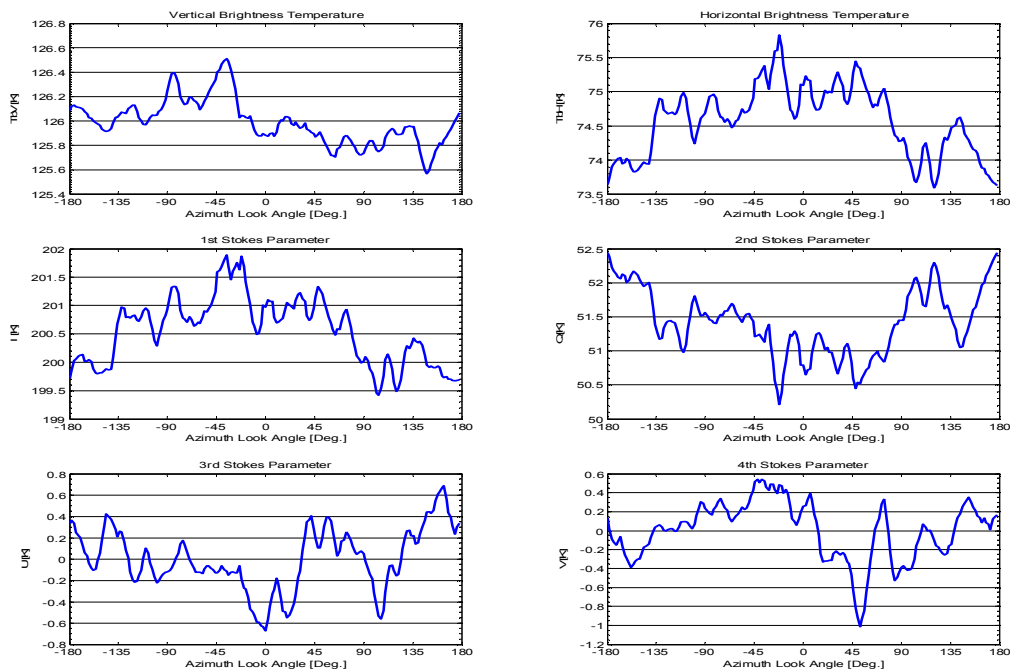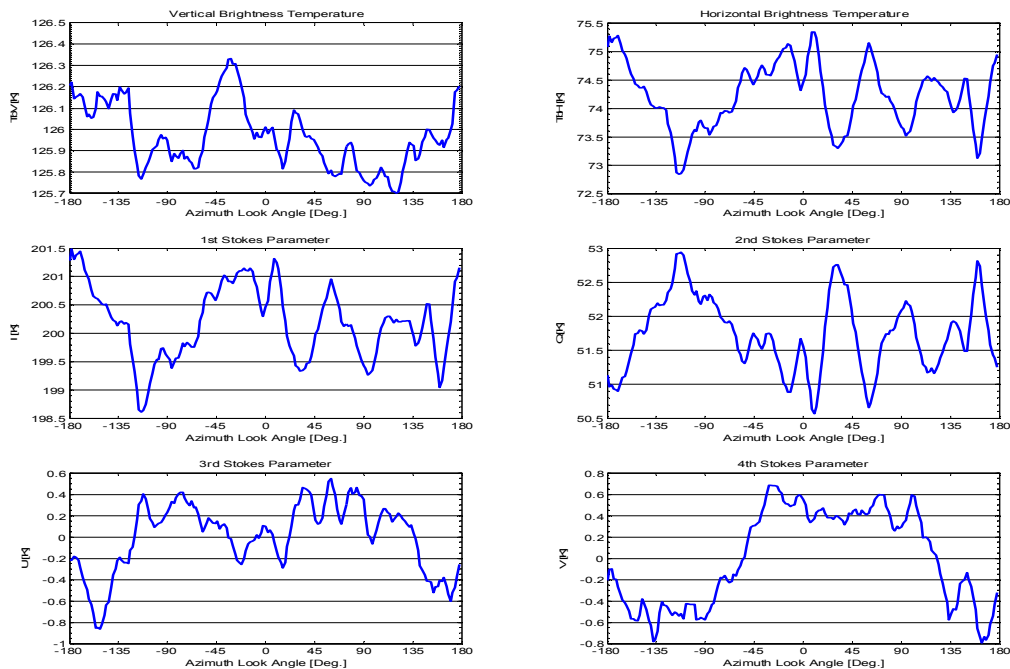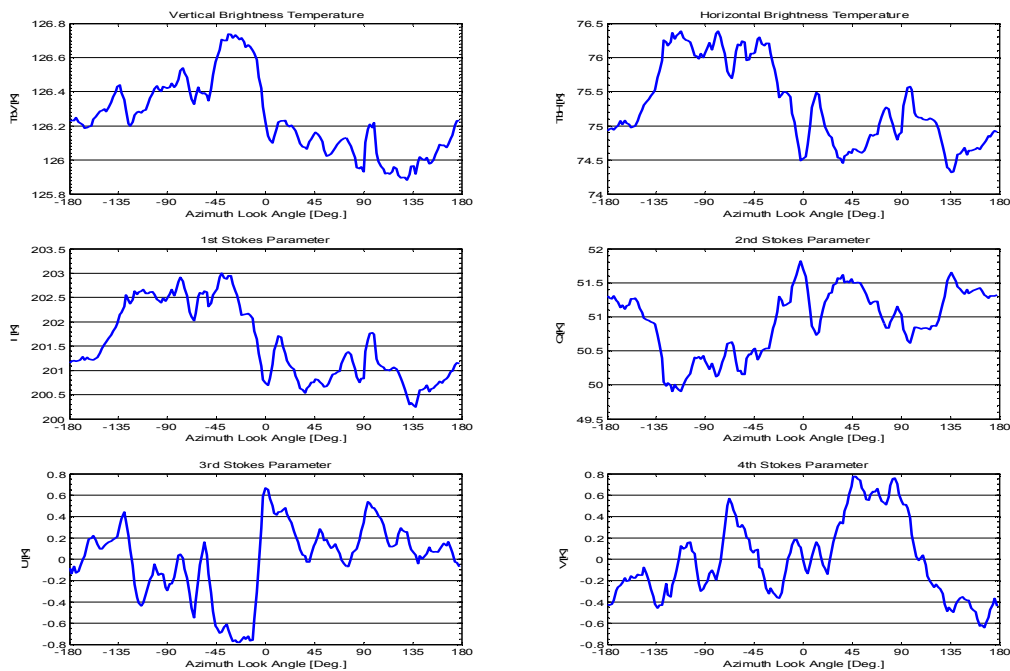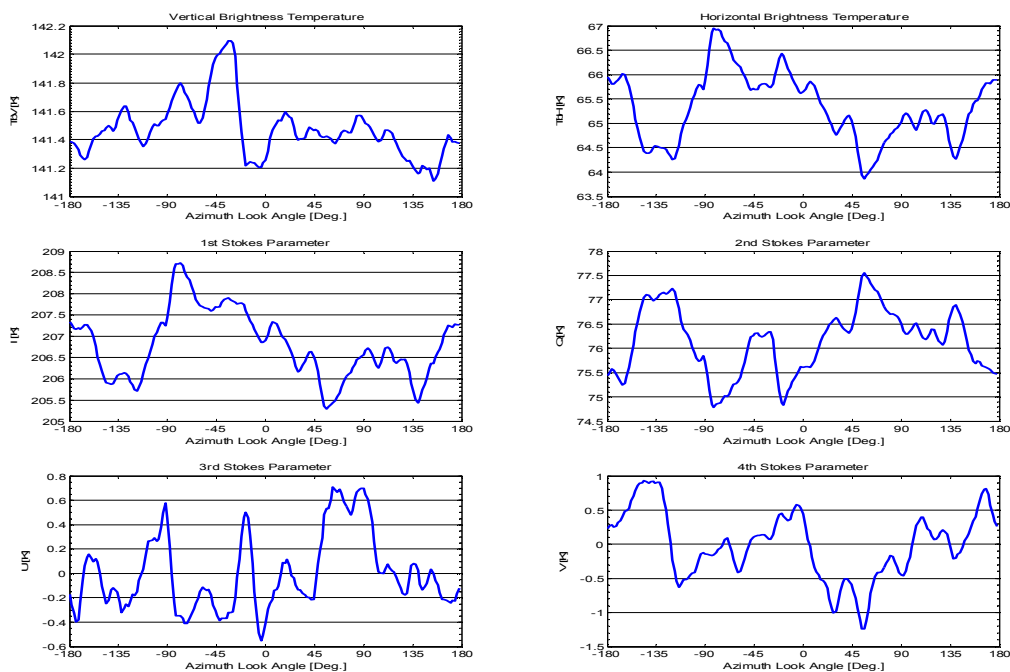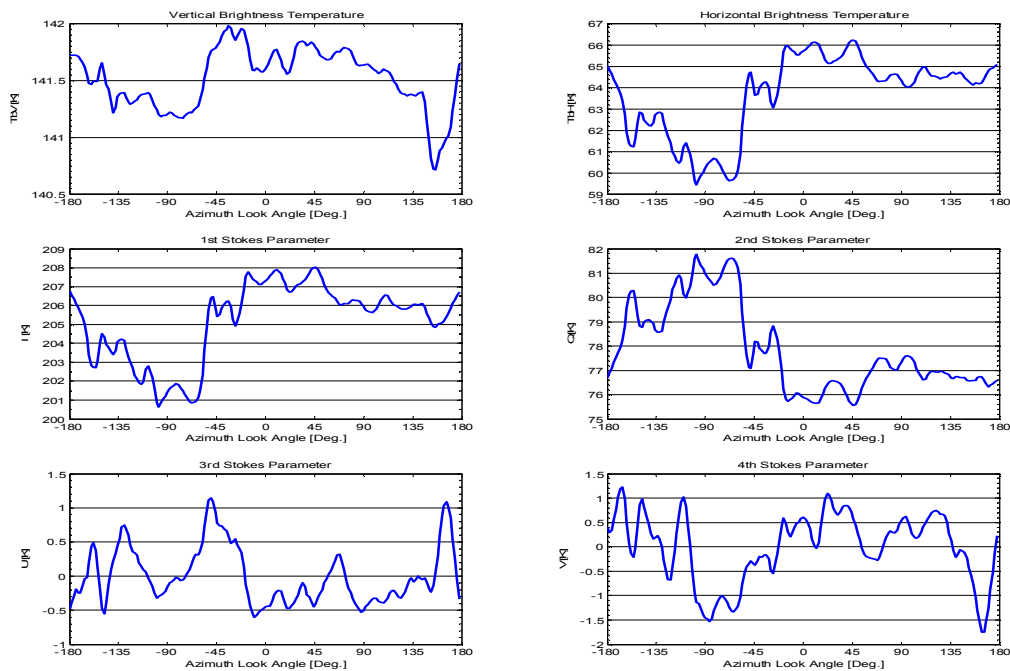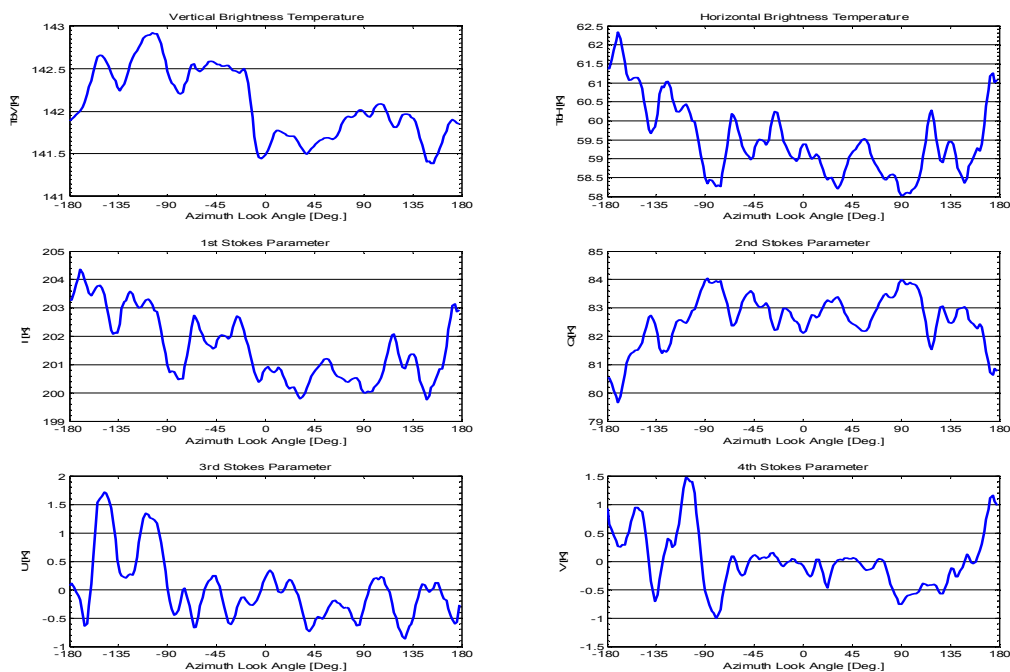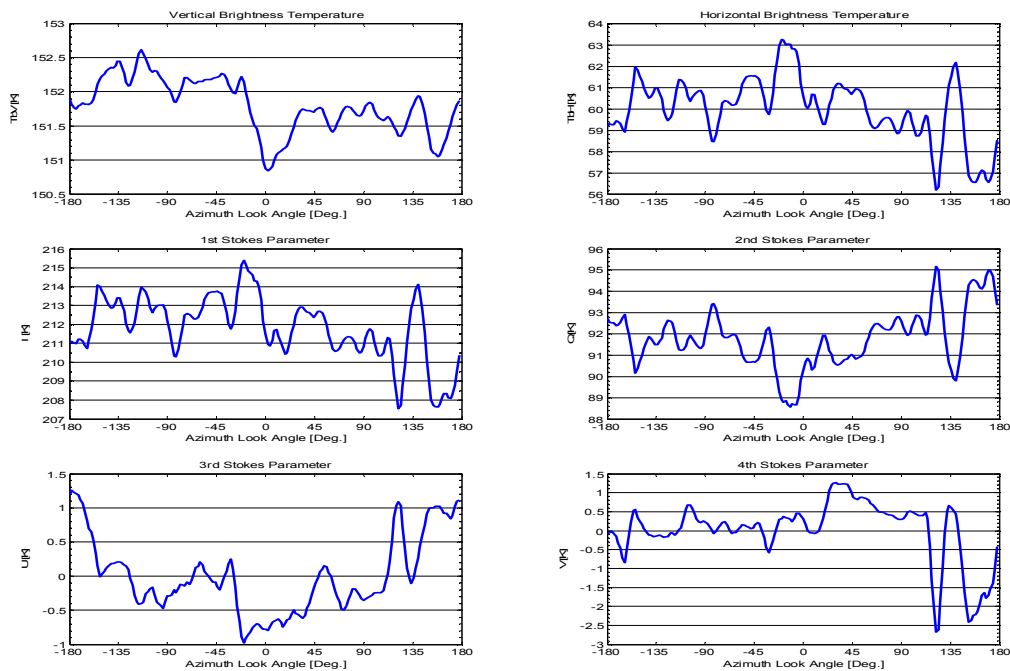
Figure 6.4. The Stokes parameters from the 3rd circle flight track with 20° incidence angle from the March 23rd 2001 flight.

Figure 6.5. The Stokes parameters from the 1st circle flight track with 35° incidence angle from the March 23rd 2001 flight.

Figure 6.6. The Stokes parameters from the 2ⁿᵈ circle flight track with 35° incidence angle from the March 23ʳᵈ 2001 flight.

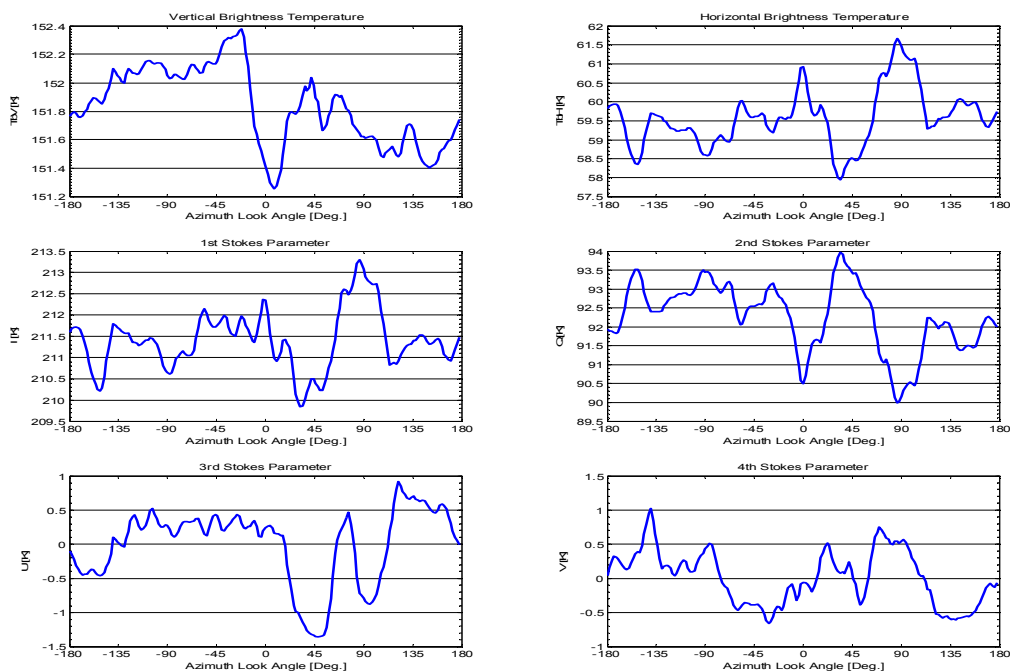*Figure 6.7. The Stokes parameters from the 3ʳᵈ circle flight track with 35° incidence angle from the March 23ʳᵈ 2001 flight.*
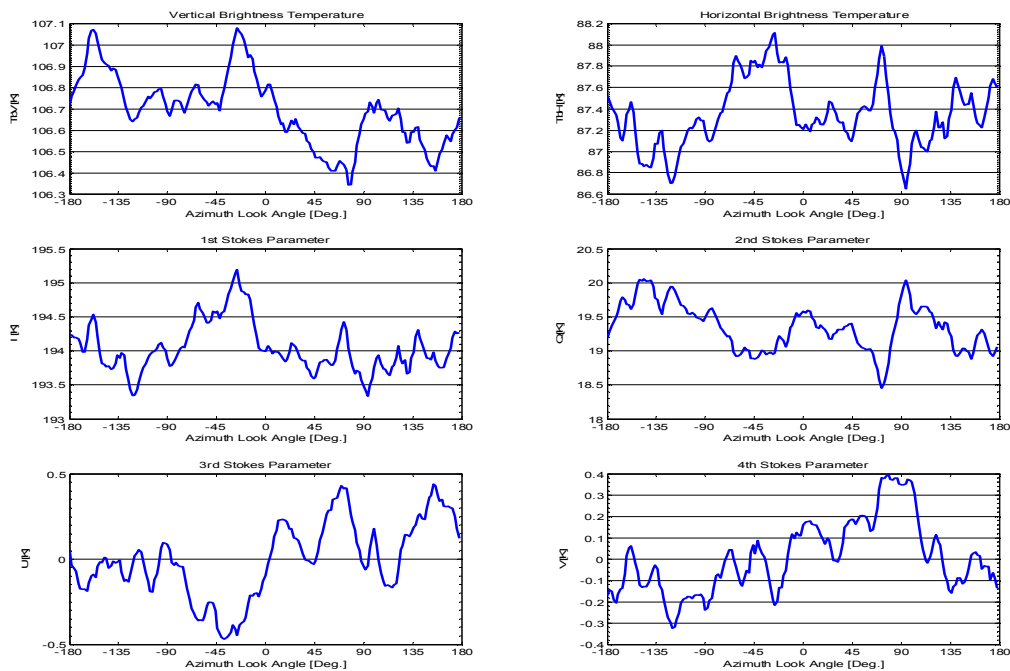
Figure 6.8. The Stokes parameters from the 1ˢᵗ circle flight track with 47° incidence angle from the March 23ʳᵈ 2001 flight.

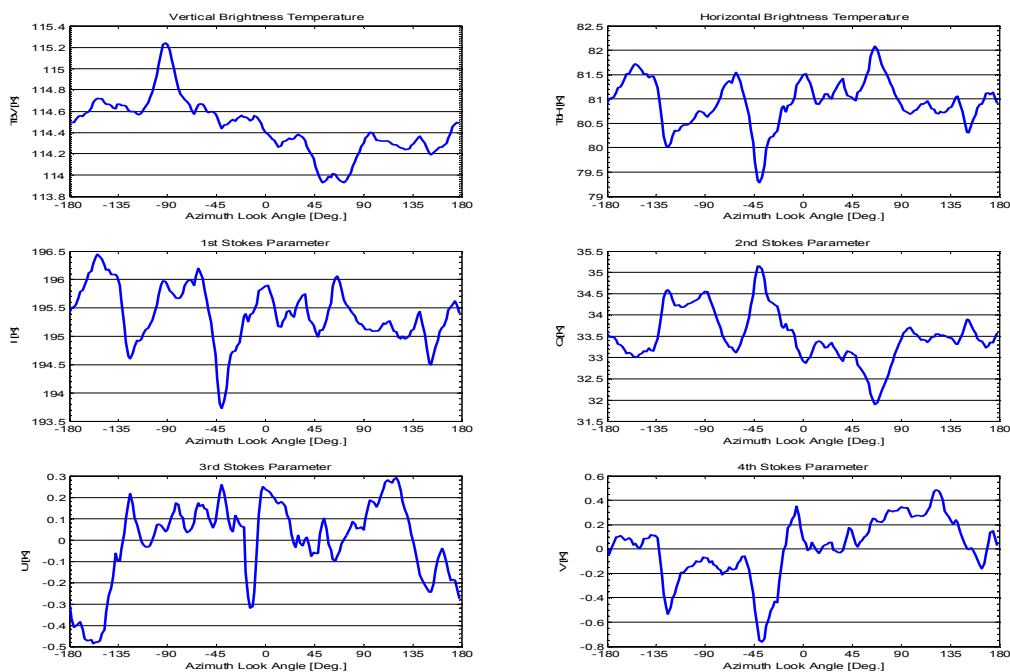*Figure 6.9. The Stokes parameters from the 2ⁿᵈ circle flight track with 47° incidence angle from the March 23ʳᵈ 2001 flight.*

Figure 6.10. The Stokes parameters from the 3rd circle flight track with 47° incidence angle from the March 23rd 2001 flight.

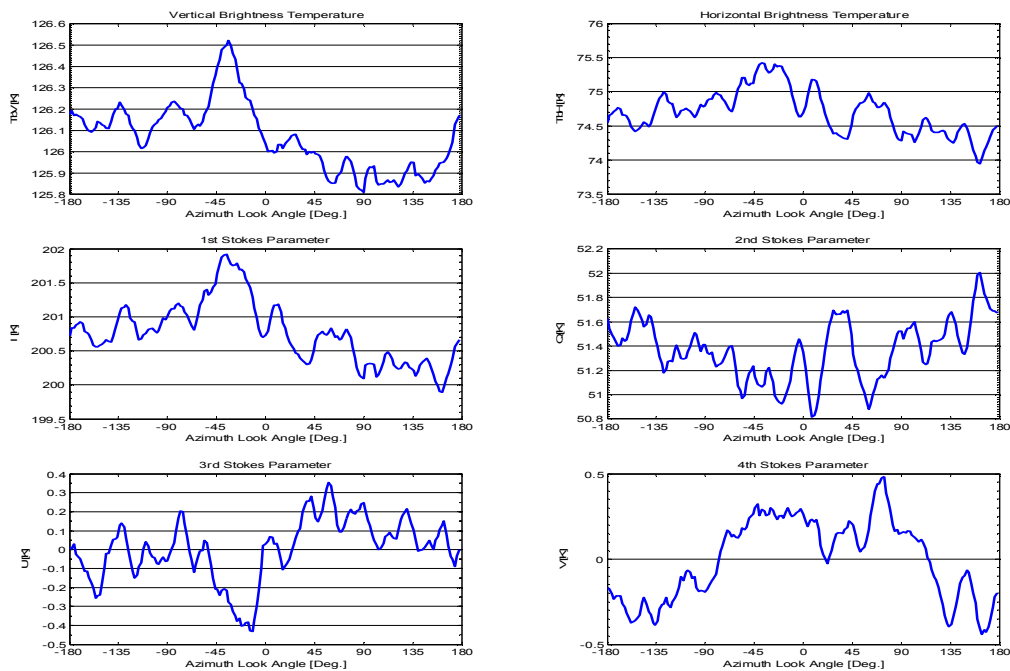*Figure 6.11. The Stokes parameters from the 1st circle flight track with 57° incidence angle from the March 23rd 2001 flight.*

Figure 6.12. The Stokes parameters from the 2ⁿᵈ circle flight track with 57° incidence angle from the March 23ʳᵈ 2001 flight.

Figure 6.13. The Stokes parameters from the 3ʳᵈ circle flight track with 57° incidence angle from the March 23ʳᵈ 2001 flight.

Figure 6.14. The Stokes parameters from the 1st circle flight track with 62° incidence angle from the March 23rd 2001 flight.

Figure 6.15. The Stokes parameters from the 2nd circle flight track with 62° incidence angle from the March 23rd 2001 flight.
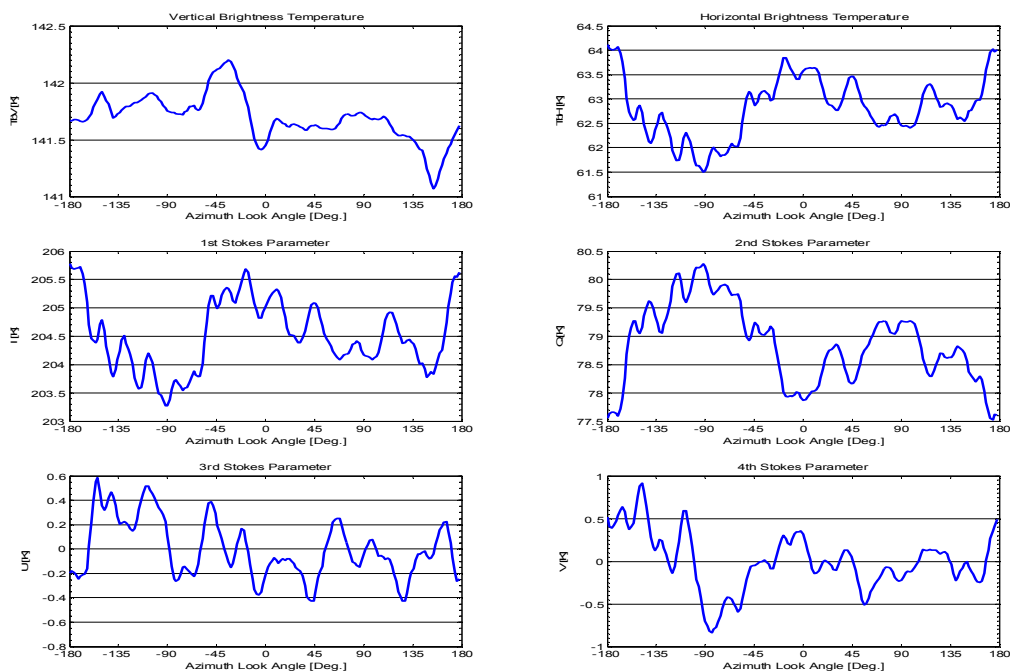
Figure 6.16. The averaged Stokes parameters from the 1st and 2nd circle flight tracks with 20° incidence angle from the March 23rd 2001 flight. The 3rd track is left out due to heavy interference.

Figure 6.17. The averaged Stokes parameters from the three circle flight tracks with 35° incidence angle from the March 23rd 2001 flight.

Figure 6.18. The averaged Stokes parameters from the three circle flight tracks with 47° incidence angle from the March 23rd 2001 flight.

Figure 6.19. The averaged Stokes parameters from the three circle flight tracks with 57° incidence angle from the March 23rd 2001 flight.
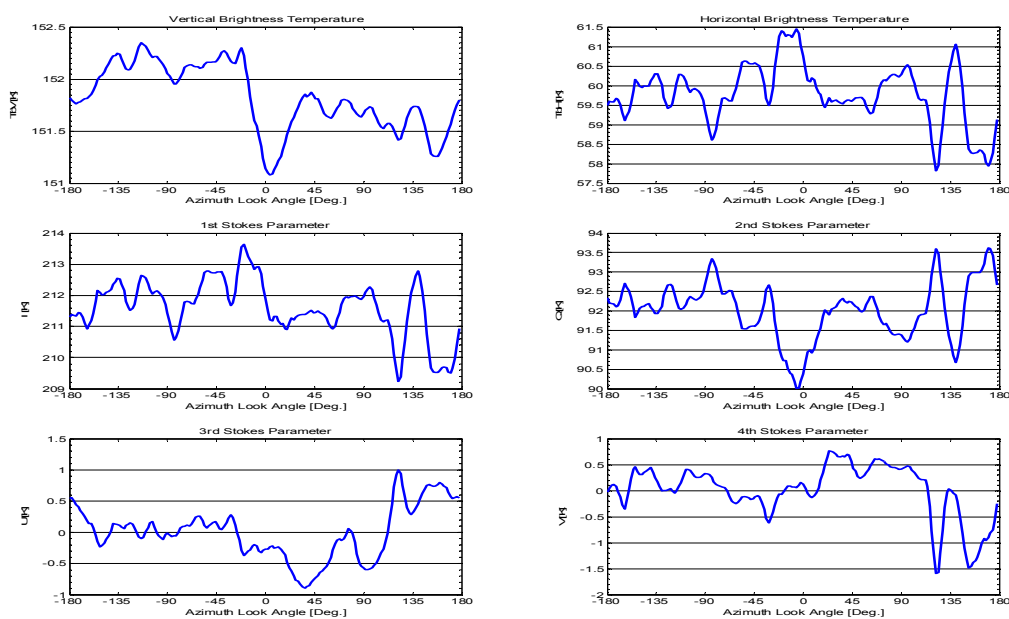
Figure 6.20. The averaged Stokes parameters from the two circle flight tracks with 62° incidence angle from the March 23rd 2001 flight.

Inc.	Harm.	TV, M.	TV, Ph.	TH, M.	TH, Ph.	U, Mag.	U, Ph.	V, Mag.	V, Ph.
20°	1	0.14	87.49	0.17	12.51	0.20	-117.97	0.19	-62.26
	2	0.07	16.03	0.23	63.10	0.09	-91.01	0.05	-151.59
	3	0.13	64.17	0.19	171.36	0.14	-100.34	0.07	121.32
	4	0.07	-68.03	0.12	115.59	0.08	60.50	0.05	-25.51
35°	1	0.32	99.78	0.19	-95.26	0.14	-10.24	0.26	-105.83
	2	0.04	149.83	0.29	-79.25	0.15	149.02	0.04	-142.99
	3	0.06	-14.93	0.20	175.04	0.10	-19.41	0.05	4.95
	4	0.11	-41.40	0.24	-61.51	0.02	-117.14	0.12	-48.35
47°	1	0.19	71.03	0.36	40.45	0.13	-104.62	0.29	-14.75
	2	0.06	26.11	0.05	86.14	0.12	-147.71	0.06	145.06
	3	0.07	116.89	0.14	98.03	0.09	-118.75	0.09	118.04
	4	0.02	149.28	0.08	116.80	0.03	-127.07	0.04	48.62
57°	1	0.18	60.22	0.32	-74.86	0.16	121.24	0.16	178.79
	2	0.08	-173.40	0.68	7.57	0.11	-126.00	0.28	-26.48
	3	0.15	96.51	0.16	111.48	0.08	80.25	0.23	53.61
	4	0.04	-155.71	0.08	-7.54	0.10	115.65	0.02	-123.23
62°	1	0.31	90.42	0.52	17.41	0.39	165.14	0.27	-1.99
	2	0.16	-164.09	0.01	22.52	0.33	74.61	0.50	-116.17
	3	0.14	118.01	0.54	57.99	0.07	-119.42	0.12	94.61
	4	0.14	159.07	0.11	104.49	0.10	109.06	0.16	-60.34
35° to 62°	1	0.24	84.43	0.21	-8.12	0.09	165.27	0.11	-45.68
	2	0.05	-178.49	0.19	-11.09	0.08	128.89	0.14	-95.95
	3	0.08	100.35	0.19	89.56	0.02	-71.69	0.10	71.39
	4	0.03	-165.40	0.04	-18.55	0.04	125.59	0.07	-50.55

Table 6.1. 1st, 2nd, 3rd, and 4th harmonic components in the averaged modified Stokes parameters from the circle flights from March 23rd 2001.

Expected phases from [5] and from the wind direction, $\psi = 120°$, would be $\theta = -120°$ and $\theta = +120°$ for the first two harmonics of the 2nd Stokes parameter, $\theta = -30°$ and $\theta = -150°$ for the 3rd and $\theta = 30°$ for the 4th. No confirmation of these values is found, and again the total average from all circles with incidence angles from 35° to 62° is calculated, resulting in the last row of table 6.1. The result shows a decrease in the magnitudes, and it is thus an indication, that the signals still have random nature, rather than systematic wind direction dependence. The resulting phases still do not comply with the expected values, and a wind driven sea surface pattern can not be identified.

7. Results from the October 25th 2001 flight

The flight on October 25th 2001 took place over the primary target area over the North Sea, and all meteorological data acquisition systems were operative. The data, received from the oilrigs, Gorm and Tyra located on either sides of the target area, is shown in figure 7.1, which also includes measurements of the sea surface temperature. The blue lines on the figure indicate the flight time, and it is noticed, that the wind speed was approximately 10 m/sec. to 11 m/sec. during the flight and that the wind direction was stable at $\theta = 190°$.

The flight altitude was increased on this flight from 1000 m to 2000 m to investigate, if the magnitude of the narrow peaks on the Stokes parameter signatures could be reduced, when the field of view, i.e. the spatial integration area, was increased. Four incidence angles were covered, and the results are shown in the figures 7.2 to 7.13. The general impression of the curves is similar to the previous two flights, and a large variation is noticed. Figure 7.5 and 7.7 show small variations for the 2nd, the 3rd and the 4th Stokes parameters, while the 1st Stokes parameter variation is of several Kelvin. The characteristic peak pattern is the same as for the two previous flights, and it is still noticed, that the width of the peaks in many cases is smaller for large incidence angles, i.e. for large circle diameters. The flight altitude is now higher, however, and even for the largest circles, flying by a point target will cause a peak of 15° width.

Calculation of averages follows the single tracks, and results are shown in the figures 7.14 to 7.17. Peaks are reduced again, and for some incidence angles, signatures similar to harmonics appear. The analysis of the 1st to 4th harmonics for each incidence angle is shown in table 7.1, and again the last row shows the harmonic analysis for the averaged track for all incidence angles from 29° to 55°. With the wind direction, $\psi = 190°$, the expected azimuth angles from [5] would be $\theta = 170°$ and $\theta = -20°$ for the 2nd Stokes parameter, $\theta = -100°$ and $\theta = 70°$ for the 3rd, and $\theta = -110°$ for the 4th. The table shows some variation, and the random impression is similar to the two previous flights, although the wind speed is 11.0 m/sec

To provide a larger statistical material, however, and to investigate the influence from the higher flight altitude, i.e. larger spatial integration, an additional data series was acquired during the October 25th 2001 flight. A constant 45° incidence angle was chosen, and circles were flown in the altitude of 1000 m, 2000 m, and 3000 m, acquiring a total of nine additional tracks. These results are shown in the figures 7.18 to 7.26, and the means from each flight altitude are presented in figure 7.27 to figure 7.29.
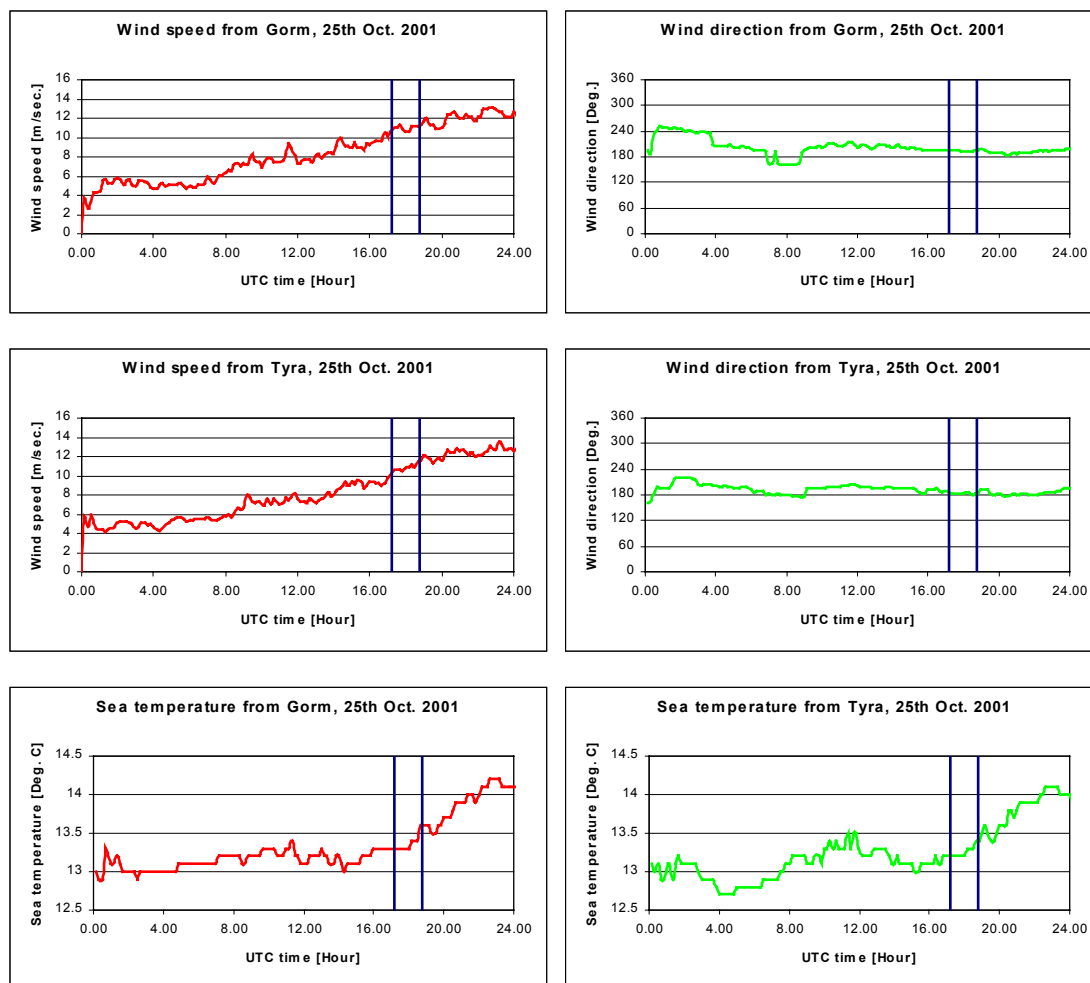
Figure 7.1. Meteorological data for October 25th 2001. Wind speed and wind direction as well as the sea surface temperature is measured at the two oilrigs Gorm and Tyra in the North Sea. The flight took place between the two locations. The blue lines indicate the flight time.

Table 7.2 shows the square root of the total power (except DC) in the Stokes parameters for the nine tracks, taken at three different altitudes. The power is averaged for each altitude, and as a noise reduction is achieved by track averaging, the power for the averaged track for each altitude is also shown. Comparing the results, it is seen, that no systematic reduction of the noise power is gained when the altitude is changed, and for three of the four modified Stokes parameters, a small increase is even noticed, when changing from 1000 m to 3000 m. The changes are very small, less than 10 % typically, and as they are not systematic, it is most likely, that they are statistical coincidences. It must thus be concluded for the present configuration, that a change in the flight altitude has very little effect on the noise represented in the data.

With the very small influence from the changing flight altitude, the nine tracks may be regarded as acquired under equal conditions, and they can be used for a statistical analysis, illustrating the effect of integration. A total of 12 tracks are acquired with a 45° incidence angle, and table 7.3 shows the square root of the power, i.e. the rms. value, in each of the four
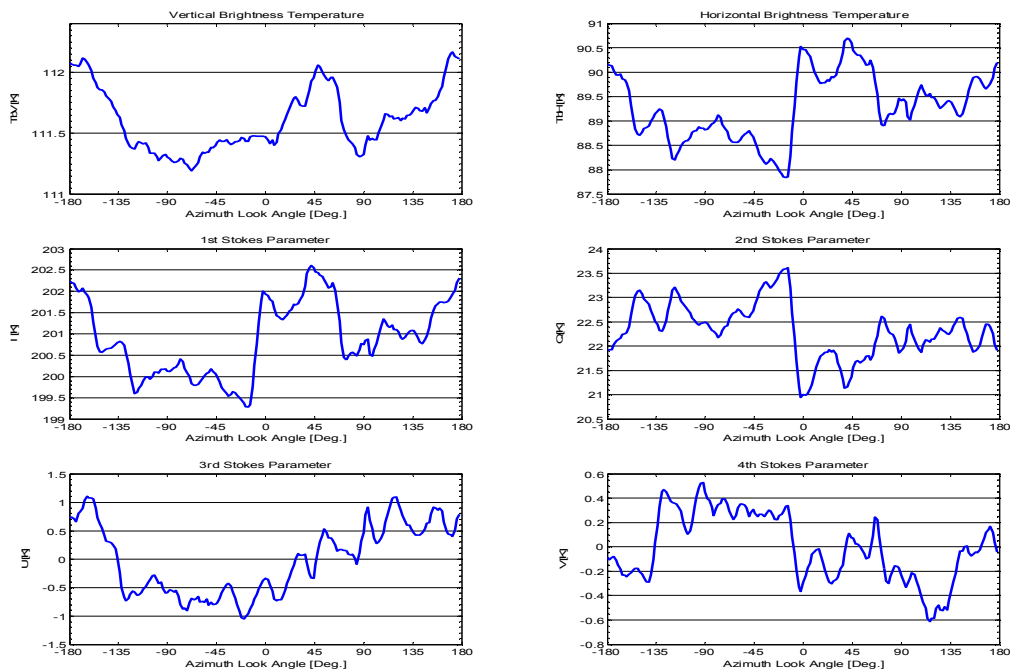
Figure 7.2. The Stokes parameters from the 1st circle flight track with 29° incidence angle from the October 25th 2001 flight.
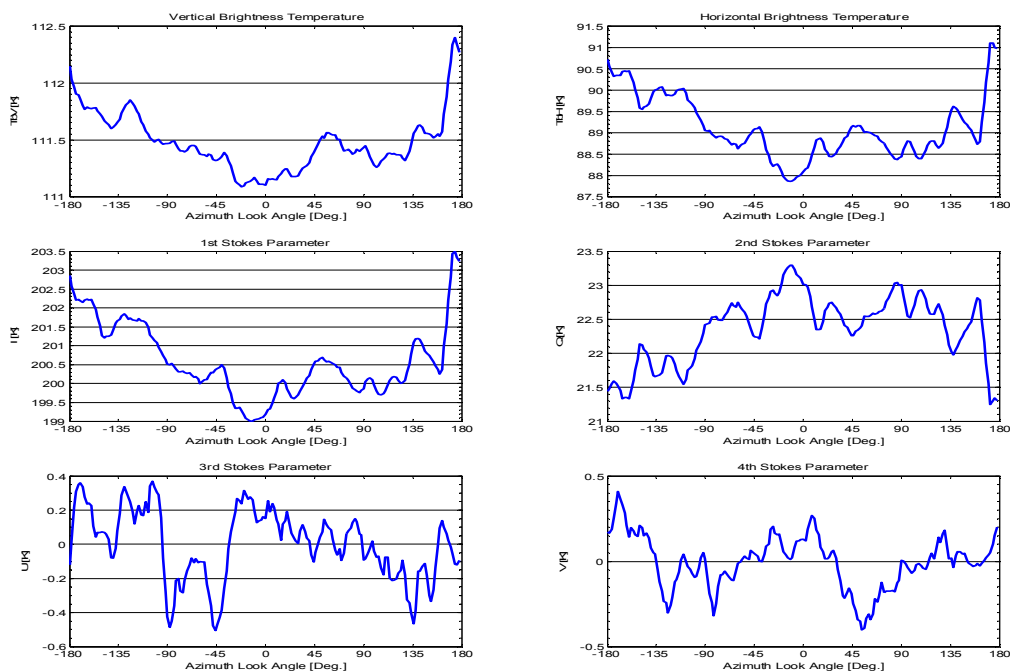
Figure 7.3. The Stokes parameters from the 2nd circle flight track with 29° incidence angle from the October 25th 2001 flight.
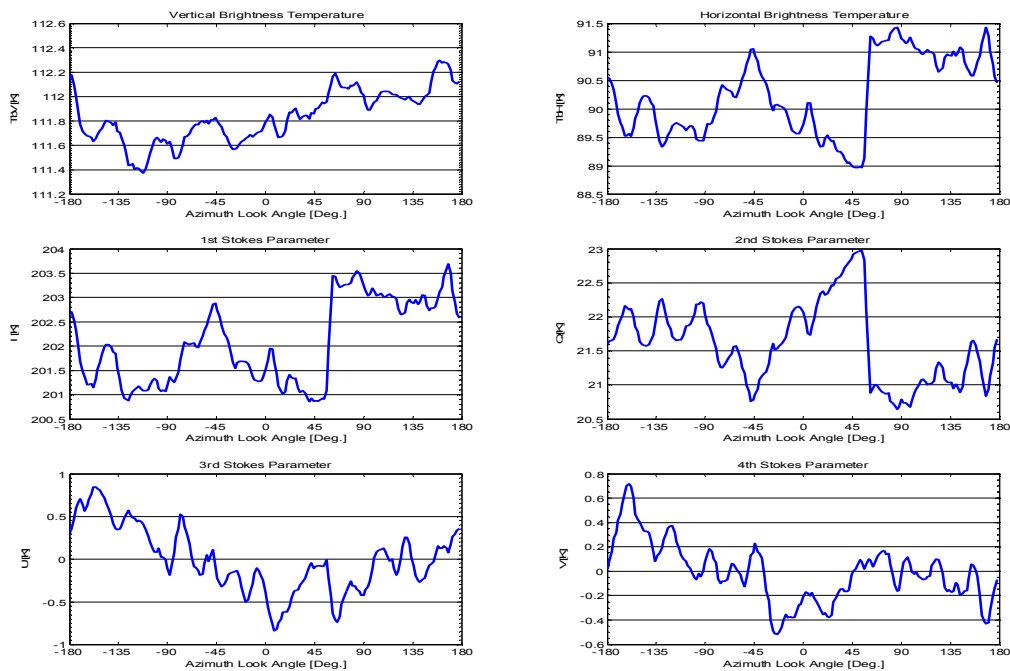
Figure 7.4. The Stokes parameters from the 3rd circle flight track with 29° incidence angle from the October 25th 2001 flight.
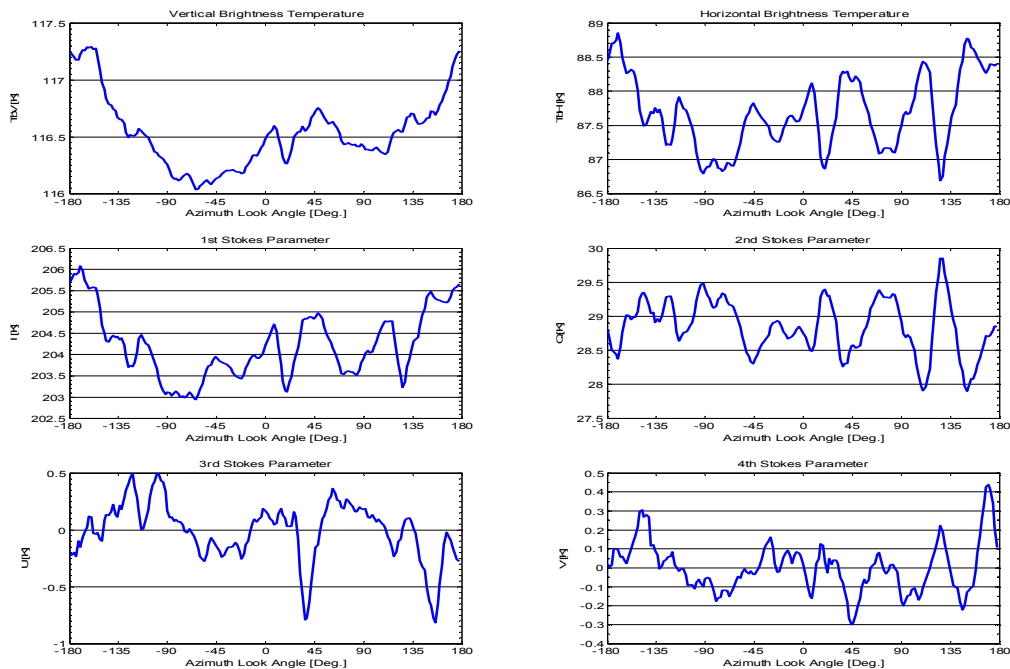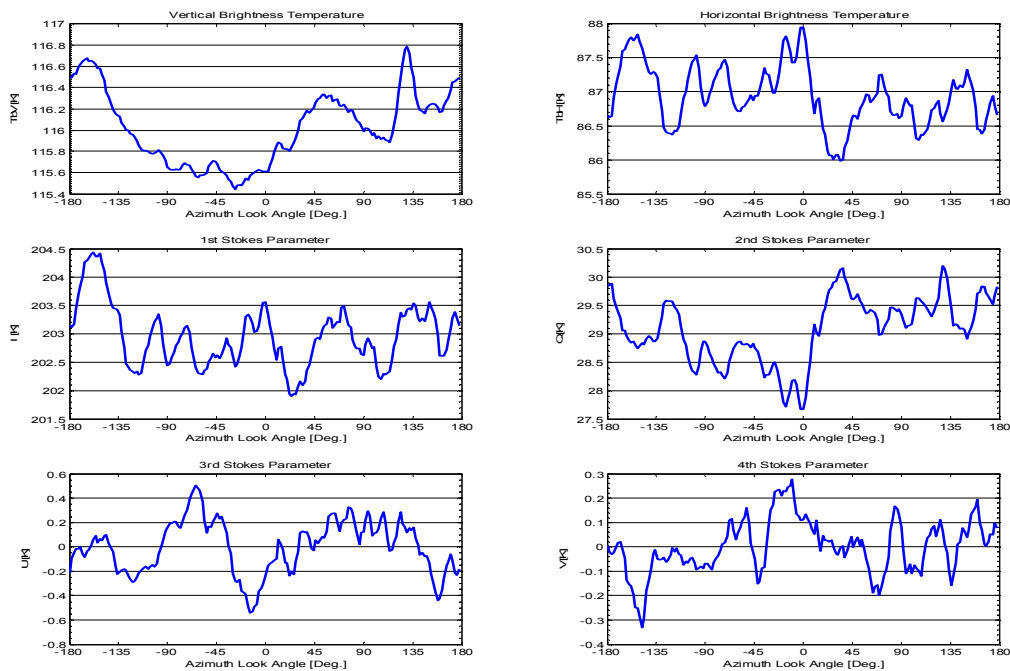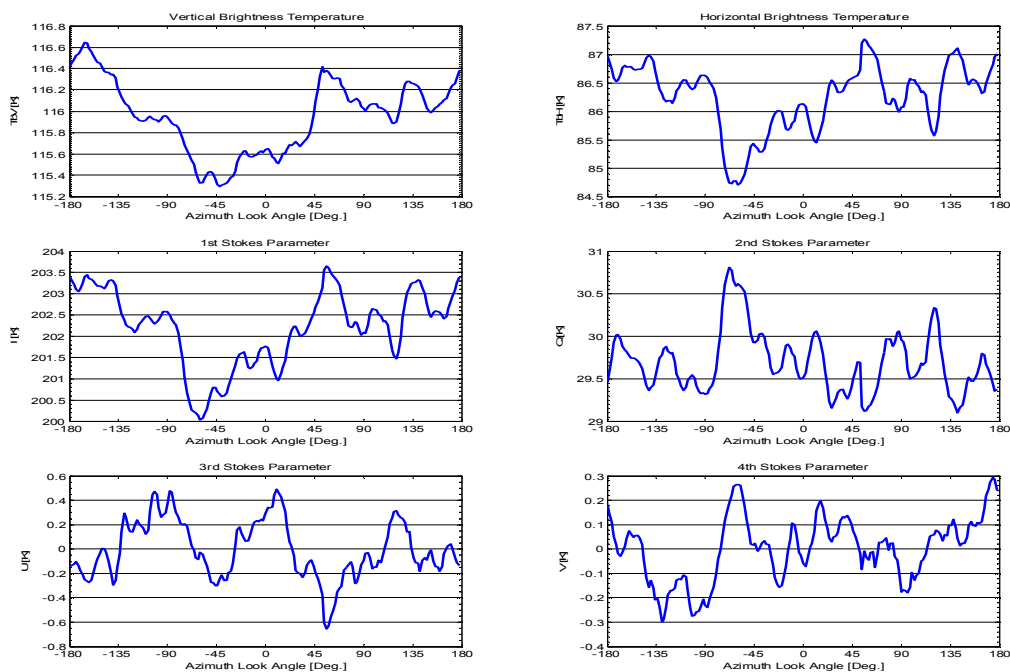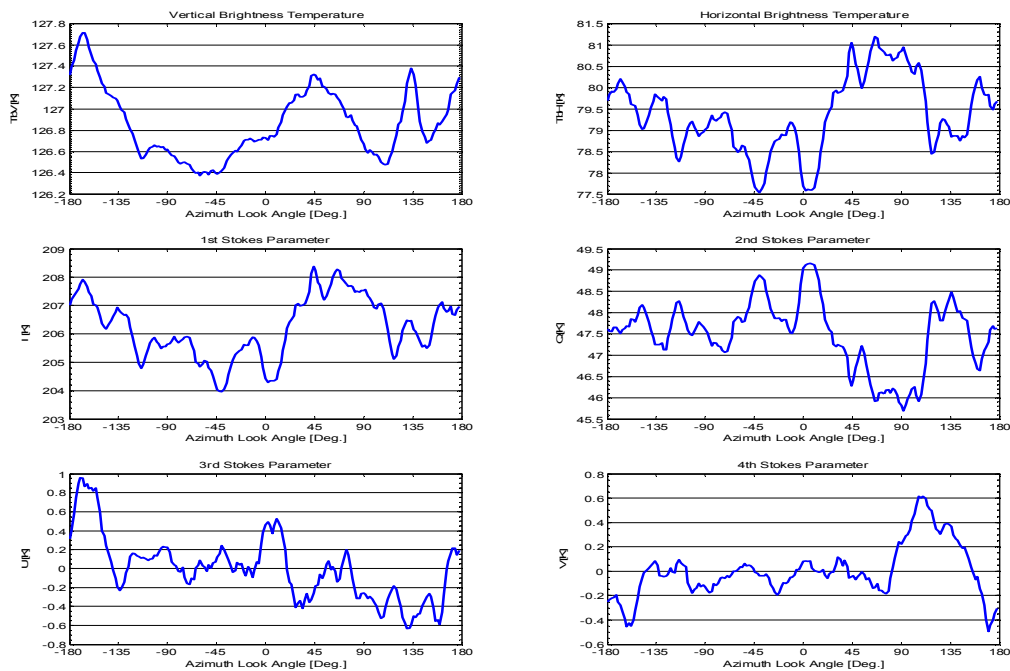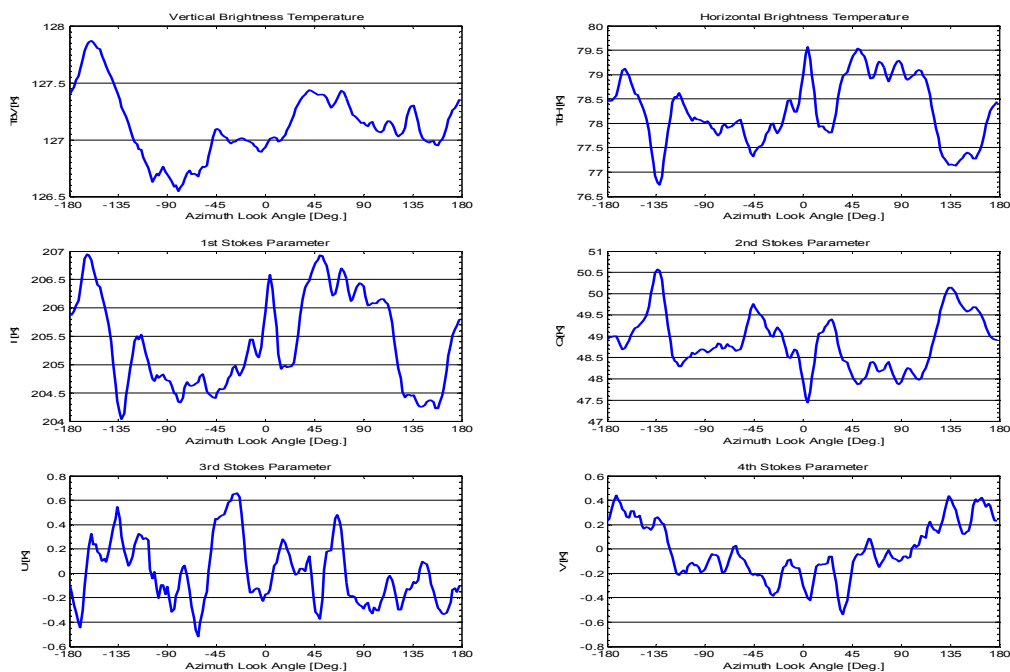

Figure 7.5. The Stokes parameters from the 1st circle flight track with 35° incidence angle from the October 25th 2001 flight.

Figure 7.6. The Stokes parameters from the 2nd circle flight track with 35° incidence angle from the October 25th 2001 flight.
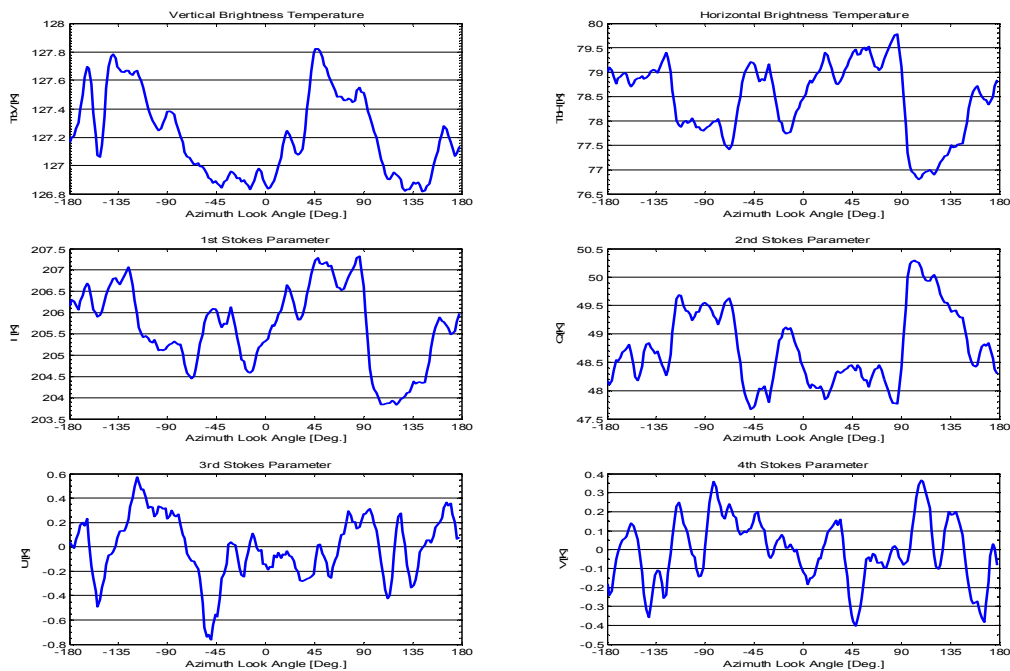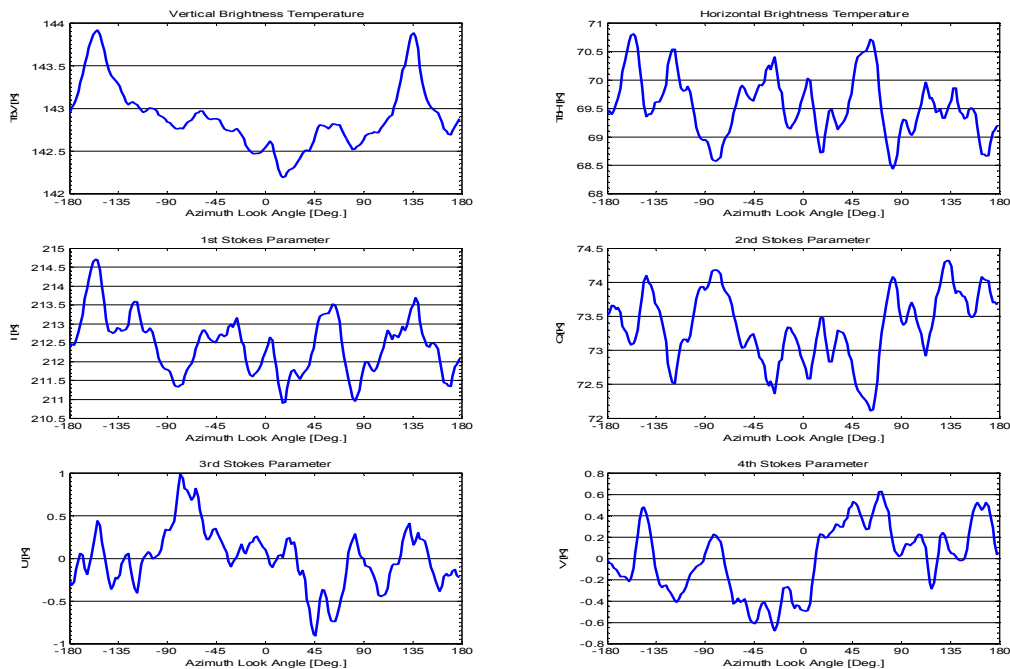

Figure 7.7. The Stokes parameters from the 3rd circle flight track with 35° incidence angle from the October 25th 2001 flight.

Figure 7.8. The Stokes parameters from the 1st circle flight track with 45° incidence angle from the October 25th 2001 flight.
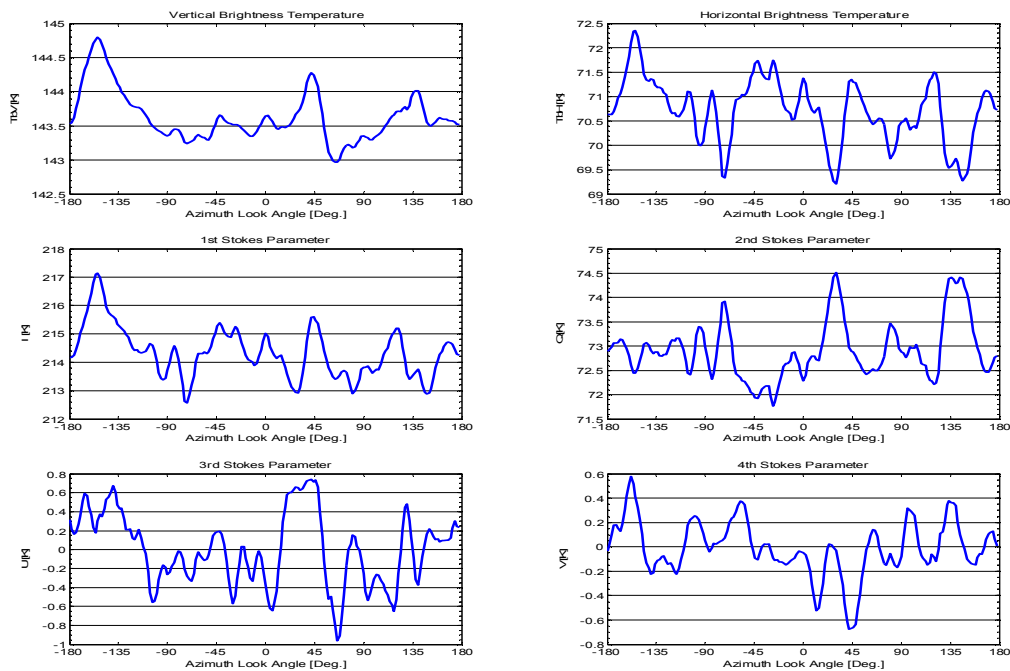

Figure 7.9. The Stokes parameters from the 2nd circle flight track with 45° incidence angle from the October 25th 2001 flight.
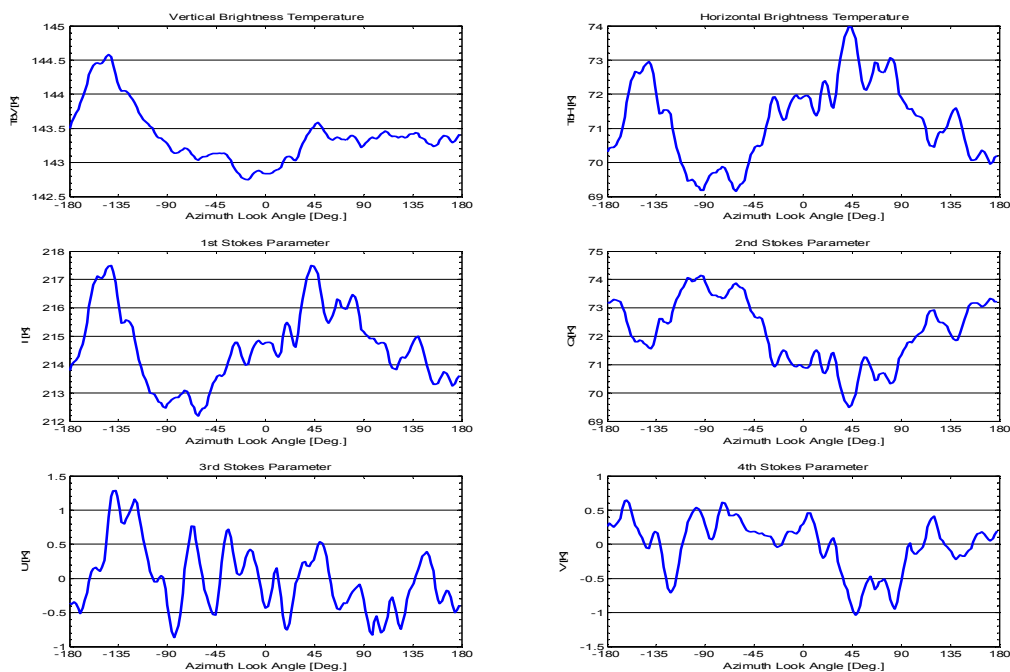
Figure 7.10. The Stokes parameters from the 3rd circle flight track with 45° incidence angle from the October 25th 2001 flight.

Figure 7.11. The Stokes parameters from the 1st circle flight track with 55° incidence angle from the October 25th 2001 flight.

Figure 7.12. The Stokes parameters from the 2nd circle flight track with 55° incidence angle from the October 25th 2001 flight.

Figure 7.13. The Stokes parameters from the 3rd circle flight track with 55° incidence angle from the October 25th 2001 flight.
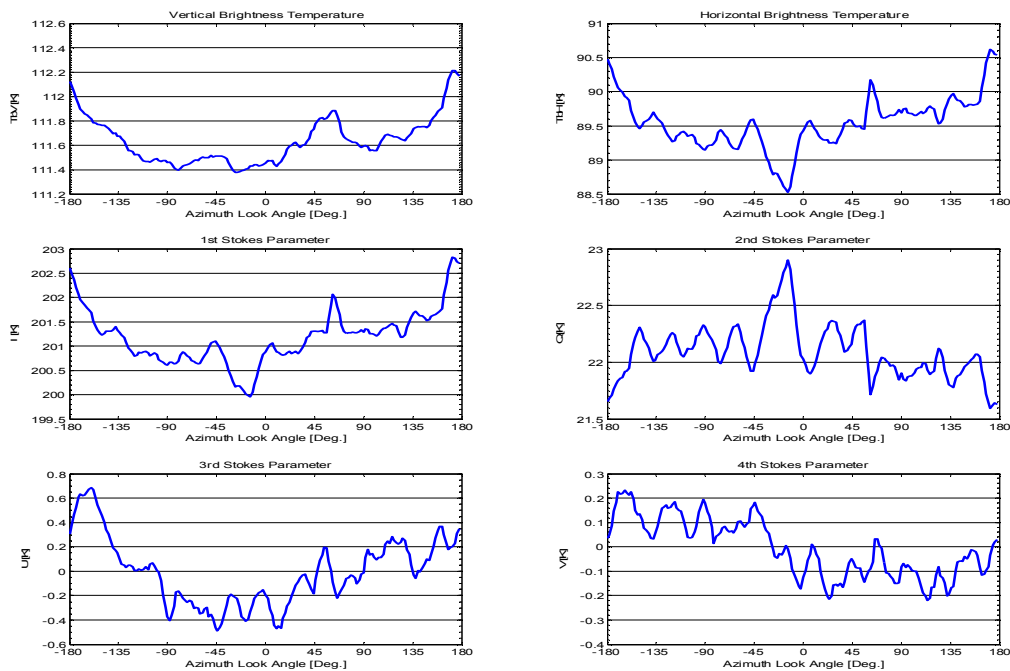
Figure 7.14. The averaged Stokes parameters from the three circle flight tracks with 29° incidence angle from the October 25th 2001 flight.
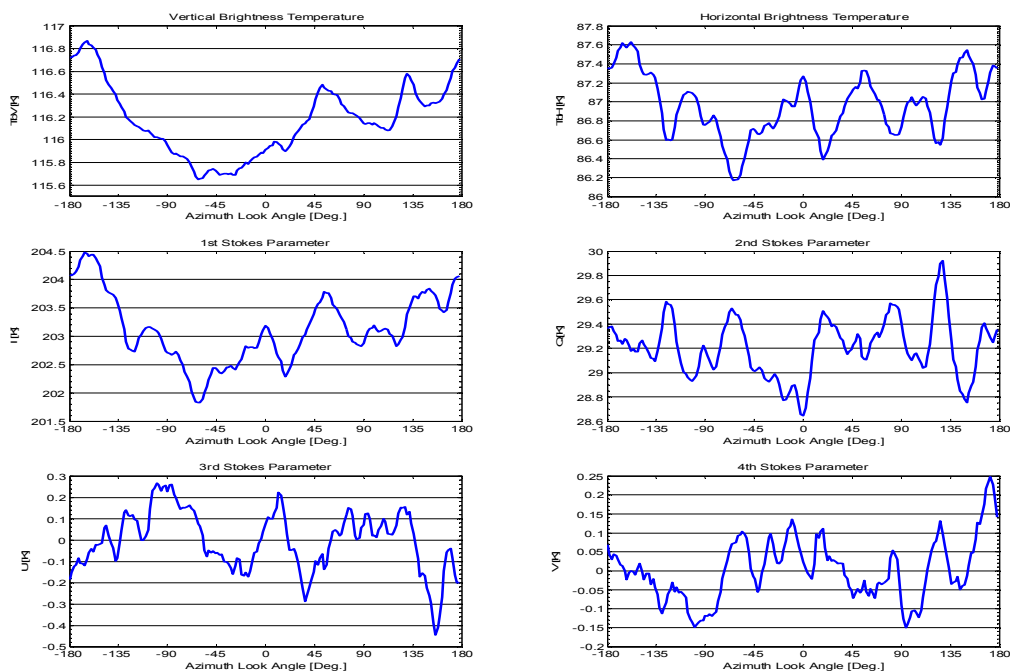

Figure 7.15. The averaged Stokes parameters from the three circle flight tracks with 35° incidence angle from the October 25th 2001 flight.
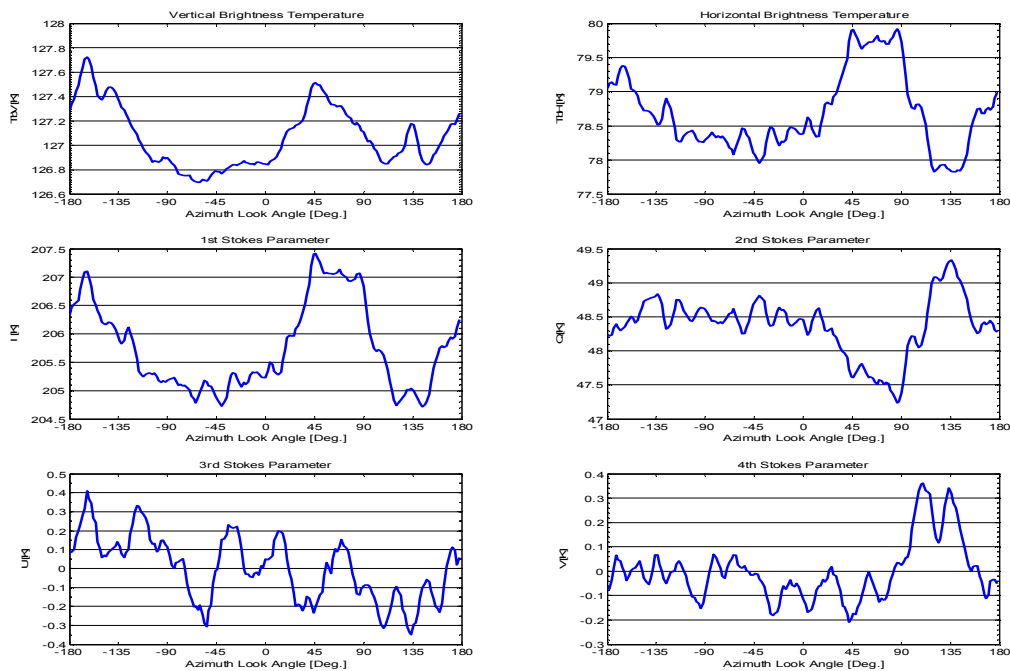
Figure 7.16. The averaged Stokes parameters from the three circle flight tracks with 45° incidence angle from the October 25th 2001 flight.
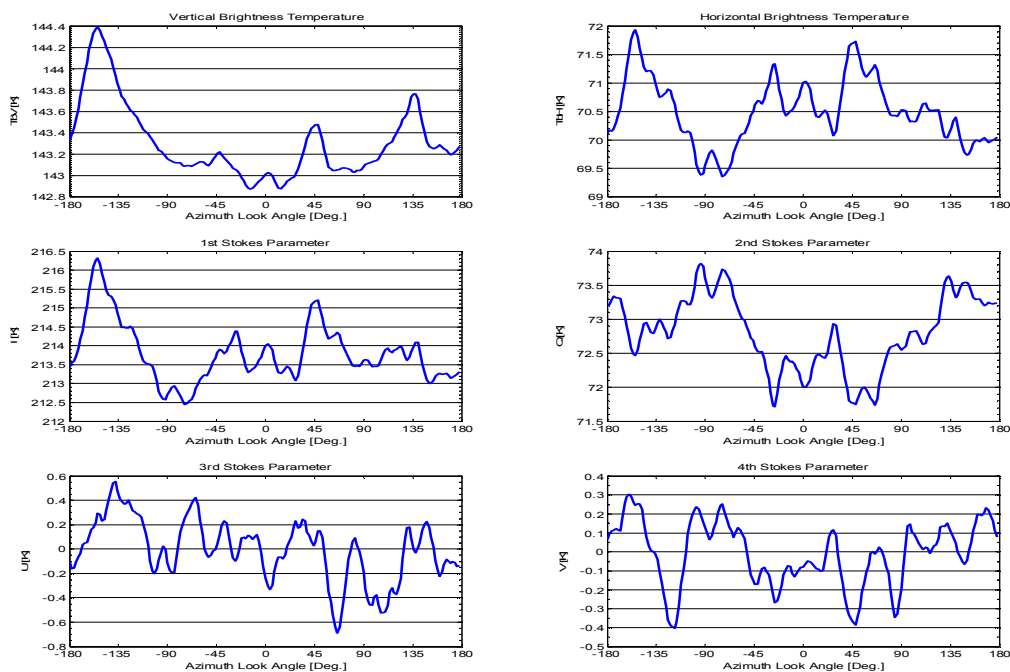
Figure 7.17. The averaged Stokes parameters from the three circle flight tracks with 55° incidence angle from the October 25th 2001 flight.

Inc.	Harm.	TV, M.	TV, Ph.	TH, M.	TH, Ph.	U, Mag.	U, Ph.	V, Mag.	V, Ph.
29°	1	0.20	-148.12	0.43	-147.99	0.33	-165.07	0.14	108.72
	2	0.10	-26.40	0.07	-25.95	0.11	-53.59	0.02	-99.96
	3	0.12	-172.72	0.20	-167.69	0.07	116.46	0.05	136.74
	4	0.02	107.78	0.06	-27.69	0.05	-81.85	0.00	122.67
35°	1	0.37	-154.40	0.27	-161.16	0.05	66.74	0.01	-84.65
	2	0.20	-58.34	0.23	-31.77	0.12	-170.22	0.08	27.61
	3	0.09	168.61	0.04	133.50	0.06	-4.88	0.02	-178.06
	4	0.02	-114.23	0.10	68.98	0.08	-41.16	0.00	-38.60
45°	1	0.17	-143.78	0.36	-82.09	0.12	101.24	0.09	-147.87
	2	0.27	-72.82	0.53	-96.79	0.11	-65.03	0.09	122.45
	3	0.11	143.88	0.42	153.37	0.06	83.13	0.05	5.28
	4	0.05	-157.68	0.15	28.47	0.09	43.88	0.07	-114.76
55°	1	0.36	165.98	0.22	-57.01	0.19	98.10	0.11	161.63
	2	0.17	-68.51	0.46	-63.67	0.09	-43.77	0.06	75.10
	3	0.10	75.32	0.42	86.28	0.02	-32.63	0.06	-140.61
	4	0.22	-149.43	0.30	176.84	0.16	-169.32	0.12	-55.07
35°, 45° and 55°	1	0.28	-168.04	0.21	-97.94	0.12	94.91	0.06	-172.80
	2	0.21	-67.14	0.37	-72.44	0.06	-90.69	0.06	76.58
	3	0.08	129.18	0.25	120.58	0.03	28.65	0.01	-113.44
	4	0.10	-148.98	0.08	126.06	0.01	-147.94	0.06	-75.14

Table 7.1. 1st, 2nd, 3rd, and 4th harmonic components in the averaged modified Stokes parameters from the circle flights from October 25th 2001.

Circles	TV, std.dev. [K]	TH, std.dev. [K]	U, std.dev. [K]	V, std.dev. [K]
1000m altitude 3 single circles	0.284	0.796	0.385	0.243
	0.173	0.532	0.343	0.118
	0.199	0.615	0.598	0.427
1000 m alt., average	0.219	0.648	0.442	0.263
1000 m alt., integrated	0.181	0.324	0.263	0.141
2000m altitude 3 single circles	0.278	0.883	0.423	0.220
	0.231	0.637	0.383	0.235
	0.304	0.674	0.219	0.283
2000 m alt., average	0.271	0.731	0.342	0.246
2000 m alt., integrated	0.225	0.482	0.242	0.139
3000m altitude 3 single circles	0.205	0.605	0.351	0.260
	0.283	0.714	0.532	0.606
	0.381	0.530	0.484	0.270
3000 m alt., average	0.290	0.616	0.456	0.379
3000 m alt., integrated	0.237	0.393	0.251	0.227
All integrated	0.199	0.290	0.156	0.079

Table 7.2. Square root of the total power (except DC) for the full signal in the modified Stokes parameters from the nine circle flights with 45° incidence angle from October 25th 2001. The power is presented for single tracks, an average of three values, and the power of the integrated track.
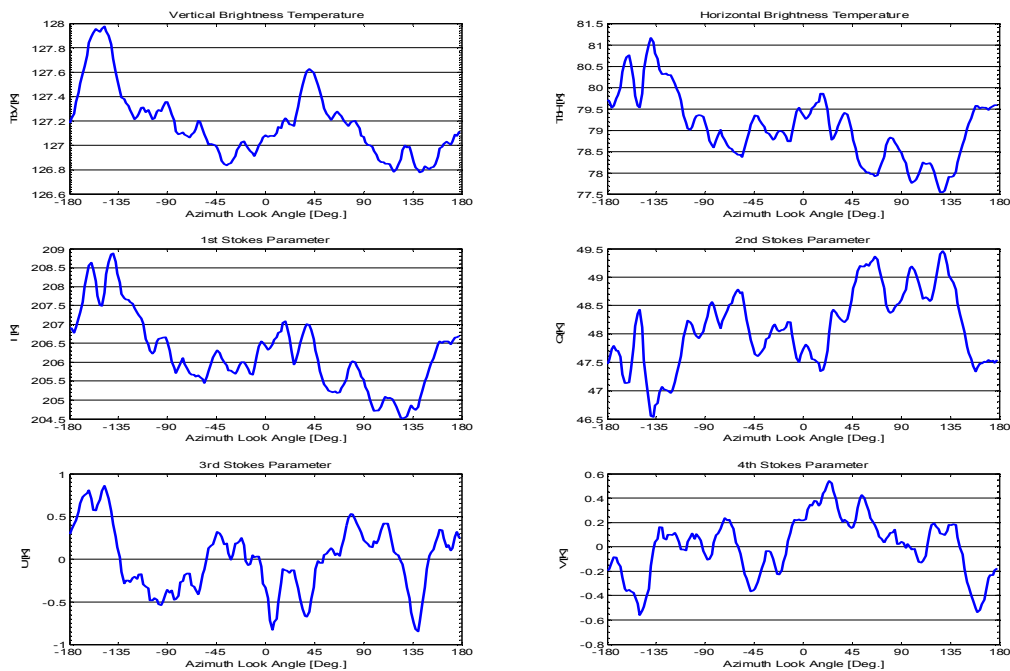
Figure 7.18. The Stokes parameters from the 1st circle flight track with 45° incidence angle and 1000 m flight altitude from the October 25th 2001 flight.
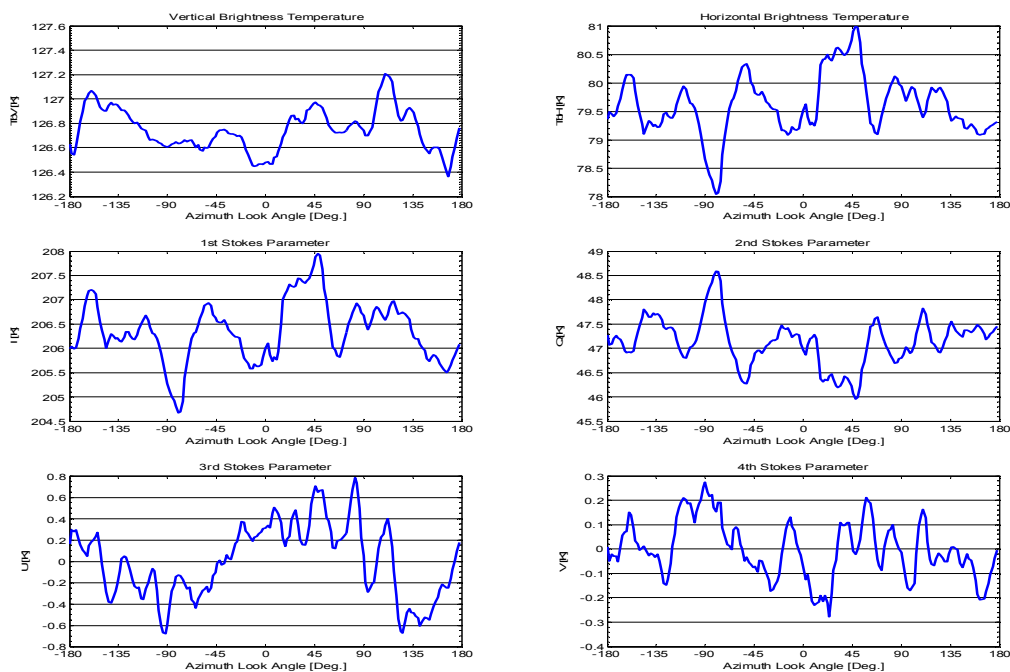

Figure 7.19. The Stokes parameters from the 2nd circle flight track with 45° incidence angle and 1000 m flight altitude from the October 25th 2001 flight.
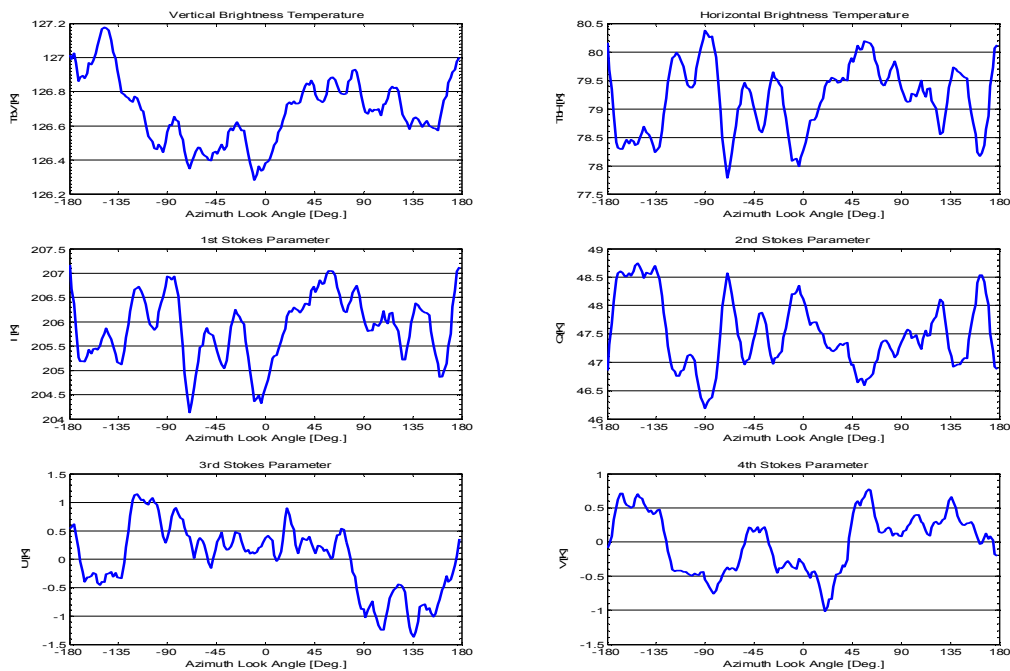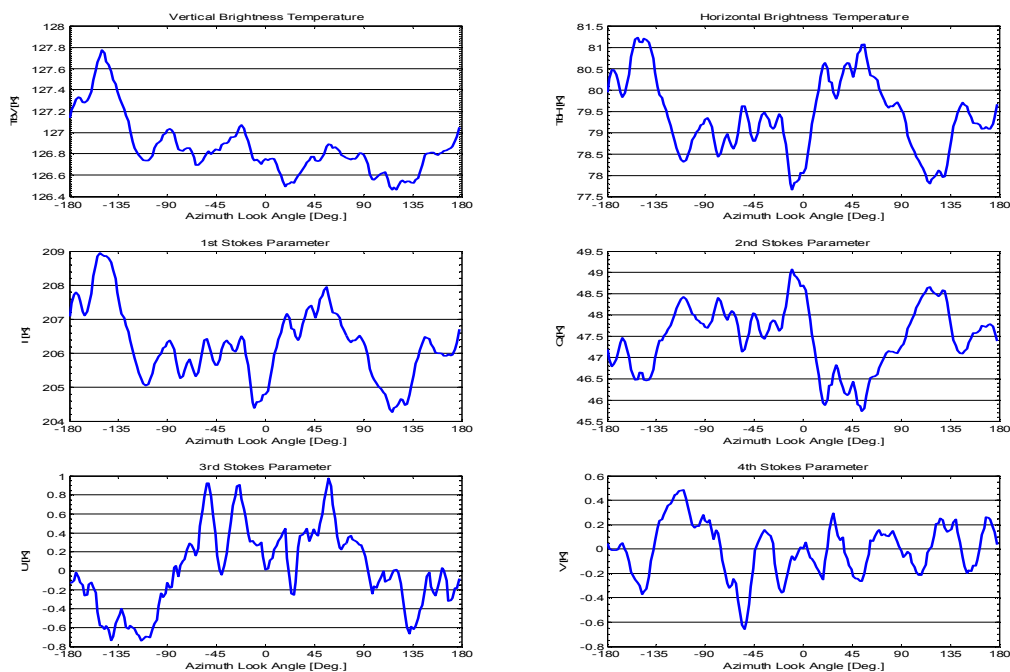
Figure 7.20. The Stokes parameters from the 3rd circle flight track with 45° incidence angle and 1000 m flight altitude from the October 25th 2001 flight.

Figure 7.21. The Stokes parameters from the 1st circle flight track with 45° incidence angle and 2000 m flight altitude from the October 25th 2001 flight.
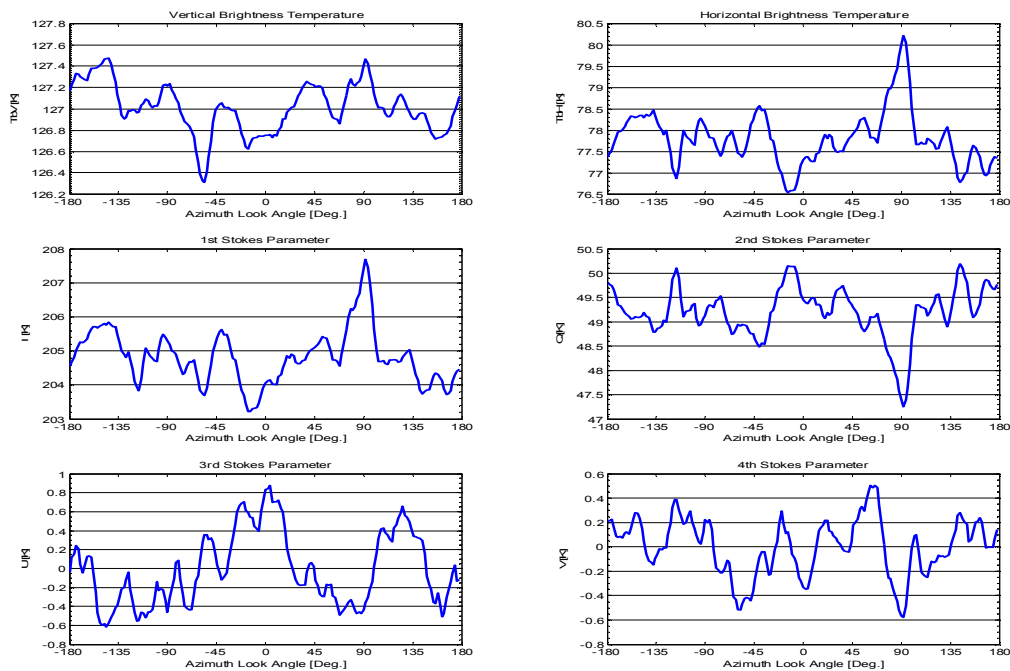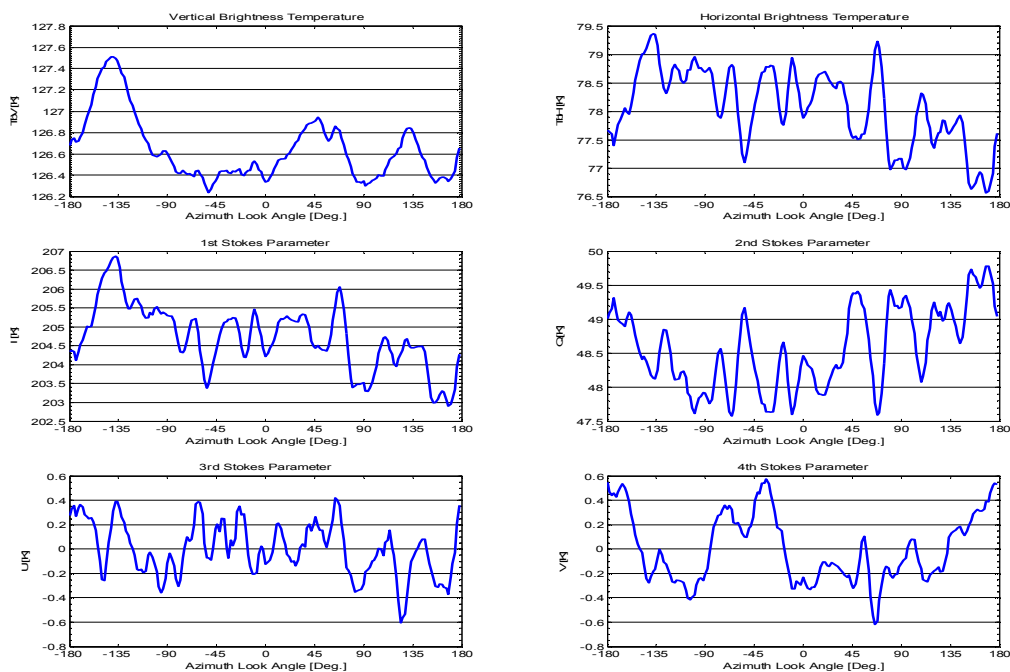
Figure 7.22. The Stokes parameters from the 2nd circle flight track with 45° incidence angle and 2000 m flight altitude from the October 25th 2001 flight.

Figure 7.23. The Stokes parameters from the 3rd circle flight track with 45° incidence angle and 2000 m flight altitude from the October 25th 2001 flight.
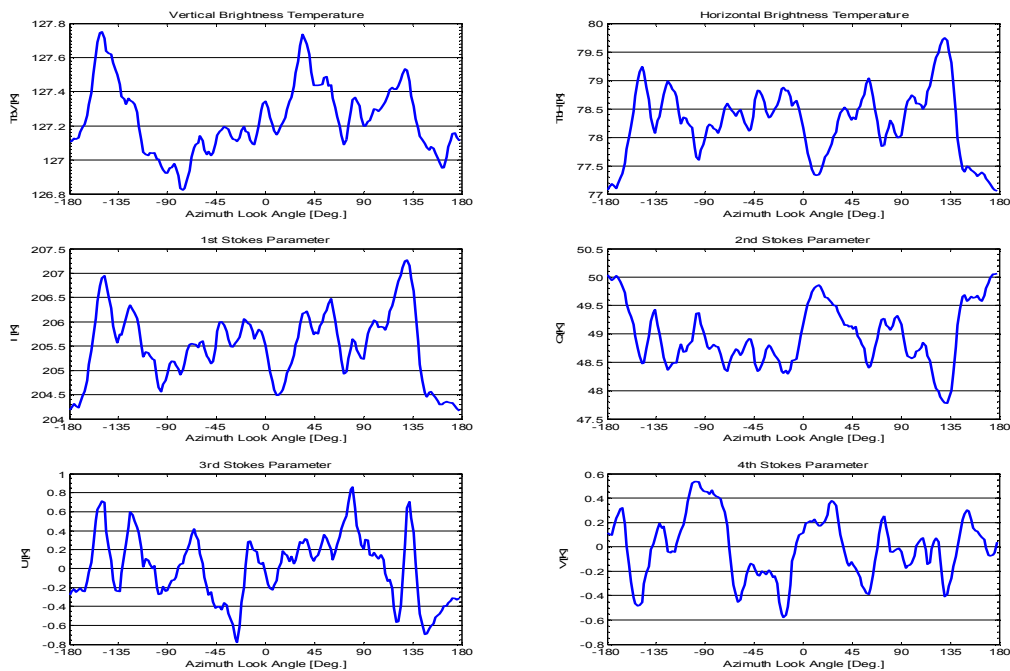
Figure 7.24. The Stokes parameters from the 1ˢᵗ circle flight track with 45° incidence angle and 3000 m flight altitude from the October 25ᵗʰ 2001 flight.
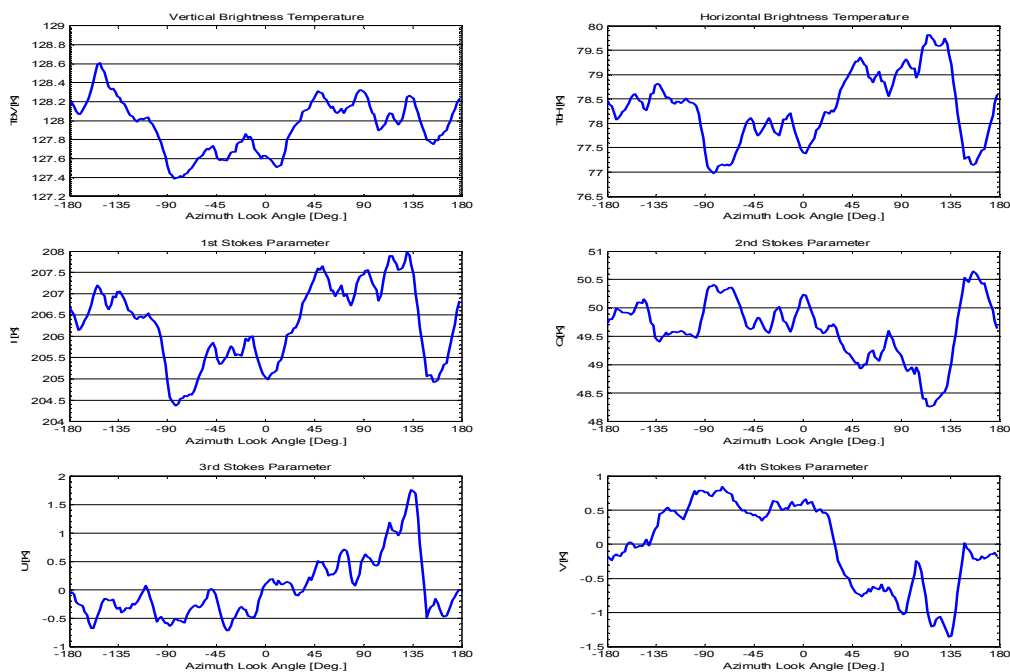

Figure 7.25. The Stokes parameters from the 2ⁿᵈ circle flight track with 45° incidence angle and 3000 m flight altitude from the October 25ᵗʰ 2001 flight.
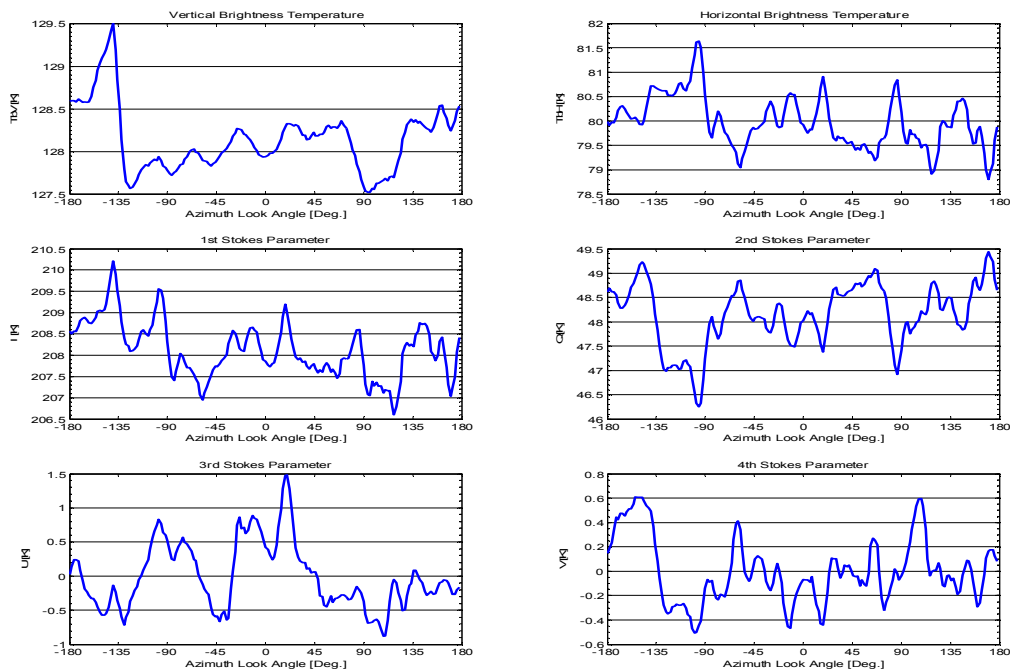
Figure 7.26. The Stokes parameters from the 3rd circle flight track with 45° incidence angle and 3000 m flight altitude from the October 25th 2001 flight.

Figure 7.27. The averaged Stokes parameters from the three circle flight tracks with 45° incidence angle and 1000 m flight altitude from the October 25th 2001 flight.
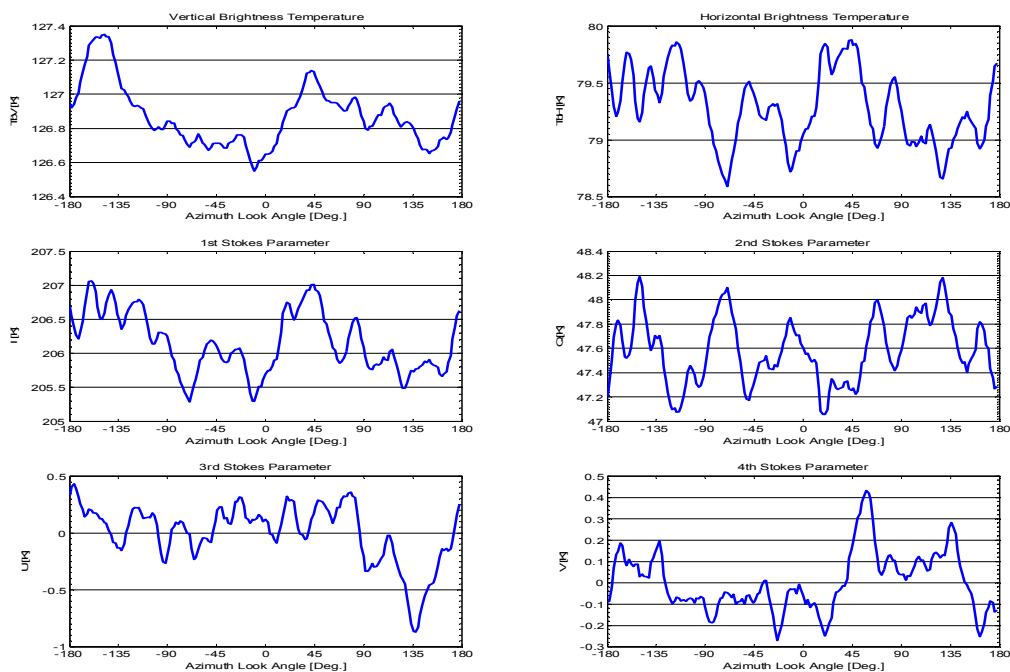
Figure 7.28. The averaged Stokes parameters from the three circle flight tracks with 45° incidence angle and 2000 m flight altitude from the October 25th 2001 flight.

Figure 7.29. The averaged Stokes parameters from the three circle flight tracks with 45° incidence angle and 3000 m flight altitude from the October 25th 2001 flight.
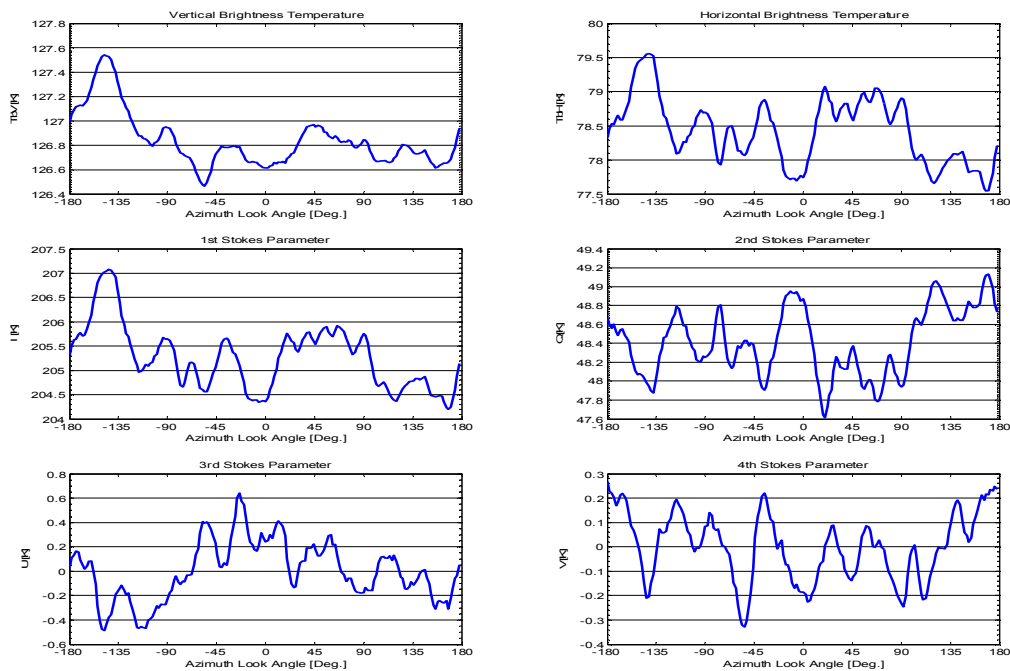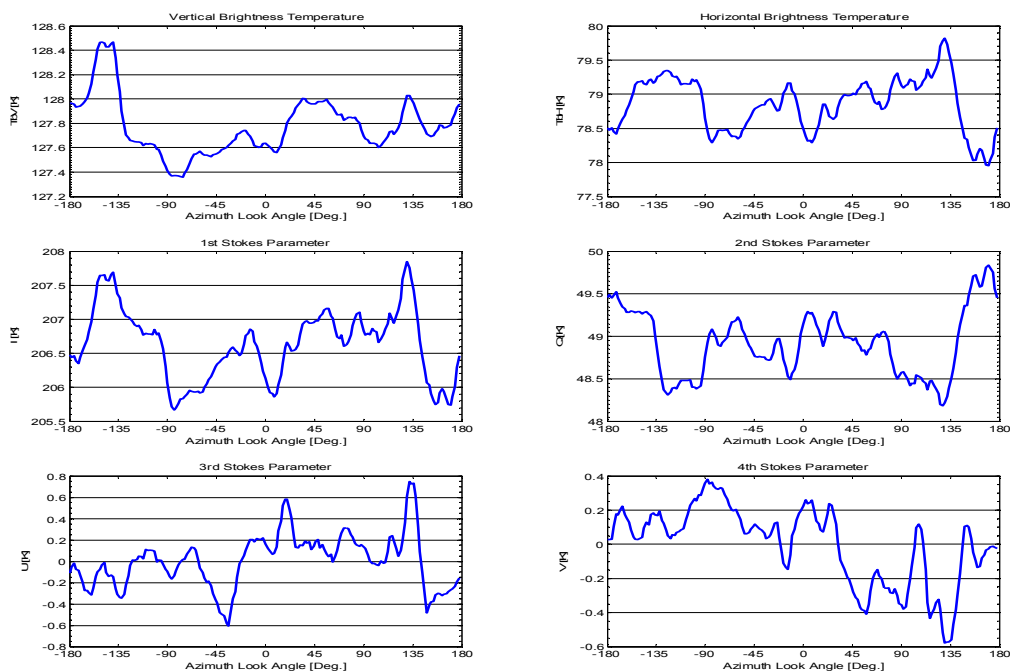
Stokes parameters, when the tracks are processed individually, and when they are averaged. After averaging the tracks three and three, the square root of the power in each of the resulting tracks is evaluated, and again the average power is calculated. Finally all tracks are fully integrated, and the power from the resulting track gives the last line in the table.

Circles		TV, std.dev. [K]	TH, std.dev. [K]	U, std.dev. [K]	V, std.dev. [K]
1000m altitude 3 single circles		0.284	0.796	0.385	0.243
		0.173	0.532	0.343	0.118
		0.199	0.615	0.598	0.427
2000m altitude 6 single circles		0.329	0.888	0.343	0.218
		0.296	0.680	0.266	0.228
		0.295	0.761	0.258	0.170
		0.278	0.883	0.423	0.220
		0.231	0.637	0.383	0.235
		0.304	0.674	0.219	0.283
3000m altitude 3 single circles		0.205	0.605	0.351	0.260
		0.283	0.714	0.532	0.606
		0.381	0.530	0.484	0.270
Average, single		0.271	0.693	0.382	0.273
3 circles integrated	1000 m	0.181	0.324	0.263	0.141
	2000 m	0.257	0.567	0.170	0.121
		0.225	0.482	0.242	0.139
	3000 m	0.237	0.393	0.251	0.227
Average, 3 integrated		0.225	0.442	0.232	0.157
All 12 integrated		0.207	0.307	0.127	0.063

Table 7.3. Total rms. noise for the full signal in the modified Stokes parameters from the 12 circle flights with 45° incidence angle from October 25th 2001. The circles are processed as single tracks, averaged as 4 times three circles and averaged totally.

The table shows reductions of rms. noise for all Stokes parameters as a result of the averaging. If the data averaged was pure Gaussian distributed random data, the effect of averaging would be a reduction by the square root of N, when N tracks are averaged. In this case the decrease of the rms. noise should be a factor of 1.73 after the first averaging and an additional factor of 2 after the second averaging. For the horizontal polarization, the reductions are 1.57 and 1.44, respectively, and for the 3rd Stokes parameter, the values are 1.65 and 1.83. The 4th Stokes parameter is improved by a factor of 1.74 from the first averaging and additional 2.49 from the second. Most of these values are near to the expected improvements, with the maximum deviations of 30 % for the horizontal polarization, being reduced too little.

For the vertical polarization, however, the improvements are poorer, and only a factor of 1.20 is gained by the first averaging, while the second gives 1.09. The conclusion from these results is, that the 2nd, 3rd, and 4th modified Stokes parameters primarily have a Gaussian nature, and the main part of their AC power is random noise. In the 3rd Stokes parameter, the improvement from second averaging was a factor of 1.83, reached by an rms. noise reduction from 232 mK to 127 mK. If a harmonic with a magnitude of 100 mK was added as a wind driven signal to the parameter, it would contribute with 70 mK to the total power, and this

contribution would not be reduced by the averaging. The reduction would then be (232 mK+70 mK)/(127 mK + 70 mK) = 1.53, which is 16% less than the measured value.

Regarding the horizontal polarization's averaging from 4 to 1, the total reduction is 1.44, while the square root of 4, equal to 2.00, would be expected. This would be equal to a non-Gaussian component with a magnitude of 243 mK. For the 1st Stokes parameter the reduced improvements are equal to the presence of a non-Gaussian component with a 266 mK magnitude, while the 3rd and 4th Stokes parameters seem to have non-Gaussian components significant below the level of the noise, and hence significantly below the approximately 150 mK signal present.

A harmonic analysis of the 1st to 4th order components of the data tracks is carried out in table 7.4, following the same integration as in the above example. The pattern from the previous flights is seen again, showing phases pointing to directions covering the full 360° range. The effect of integration is thus again a reduction of the magnitudes, illustrated in the last row. The expected azimuth angles would be $\theta = 170°$ and $\theta = -20°$ for the first two harmonics of the 2nd Stokes parameter, $\theta = -100°$ and $\theta = 70°$ for the 3rd, and $\theta = -110°$ for the 4th. Like in the previous tables, no correlation is observed, and magnitudes are found to be less than 150 mK, except for the 2nd harmonics of the horizontal and vertical polarizations.

Altitude	Har.	I, Mag.	I, Phase	Q, Mag.	Q, Ph.	U, Mag.	U, Ph.	V, Mag.	V, Ph.
1000 m	1	0.10	-170.94	0.06	90.79	0.16	32.57	0.10	-112.59
	2	0.18	-90.10	0.30	-78.05	0.20	-74.53	0.07	-134.89
	3	0.07	116.88	0.05	-143.75	0.16	132.89	0.05	116.44
	4	0.10	-126.46	0.09	167.63	0.09	21.94	0.07	-177.96
2000 m 1st group	1	0.17	-143.78	0.36	-82.09	0.12	101.24	0.09	-147.87
	2	0.27	-72.82	0.53	-96.79	0.11	-65.03	0.09	122.45
	3	0.11	143.88	0.42	153.37	0.06	83.13	0.05	5.28
	4	0.05	-157.68	0.15	28.47	0.09	43.88	0.07	-114.76
2000 m 2nd group	1	0.16	155.30	0.08	64.15	0.23	-14.02	0.10	160.65
	2	0.20	-81.83	0.46	-99.75	0.14	39.81	0.05	-6.34
	3	0.10	97.88	0.25	126.99	0.08	131.80	0.06	-132.11
	4	0.08	-146.98	0.19	-144.89	0.04	-109.39	0.06	85.88
2000 m All 6 circ.	1	0.14	-173.36	0.15	-73.99	0.10	16.97	0.08	-174.21
	2	0.24	-76.66	0.49	-98.16	0.08	-3.76	0.03	90.38
	3	0.10	121.98	0.33	143.55	0.06	110.58	0.02	-70.18
	4	0.06	-151.49	0.02	-123.15	0.03	21.15	0.01	172.80
3000 m	1	0.16	-145.31	0.11	-106.99	0.18	-55.84	0.25	81.57
	2	0.20	-55.26	0.25	-150.32	0.08	-133.75	0.05	-34.84
	3	0.09	107.90	0.34	31.76	0.14	-39.40	0.03	-89.91
	4	0.13	-161.62	0.20	177.43	0.07	-63.11	0.11	-32.90
All 45° inc. circles	1	0.13	-164.69	0.08	-81.55	0.11	-0.37	0.05	142.31
	2	0.21	-74.49	0.36	-102.09	0.07	-58.96	0.00	-106.66
	3	0.09	117.40	0.15	117.53	0.04	105.76	0.01	-102.76
	4	0.09	-148.18	0.08	-178.03	0.04	-4.39	0.02	-90.24

Table 7.4. 1st, 2nd, 3rd, and 4th harmonic components in the averaged modified Stokes parameters from the circle flights from October 25th 2001. The incidence angle is kept constant at 45°, and the flight altitude is varied.

8. Results from the March 6th 2003 flight

The results from the first three LOSAC flights, carried out during 2001, clearly pointed out the presence of some noise in the measured data, and it was demonstrated, how averaging could improve the overall signal-to-noise-ratio. The March 6th 2003 thus focused on coverage of only two incidence angles, 35° and 45°, enabling for a total acquisition of 12 to 16 circles of each angle, hence improving the integration gain, by up to a factor of four. Another way of improving the integration would be to carry out a cloverleaf pattern, as illustrated in figure 8.1. With a length of each leg of e.g. 2 minutes, the observation time for a specific direction would improve by a factor of about 100, compared to the circle flights. The drawbacks are longer temporal sampling interval between observation directions, causing risk of drift and geophysical changes, and the relatively low number of samples around the circle. Looking for 1st and 2nd order harmonics, the latter drawback is acceptable, but the result of geophysical sampling, spaced by up to 30 minutes, due to maneuvering between data tracks, is unknown.
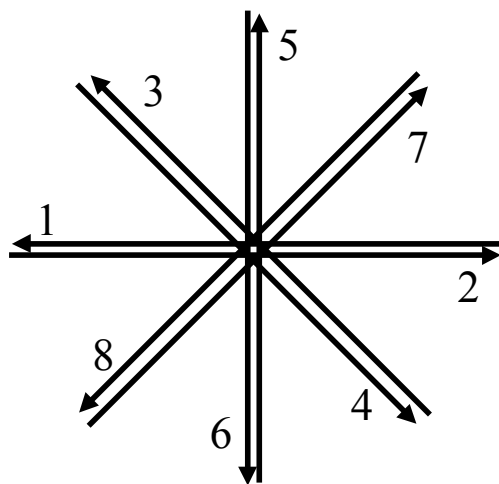

Figure 8.1. Cloverleaf flight pattern, providing excellent integration along each of the eight legs, but reducing the number of samples along the circle signature to eight. A serious drawback is also the data acquisition time, being approximately 30 minutes.

A second important issue in the choice of target for the March 6th 2003 flight, was the wind condition. During the previous flights, the wind had been between 3 m/sec. and 10 m/sec, and a real high-wind case was desired. As the flight could not be time-shifted, meteorological maps were studied prior to take-off, and a site between the Norwegian West Coast and the Faeroe Islands was chosen. The most important drawback for this site was its remote location, making the access to ground measured meteorological data difficult. The reference for this flight is thus an estimated wind map from the Danish Meteorological Institute, based on interpolations between point observations. This resulted in a wind speed of 20 m/sec., coming from straight North. The wind field was stable for at least 12 hours prior to the flight, and from a scientific point of view, it was the ideal condition. The flight altitude was chosen to be 2000 m, as no obvious advantage was observed from any specific altitude on the October 25th 2001 flight.

The results from the circle flights with 45° incidence angle are illustrated in the figures 8.2 to 8.14. Likewise the circle signatures, sampled at 35° incidence angle are shown in the figures

8.18 to 8.33, providing 13 and 16 individual signatures, respectively. As averaging has proved to be efficient in the improvement of the signal-to-noise ratio, the signatures are integrated partly and fully. The figures 8.15 and 8.16 illustrate the 45° incidence angle signatures when the first 6 and the latter 7 circles are integrated, respectively. Figure 8.18 is the fully integrated signature for all 13 circles. Likewise the figures 8.34 and 8.35 each show 8 circles of the 35° incidence angle case, while 8.36 is fully integrated.

As expected, the signatures seem to contain less noise after integration, and table 8.1 contains the full statistics of the root-mean-square noise within the 45° incidence angle signatures. The table is divided into four subsections, containing the signatures individually, averaged three, averaged seven, and fully integrated, respectively. As it was discussed for the October 25th 2001 flight, the integration gain should be the square root of N, when N circles are integrated, provided that the circles are statistically independent and that only Gaussian noise is present. In this case, the improvement factors should thus be 1.73, 1.52, and 1.36, between the sections of the table. For the 4th Stokes parameter, this almost holds, and for the horizontal polarization as well as for the 3rd Stokes parameter, the numbers are partly reached. Hence the horizontal polarization returns numbers of 1.57, 1.21 and 1.15. The vertical polarization, however, provides a much poorer gain, and its improvement coefficients are found to be 1.31, 1.17, and 1.04, being the result of a sinusoidal with a magnitude of 157 mK present within the signal.

Circles	TV, std.dev. [K]	TH, std.dev. [K]	U, std.dev. [K]	V, std.dev. [K]
Single circles	0.419	3.515	2.725	0.815
45° incidence angle	0.368	10.414	1.958	1.533
	0.367	8.413	4.214	0.856
	0.634	6.042	4.027	0.819
	0.566	6.598	2.812	0.733
	0.447	5.300	2.605	0.598
	0.233	3.865	3.381	0.778
	0.399	4.388	2.748	0.731
	0.312	7.631	4.976	1.166
	0.359	7.392	4.485	0.845
	0.821	6.116	3.731	1.424
	0.632	7.067	3.737	0.894
	0.396	5.229	4.222	1.472
Average, single	0.458	6.305	3.509	0.974
3 circles	0.256	5.590	1.711	0.649
integrated	0.405	3.573	2.176	0.448
	0.282	2.718	1.928	0.508
	0.295	4.591	3.043	0.472
	0.498	3.663	2.323	0.624
Average, 3 integrated	0.347	4.027	2.236	0.540
7 integrated	0.310	3.862	1.226	0.370
	0.280	2.804	2.084	0.390
Average, 7 integrated	0.295	3.333	1.655	0.380
All 13 integrated	0.284	2.908	1.457	0.188

Table 8.1. Total rms. noise for the full signal in the modified Stokes parameters from the 13 circle flights with 45° incidence angle from March 6th 2003. The circles are processed as single tracks, averaged as three circles, seven circles, and averaged totally.
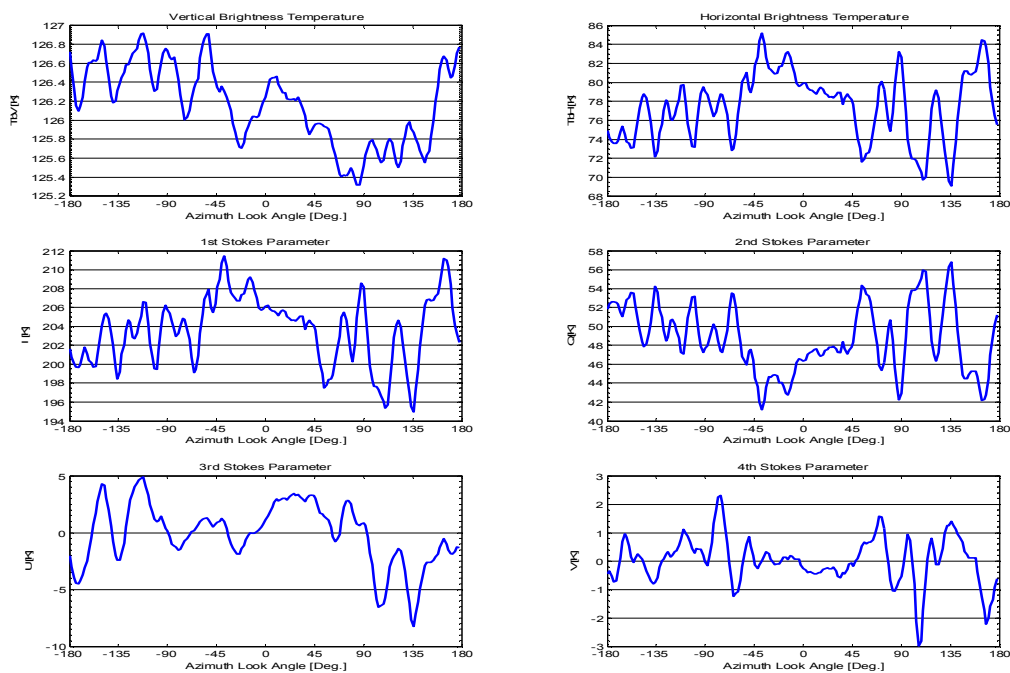
Figure 8.2. The Stokes parameters from the 1st circle flight track with 45° incidence angle from the March 6th 2003 flight.
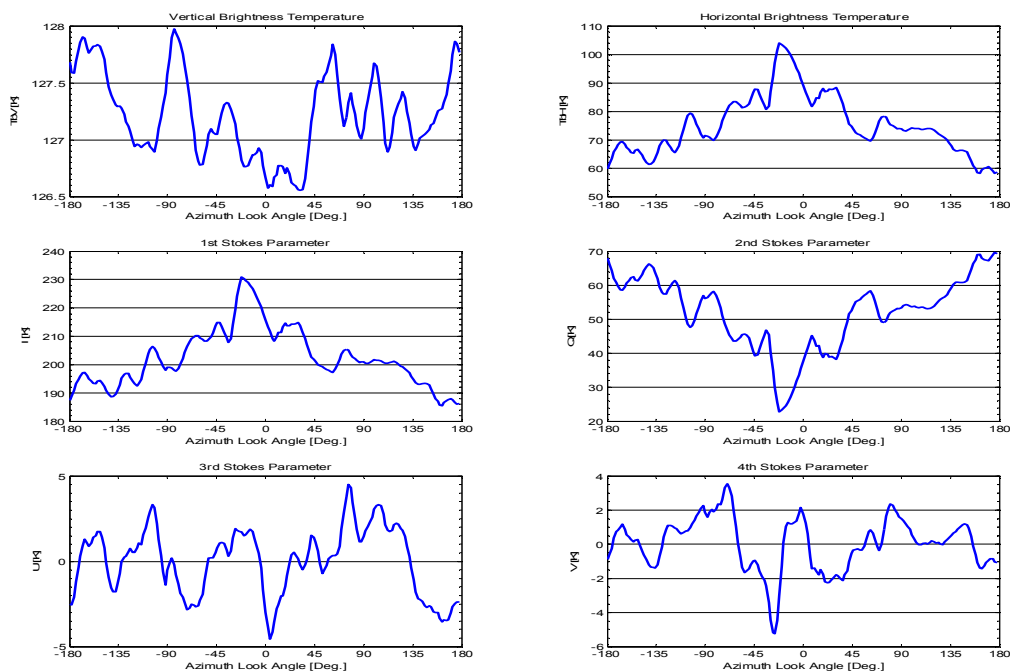

Figure 8.3. The Stokes parameters from the 2nd circle flight track with 45° incidence angle from the March 6th 2003 flight.
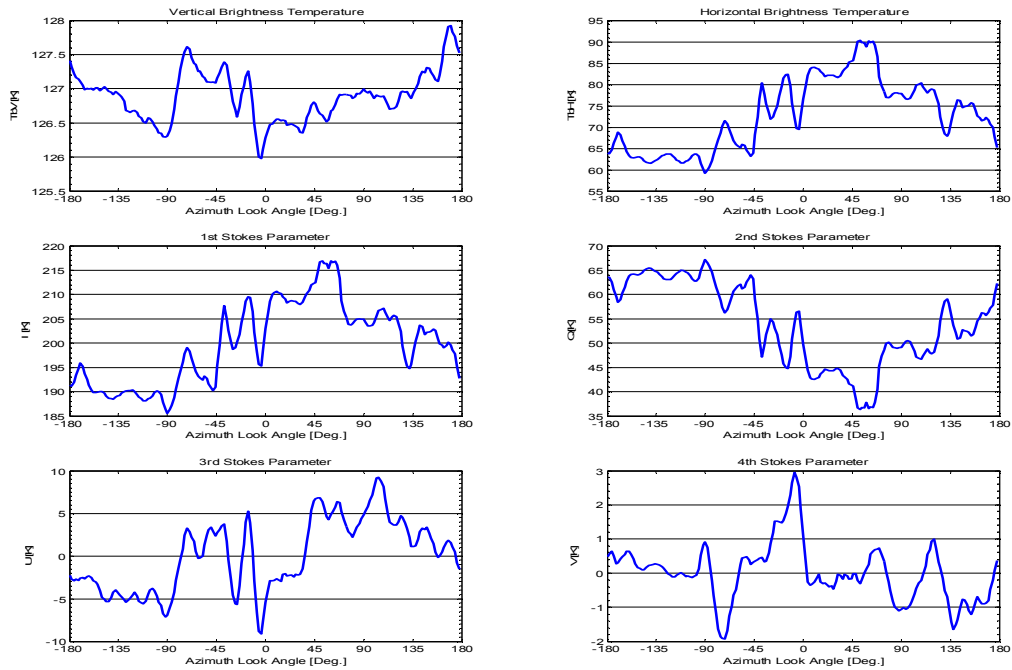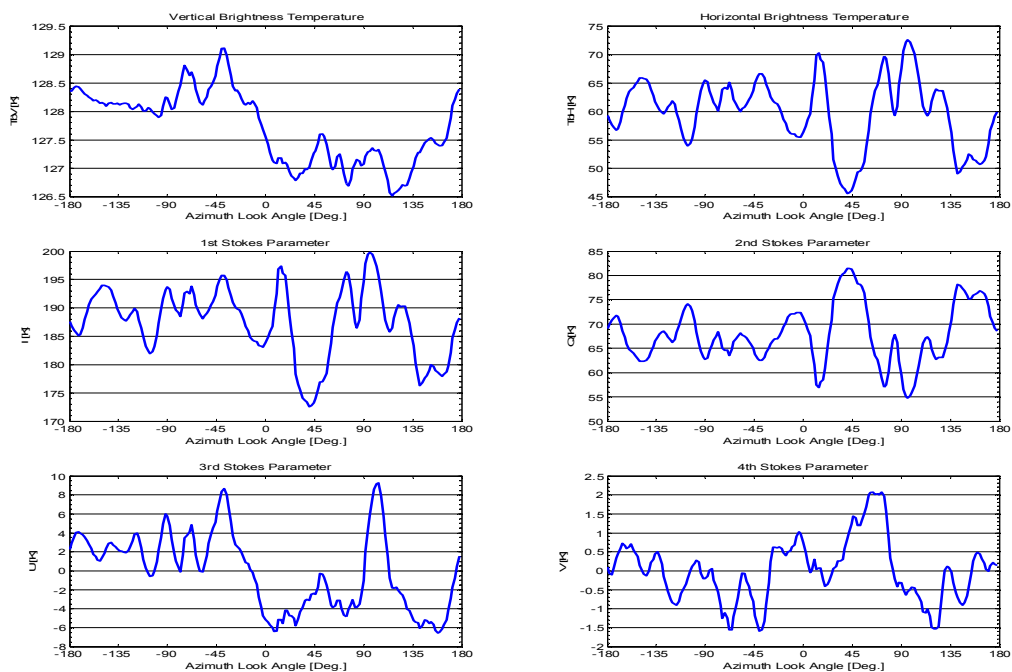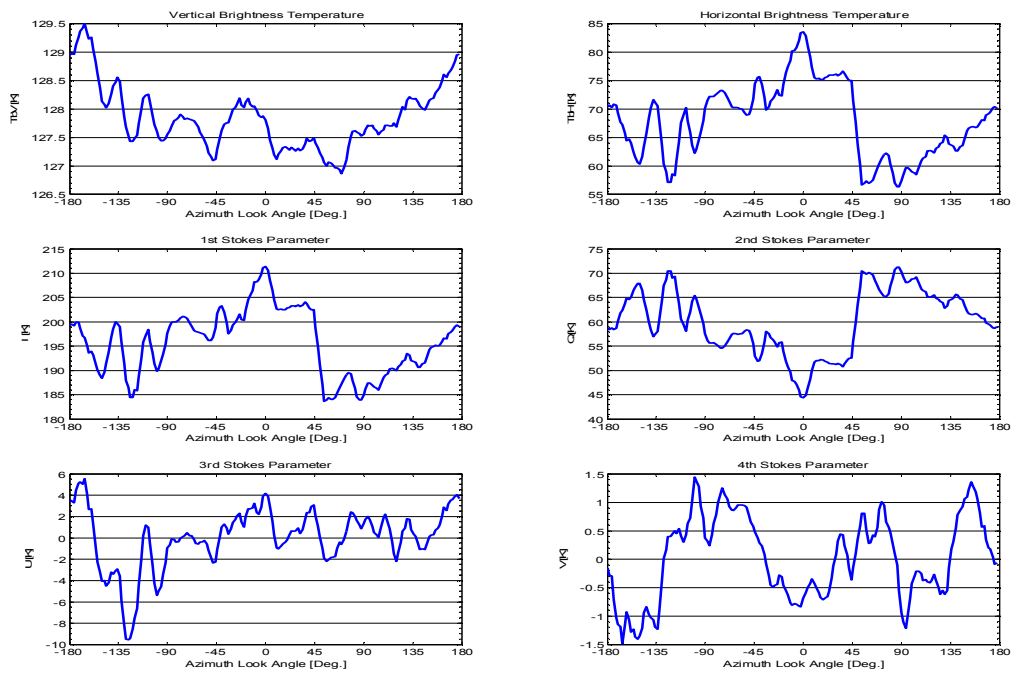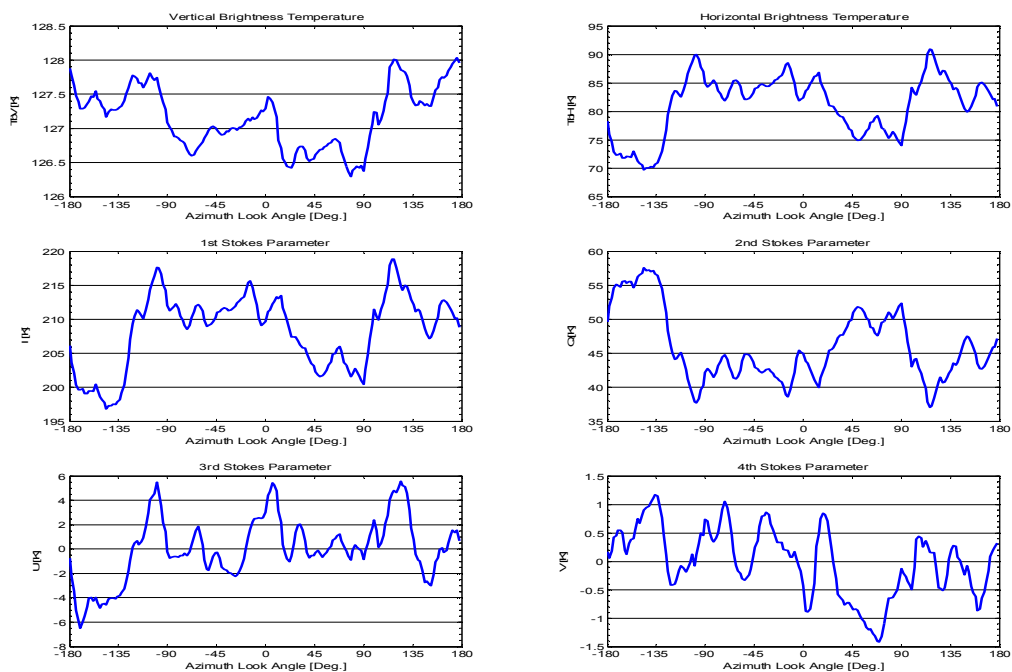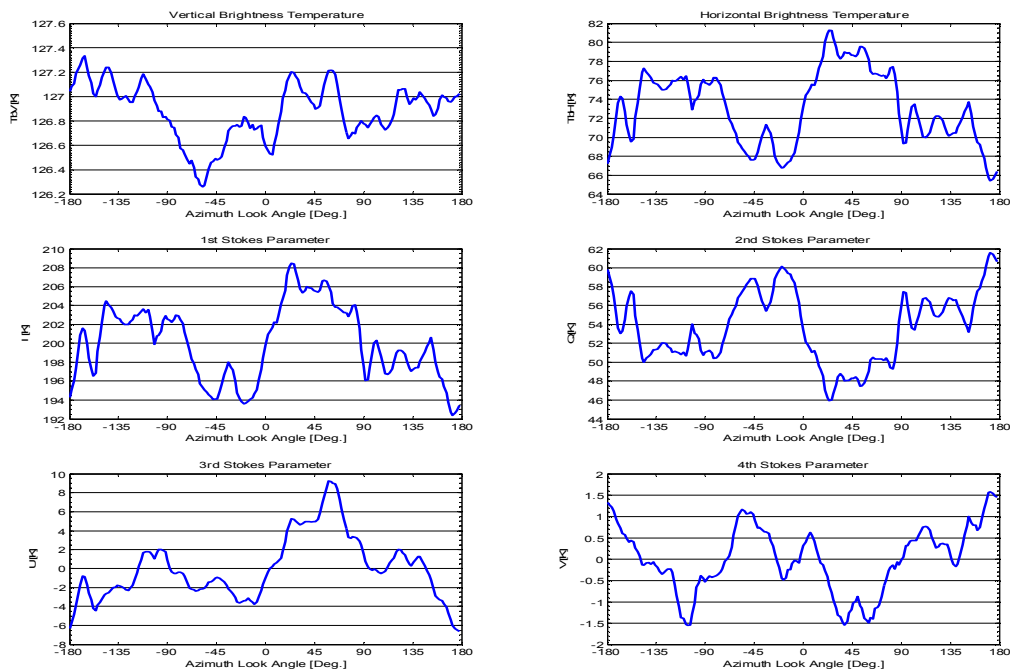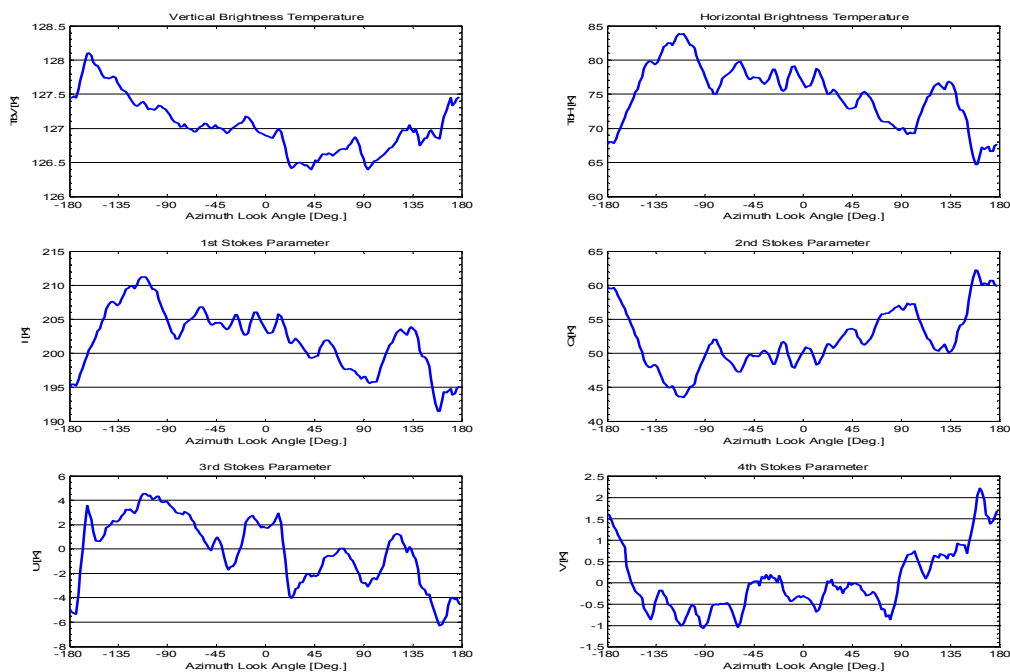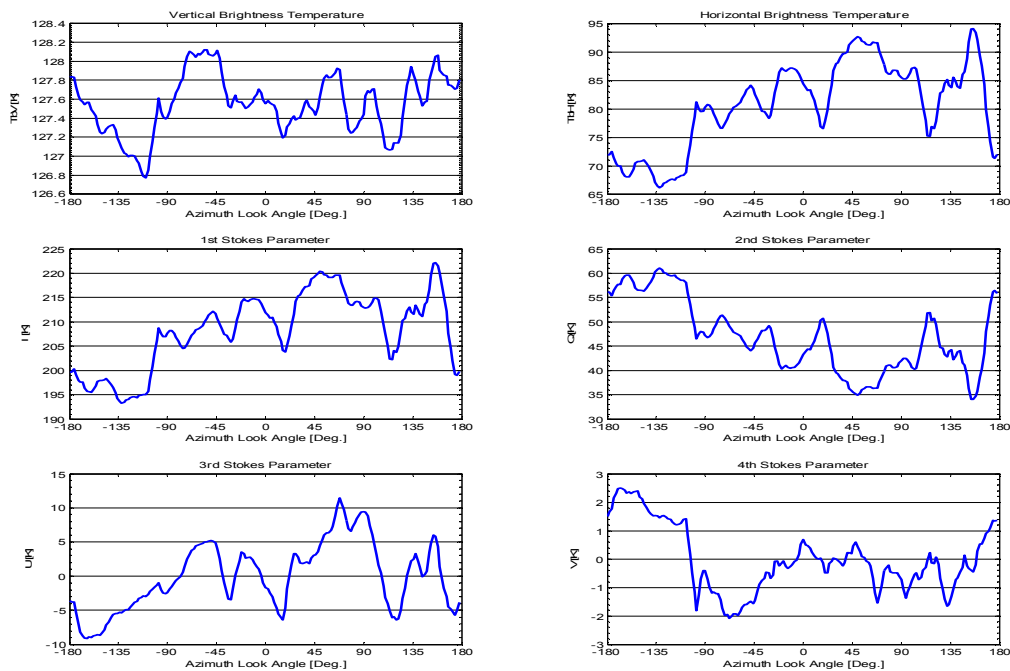
Figure 8.4. The Stokes parameters from the 3ʳᵈ circle flight track with 45° incidence angle from the March 6ᵗʰ 2003 flight.

Figure 8.5. The Stokes parameters from the 4ᵗʰ circle flight track with 45° incidence angle from the March 6ᵗʰ 2003 flight.

Figure 8.6. The Stokes parameters from the 5th circle flight track with 45° incidence angle from the March 6th 2003 flight.

Figure 8.7. The Stokes parameters from the 6th circle flight track with 45° incidence angle from the March 6th 2003 flight.

Figure 8.8. The Stokes parameters from the 7th circle flight track with 45° incidence angle from the March 6th 2003 flight.
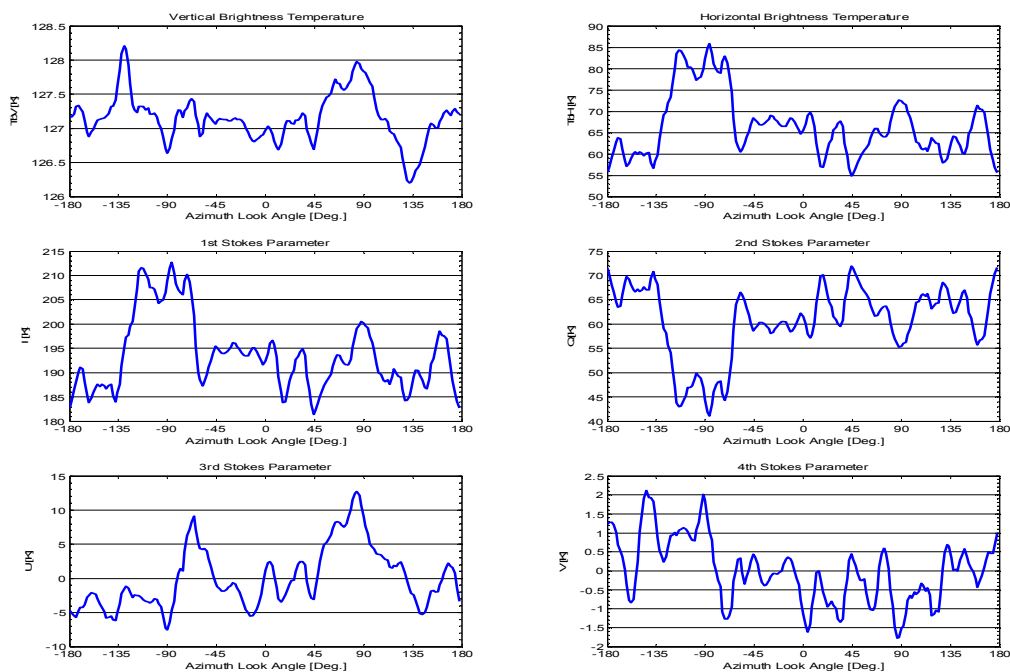

Figure 8.9. The Stokes parameters from the 8th circle flight track with 45° incidence angle from the March 6th 2003 flight.
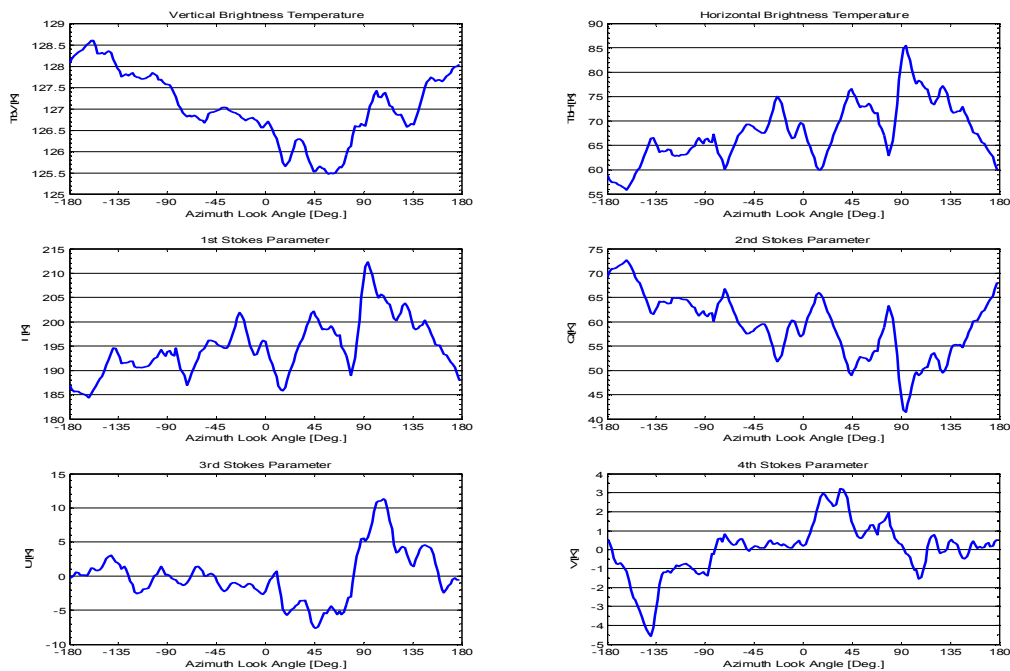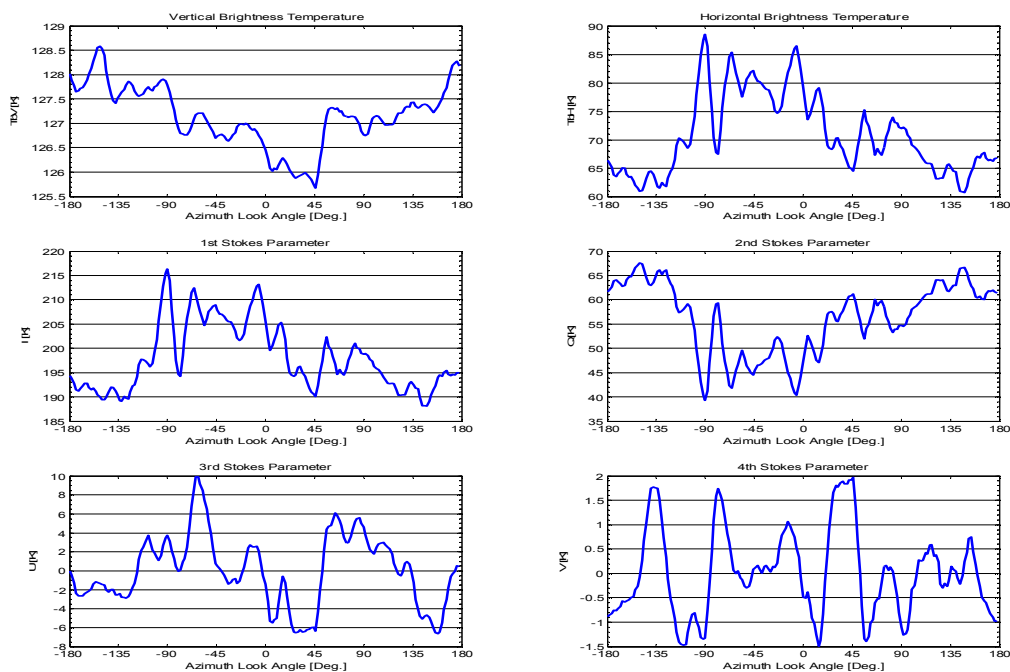
Figure 8.10. The Stokes parameters from the 9th circle flight track with 45° incidence angle from the March 6th 2003 flight.

Figure 8.11. The Stokes parameters from the 10th circle flight track with 45° incidence angle from the March 6th 2003 flight.
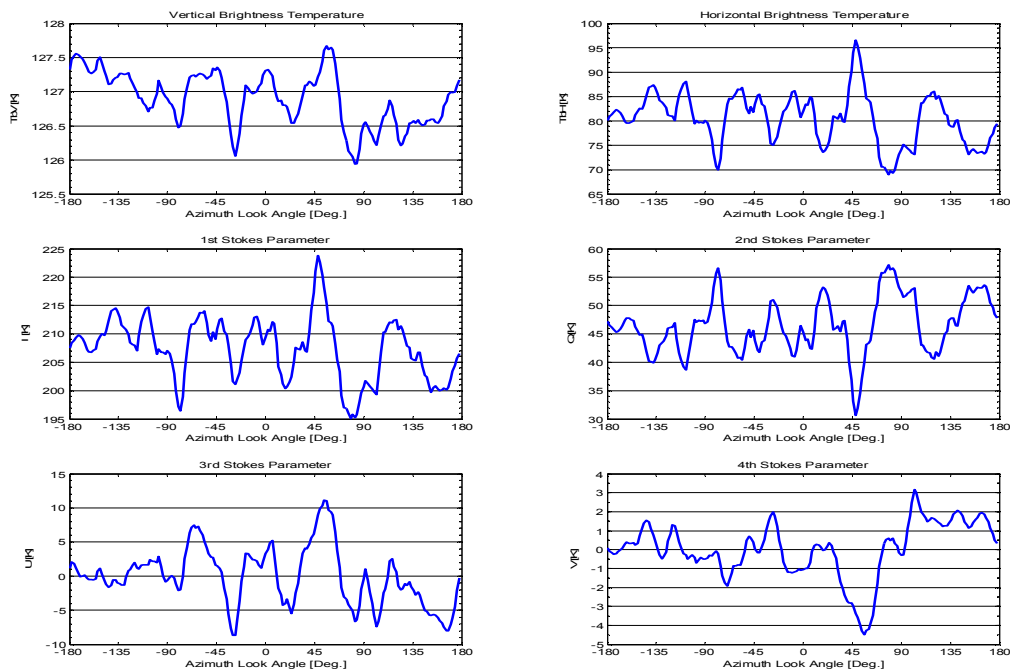
Figure 8.12. The Stokes parameters from the 11th circle flight track with 45° incidence angle from the March 6th 2003 flight.

Figure 8.13. The Stokes parameters from the 12th circle flight track with 45° incidence angle from the March 6th 2003 flight.

Figure 8.14. The Stokes parameters from the 13th circle flight track with 45° incidence angle from the March 6th 2003 flight.
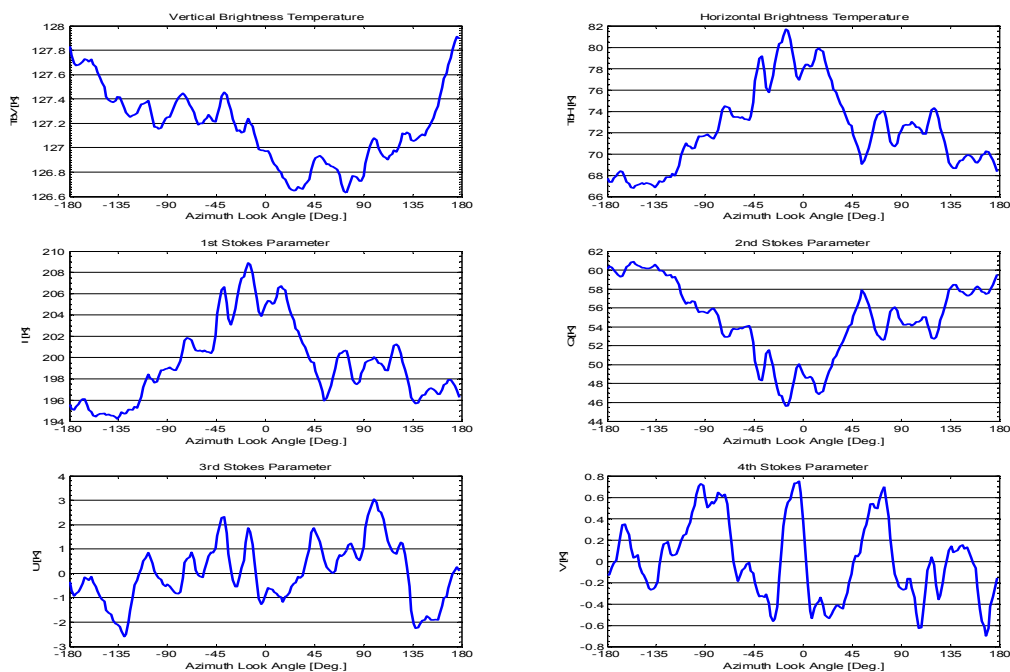

Figure 8.15. The averaged Stokes parameters from the 1st to the 6th circle flight tracks with 45° incidence angle from the March 6th 2003 flight.
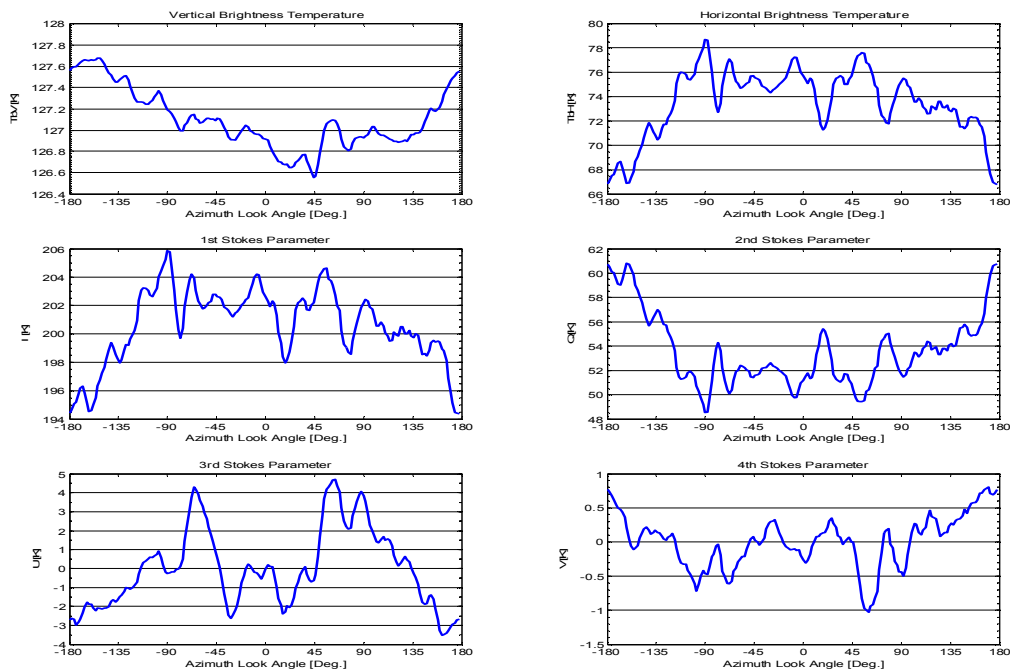
Figure 8.16. The averaged Stokes parameters from the 7th to the 13th circle flight tracks with 45° incidence angle from the March 6th 2003 flight.
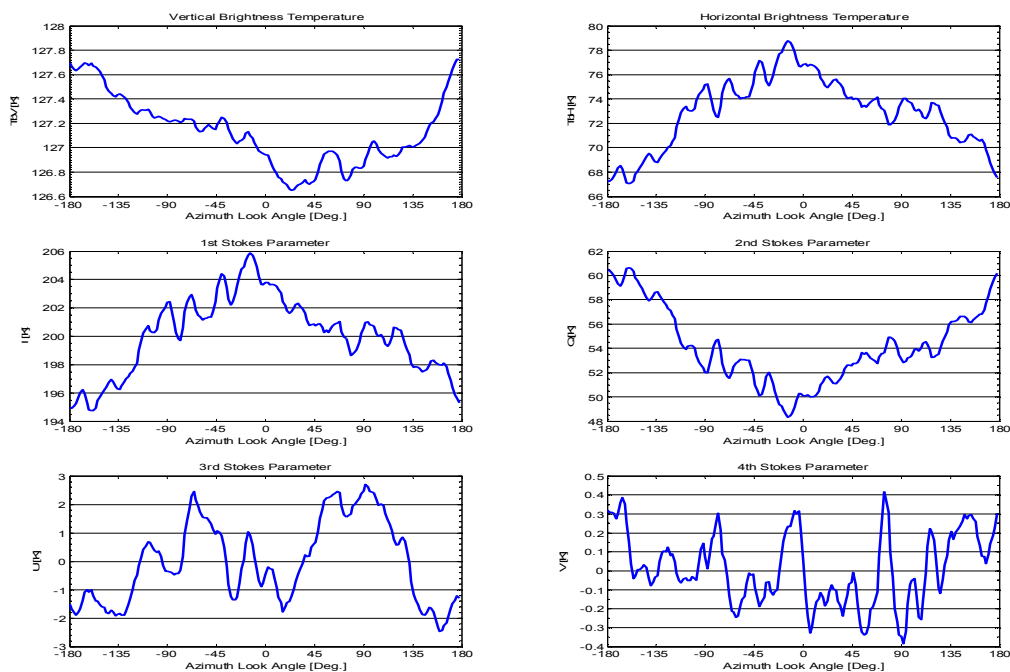

Figure 8.17. The averaged Stokes parameters from all 13 circle flight tracks with 45° incidence angle from the March 6th 2003 flight.
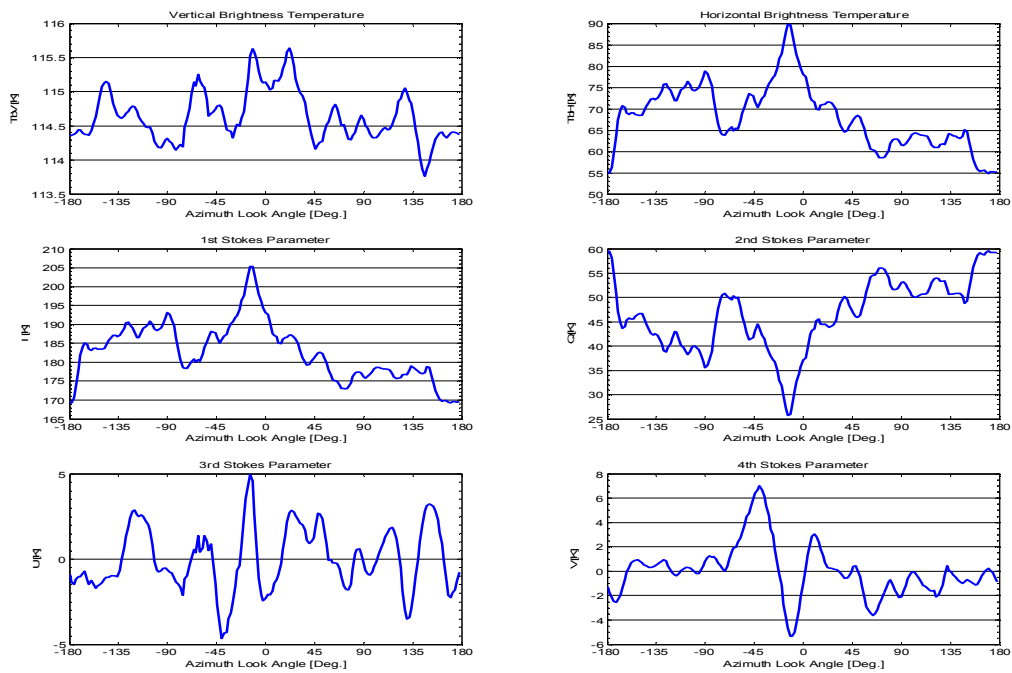
Figure 8.18. The Stokes parameters from the 1ˢᵗ circle flight track with 35° incidence angle from the March 6ᵗʰ 2003 flight.

Figure 8.19. The Stokes parameters from the 2ⁿᵈ circle flight track with 35° incidence angle from the March 6ᵗʰ 2003 flight.

Figure 8.20. The Stokes parameters from the 3rd circle flight track with 35° incidence angle from the March 6th 2003 flight.

Figure 8.21. The Stokes parameters from the 4th circle flight track with 35° incidence angle from the March 6th 2003 flight.
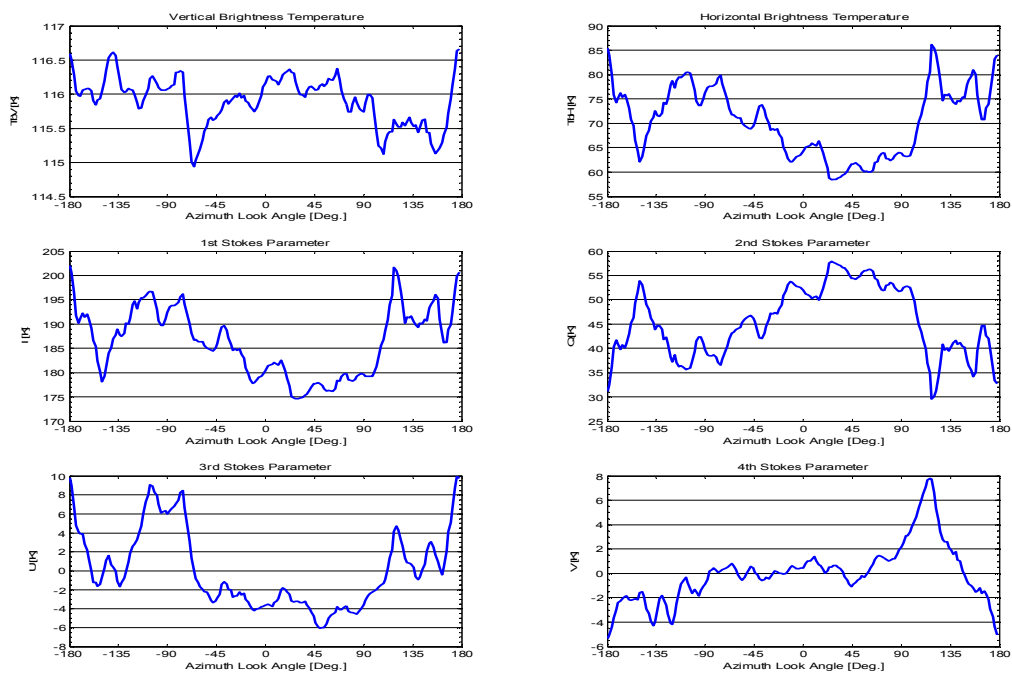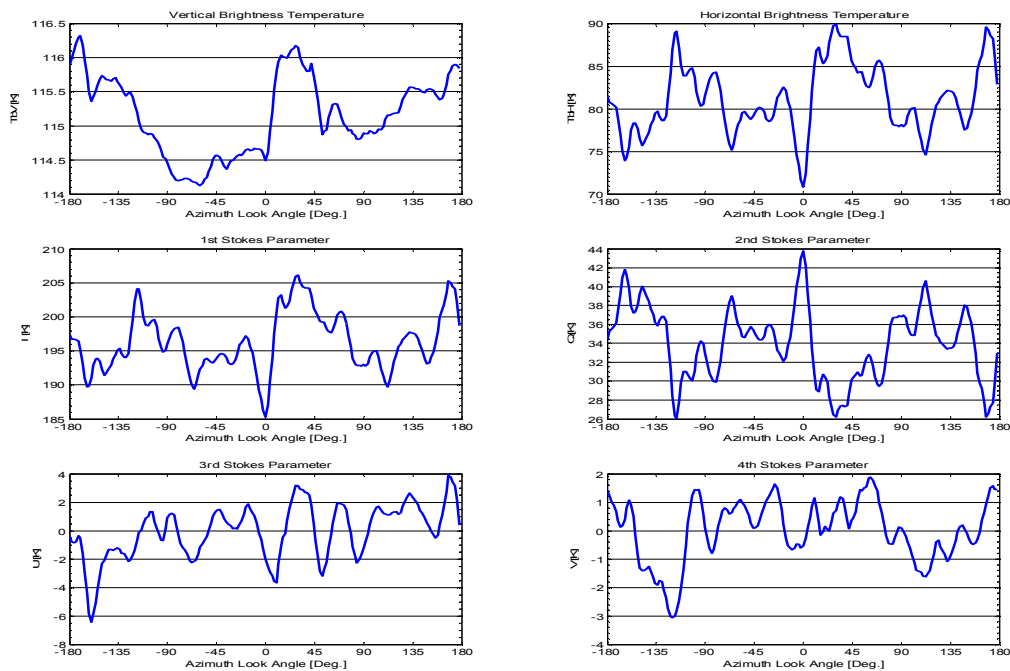
Figure 8.22. The Stokes parameters from the 5th circle flight track with 35° incidence angle from the March 6th 2003 flight.

Figure 8.23. The Stokes parameters from the 6th circle flight track with 35° incidence angle from the March 6th 2003 flight.

Figure 8.24. The Stokes parameters from the 7th circle flight track with 35° incidence angle from the March 6th 2003 flight.
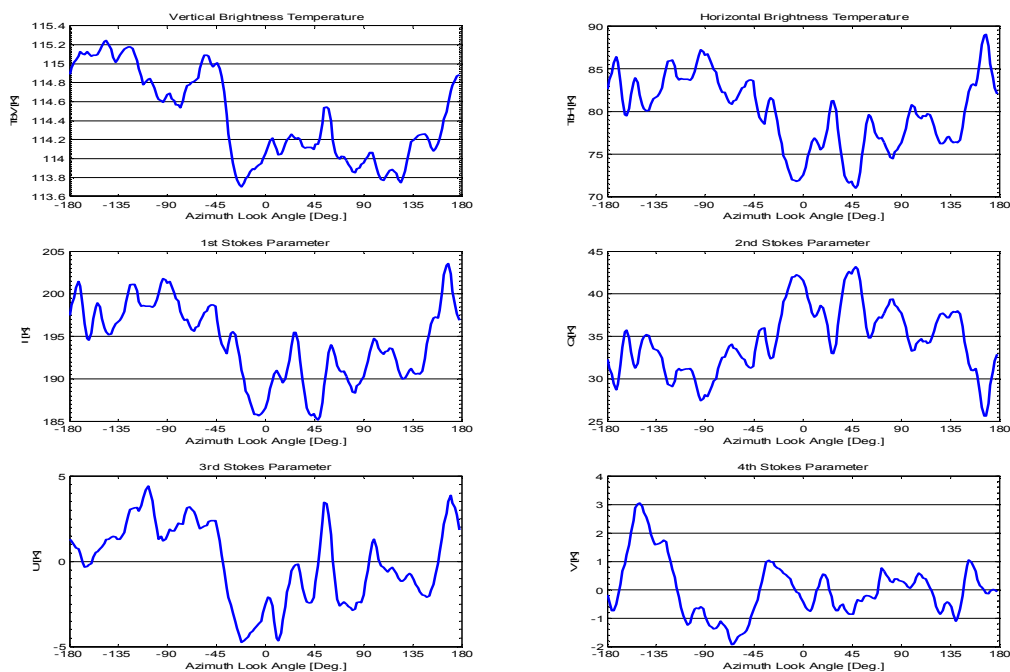

Figure 8.25. The Stokes parameters from the 8th circle flight track with 35° incidence angle from the March 6th 2003 flight.

Figure 8.26. The Stokes parameters from the 9th circle flight track with 35° incidence angle from the March 6th 2003 flight.
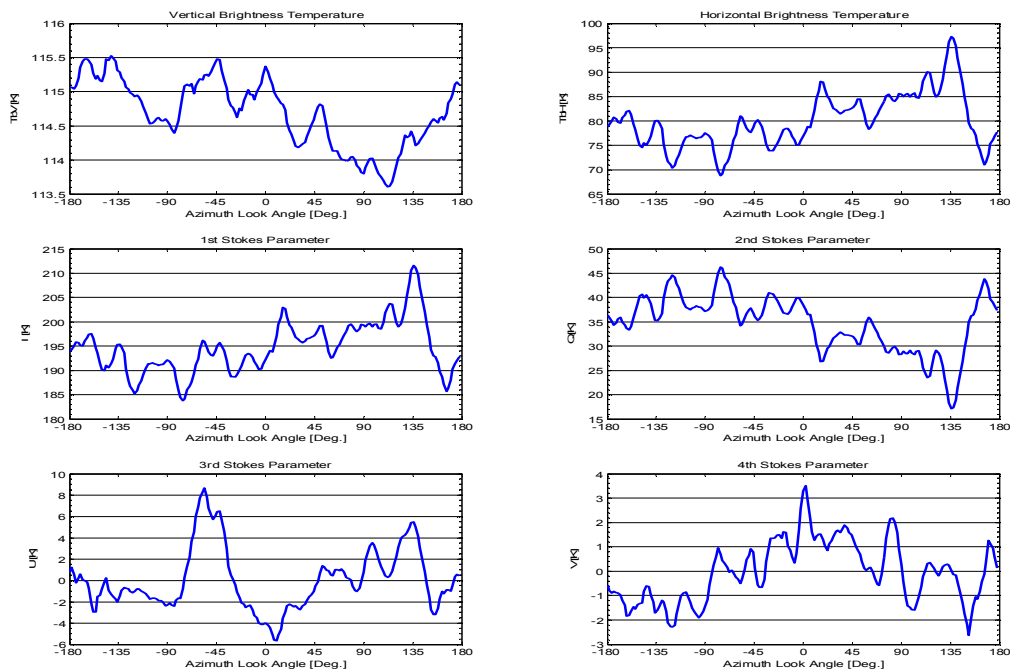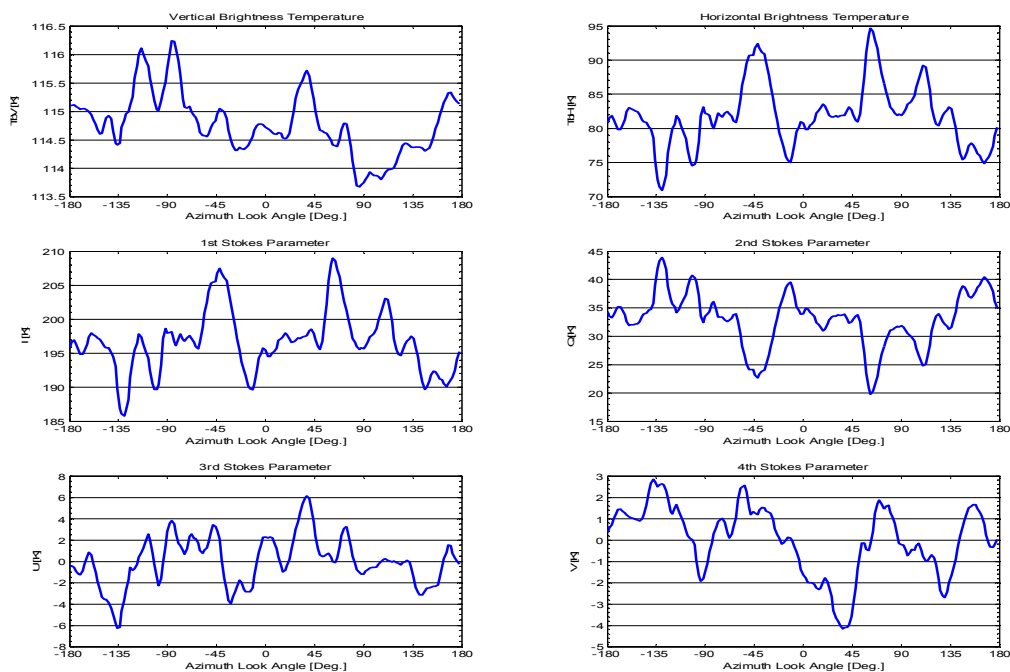

Figure 8.27. The Stokes parameters from the 10th circle flight track with 35° incidence angle from the March 6th 2003 flight.
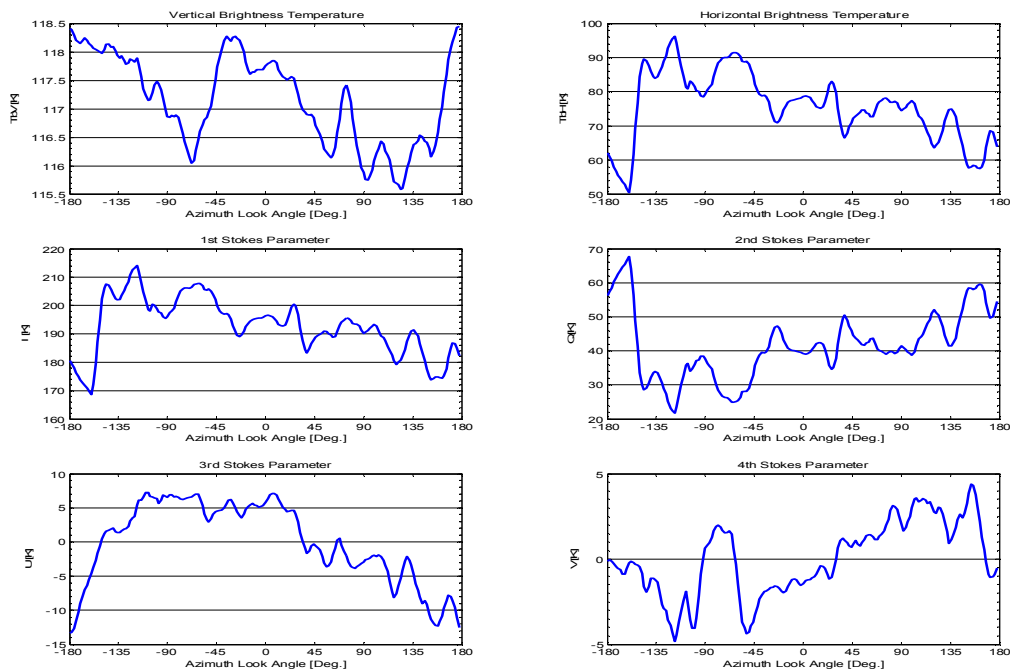
Figure 8.28. The Stokes parameters from the 11th circle flight track with 35° incidence angle from the March 6th 2003 flight.
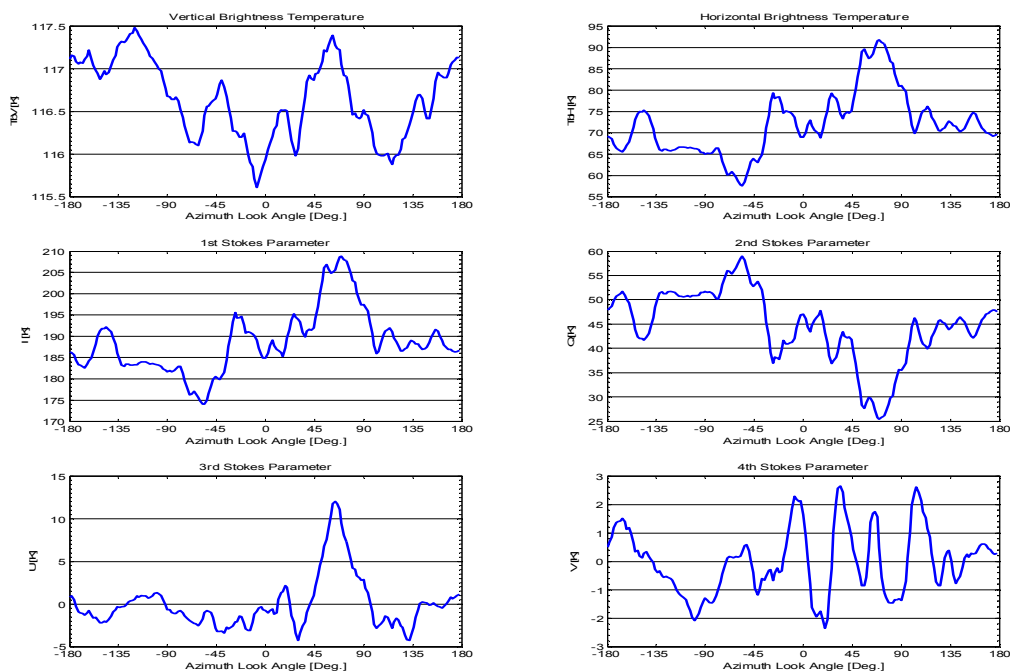
Figure 8.29. The Stokes parameters from the 12th circle flight track with 35° incidence angle from the March 6th 2003 flight.
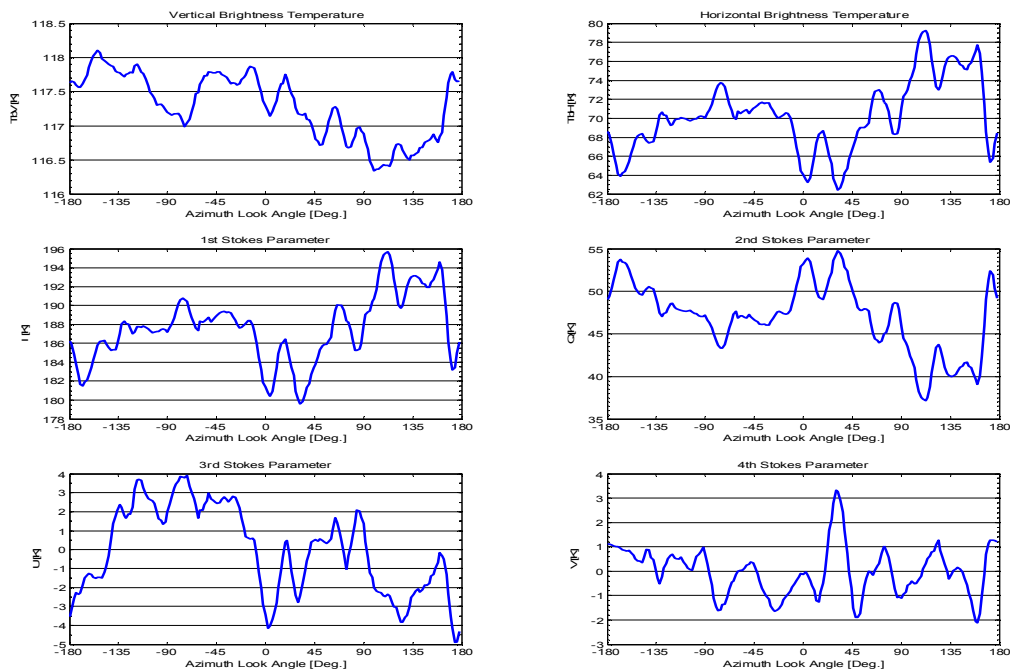
Figure 8.30. The Stokes parameters from the 13th circle flight track with 35° incidence angle from the March 6th 2003 flight.
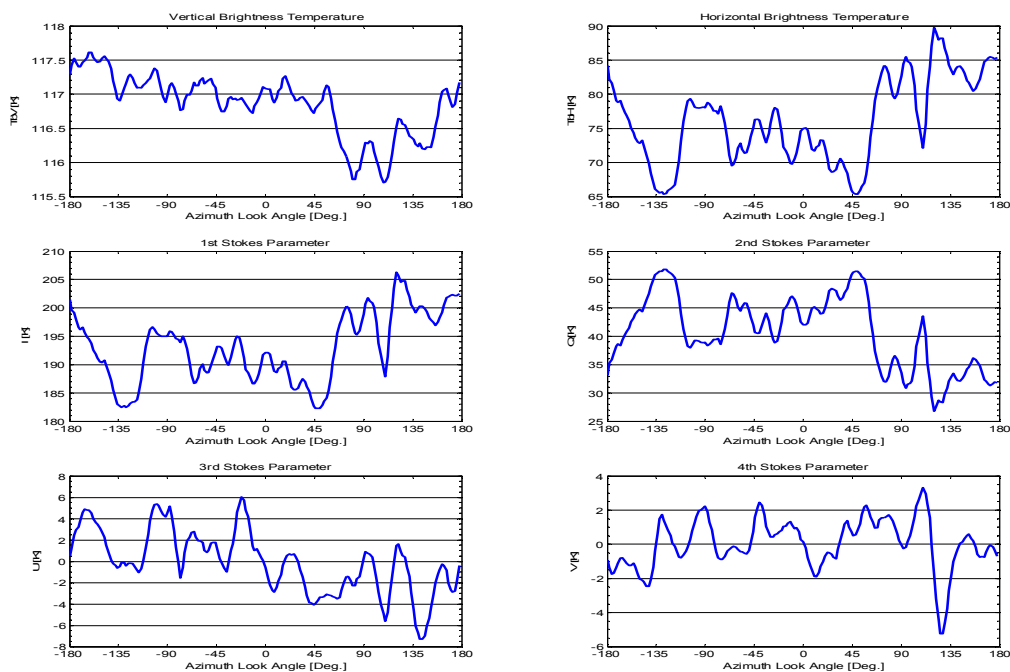
Figure 8.31. The Stokes parameters from the 14th circle flight track with 35° incidence angle from the March 6th 2003 flight.
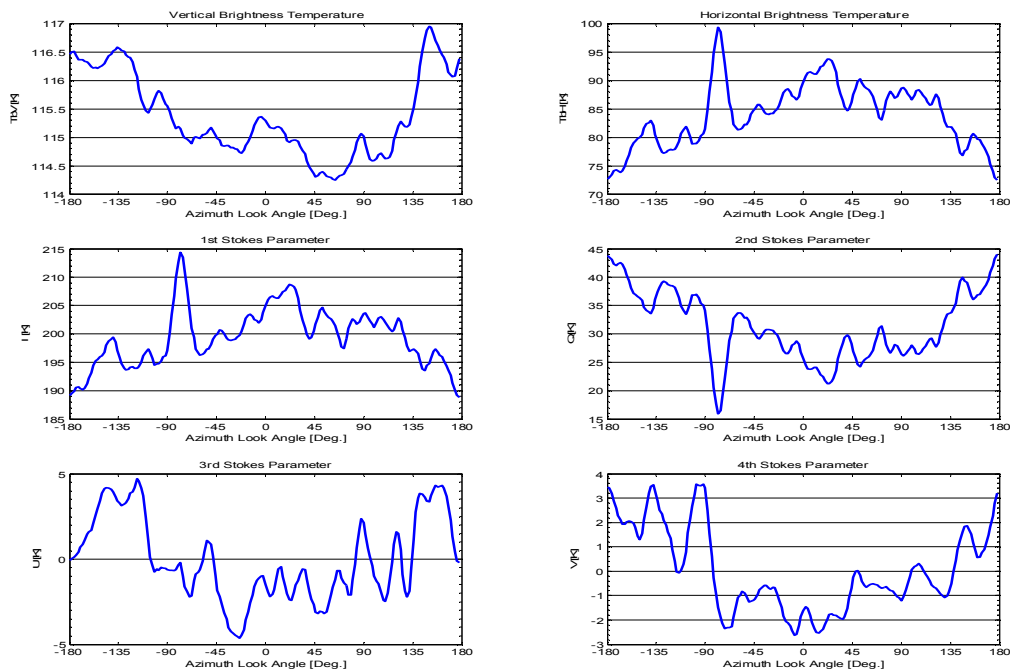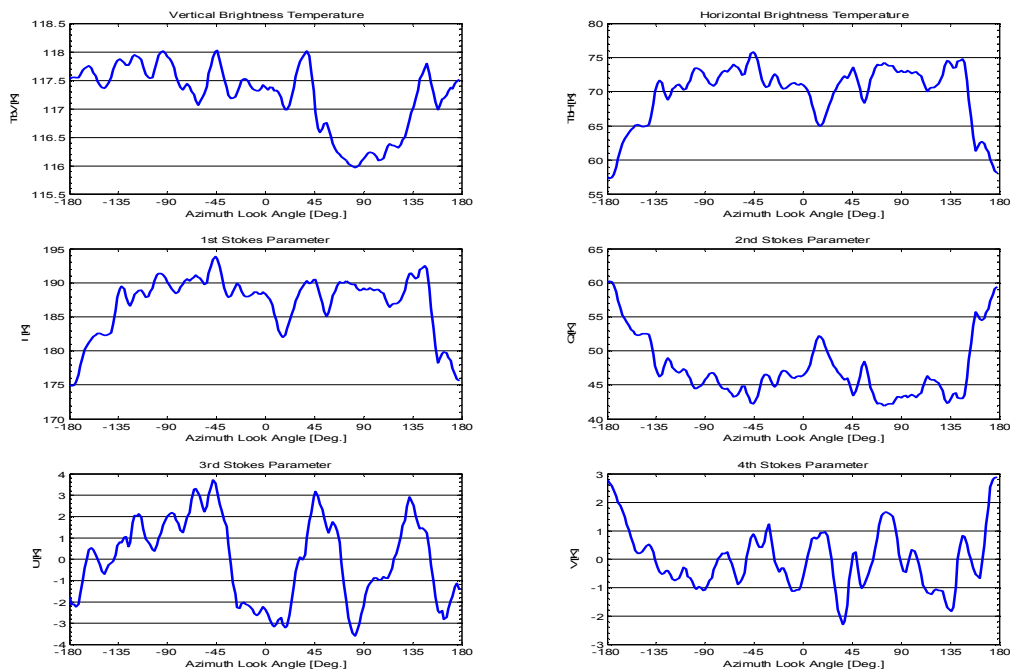
Figure 8.32. The Stokes parameters from the 15th circle flight track with 35° incidence angle from the March 6th 2003 flight.
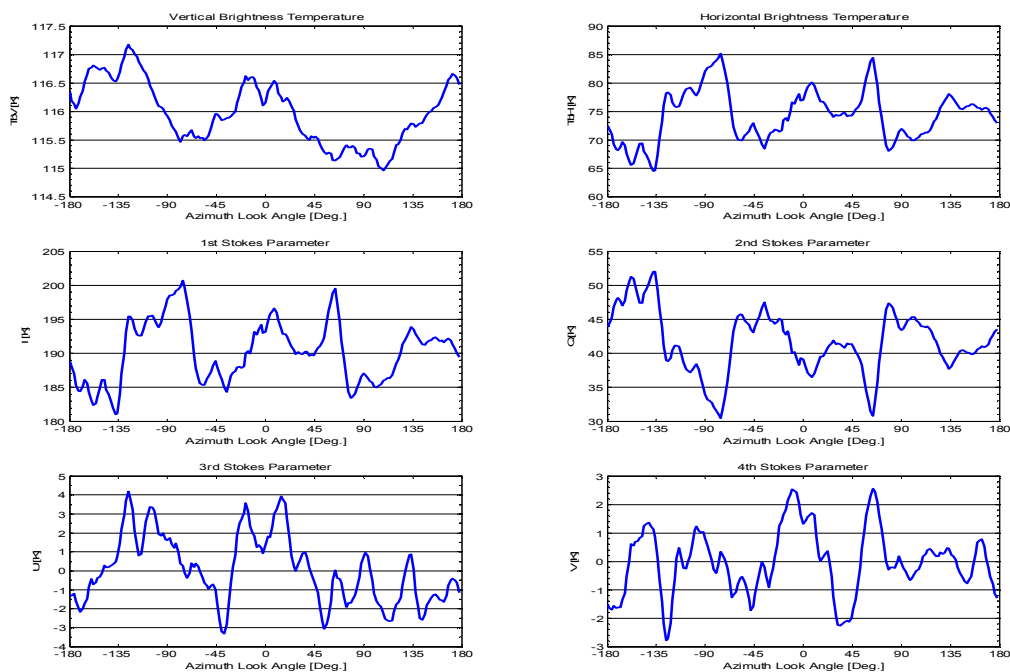
Figure 8.33. The Stokes parameters from the 16th circle flight track with 35° incidence angle from the March 6th 2003 flight.
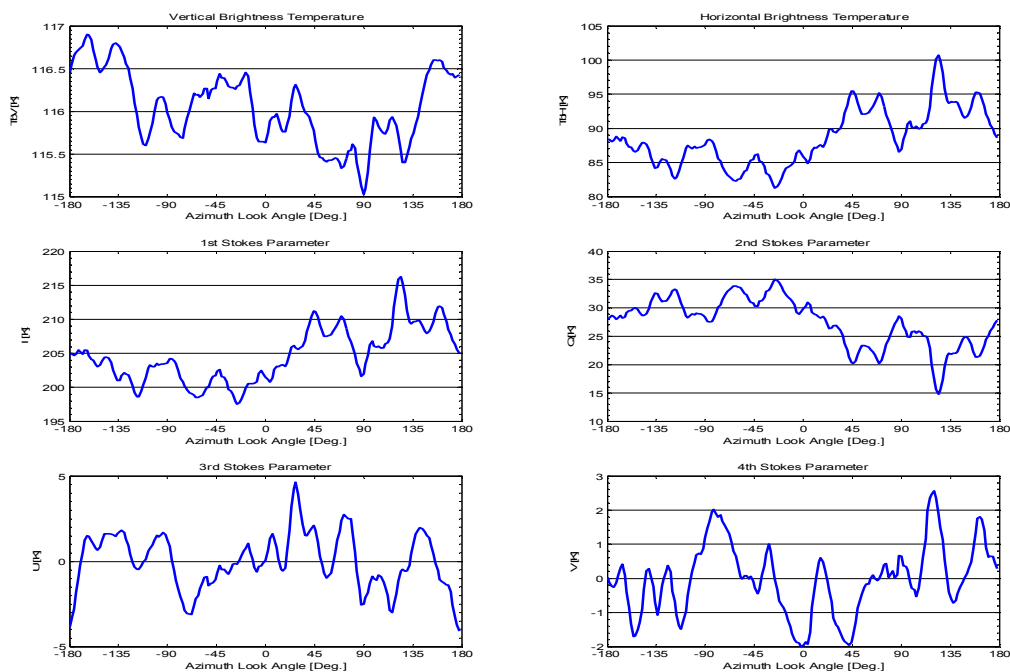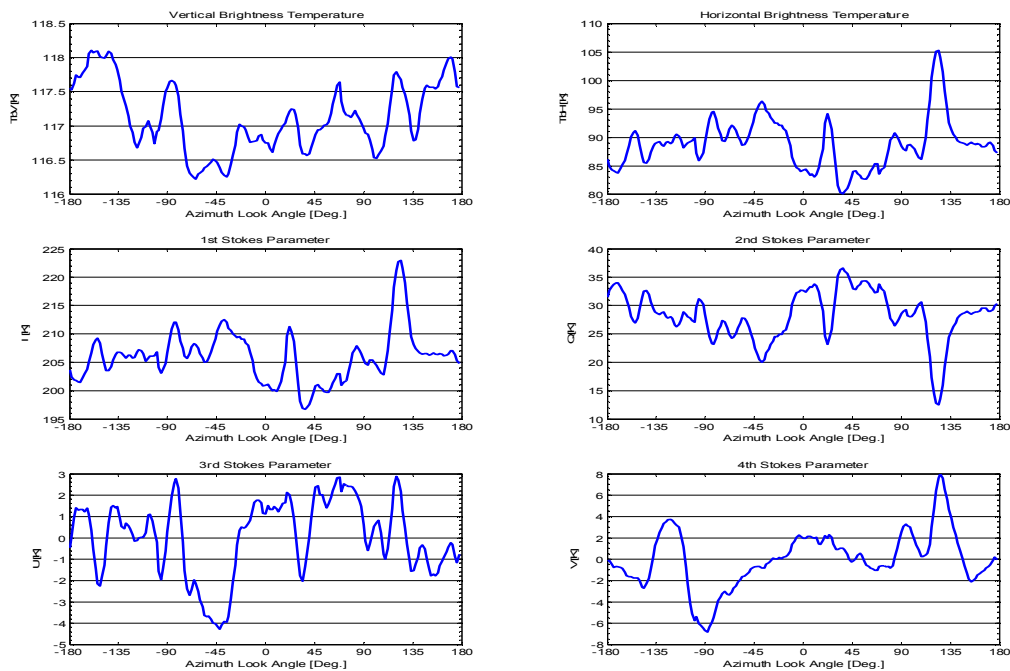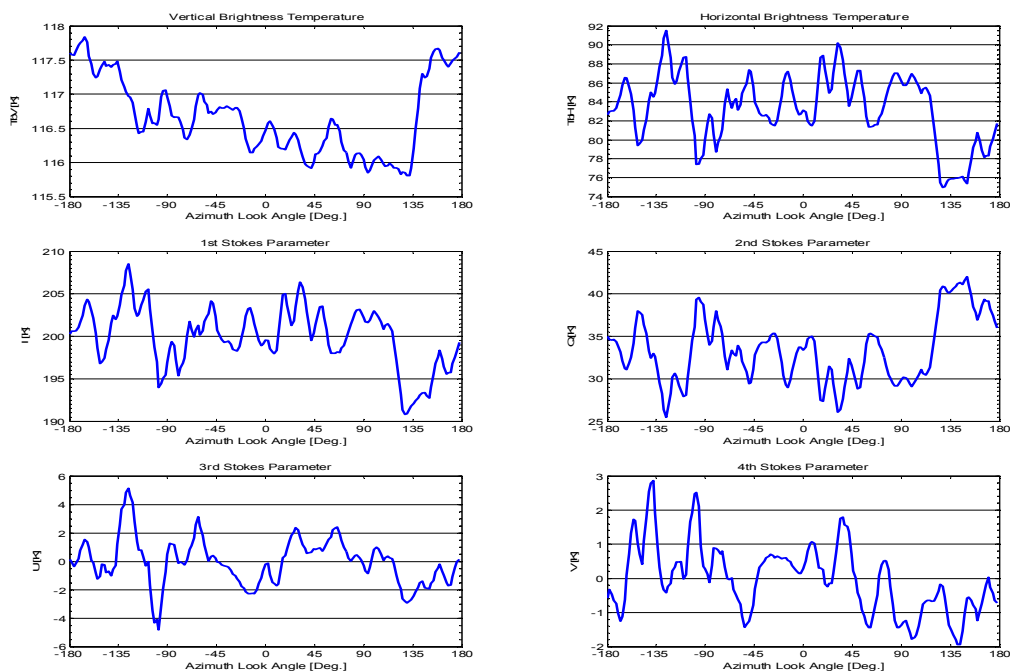
Figure 8.34. The averaged Stokes parameters from the 1ˢᵗ to the 8ᵗʰ circle flight tracks with 35° incidence angle from the March 6ᵗʰ 2003 flight.

Figure 8.35. The averaged Stokes parameters from the 9ˢᵗ to the 16ᵗʰ circle flight tracks with 35° incidence angle from the March 6ᵗʰ 2003 flight.
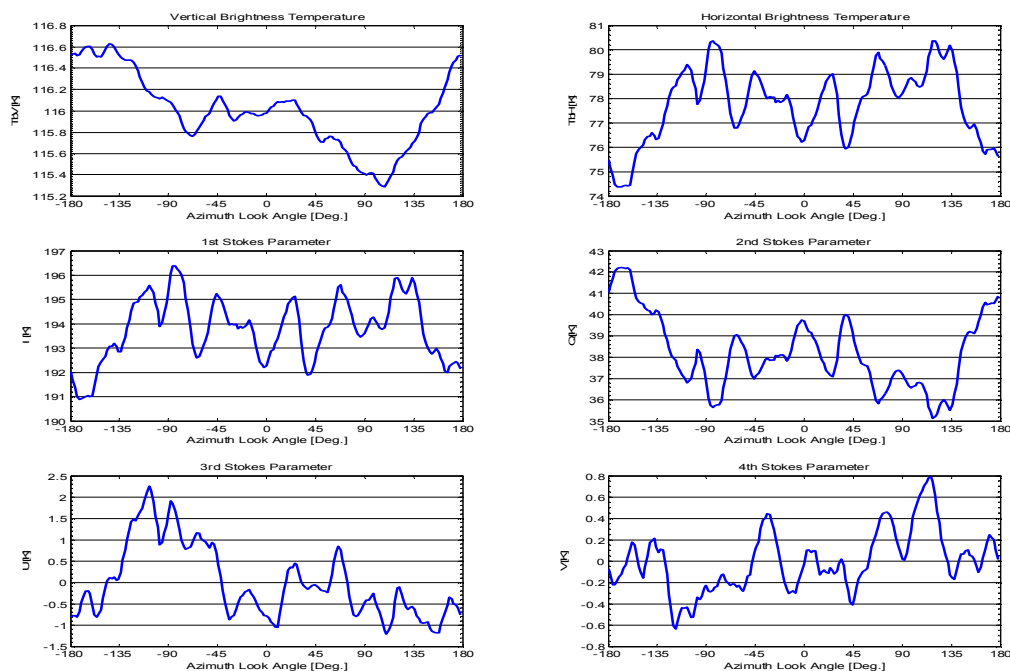
Figure 8.36. The averaged Stokes parameters from all 16 circle flight tracks with 35° incidence angle from the March 6th 2003 flight.
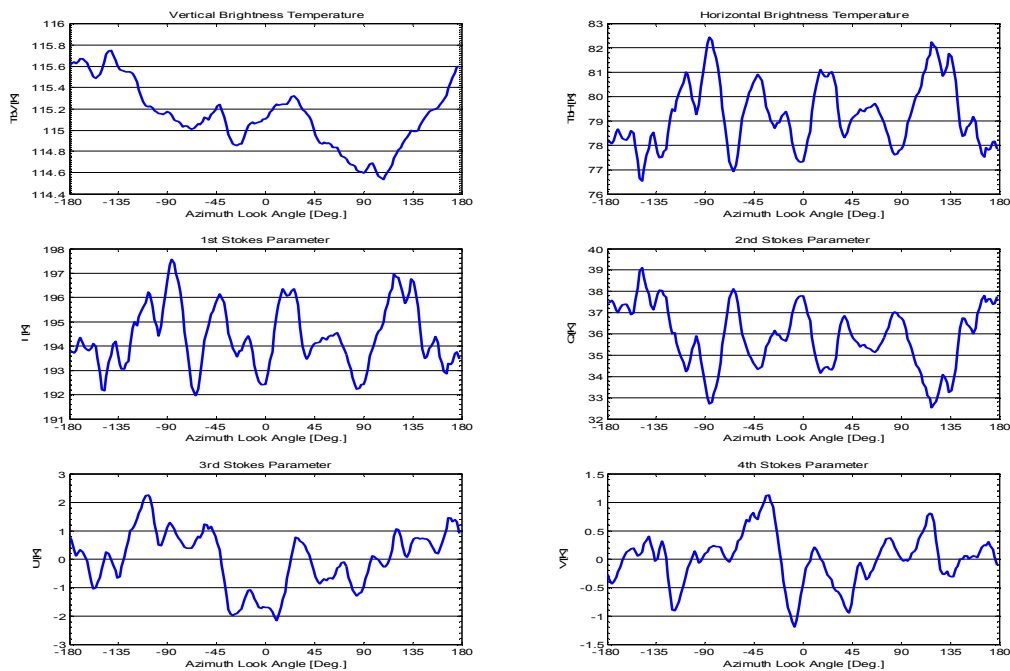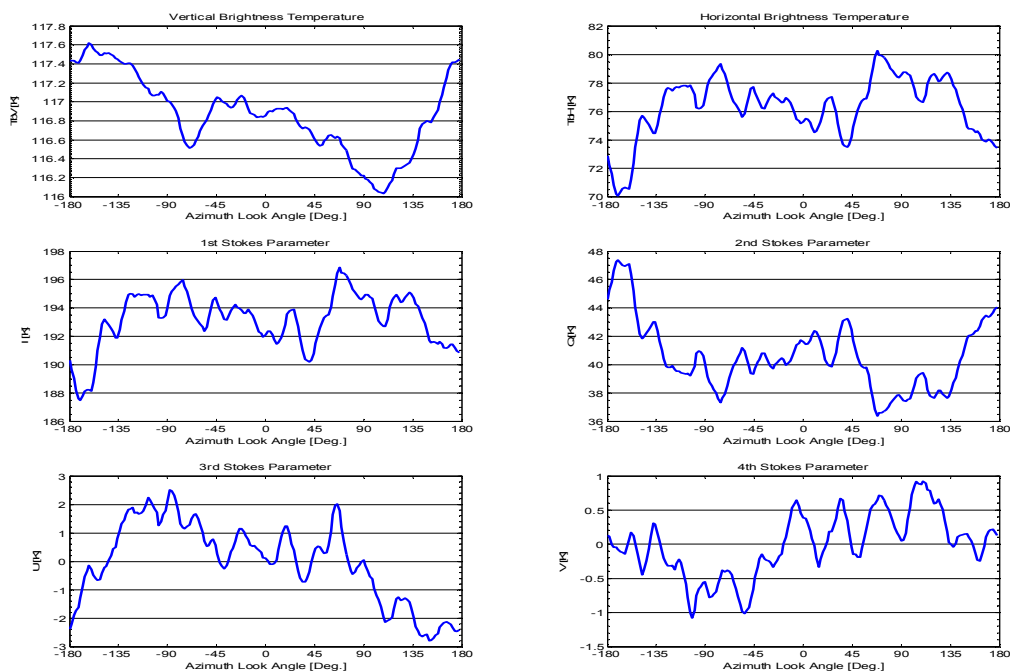
Generally it is noticed, that the noise level is significantly above the level seen for the previous flights, and it is especially noticed, that the noise for the horizontal polarization has increased. This may be due to the stronger wind, and also a result of a fully developed sea state, as the wind had been stable for many hours, and as the test site was located in the Northern Atlantic, having a water depth of several kilometers. This should be compared to the relatively low depth in the North Sea and in Kattegat, being only in the order of 20 meters.

For the circles with 35° incidence angle, the same analysis of root-mean-square noise has been carried out, and table 8.2 shows the results. As it was shown for 45° incidence angle, the general noise has increased compared to the previous flights, and especially the horizontal channel shows large values. The integration gain almost reaches the expected values, 2.00, 1.41, and 1.41, respectively, for the horizontal polarization and for the 3rd and 4th Stokes parameters, and again the vertical polarization is the only one, which has very poor improvement. The reduced improvement is corresponds to a non-Gaussian signal of 294 mK within the signal. It is noticed, that the order of magnitude is comparable to the result from the 45° incidence angle, and it is also noticed, that a signal of this size will be masked within the noise of the horizontal channel, thus being impossible to identify within the present data.

Table 8.3 contains a harmonic analysis of the fully integrated signatures, and the theory of some systematic signal within the vertical polarization seems to be confirmed by the consistence in the 1st harmonic. The expected phase for a straight North wind direction is expected to be 0, but this is obviously not the case. The statistical material is too small to conclude, however, and for the remaining parameters it is hard to find any systematic effect.

Circles	TV, std.dev. [K]	TH, std.dev. [K]	U, std.dev. [K]	V, std.dev. [K]
Single circles	0.376	7.479	1.862	2.172
35° incidence angle	0.360	7.064	4.106	2.395
	0.580	4.054	1.910	1.089
	0.471	4.258	2.322	1.011
	0.496	5.578	2.923	1.255
	0.547	4.616	2.295	1.617
	0.737	5.574	2.431	1.727
	0.433	4.147	1.646	1.037
	0.505	4.420	1.779	2.675
	0.561	3.652	1.651	1.014
	0.797	10.075	5.896	2.185
	0.458	7.397	3.091	1.157
	0.472	3.790	2.290	0.990
	0.455	6.215	2.918	1.484
	0.581	4.342	1.954	1.054
	0.552	4.508	1.785	1.152
Average, single	0.524	5.448	2.554	1.501
4 circles	0.265	2.913	1.572	0.747
integrated	0.421	3.203	0.971	0.613
	0.437	3.137	1.822	0.911
	0.454	2.878	1.450	0.495
Average, 4 integrated	0.394	3.033	1.454	0.691
8 integrated	0.303	1.357	1.005	0.447
	0.413	2.156	1.409	0.460
Average, 8 integrated	0.358	1.757	1.207	0.454
All 16 integrated	0.352	1.498	0.852	0.286

Table 8.2. Total rms. noise for the full signal in the modified Stokes parameters from the 16 circle flights with 35° incidence angle from March 6th 2003. The circles are processed as single tracks, averaged as 4 times four circles, 2 times eight, and averaged totally.

Inc.	Harm.	TV, M.	TV, Ph.	TH, M.	TH, Ph.	U, Mag.	U, Ph.	V, Mag.	V, Ph.
45°	1	0.36	141.01	3.71	-0.18	1.04	-34.80	0.13	165.67
	2	0.10	0.57	1.11	111.83	1.43	171.72	0.09	32.21
	3	0.12	137.18	0.90	-22.01	0.60	128.11	0.02	-95.80
	4	0.04	14.85	0.43	43.61	0.16	-41.47	0.07	39.90
35°	1	0.36	120.45	0.66	-24.49	0.77	79.43	0.22	-99.21
	2	0.33	-34.87	1.52	158.15	0.72	-154.03	0.11	99.15
	3	0.04	-177.50	0.71	-29.71	0.29	-97.27	0.18	85.64
	4	0.03	140.22	0.30	138.01	0.10	129.73	0.06	-106.35

Table 8.3. 1st, 2nd, 3rd, and 4th harmonic components in the averaged modified Stokes parameters from the circle flights from March 6th 2003.

The last data set from the March 6th 2003 flight is the level flight set. Eight legs, each 2 minutes long, were measured at different headings, and the tracks, integrated to 1 sec. points, are shown in the figures 8.37 to 8.44. The horizontal axis shows the time-of-day of the data acquisition, and it is noticed, that all tracks show some kind of periodic variation, the period in some cases being up to 1 minute.

Figure 8.37. The modified Stokes parameters from the level flight track from March 6th 2003, 50° incidence angle, heading -62°.

Figure 8.38. The modified Stokes parameters from the level flight track from March 6th 2003, 50° incidence angle, heading -172°.

Figure 8.39. The modified Stokes parameters from the level flight track from March 6th 2003, 50° incidence angle, heading +36°.

Figure 8.40. The modified Stokes parameters from the level flight track from March 6th 2003, 50° incidence angle, heading -100°.

Figure 8.41. The modified Stokes parameters from the level flight track from March 6th 2003, 50° incidence angle, heading +144°.

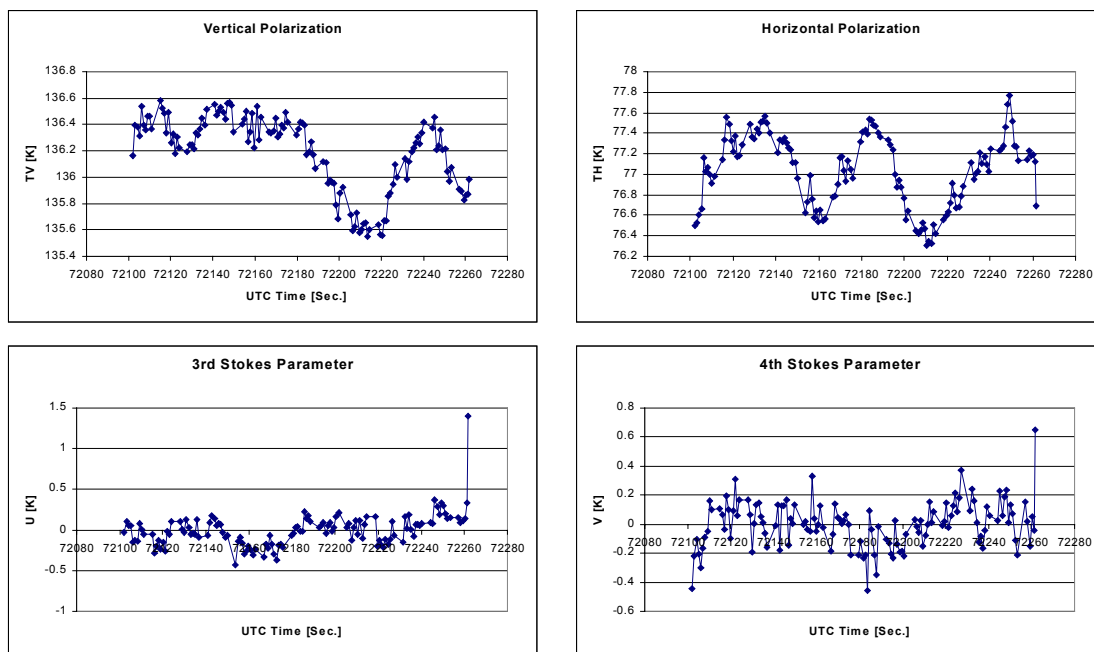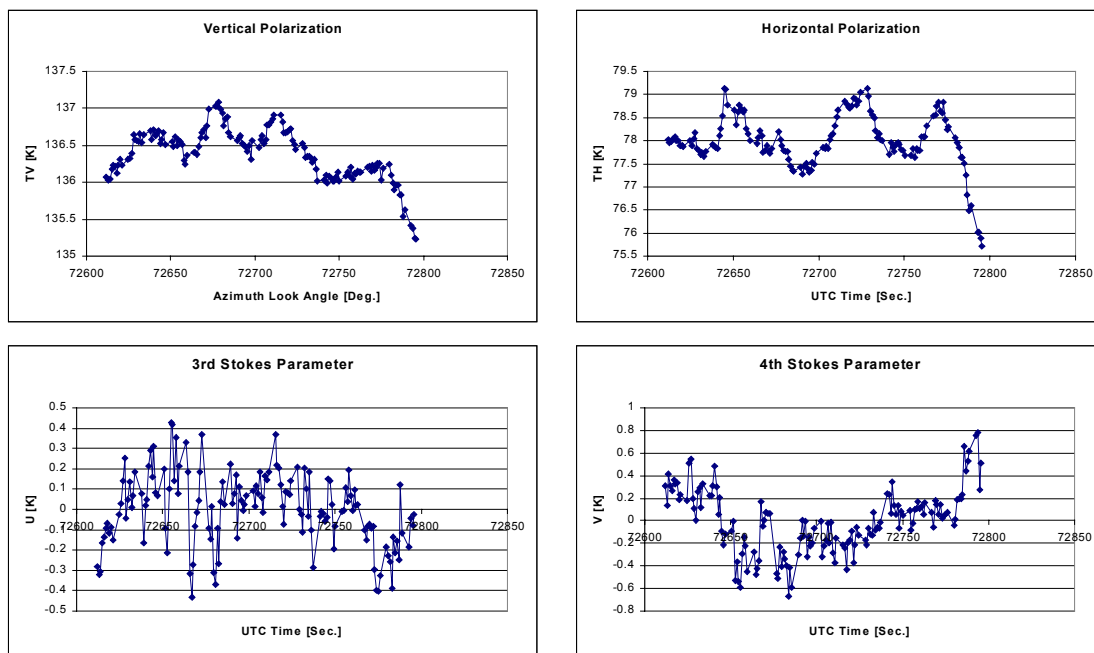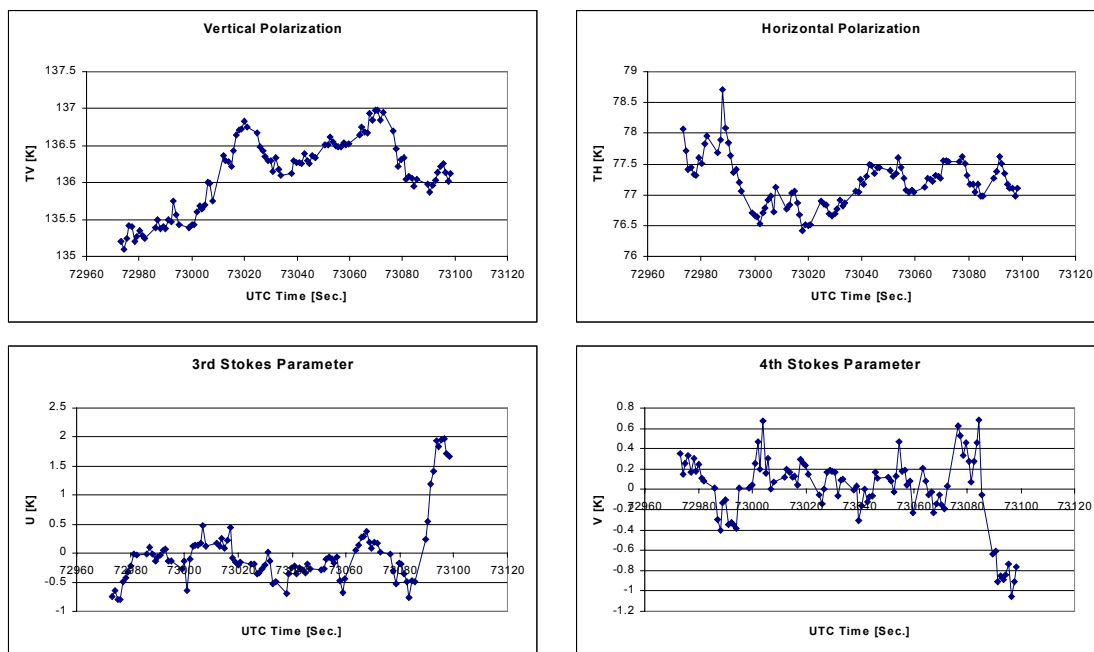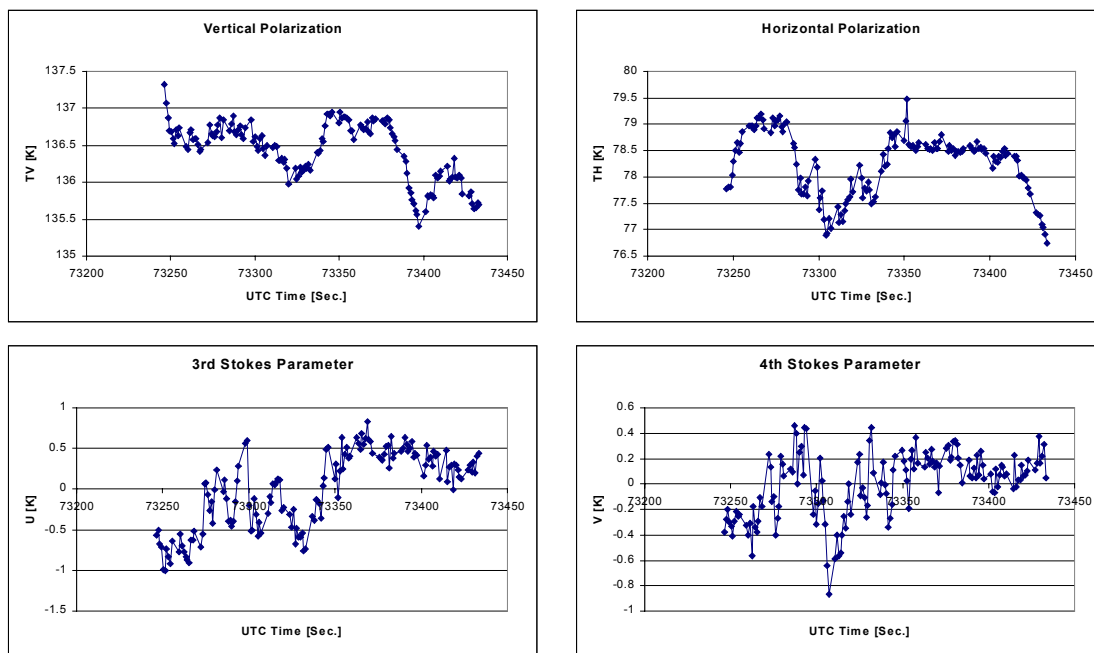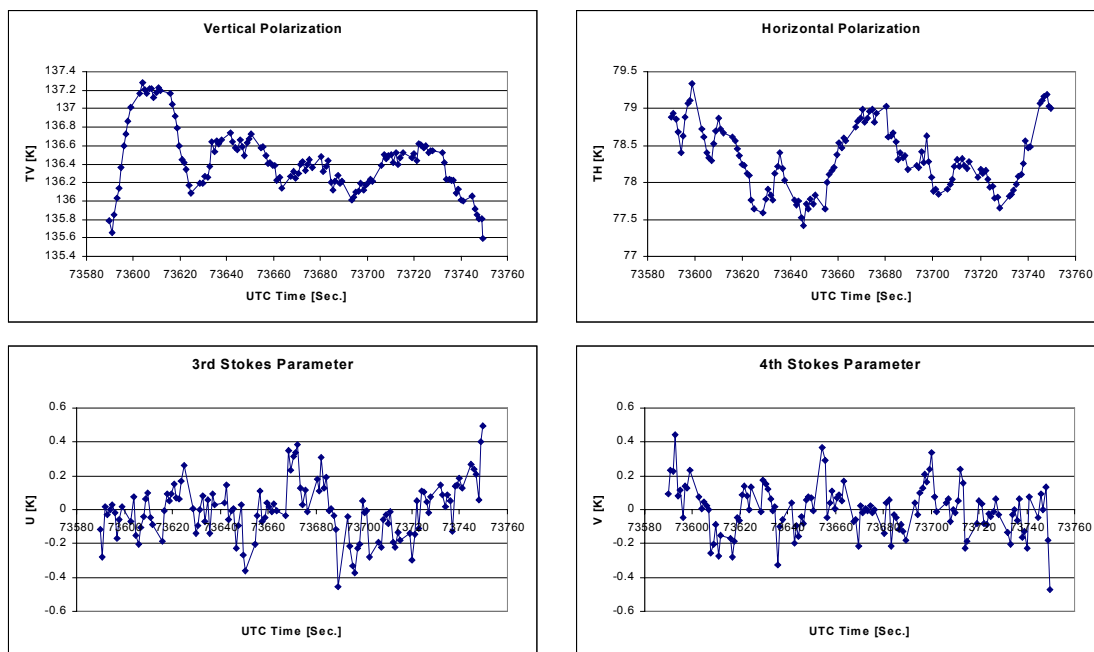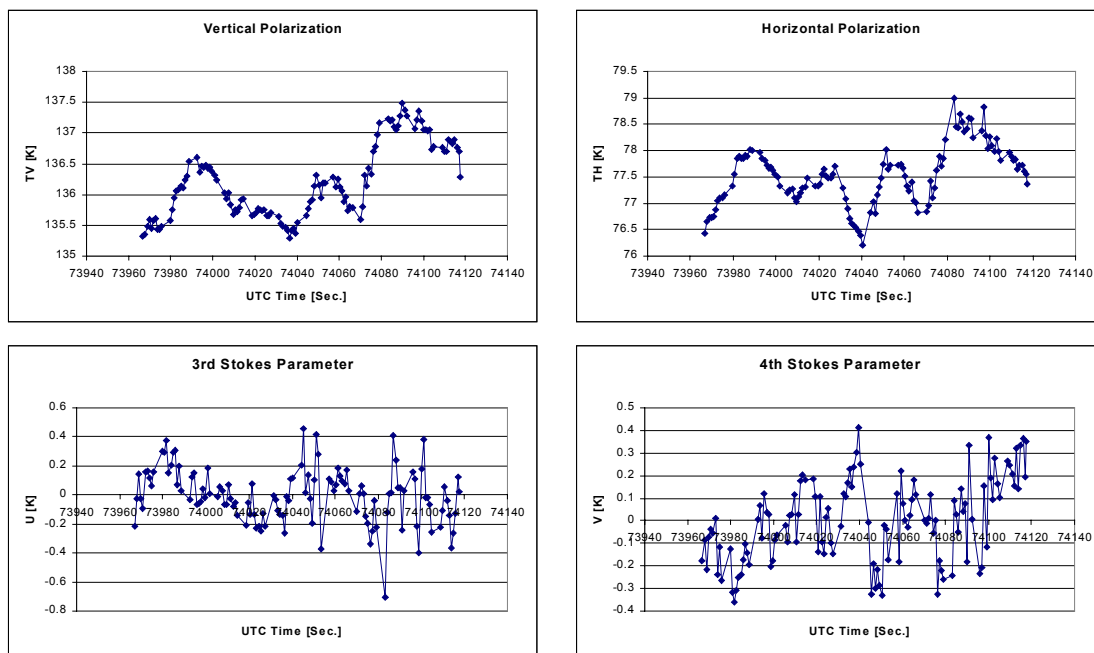*Figure 8.42. The modified Stokes parameters from the level flight track from March 6th 2003, 50° incidence angle, heading -18°.*
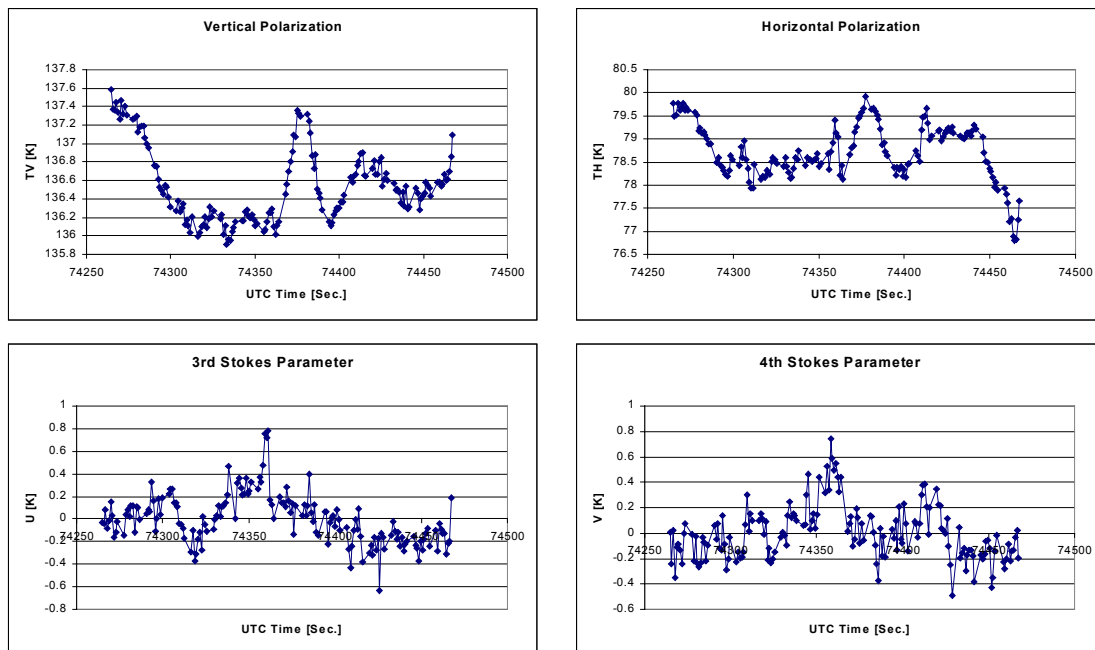
Figure 8.43. The modified Stokes parameters from the level flight track from March 6th 2003, 50° incidence angle, heading -135°.
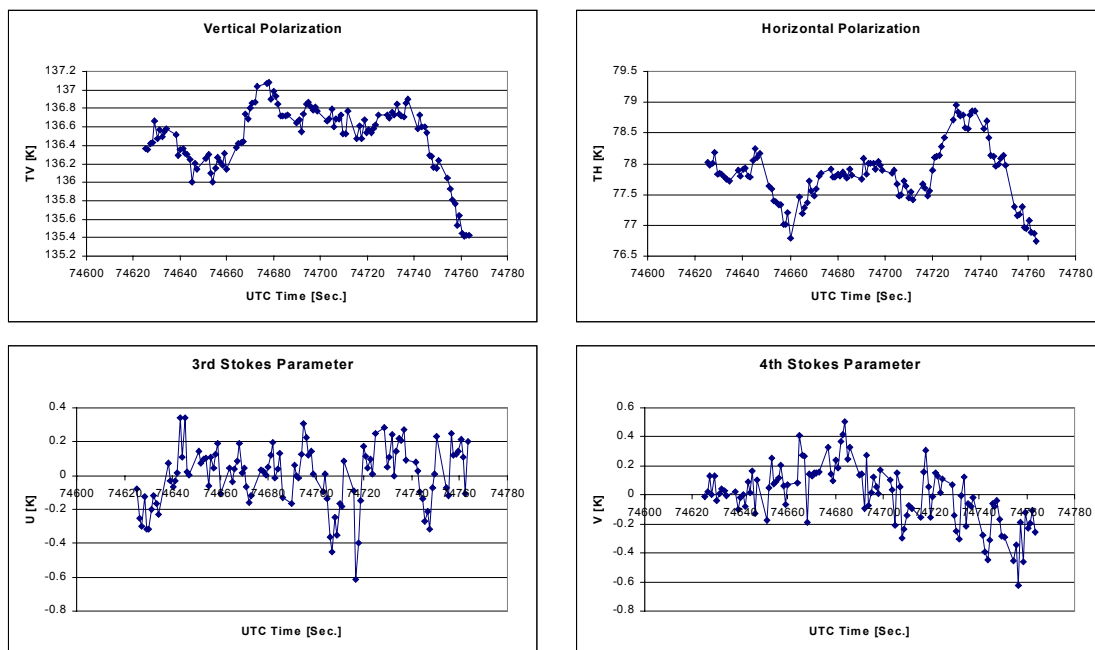

Figure 8.44. The modified Stokes parameters from the level flight track from March 6th 2003, 50° incidence angle, heading +90°.

The variations seem to be smaller than for the circle tracks, but the general impression, that especially the horizontal polarization is influenced, seems to be confirmed. In the circle tracks, these variations will directly overlay an eventual signature, and it is obvious, that it may lead to the conclusion, that a Gaussian noise signal is present, which will average out, when integrating the circles. For the level flights, each track may be fully integrated, thus representing one sample of a circle signature, and finally the eight points may be combined in one figure. This is done in figure 8.45, where the points are connected, using a low pass filter, and where the DC-content of each parameter has been removed to make them fit into one figure.

To identify an eventual signature in the combined circle, the 1st and 2nd order harmonics are estimated, using a least-mean-square algorithm, and the result is seen in table 8.4. It is noticed, that the vertical polarization contains a 1st harmonic, which confirms the finding from the two sets of circle flights. The horizontal polarization as well as the 3rd Stokes parameter seem to have approximately the same phase in their 1st harmonics, but as this does not correspond to the finding for the circle flights, no conclusion can be made, as the statistical materiel is too small.

Figures of the 1st and 2nd order harmonics for each of the four modified Stokes parameters have been plotted, and the result is seen in figure 8.46. It illustrates, that all parameters, except the horizontal polarization, have variations with magnitudes in the order of 200 mK, and it points out some dependence between the first three modified Stokes parameters.
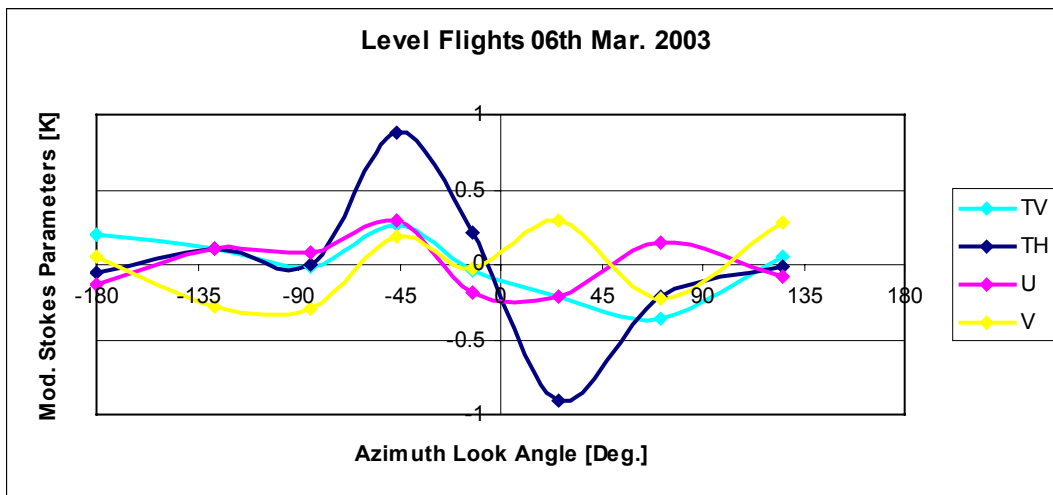
Figure 8.45. The modified Stokes parameters from the level flight tracks
March 6th 2003, 50° incidence angle.

Inc.	Harm.	TV, M.	TV, Ph.	TH, M.	TH, Ph.	U, Mag.	U, Ph.	V, Mag.	V, Ph.
Level	1	0.21	129.95	0.32	97.36	0.08	82.24	0.14	-76.22
50° inc.	2	0.17	59.07	0.41	100.01	0.16	170.06	0.21	43.96

Table 8.4. The modified Stokes parameters from the level flight tracks
March 6th 2003, 50° incidence angle. Result of 1st and 2nd harmonic fit.
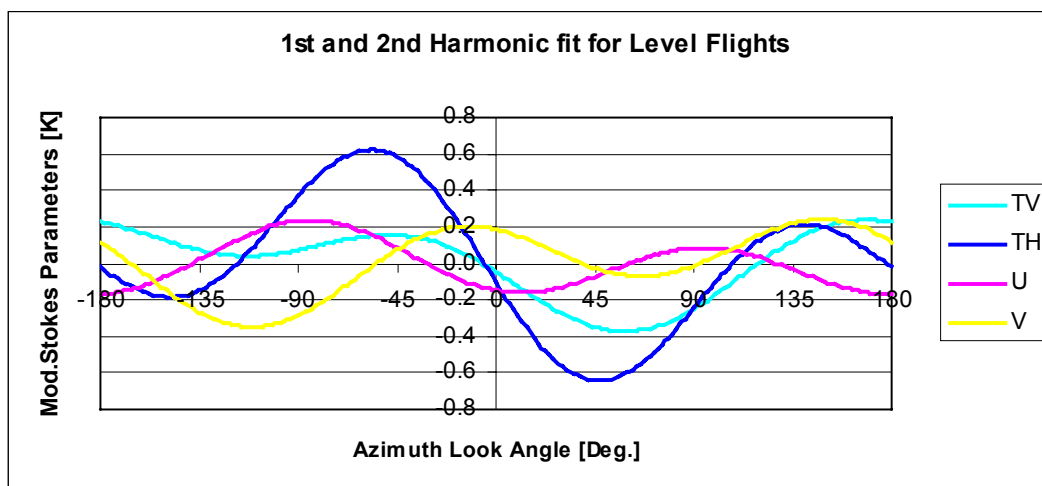
Figure 8.46. The modified Stokes parameters from the level flight tracks March 6th 2003, 50° incidence angle. Result of 1st and 2nd harmonic fit.

9. Results from the October 20th 2003 flight

The October 20th 2003 flight was known to be the last science flight within the LOSAC campaign, and it was decided to divide it into two parts in order to fill the voids, identified by the earlier flights. Again the primary focus was on a medium wind case, around 10 m/sec., as this wind speed on the October 25th 2001 flight turned out to provide less noise than the high wind, around 20 m/sec. It was decided to repeat the full flight pattern from the March 6th 2003 flight, thus providing a relatively large number of circles, concentrated at two incidence angles, 45° and 35°. Likewise it was decided to repeat the eight level flights, as they turned out to provide a good, alternative sampling of the eventual signature, and as it was interesting to investigate, if the consistence of the harmonics of the vertical polarization from circle flights to level flights could be reproduced.

As a secondary priority it was decided to perform a number of circle tracks over a target area with almost no wind. Two targets were thus identified, the primary site (Target A) being in the central North Sea between the oilrigs as in two earlier flights, while the secondary target was found to be off the South coast of Norway, near Lista (Target B). The latter point was chosen from meteorological data, forecasting the point to be right in the center of a low-pressure front, thus providing a local area with no wind. No measured meteorological data was available directly from the Lista flight point, but interpolated wind maps from the Danish Meteorological Institute confirm wind speeds below 1 m/sec. at the time of the flight. Prior to the flight, however, the wind was stronger, up to 10 m/sec., and some swell was to anticipate. For the North Sea site the wind conditions were stable during a period of 12 hours before the flight, and at the flight time 9.8 m/sec. was measured from a direction of 40°.

For the circle flights, 16 circles were measured with each of the two incidence angles, and the results are seen in the figures 9.1 to 9.16 and 9.19 to 9.34, respectively. Figure 9.17 and 9.18 for 45° incidence angle and figure 9.36 and 9.36 for 35° incidence angle, show the circles, when they are integrated eight by eight, and finally the figures 9.37 and 9.38 show the tracks fully integrated.

Figure 9.1. The Stokes parameters from the 1st circle flight track with 45° incidence angle from the October 20th 2003, Target A, flight.

Figure 9.2. The Stokes parameters from the 2nd circle flight track with 45° incidence angle from the October 20th 2003, Target A, flight.

Figure 9.3. The Stokes parameters from the 3rd circle flight track with 45°incidence angle from the October 20th 2003, Target A, flight.

Figure 9.4. The Stokes parameters from the 4th circle flight track with 45°incidence angle from the October 20th 2003, Target A, flight.

Figure 9.5. The Stokes parameters from the 5th circle flight track with 45° incidence angle from the October 20th 2003, Target A, flight.

Figure 9.6. The Stokes parameters from the 6th circle flight track with 45° incidence angle from the October 20th 2003, Target A, flight.

Figure 9.7. The Stokes parameters from the 7th circle flight track with 45° incidence angle from the October 20th 2003, Target A, flight.

Figure 9.8. The Stokes parameters from the 8th circle flight track with 45° incidence angle from the October 20th 2003, Target A, flight.

Figure 9.9. The Stokes parameters from the 9th circle flight track with 45° incidence angle from the October 20th 2003, Target A, flight.

Figure 9.10. The Stokes parameters from the 10th circle flight track with 45° incidence angle from the October 20th 2003, Target A, flight.

Figure 9.11. The Stokes parameters from the 11th circle flight track with 45° incidence angle from the October 20th 2003, Target A, flight.

Figure 9.12. The Stokes parameters from the 12th circle flight track with 45° incidence angle from the October 20th 2003, Target A, flight.
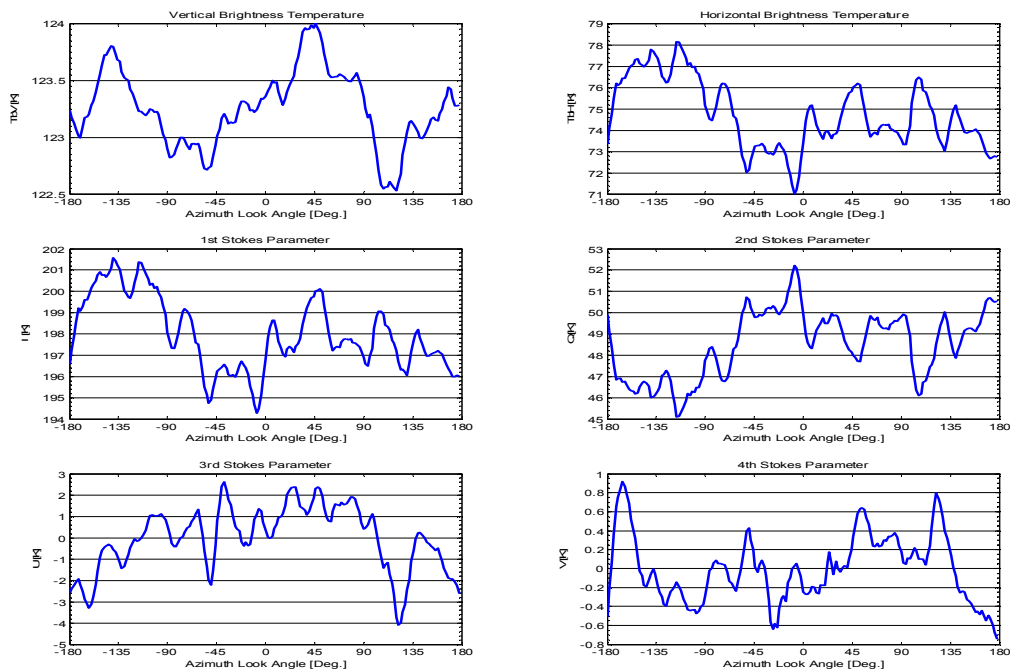
Figure 9.13. The Stokes parameters from the 13th circle flight track with 45° incidence angle from the October 20th 2003, Target A, flight.

Figure 9.14. The Stokes parameters from the 14th circle flight track with 45° incidence angle from the October 20th 2003, Target A, flight.

Figure 9.15. The Stokes parameters from the 15th circle flight track with 45° incidence angle from the October 20th 2003, Target A, flight.
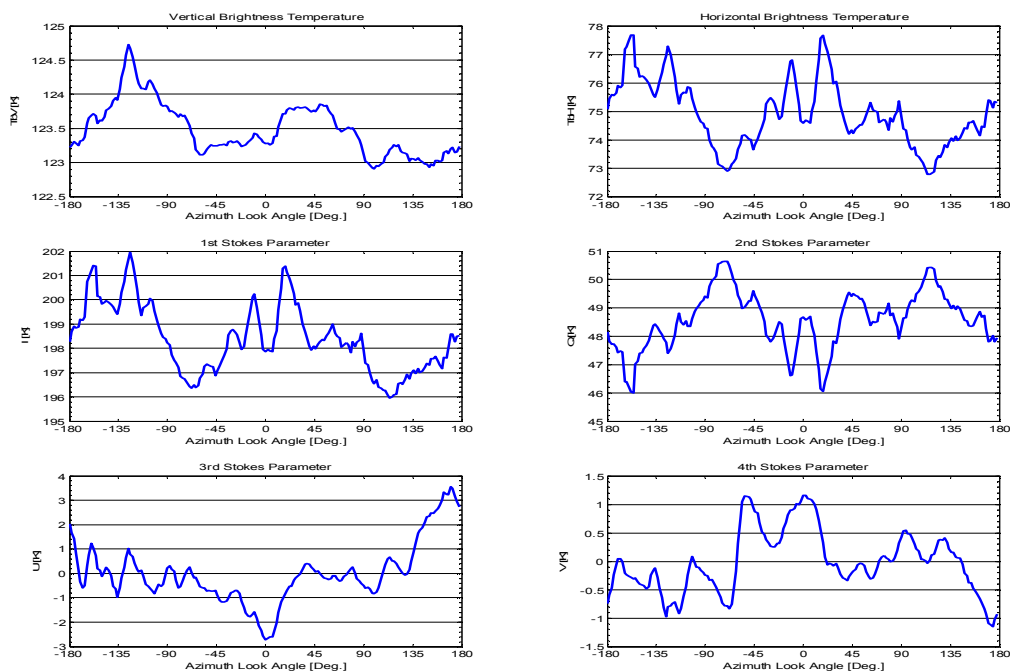

Figure 9.16. The Stokes parameters from the 16th circle flight track with 45° incidence angle from the October 20th 2003, Target A, flight.
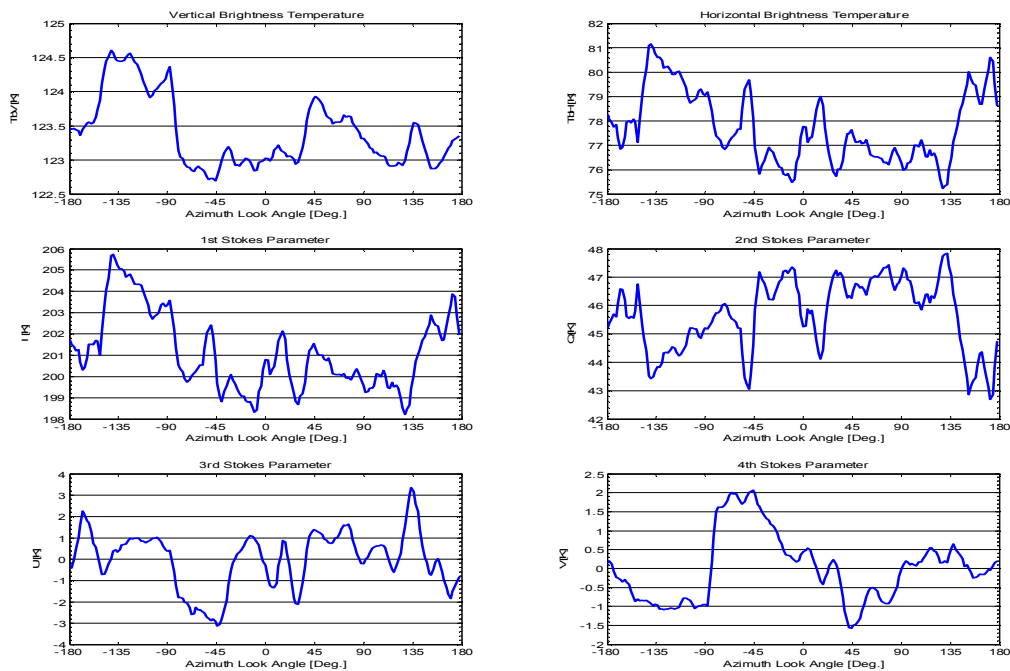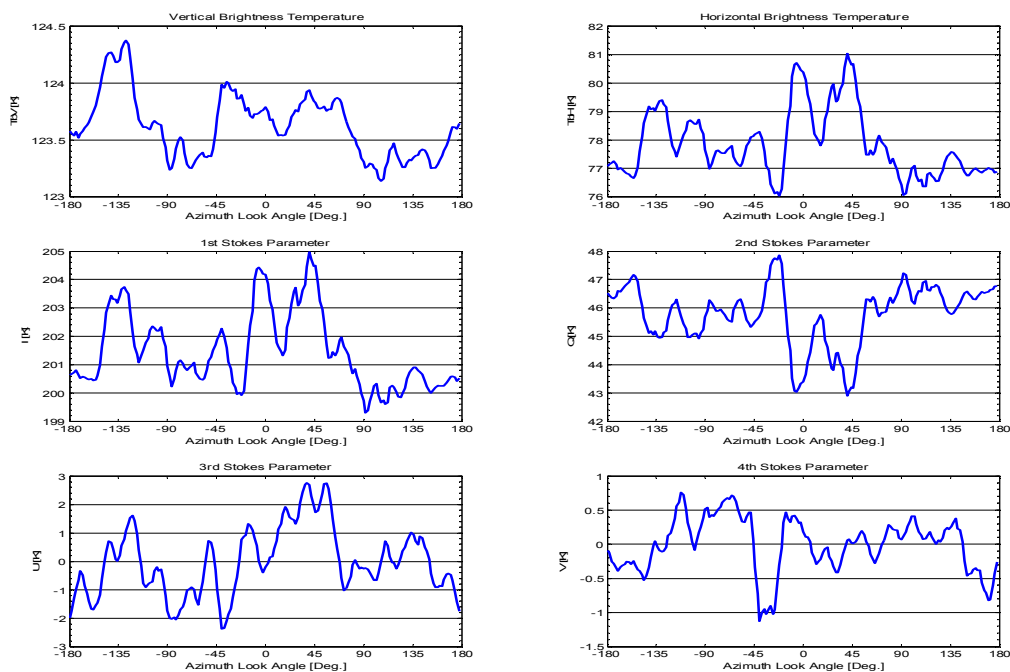
Figure 9.17. The averaged Stokes parameters from the 1ˢᵗ to the 8ᵗʰ circle flight tracks with 45° incidence angle from the October 20ᵗʰ 2003, Target A, flight.

Figure 9.18. The averaged Stokes parameters from the 9ᵗʰ to the 16ᵗʰ circle flight tracks with 45° incidence angle from the October 20ᵗʰ 2003, Target A, flight.
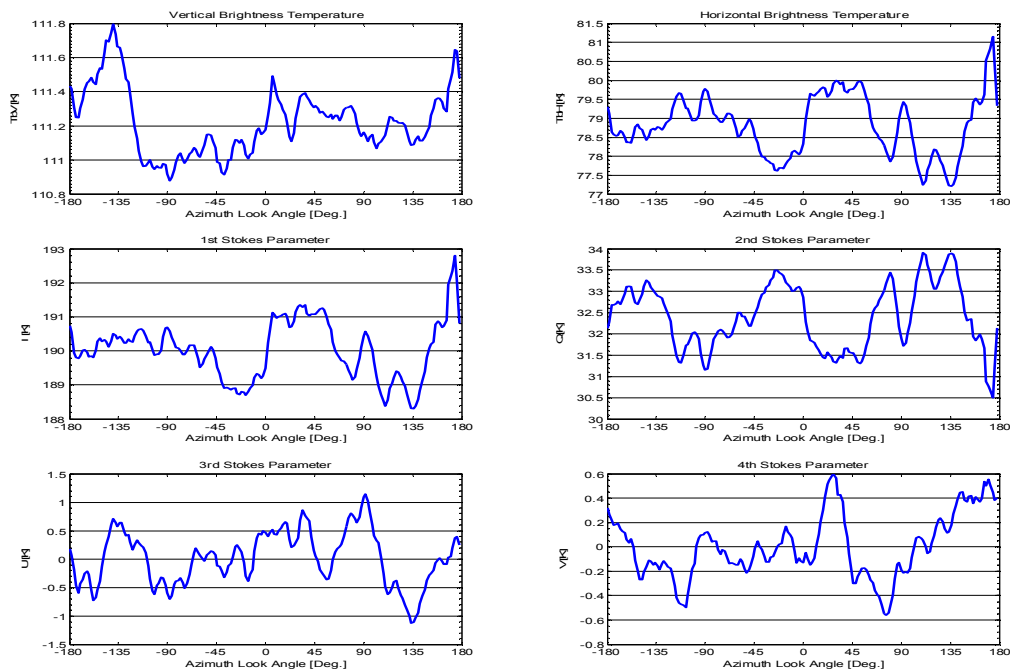
Figure 9.19. The Stokes parameters from the 1st circle flight track with 35° incidence angle from the October 20th 2003, Target A, flight.
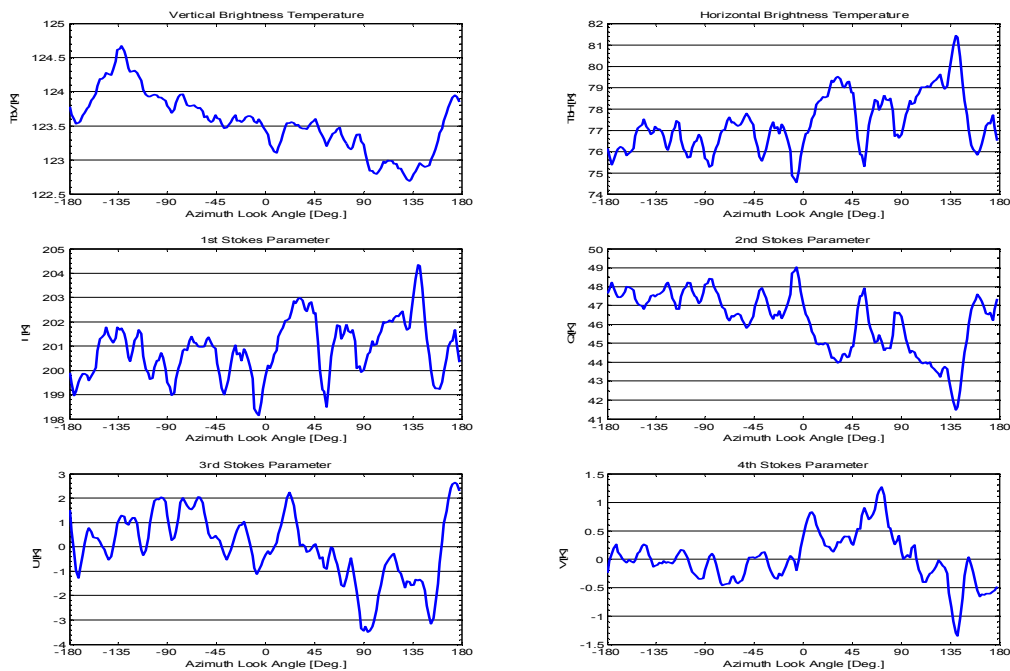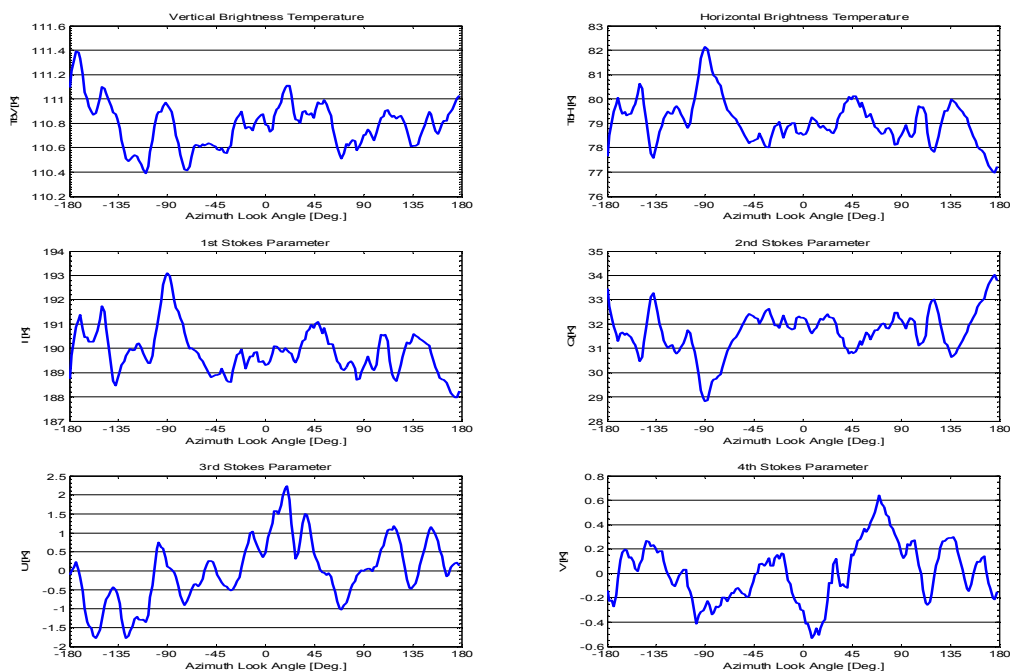

Figure 9.20. The Stokes parameters from the 2nd circle flight track with 35° incidence angle from the October 20th 2003, Target A, flight.
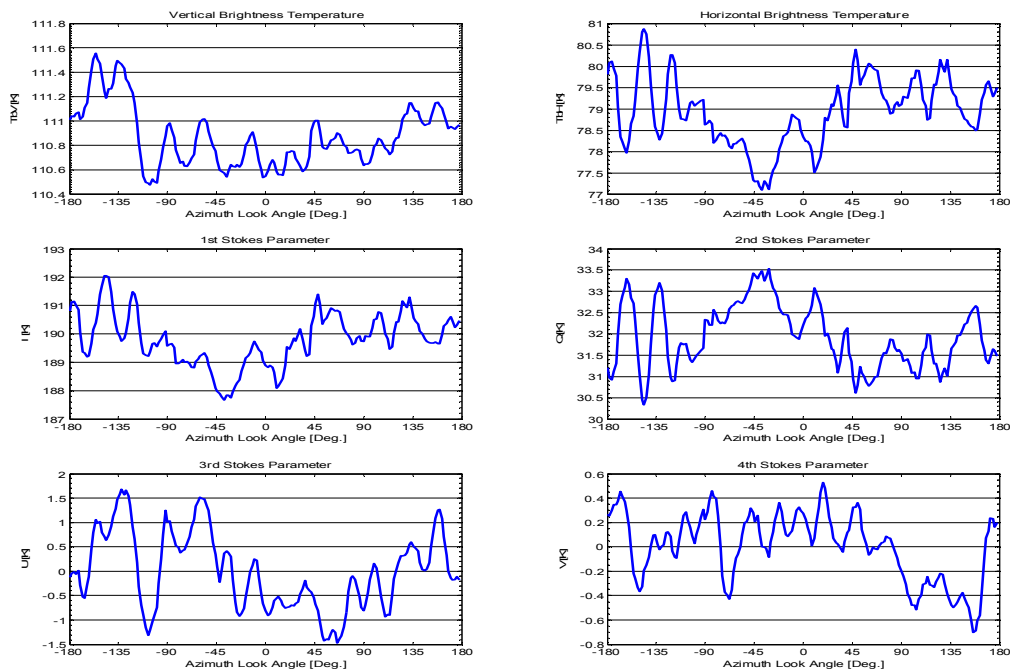
F*igure 9.21. The Stokes parameters from the 3rd circle flight track with 35° incidence angle from the October 20th 2003, Target A, flight.*
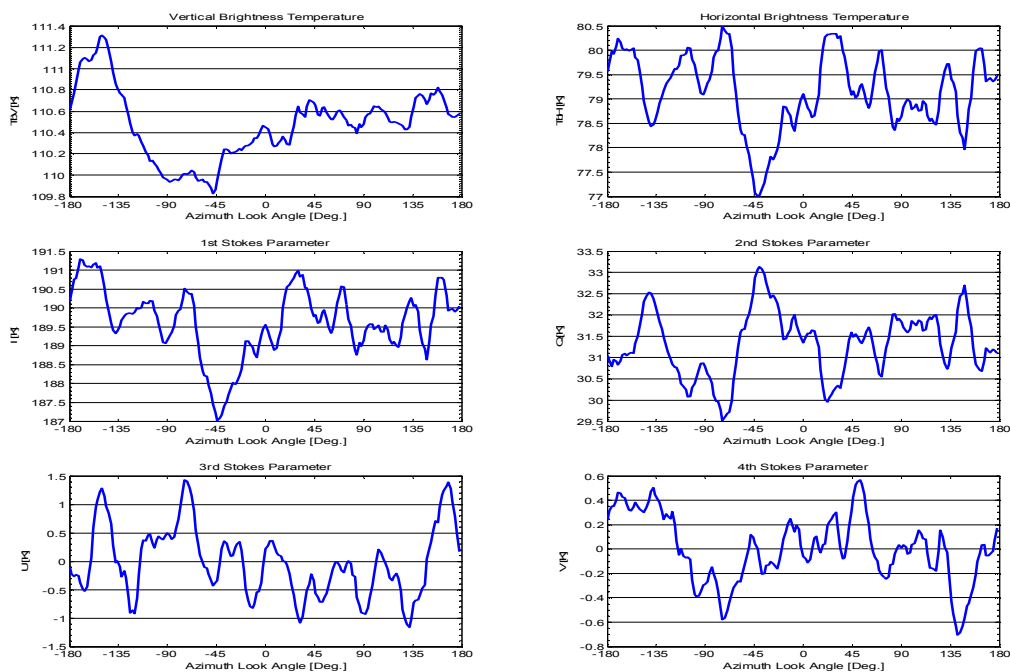
Figure 9.22. The Stokes parameters from the 4th circle flight track with 35° incidence angle from the October 20th 2003, Target A, flight.
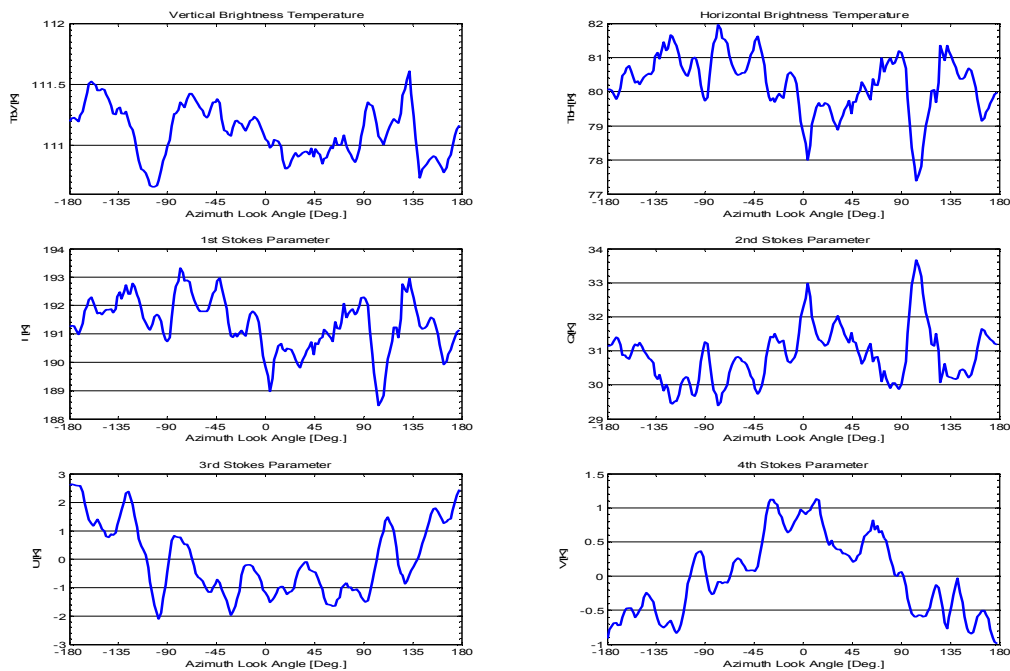
Figure 9.23. The Stokes parameters from the 5th circle flight track with 35° incidence angle from the October 20th 2003, Target A, flight.
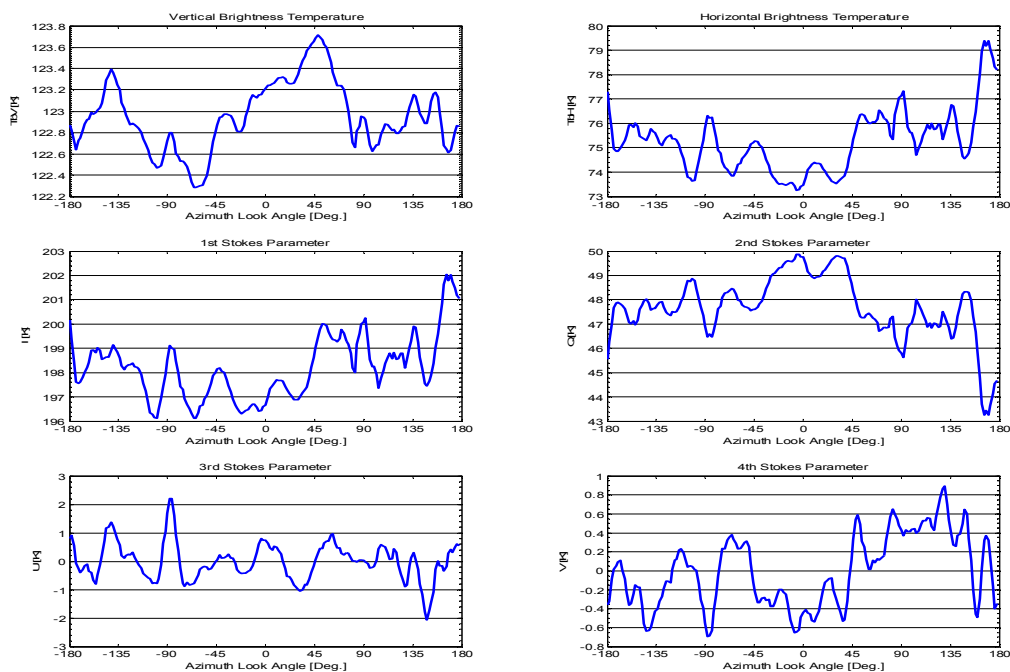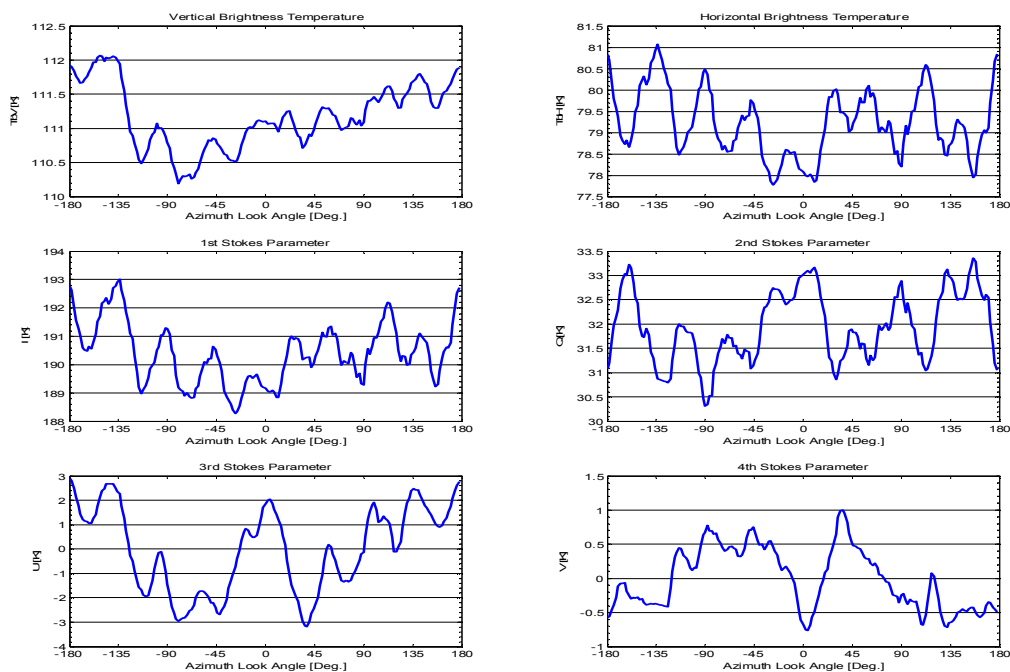

Figure 9.24. The Stokes parameters from the 6th circle flight track with 35° incidence angle from the October 20th 2003, Target A, flight.
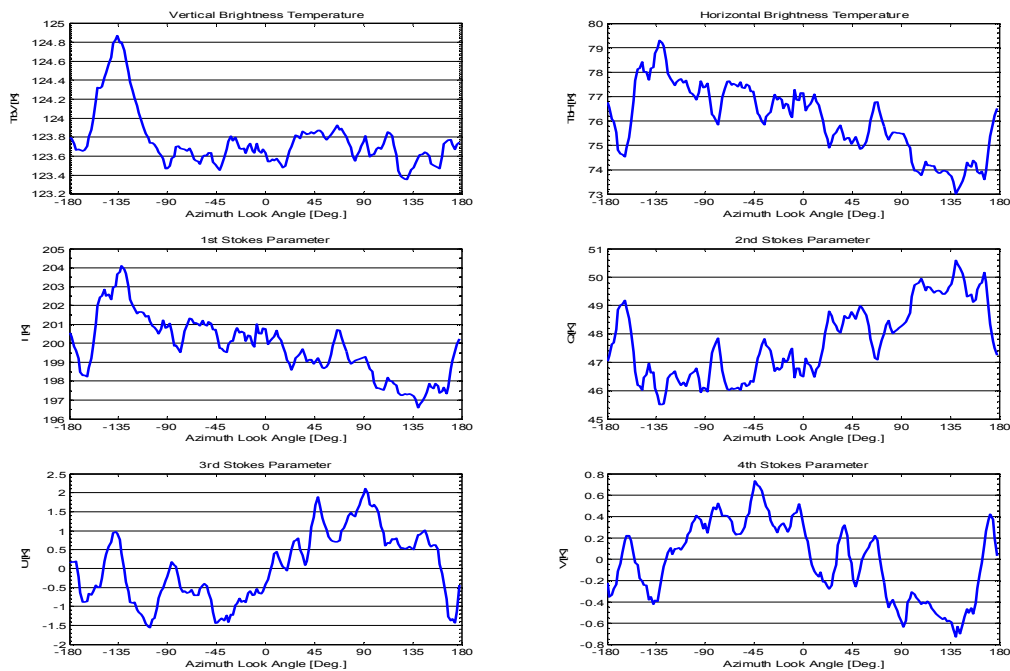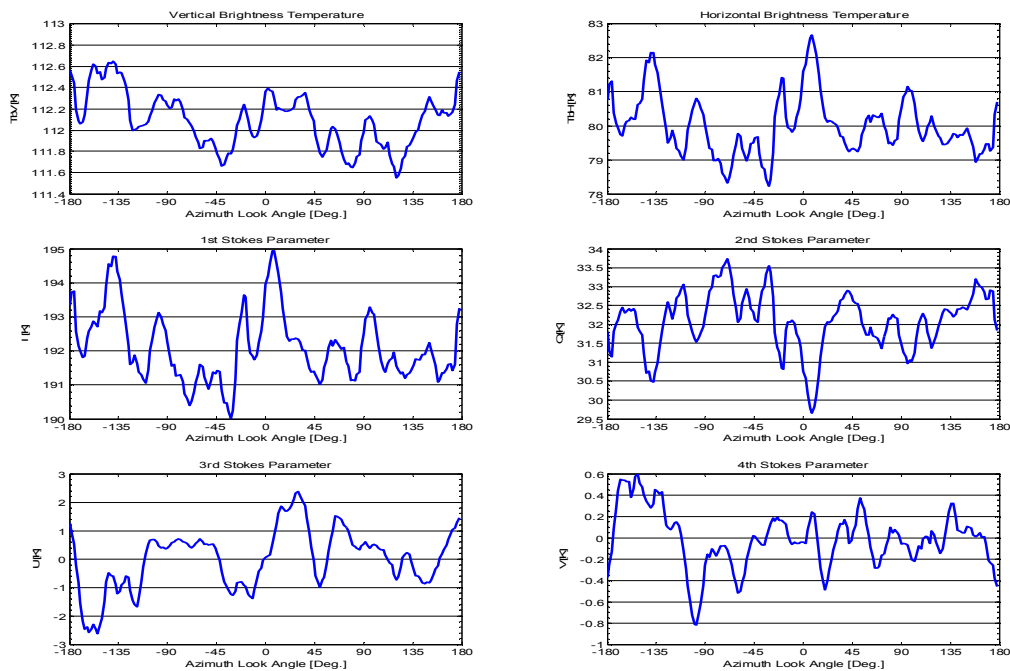
Figure 9.25. The Stokes parameters from the 7th circle flight track with 35° incidence angle from the October 20th 2003, Target A, flight.
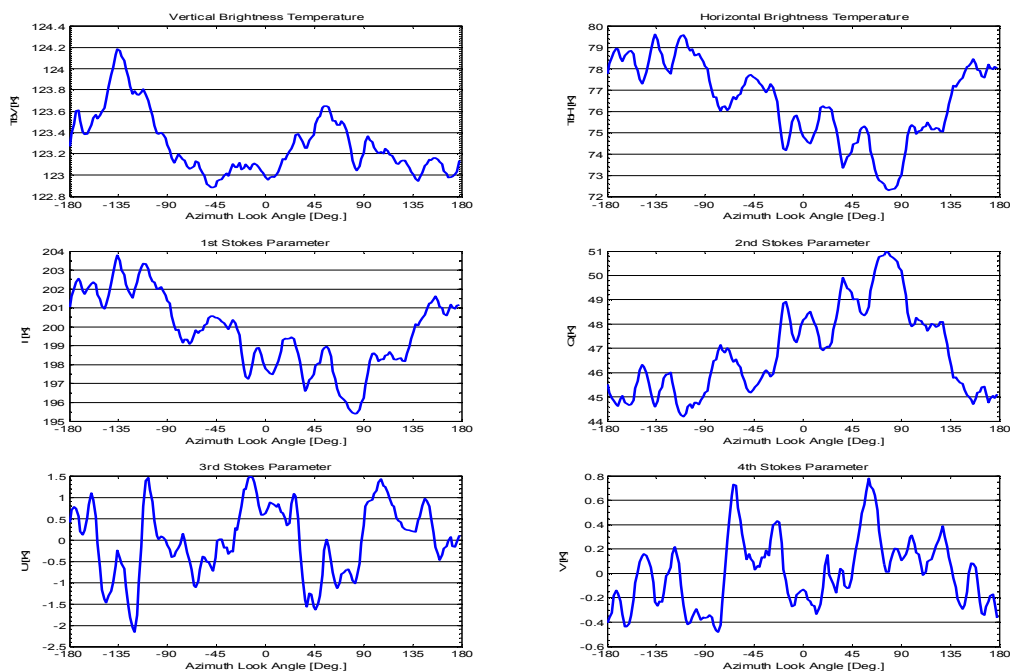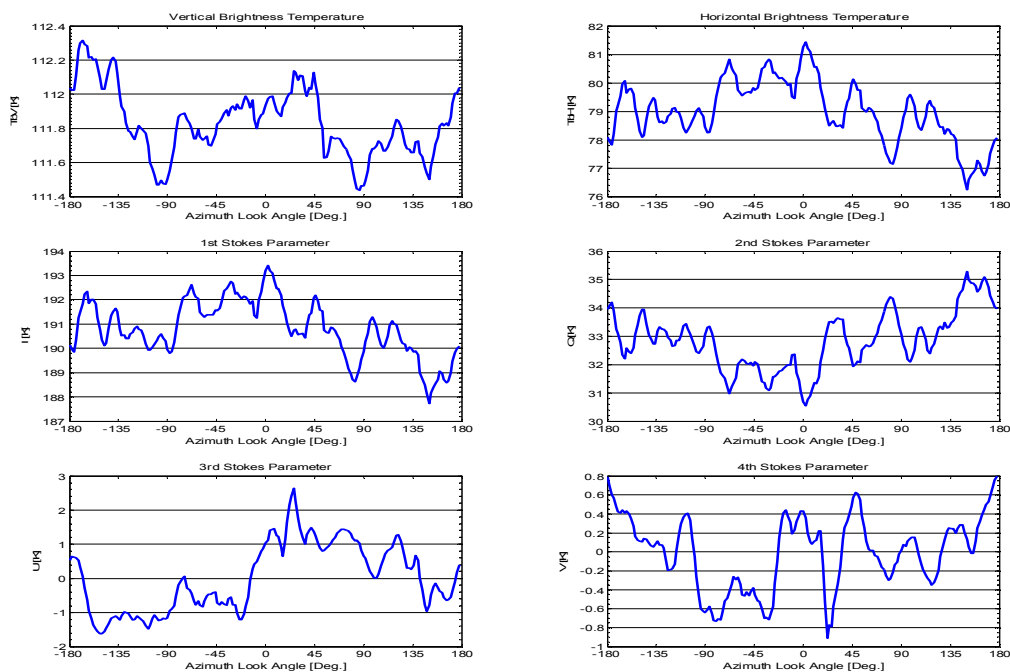

Figure 9.26. The Stokes parameters from the 8th circle flight track with 35° incidence angle from the October 20th 2003, Target A, flight.
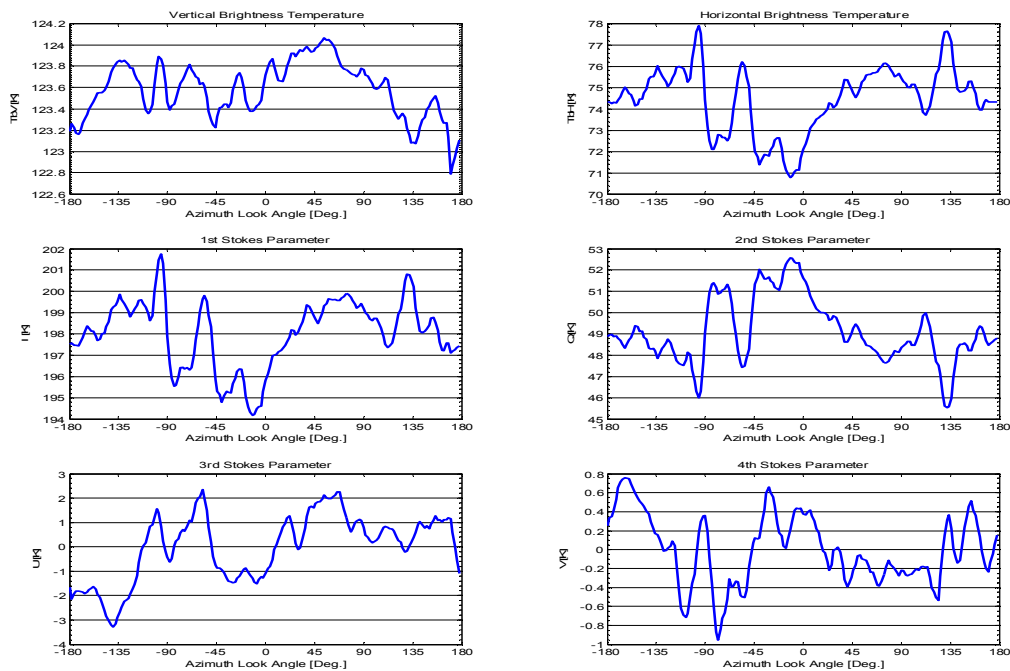
Figure 9.27. The Stokes parameters from the 9th circle flight track with $35°$ incidence angle from the October 20th 2003, Target A, flight.

Figure 9.28. The Stokes parameters from the 10th circle flight track with $35°$ incidence angle from the October 20th 2003, Target A, flight.

Figure 9.29. The Stokes parameters from the 11th circle flight track with 35° incidence angle from the October 20th 2003, Target A, flight.
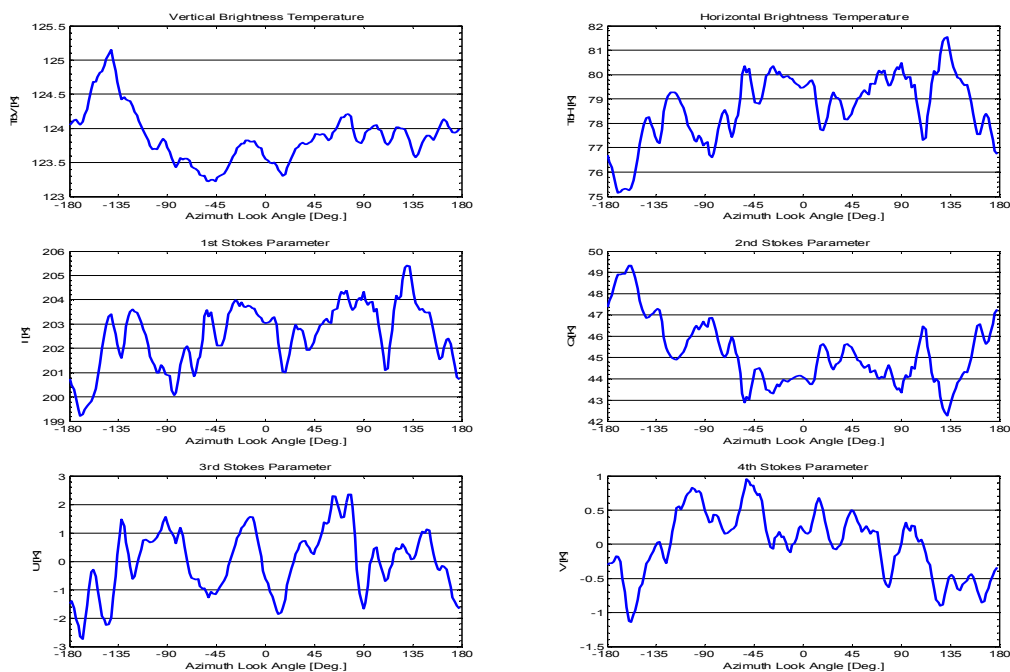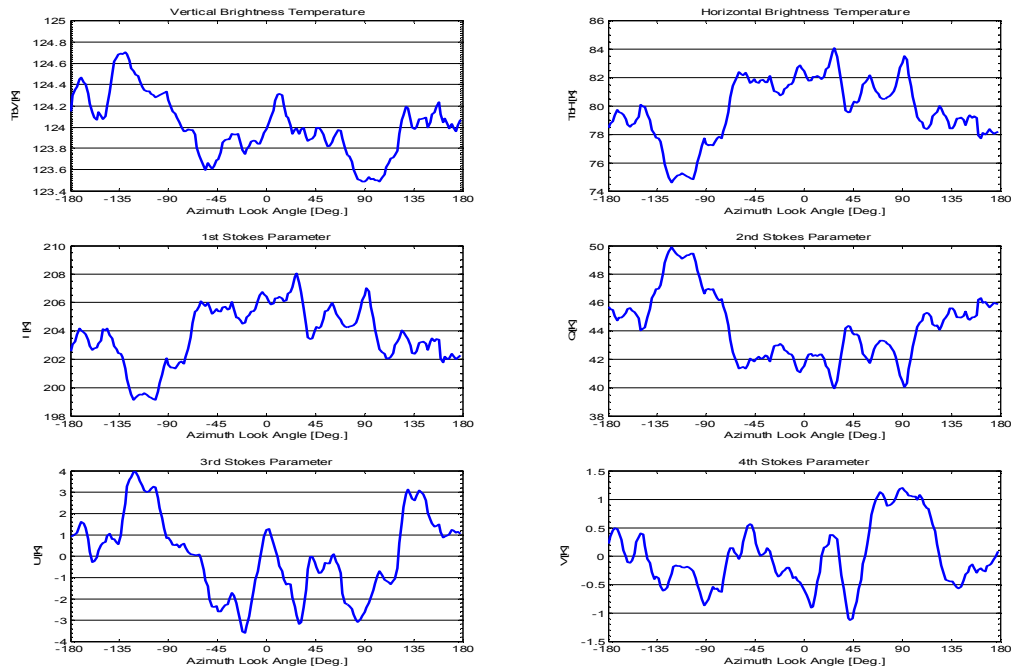

Figure 9.30. The Stokes parameters from the 12th circle flight track with 35° incidence angle from the October 20th 2003, Target A, flight.

Figure 9.31. The Stokes parameters from the 13th circle flight track with 35° incidence angle from the October 20th 2003, Target A, flight.

Figure 9.32. The Stokes parameters from the 14th circle flight track with 35° incidence angle from the October 20th 2003, Target A, flight.
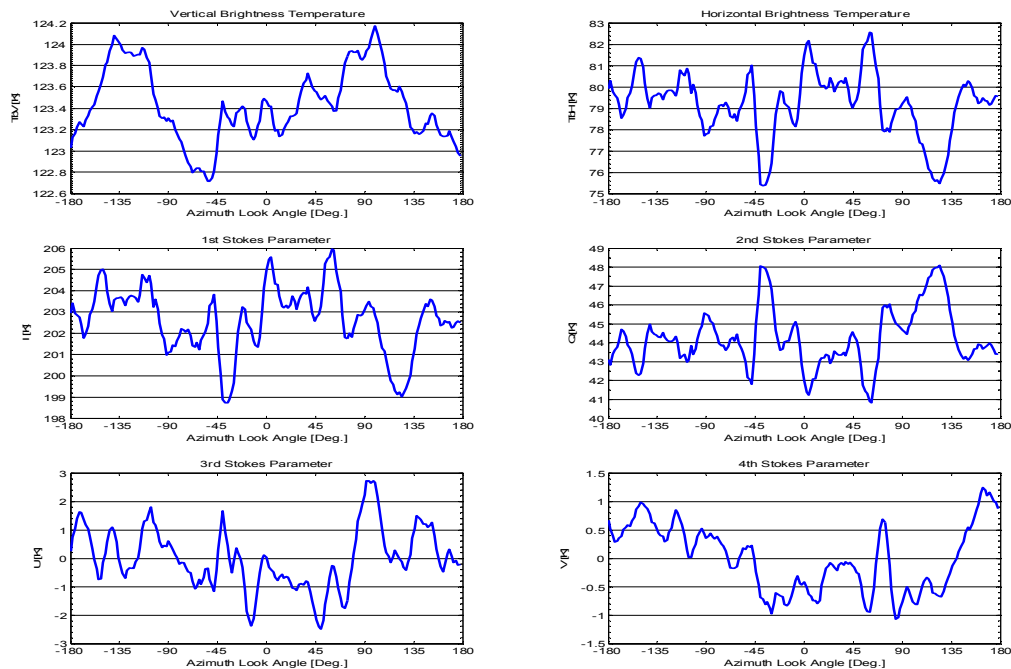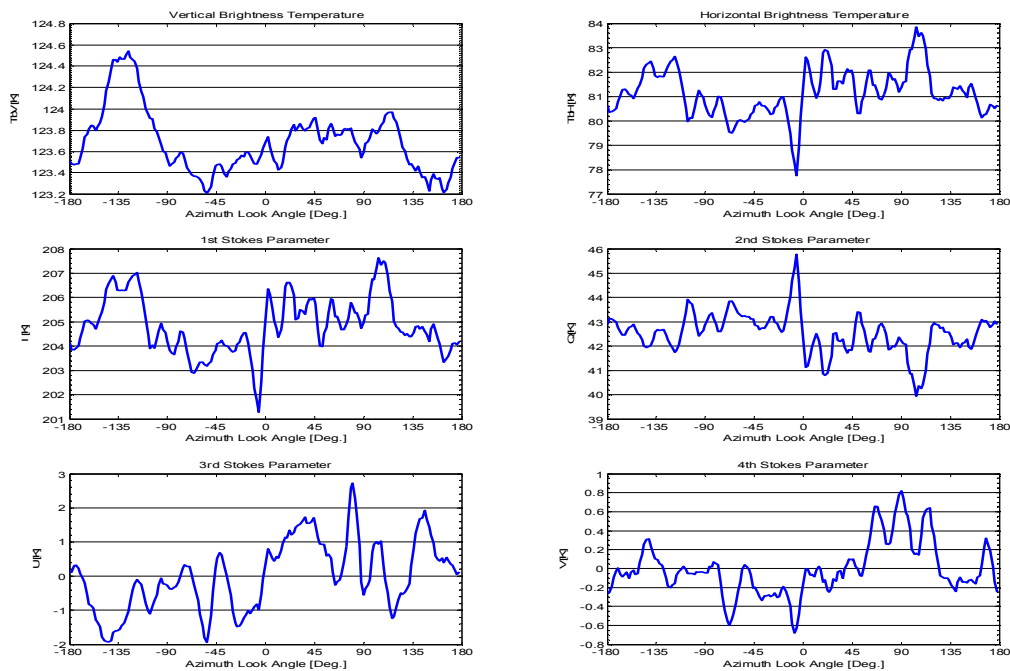
Figure 9.33. The Stokes parameters from the 15th circle flight track with 35° incidence angle from the October 20th 2003, Target A, flight.
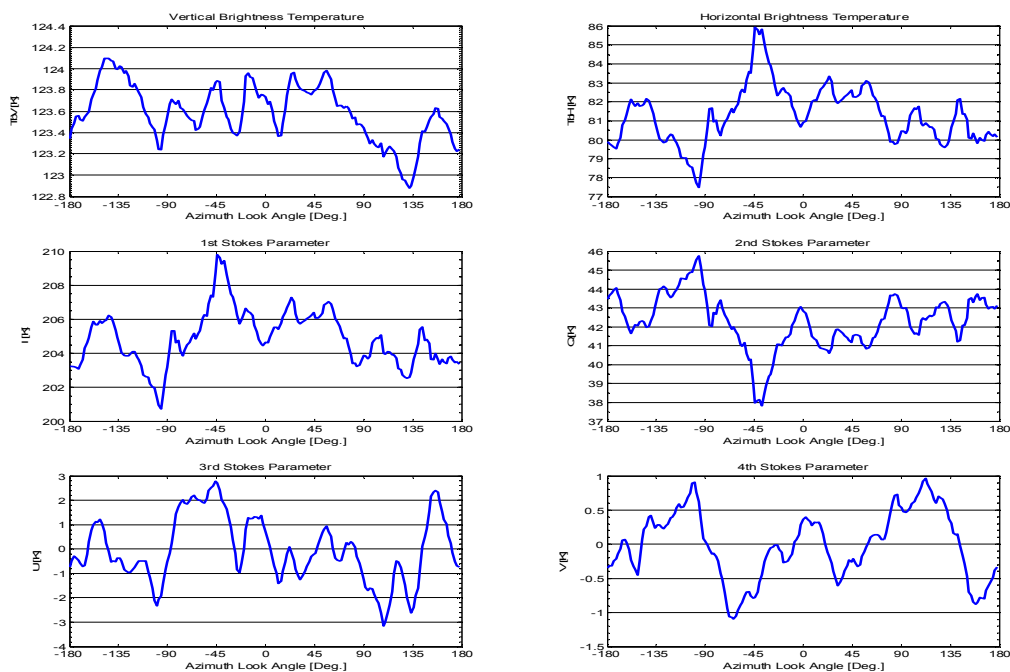

Figure 9.34. The Stokes parameters from the 16th circle flight track with 35° incidence angle from the October 20th 2003, Target A, flight.

Figure 9.35. The averaged Stokes parameters from the 1st to the 8th circle flight tracks with 35° incidence angle from the October 20th 2003, Target A, flight.

Figure 9.36. The averaged Stokes parameters from the 9st to the 16th circle flight tracks with 35° incidence angle from the October 20th 2003, Target A, flight.

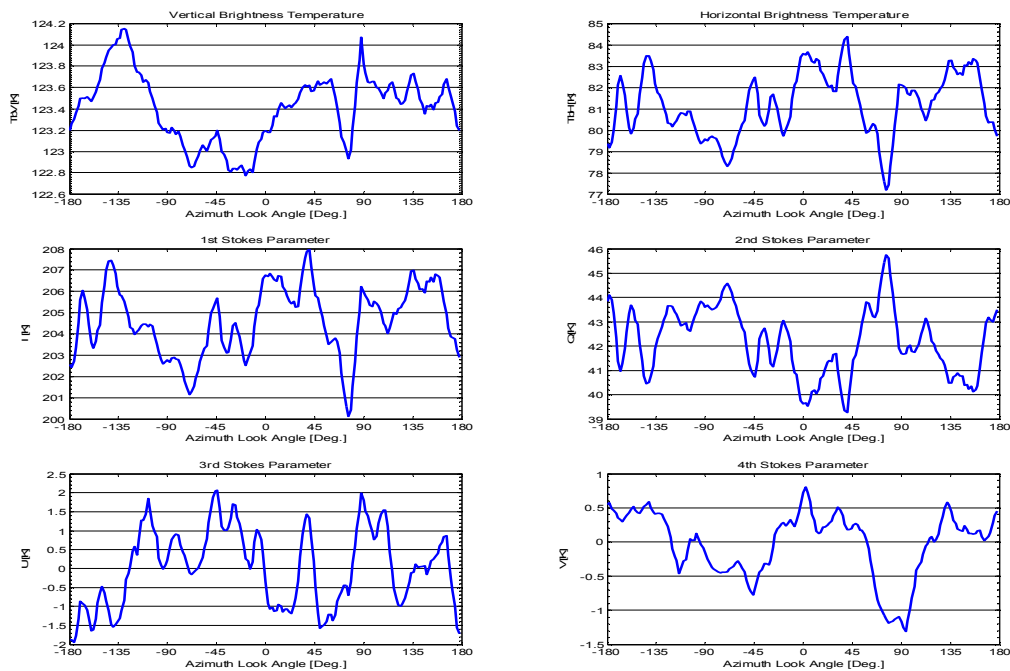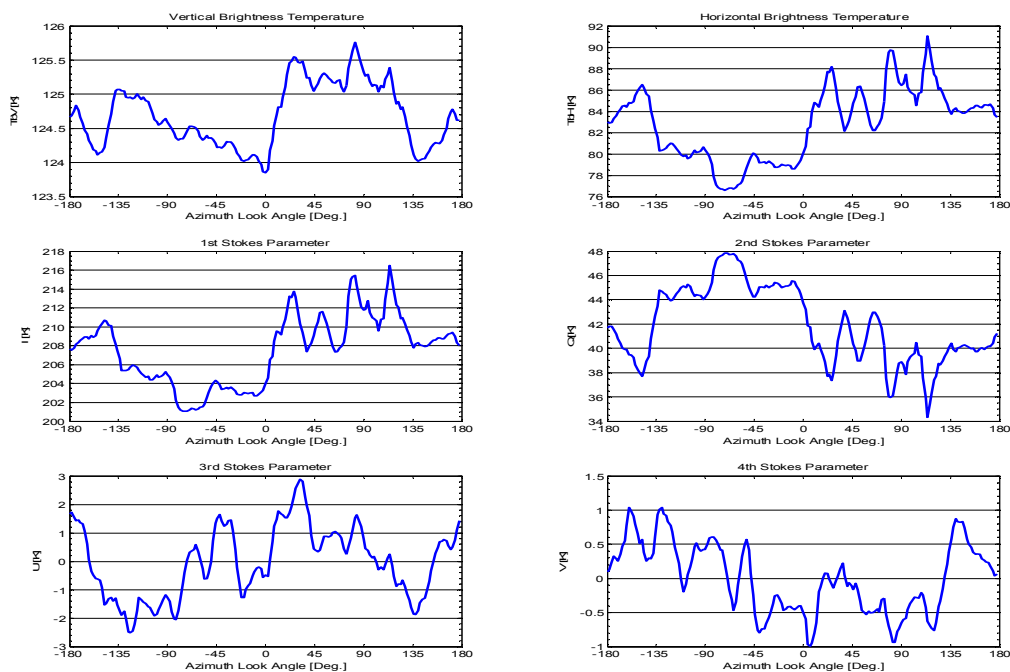*Figure 9.37. The averaged Stokes parameters from all 16 circle flight tracks with 45° incidence angle from the October 20th 2003, Target A, flight.*

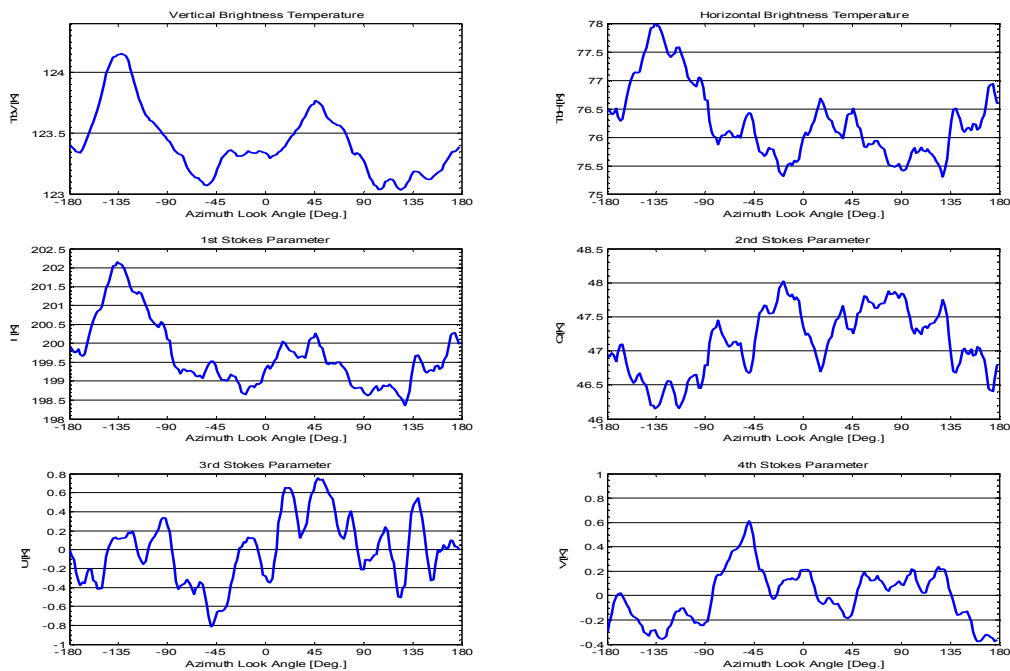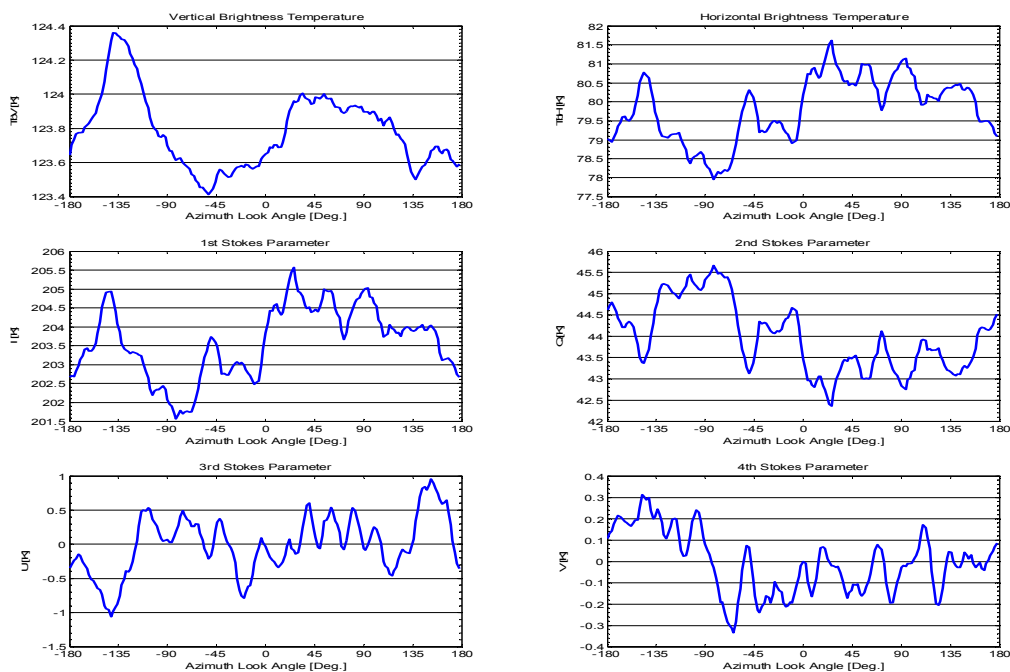*Figure 9.38. The averaged Stokes parameters from all 16 circle flight tracks with 35° incidence angle from the October 20th 2003, Target A, flight.*

The general impression of the tracks is quite similar to the earlier flights, and the root-mean-square analysis of the integration gain is done for each of the incidence angles. The results are seen in the tables 9.1 and 9.2, for 45° incidence angle and 35° incidence angle, respectively. Again it is seen, that the 3rd and the 4th Stokes parameters provide the full integration gain, while the horizontal polarization provides almost the full improvement. The results from the vertical polarization provide only improvement factors of 1.45 and 1.56 for the two incidence angles, while a pure Gaussian signal would improve by 4. The reduction corresponds to the presence of a sinusoidal with rms. power of 201 mK and 151 mK in each of the two cases, respectively, and this order of magnitude is comparable to the results from the earlier flights.

Finally the first four harmonics for each of the integrated tracks are calculated in table 9.3, but no clear signature seems to be present. For the wind direction, $\psi = 40°$, [5] provides expected phases of $\theta = -40°$ and $\theta = -80°$ for the 1st and 2nd harmonics of the vertical and horizontal polarizations, $\theta = +50°$ and $\theta = +10°$ for the harmonics of the 3rd Stokes parameter, and $\theta = -170°$ for the 2nd harmonic of the 4th. Only the 2nd harmonics of horizontal polarizations seem to follow these results, however, and no conclusions regarding wind driven signatures can be made from these results.

Circles	TV, std.dev. [K]	TH, std.dev. [K]	U, std.dev. [K]	V, std.dev. [K]
Single circles	0.333	1.606	1.510	0.354
45° incidence angle	0.387	1.165	1.245	0.553
	0.513	1.455	1.335	0.912
	0.281	1.174	1.195	0.400
	0.440	1.323	1.391	0.432
	0.322	1.265	0.656	0.384
	0.301	1.435	0.924	0.360
	0.292	1.888	0.834	0.285
	0.262	1.531	1.372	0.366
	0.390	1.382	1.125	0.484
	0.287	2.203	1.877	0.558
	0.344	1.496	1.071	0.590
	0.302	0.965	1.020	0.283
	0.268	1.505	1.340	0.500
	0.325	1.482	1.021	0.482
	0.464	3.366	1.247	0.512
Average, single	0.344	1.578	1.198	0.466
4 circles	0.316	0.878	0.653	0.352
integrated	0.253	0.615	0.335	0.179
	0.219	0.850	0.698	0.181
	0.249	1.197	0.655	0.228
Average, 4 integrated	0.259	0.885	0.585	0.235
8 integrated	0.278	0.654	0.348	0.218
	0.221	0.854	0.423	0.144
Average, 8 integrated	0.249	0.754	0.386	0.181
All 16 integrated	0.237	0.481	0.285	0.090

Table 9.1. Total rms. noise for the full signal in the modified Stokes parameters from the 16 circle flights with 45° incidence angle from October 20th 2003, Target A. The circles are processed as single tracks, averaged as 4 times four circles, 2 times eight, and totally.

Circles	TV, std.dev. [K]	TH, std.dev. [K]	U, std.dev. [K]	V, std.dev. [K]
Single circles	0.195	0.787	0.475	0.262
35° incidence angle	0.192	0.909	0.846	0.241
	0.249	0.805	0.793	0.279
	0.331	0.768	0.610	0.276
	0.214	0.856	1.247	0.585
	0.475	0.783	1.733	0.451
	0.256	0.867	1.060	0.271
	0.201	1.078	1.005	0.386
	0.296	1.672	0.838	0.300
	0.246	0.980	0.827	0.336
	0.284	1.600	1.085	0.450
	0.429	1.138	1.037	0.351
	0.250	1.086	1.222	0.378
	0.322	1.814	0.984	0.559
	0.473	1.004	0.934	0.456
	0.241	1.144	1.035	0.301
Average, single	0.291	1.081	0.983	0.368
4 circles	0.196	0.526	0.312	0.126
integrated	0.200	0.405	0.634	0.195
	0.231	0.913	0.490	0.214
	0.241	0.510	0.511	0.182
Average, 4 integrated	0.217	0.589	0.487	0.179
8 integrated	0.192	0.323	0.376	0.131
	0.198	0.537	0.411	0.118
Average, 8 integrated	0.195	0.430	0.393	0.124
All 16 integrated	0.186	0.334	0.304	0.062

Table 9.2. Total rms. noise for the full signal in the modified Stokes parameters from the 16 circle flights with 35° incidence angle from October 20th 2003, Target A. The circles are processed as single tracks, averaged as 4 times four circles, 2 times eight, and totally.

Inc.	Harm.	TV, M.	TV, Ph.	TH, M.	TH, Ph.	U, Mag.	U, Ph.	V, Mag.	V, Ph.
45°	1	0.07	144.62	0.24	-120.43	0.17	-77.95	0.03	15.16
	2	0.30	-95.66	0.40	-71.61	0.11	-148.83	0.04	143.52
	3	0.07	39.88	0.11	2.91	0.26	-103.94	0.05	92.61
	4	0.09	156.26	0.27	-161.64	0.15	88.71	0.05	-95.74
35°	1	0.15	-168.30	0.16	-25.70	0.29	-129.11	0.05	-6.25
	2	0.19	-36.10	0.33	-92.28	0.19	-56.06	0.02	5.02
	3	0.04	112.44	0.05	-34.26	0.03	-66.93	0.03	92.66
	4	0.06	-147.51	0.18	-134.93	0.13	-55.44	0.00	28.52

Table 9.3. 1st, 2nd, 3rd, and 4th harmonic components in the averaged modified Stokes parameters from the circle flights from October 20th 2003, target A.

Data from the 2nd set of circle flights from the October 20th 2003 flight, taken over target B at a 45° incidence angle, are presented in the figures 9.39 to 9.54. These figures are followed by the integrated signatures from eight circles in figure 9.55 and figure 9.56, and finally the fully integrated result in figure 9.57. Root-mean-square data is presented in table 9.4, and the result from the harmonic analysis is shown in table 9.5.
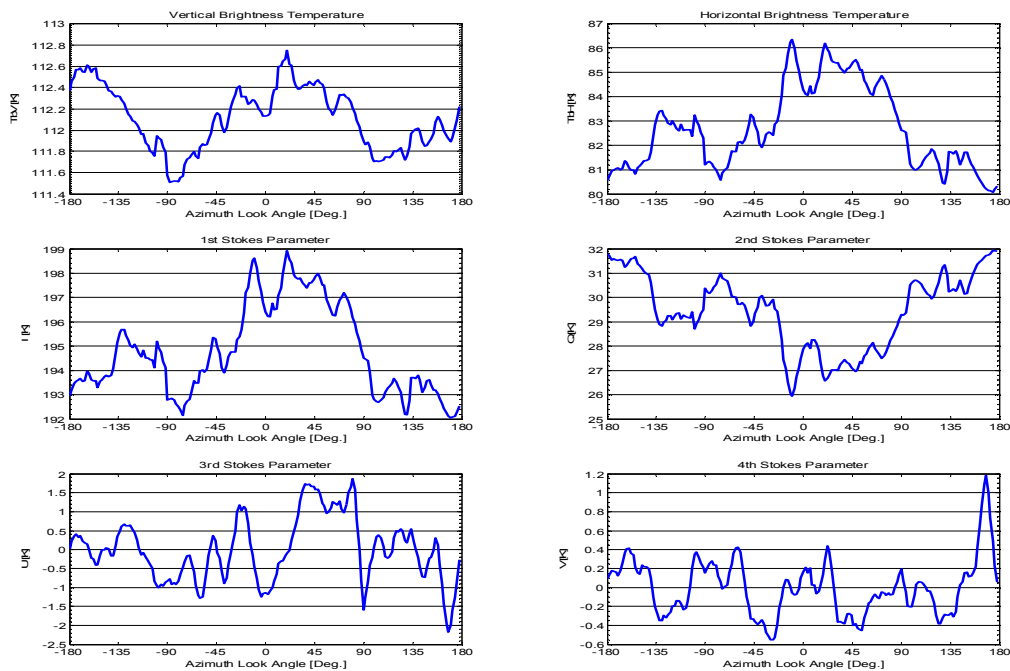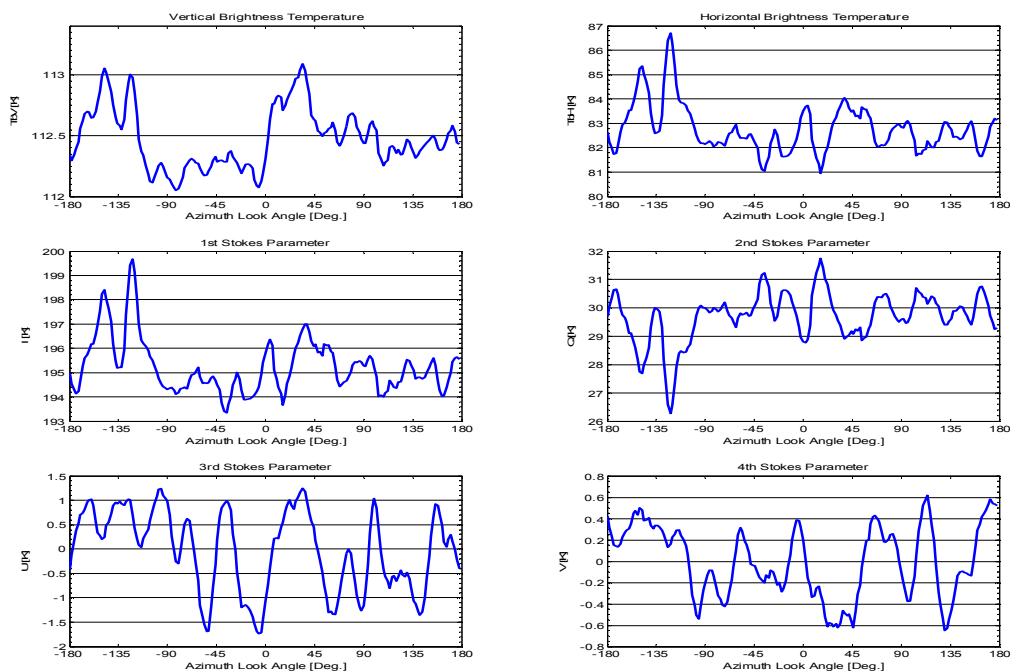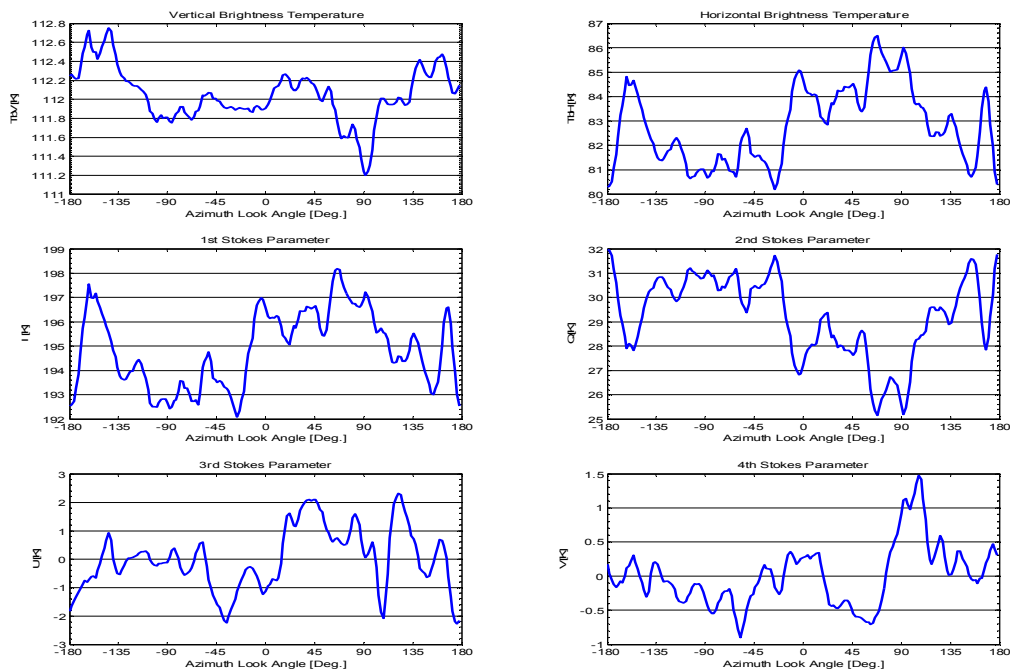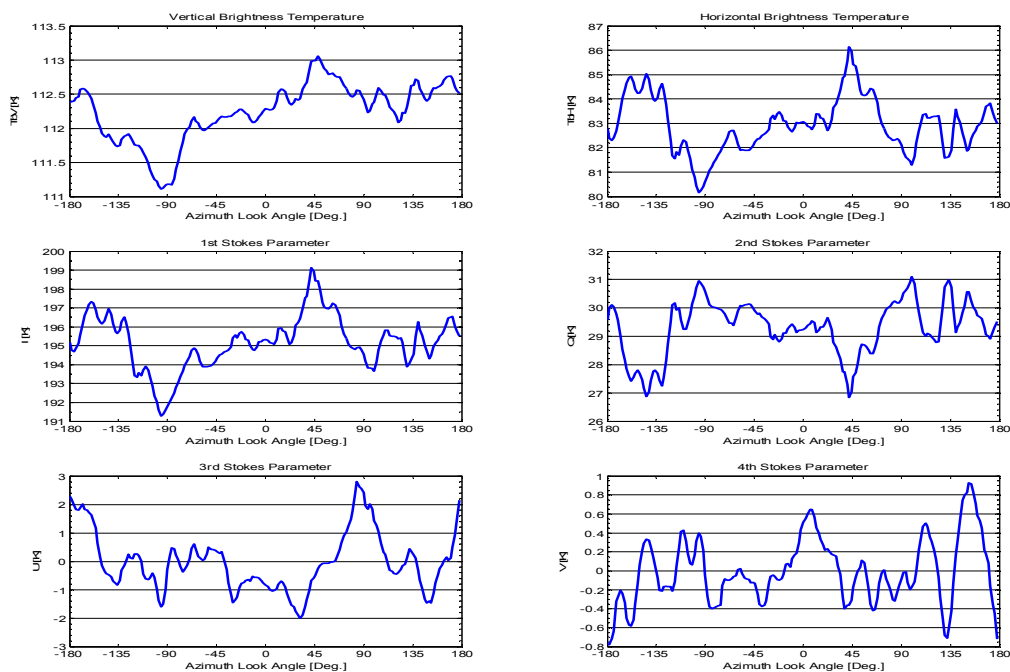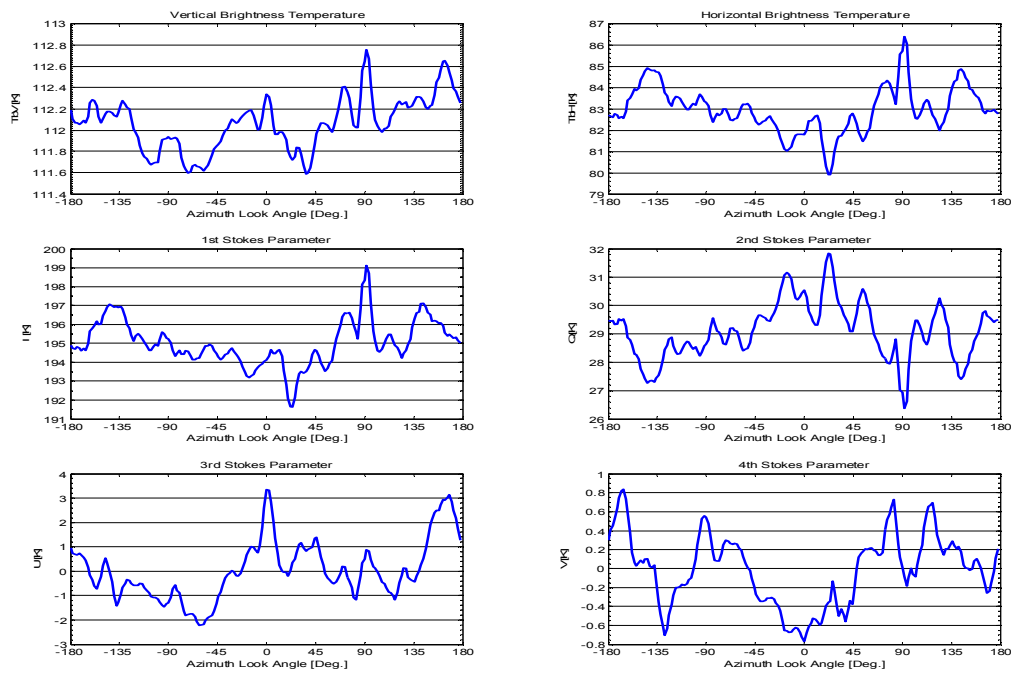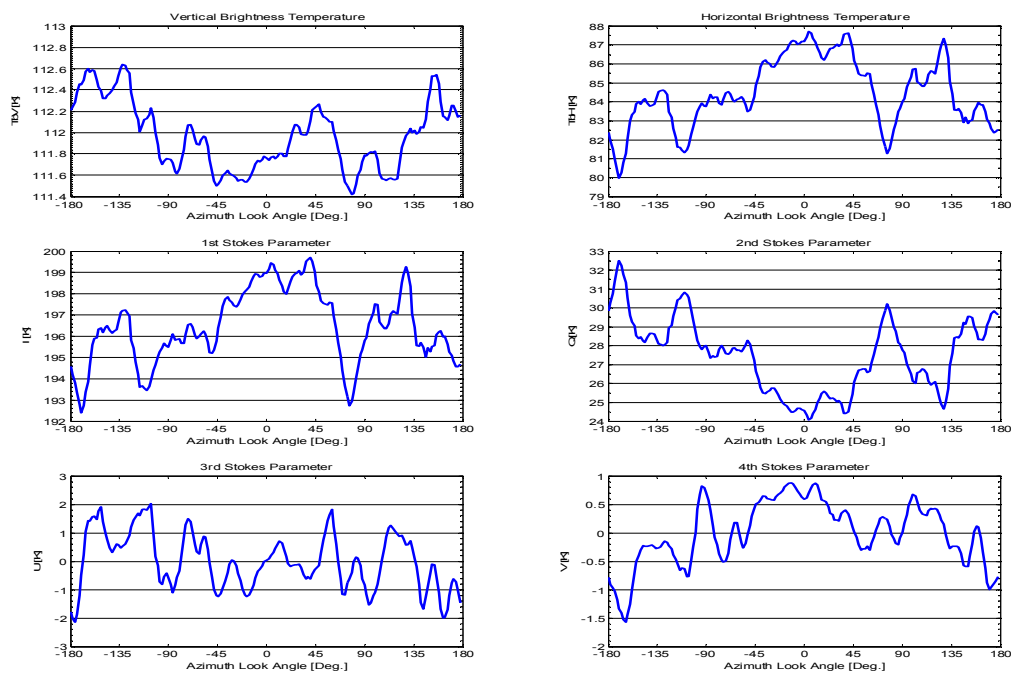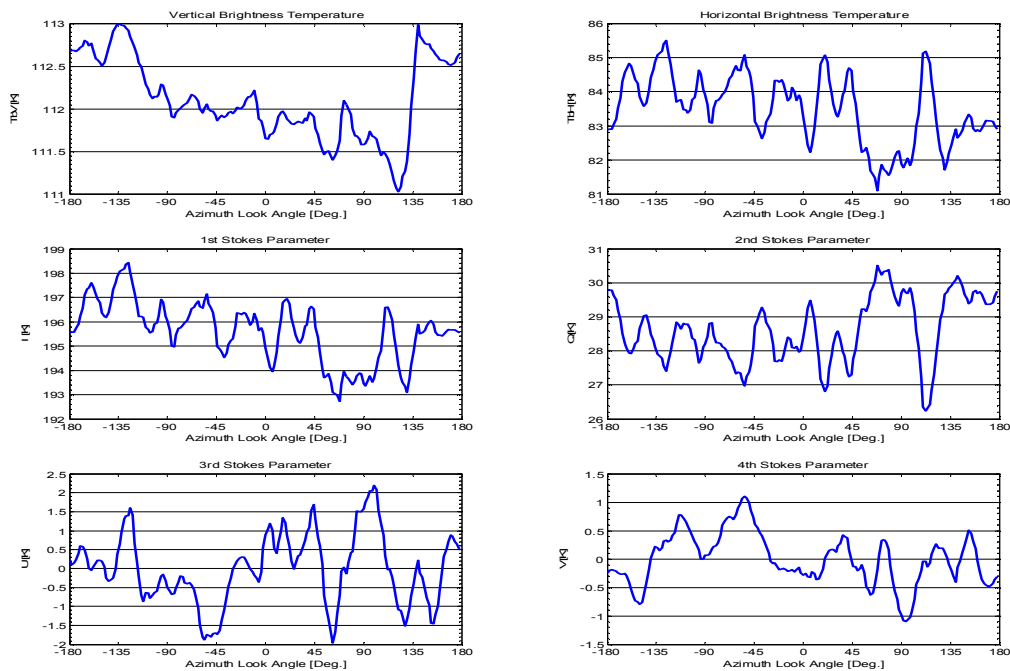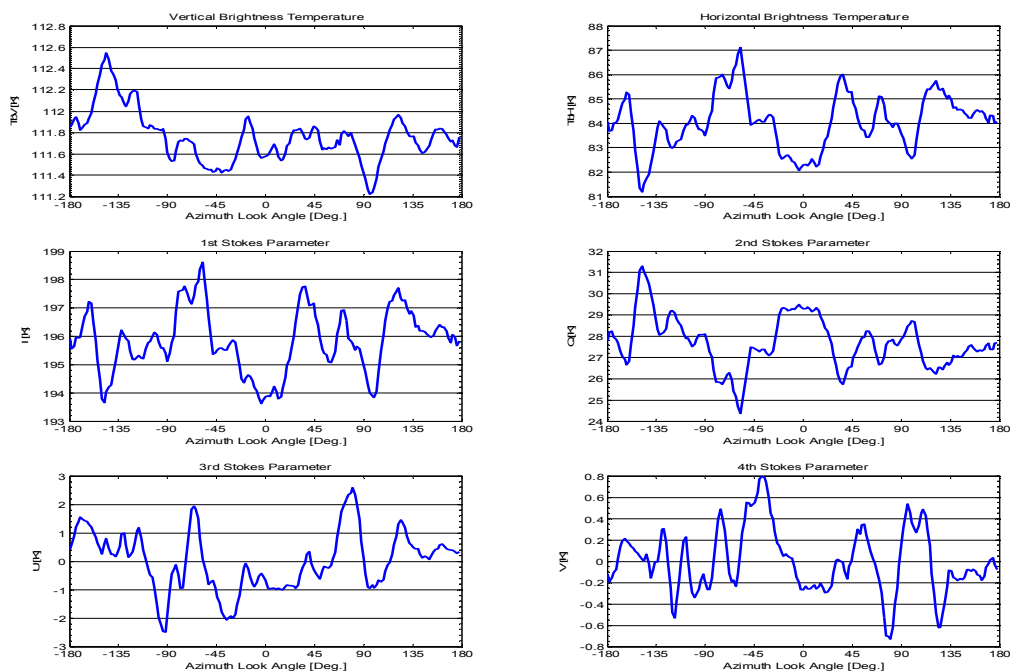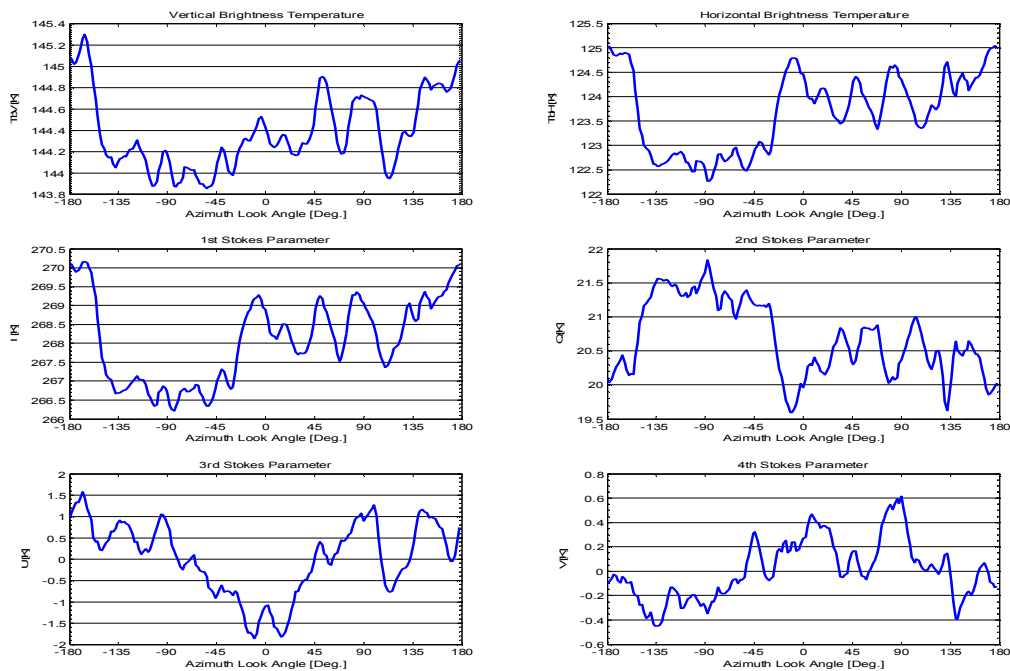
Figure 9.39. The Stokes parameters from the 1ˢᵗ circle flight track with 45° incidence angle from the October 20ᵗʰ 2003, Target B, flight.
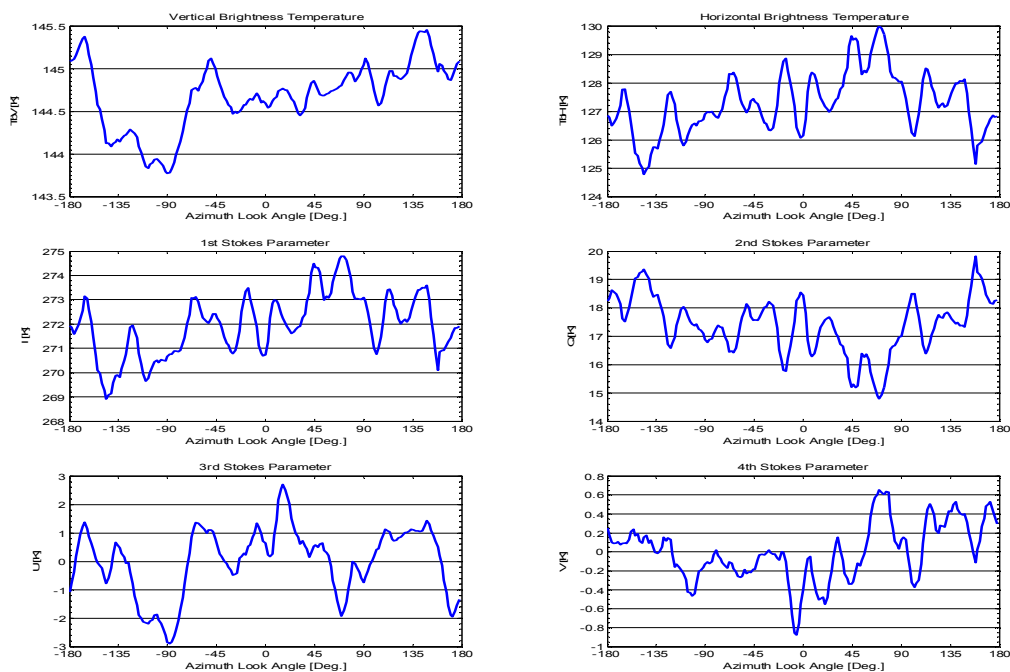
Figure 9.40. The Stokes parameters from the 2ⁿᵈ circle flight track with 45° incidence angle from the October 20ᵗʰ 2003, Target B, flight.
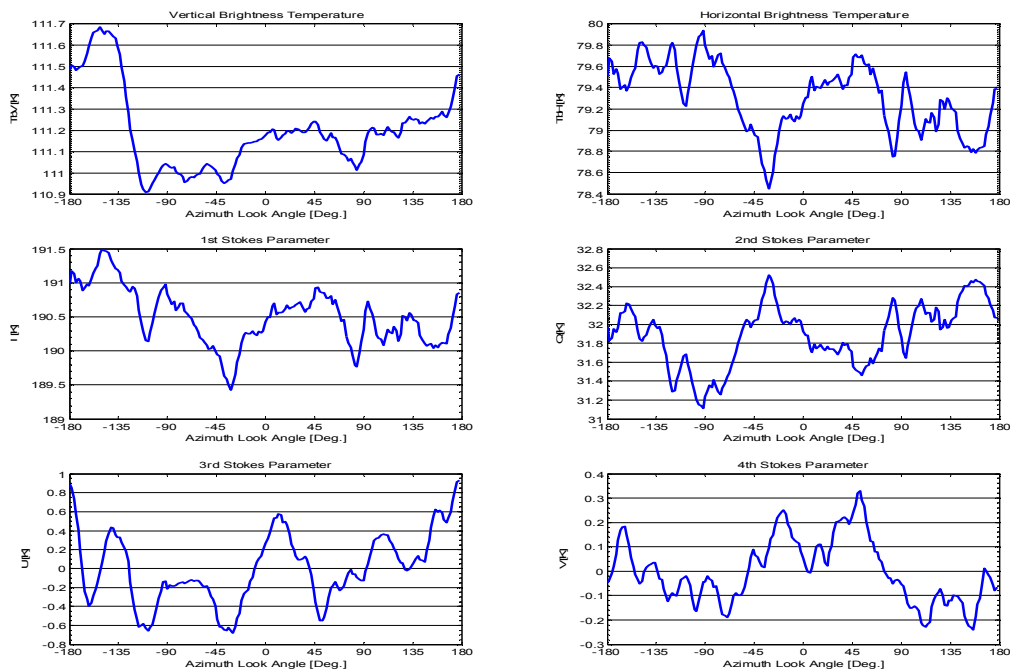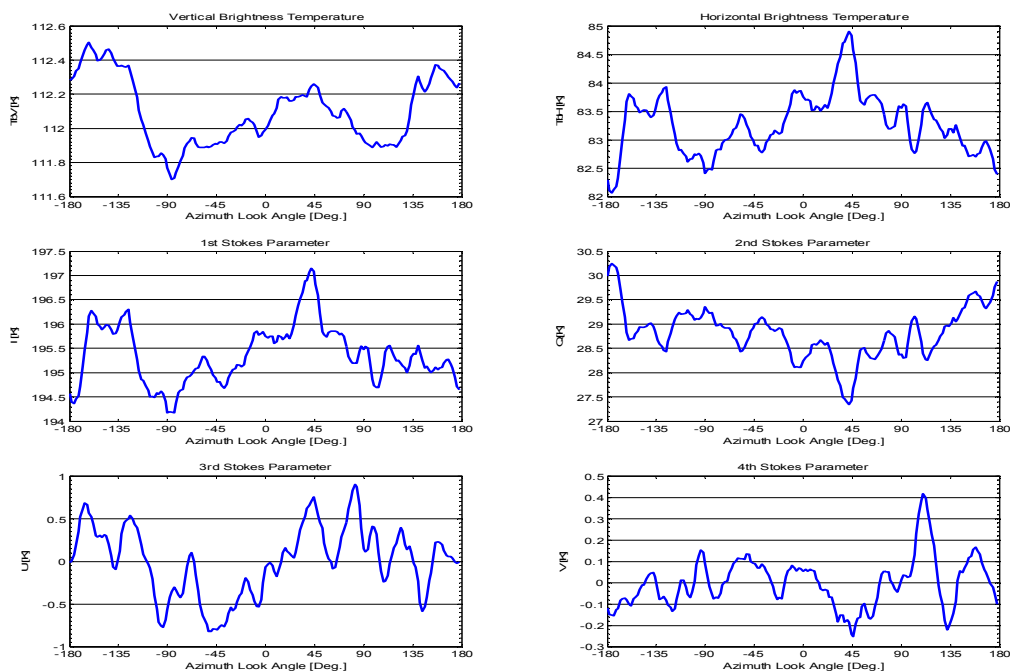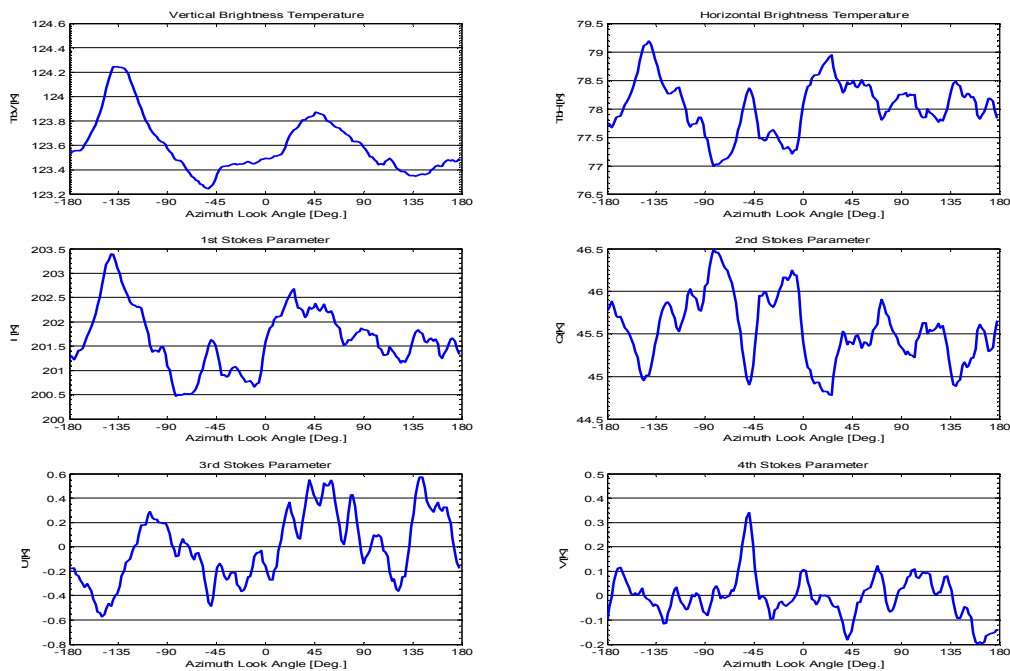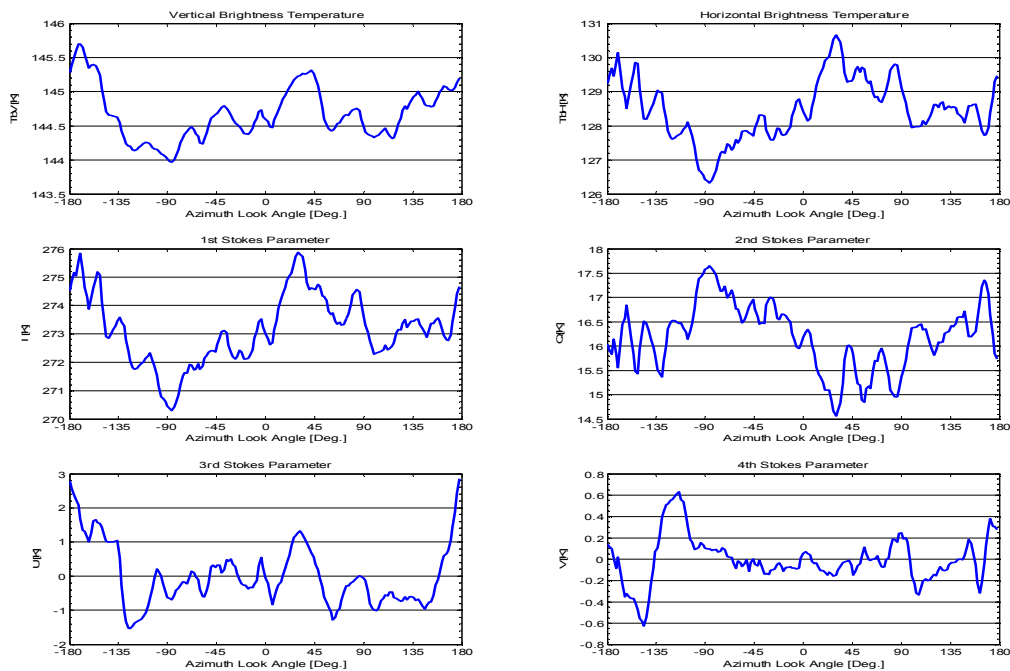
Figure 9.41. The Stokes parameters from the 3ʳᵈ circle flight track with 45° incidence angle from the October 20ᵗʰ 2003, Target B, flight.
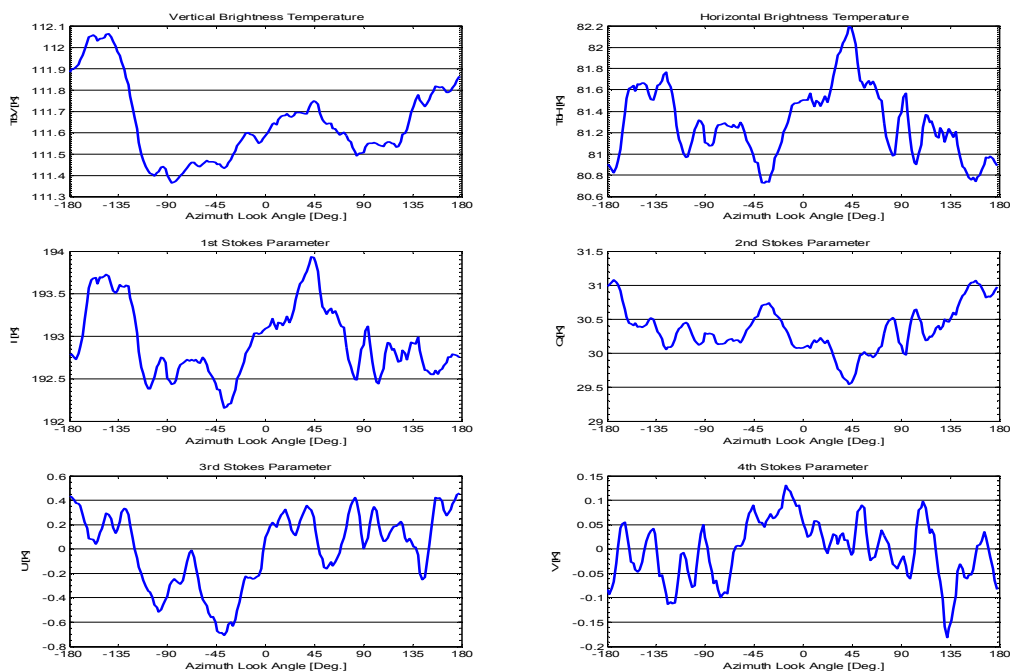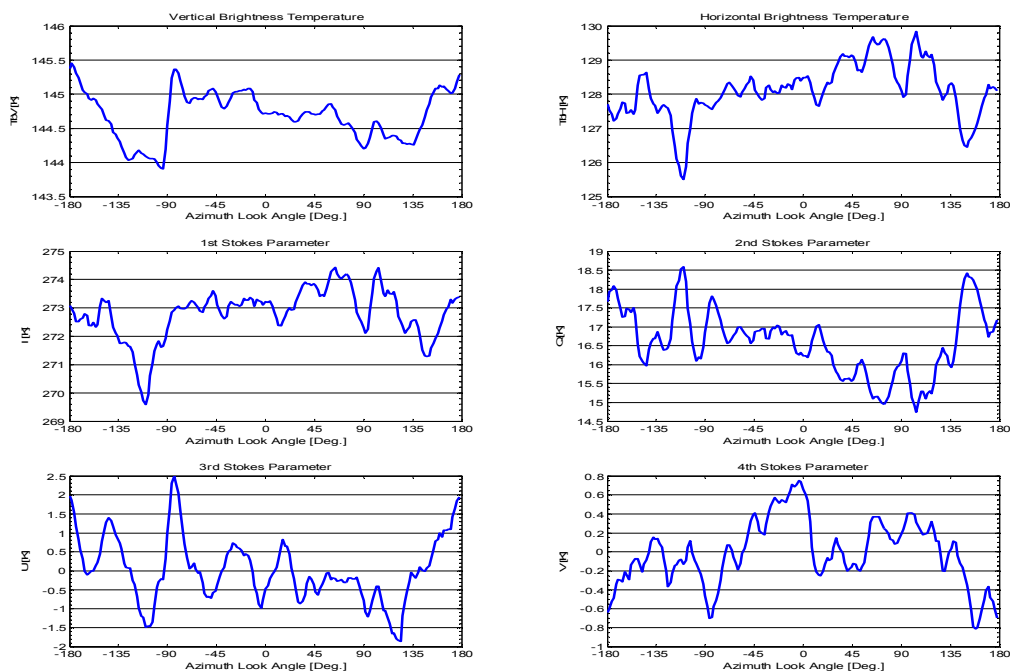

Figure 9.42. The Stokes parameters from the 4ᵗʰ circle flight track with 45° incidence angle from the October 20ᵗʰ 2003, Target B, flight.
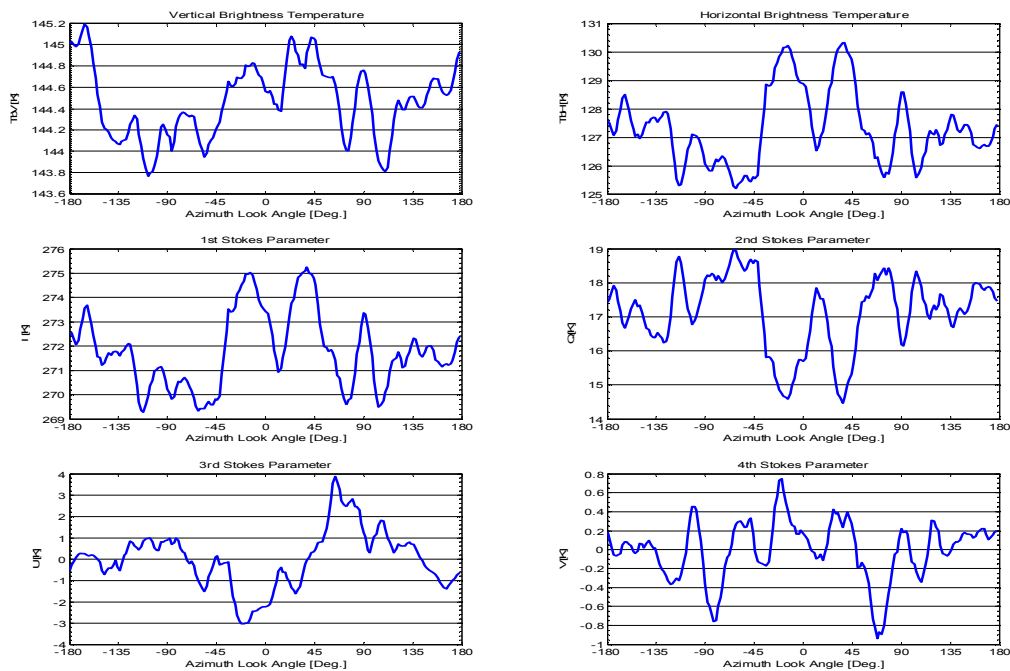
Figure 9.43. The Stokes parameters from the 5th circle flight track with 45° incidence angle from the October 20th 2003, Target B, flight.
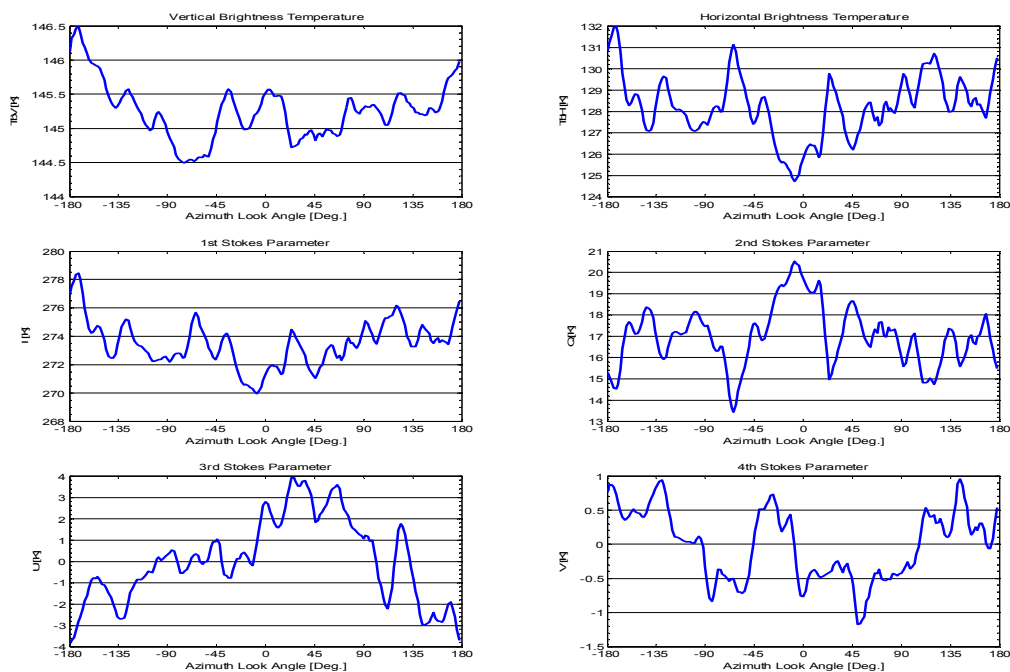
Figure 9.44. The Stokes parameters from the 6th circle flight track with 45° incidence angle from the October 20th 2003, Target B, flight.
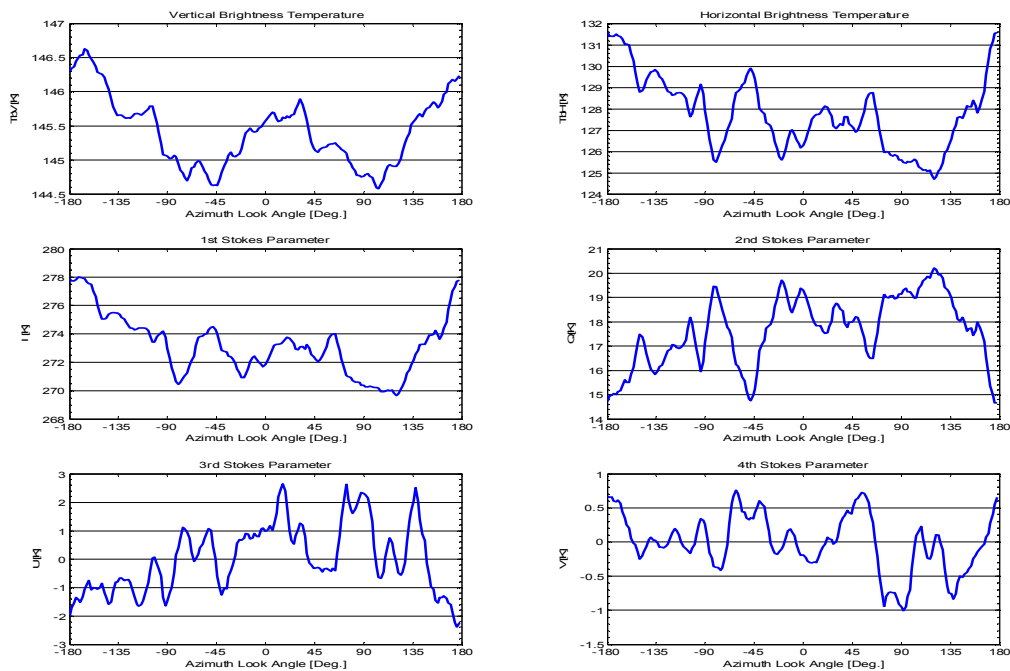
Figure 9.45. The Stokes parameters from the 7th circle flight track with $45°$ incidence angle from the October 20th 2003, Target B, flight.
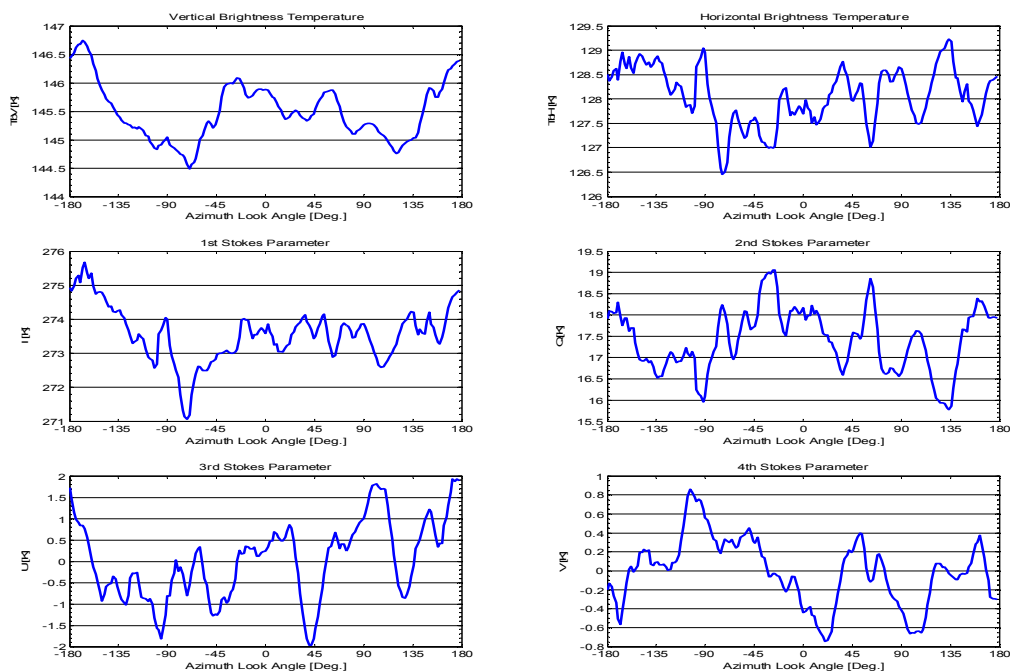
Figure 9.46. The Stokes parameters from the 8th circle flight track with $45°$ incidence angle from the October 20th 2003, Target B, flight.

117
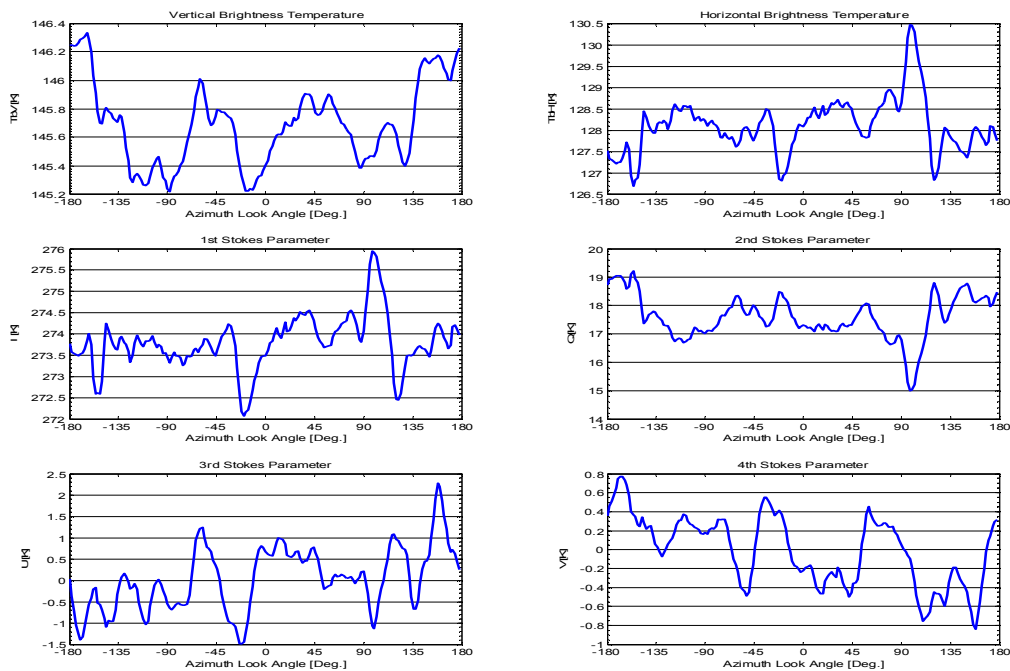
Figure 9.47. The Stokes parameters from the 9th circle flight track with 45° incidence angle from the October 20th 2003, Target B, flight.
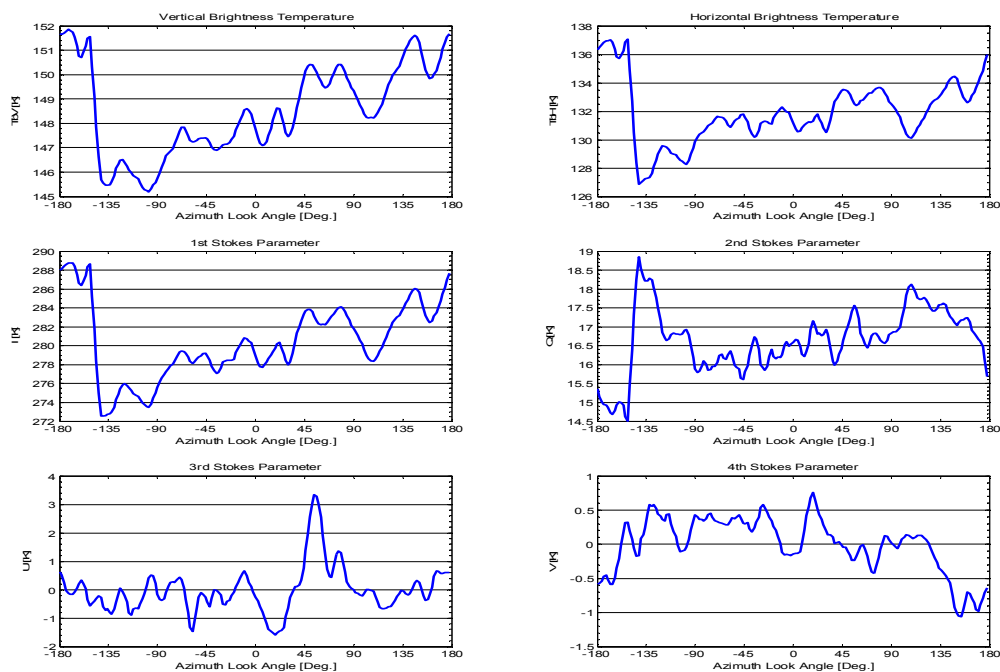
Figure 9.48. The Stokes parameters from the 10th circle flight track with 45° incidence angle from the October 20th 2003, Target B, flight.
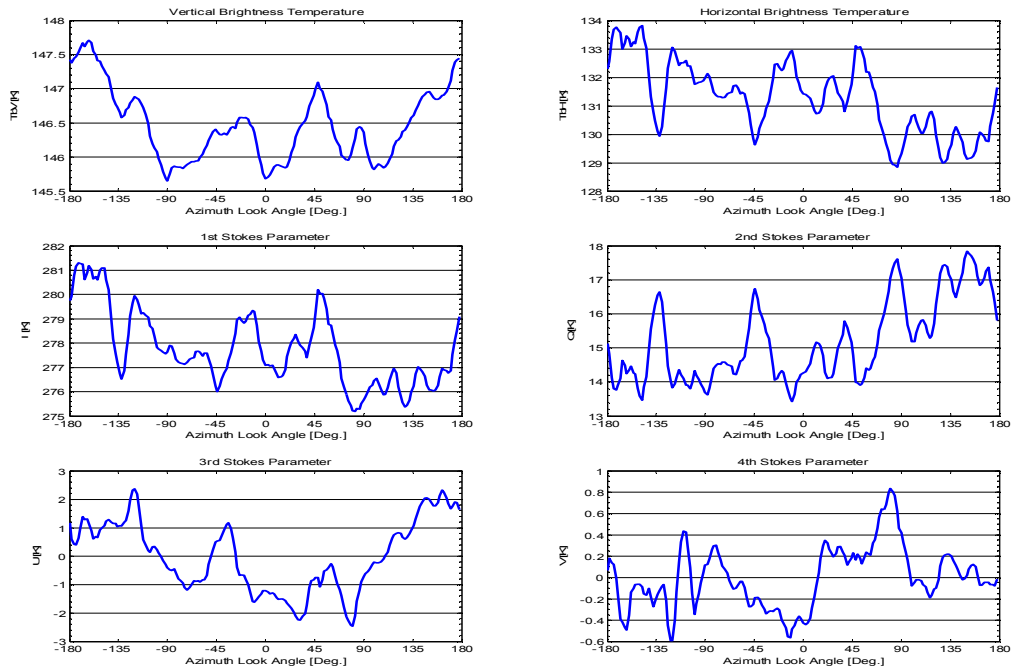
Figure 9.49. The Stokes parameters from the 11th circle flight track with 45° incidence angle from the October 20th 2003, Target B, flight.
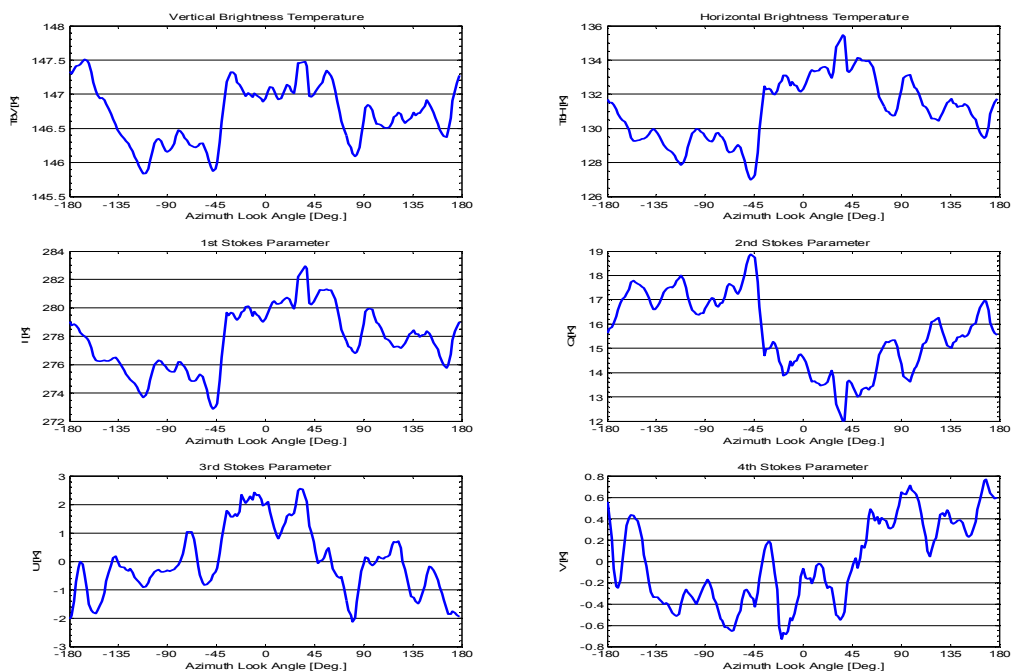
Figure 9.50. The Stokes parameters from the 12th circle flight track with 45° incidence angle from the October 20th 2003, Target B, flight.
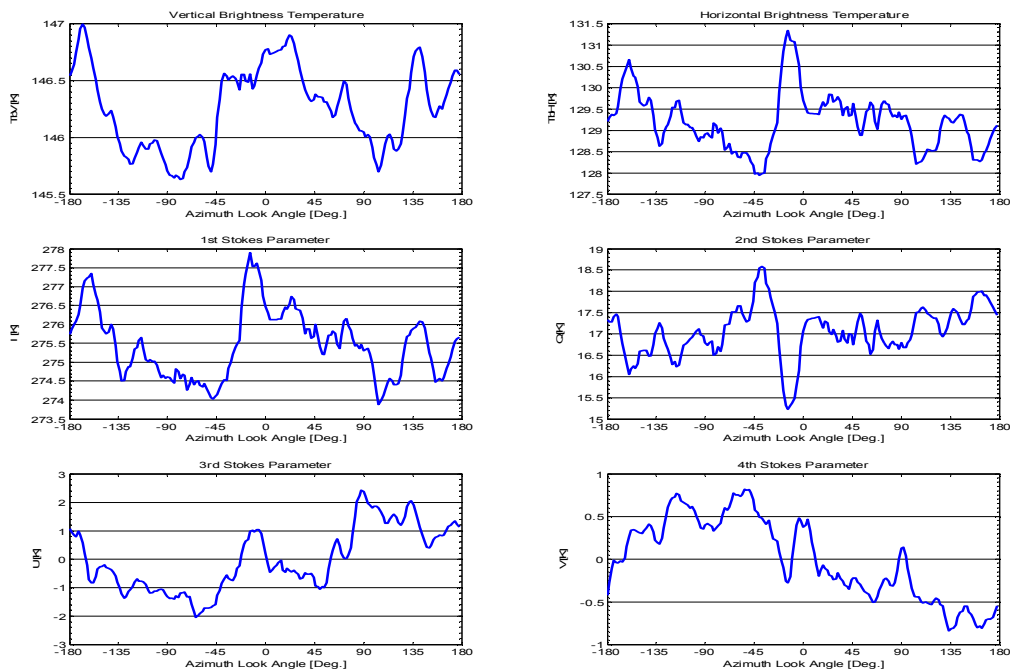
Figure 9.51. The Stokes parameters from the 13th circle flight track with 45° incidence angle from the October 20th 2003, Target B, flight.
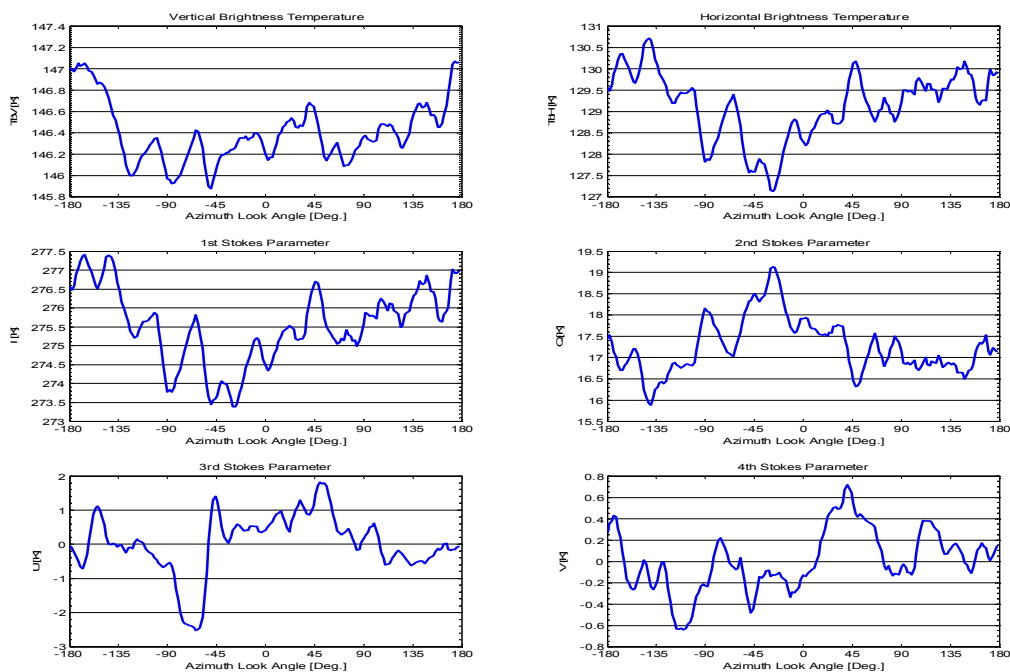
Figure 9.52. The Stokes parameters from the 14th circle flight track with 45° incidence angle from the October 20th 2003, Target B, flight.
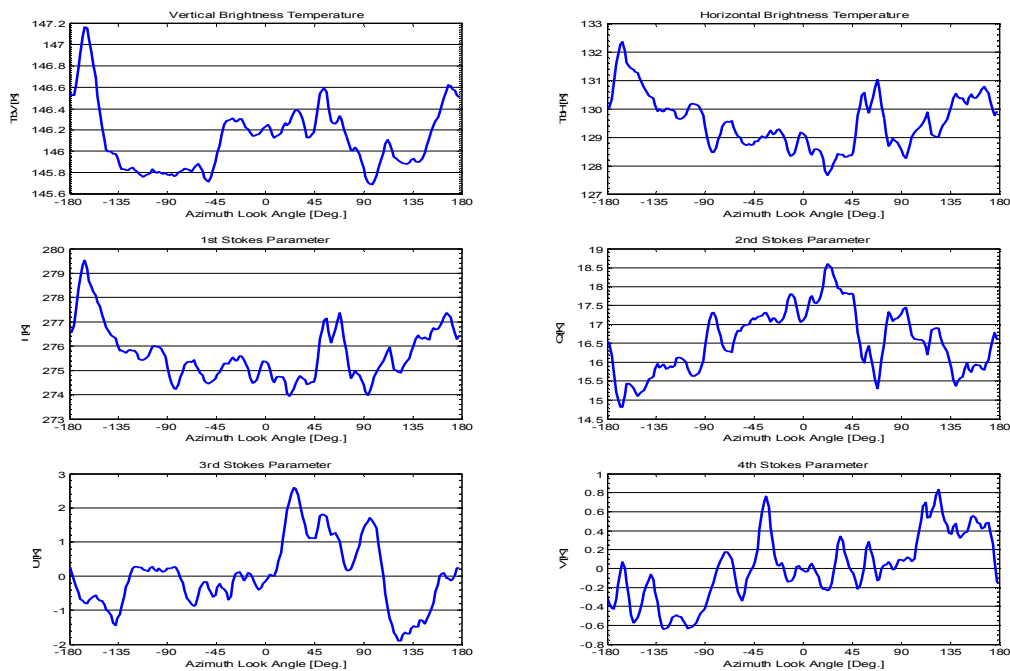
Figure 9.53. The Stokes parameters from the 15th circle flight track with 45° incidence angle from the October 20th 2003, Target B, flight.
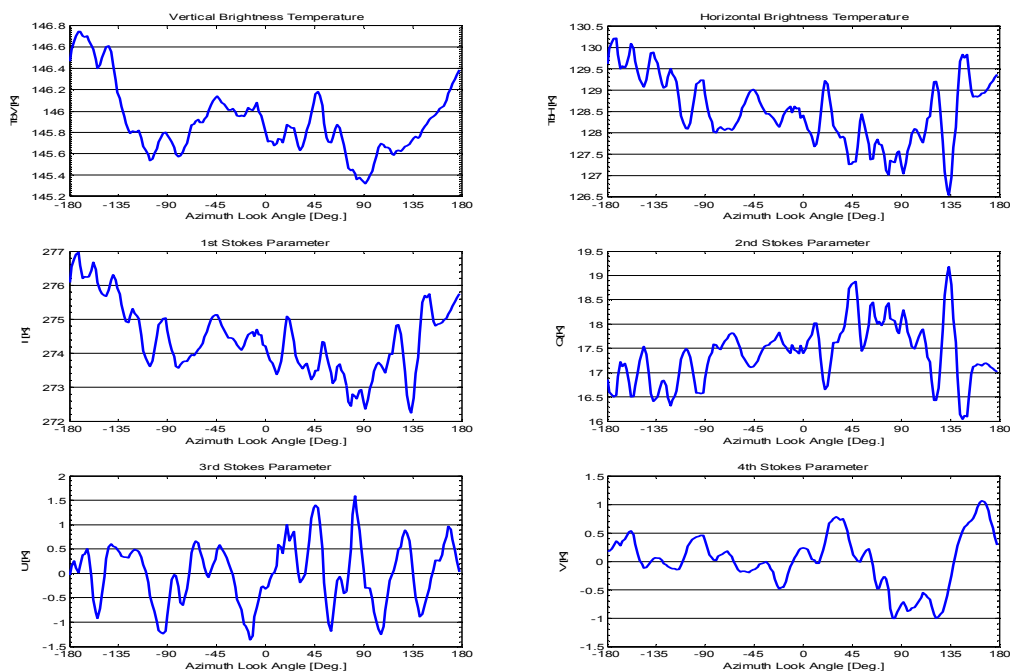
Figure 9.54. The Stokes parameters from the 16th circle flight track with 45° incidence angle from the October 20th 2003, Target B, flight.
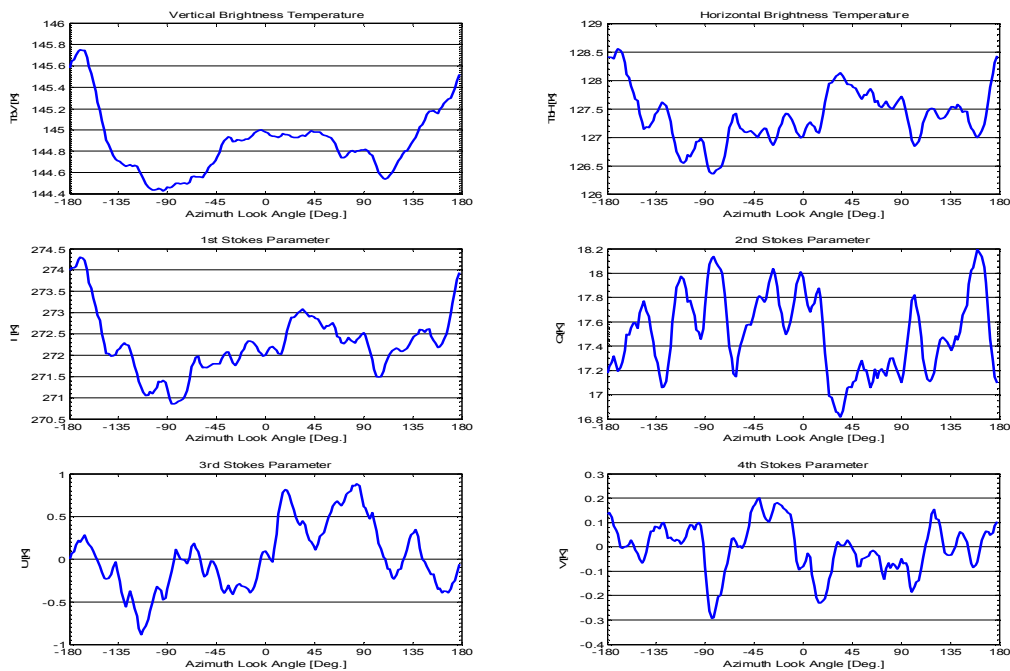
Figure 9.55. The averaged Stokes parameters from the 1st to the 8th circle flight tracks with 45° incidence angle from the October 20th 2003, Target B, flight.
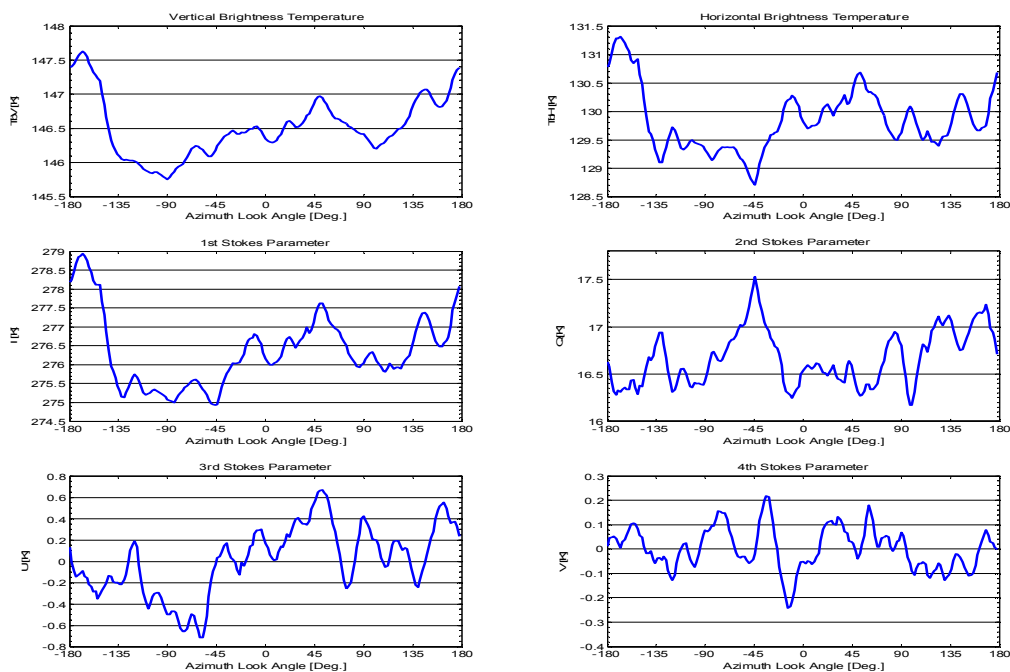
Figure 9.56. The averaged Stokes parameters from the 9th to the 16th circle flight tracks with 45° incidence angle from the October 20th 2003, Target B, flight.
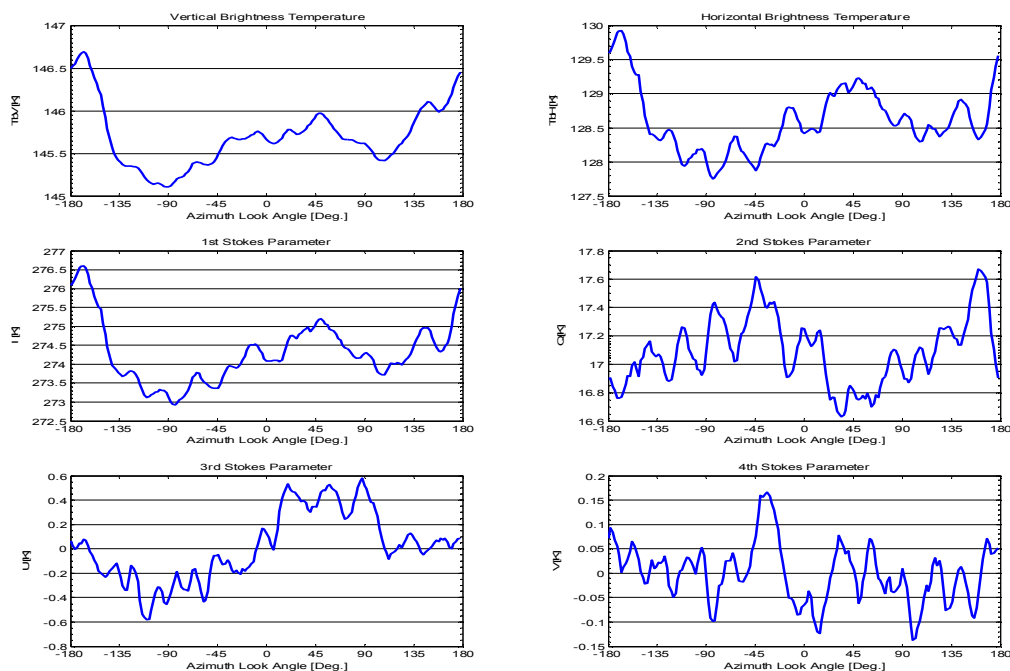
Figure 9.57. The averaged Stokes parameters from all 16 circle flight tracks with 45° incidence angle from the October 20th 2003, Target B, flight.

The results from the secondary target, measured with almost no wind, also show very similar results, compared to the earlier results. It is thus again seen, that the vertical and horizontal polarizations do not reach the full integration gain, while the 3rd and 4th Stokes parameters seem to be almost fully Gaussian. Interpreted as Gaussian signals with an overlaid sinusoidal, the non-Gaussian parts of the vertical and horizontal polarizations are 332 mK and 266 mK, respectively. These values seem to be quite constant from flight to flight, and one reason may be the swell, obviously present at target B on October 20th 2003.

The harmonic analysis of the target B measurements also show some consistence with the results from target A. Comparing the phases of the vertical and horizontal polarizations, it is noticed, that a slight shift has taken place, but it seems, that the overall relation between 1st and 2nd harmonics is quite the same. Comparison of the results to the expected phases from [5] may be relevant in the case of swell, as the wind field, measured at target A was present also at target B until a few hours prior to the flight. It seems, however, as it was seen for the target A results, that very little consistence is present, and no conclusion can be made about the eventual wind driven signature from the circle flight data.

At target A on October 20th 2003, eight legs of a cloverleaf were measured as well, and results from these measurements is seen in the figures 9.58 to 9.65, presented as points, integrated to 1 sec., and plotted with the time-of-day on the horizontal axis. Similar to the high-wind case from March 6th 2003, these legs illustrate the same variability, and it is clear, that the signals may easily change by 1 K within a 30 sec. period. Especially the horizontal polarization seems to contain noise, and it is obvious, that a 2 minute integration period may

be too small to cancel out all variations. The legs are fully integrated, however, and finally they are combined into a full circle signature with eight samples. After low-pass filtering, the signature appears as illustrated in figure 9.66, showing all four parameters with a zero mean to make them fit into the figure. Estimations of the 1st and 2nd order harmonic content in the signatures are made, based on the least-mean-square method, and these results are seen in table 9.6. Finally a plot of the harmonic estimates is seen in figure 9.67, providing a full 360° signature. It is noticed, that the 3rd Stokes parameter has some presence of noise, but all other parameters clearly have variations below 200 mK of magnitude.

Circles	TV, std.dev. [K]	TH, std.dev. [K]	U, std.dev. [K]	V, std.dev. [K]
Single circles	0.353	0.807	0.856	0.244
45° incidence angle	0.400	1.074	1.193	0.304
	0.392	0.908	0.908	0.219
	0.356	0.808	0.862	0.346
	0.343	1.291	1.360	0.308
	0.418	1.460	1.960	0.514
	0.515	1.721	1.196	0.414
	0.510	0.585	0.920	0.353
	0.291	0.648	0.752	0.369
	1.879	2.228	0.825	0.404
	0.530	1.279	1.248	0.290
	0.433	1.878	1.191	0.402
	0.359	0.670	1.122	0.474
	0.287	0.788	0.872	0.290
	0.314	0.944	0.981	0.357
	0.325	0.790	0.632	0.475
Average, single	0.482	1.118	1.055	0.360
4 circles	0.293	0.623	0.477	0.137
integrated	0.372	0.678	0.819	0.225
	0.667	0.852	0.356	0.156
	0.271	0.543	0.513	0.147
Average, 4 integrated	0.401	0.674	0.541	0.166
8 integrated	0.307	0.477	0.394	0.104
	0.446	0.552	0.323	0.086
Average, 8 integrated	0.377	0.514	0.359	0.095
All 16 integrated	0.370	0.479	0.284	0.060

Table 9.4. Total rms. noise for the full signal in the modified Stokes parameters from the 16 circle flights with 45° incidence angle from October 20th 2003, Target B. The circles are processed as single tracks, averaged as 4 times four circles, 2 times eight, and totally.

Inc.	Harm.	TV, M.	TV, Ph.	TH, M.	TH, Ph.	U, Mag.	U, Ph.	V, Mag.	V, Ph.
45°	1	0.27	-135.32	0.33	-119.10	0.35	-72.96	0.02	92.65
	2	0.37	-6.91	0.43	-38.19	0.11	-62.21	0.01	6.70
	3	0.21	166.78	0.23	162.42	0.08	-179.36	0.04	151.00
	4	0.03	-36.58	0.09	-68.79	0.03	-55.62	0.03	149.28

Table 9.5. 1st, 2nd, 3rd, and 4th harmonic components in the averaged modified Stokes parameters from the circle flights from October 20th 2003, Target B.
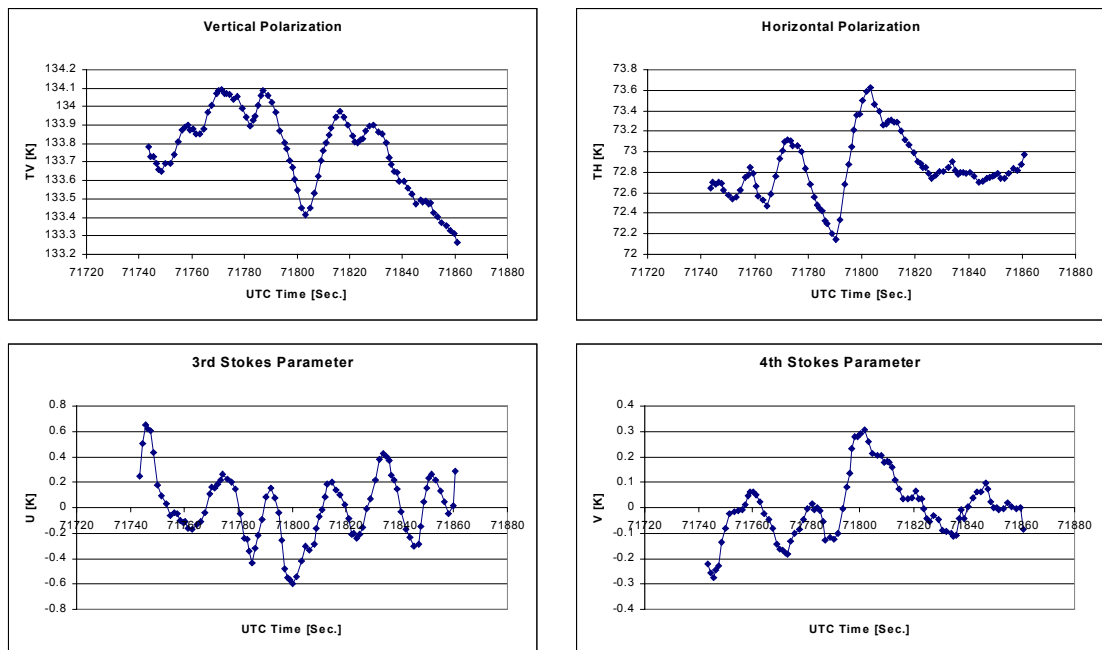
Figure 9.58. The modified Stokes parameters from the level flight track from October 20th 2003, Target A, 50° incidence angle, heading 180°.
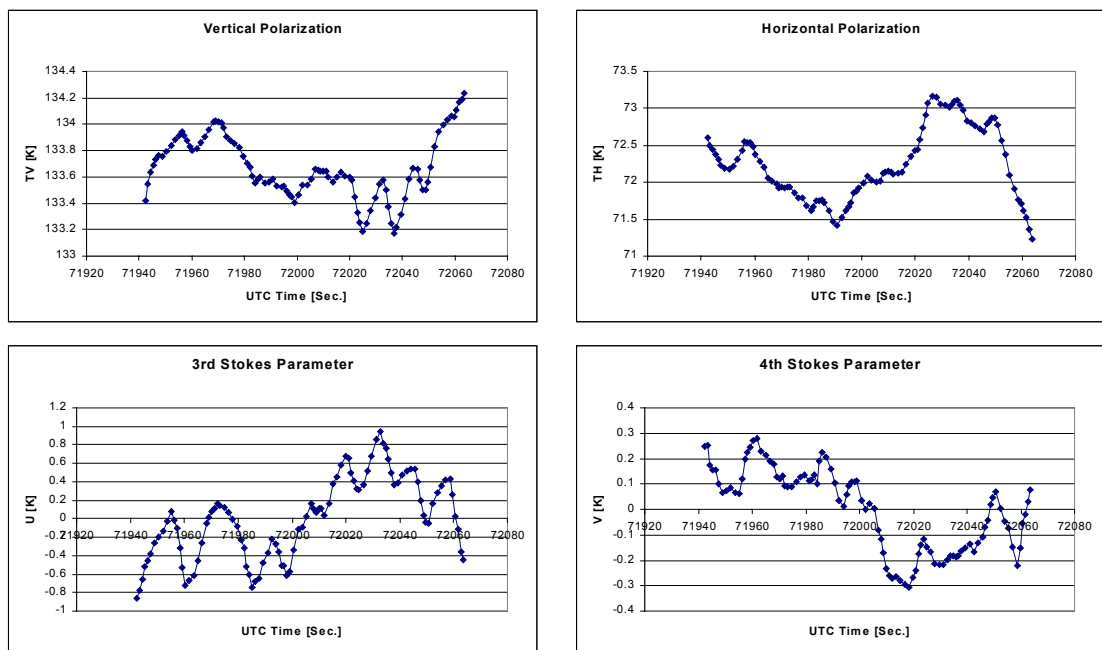
Figure 9.59. The modified Stokes parameters from the level flight track from October 20th 2003, Target A, 50° incidence angle, heading +45°.
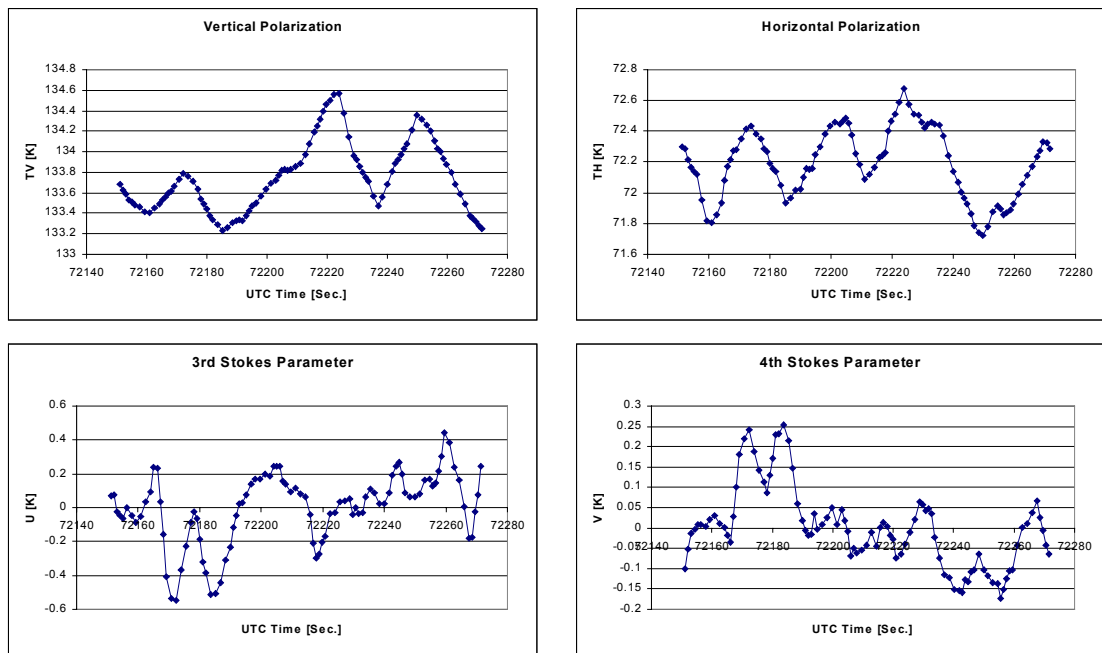
Figure 9.60. The modified Stokes parameters from the level flight track from October 20th 2003, Target A, 50° incidence angle, heading -90°.
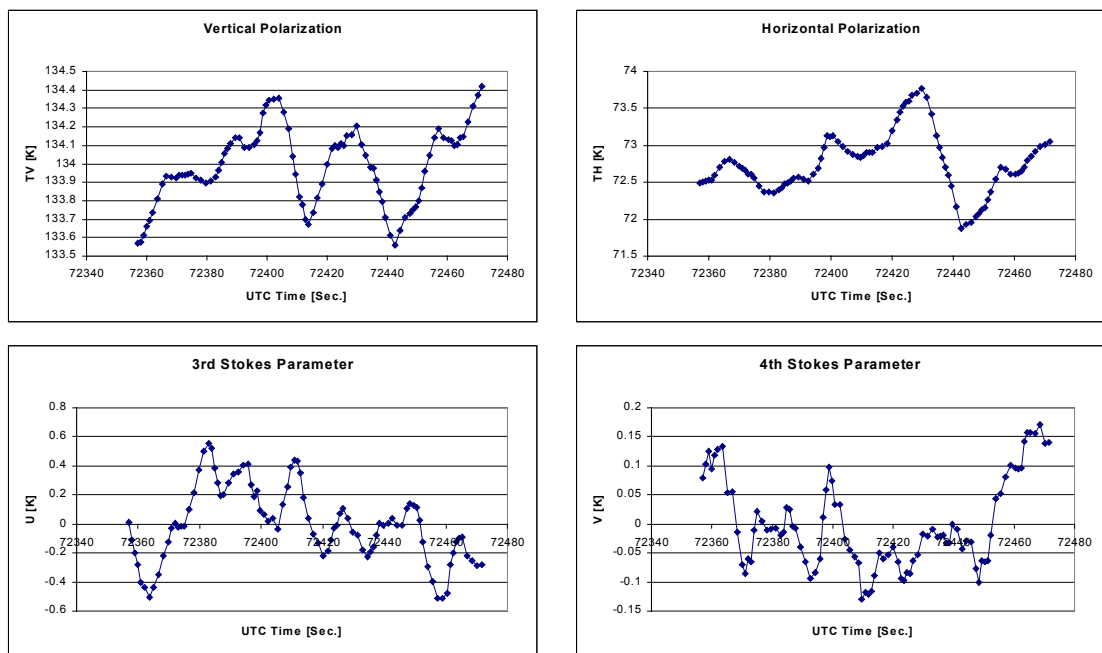
Figure 9.61. The modified Stokes parameters from the level flight track from October 20th 2003, Target A, 50° incidence angle, heading +135°.
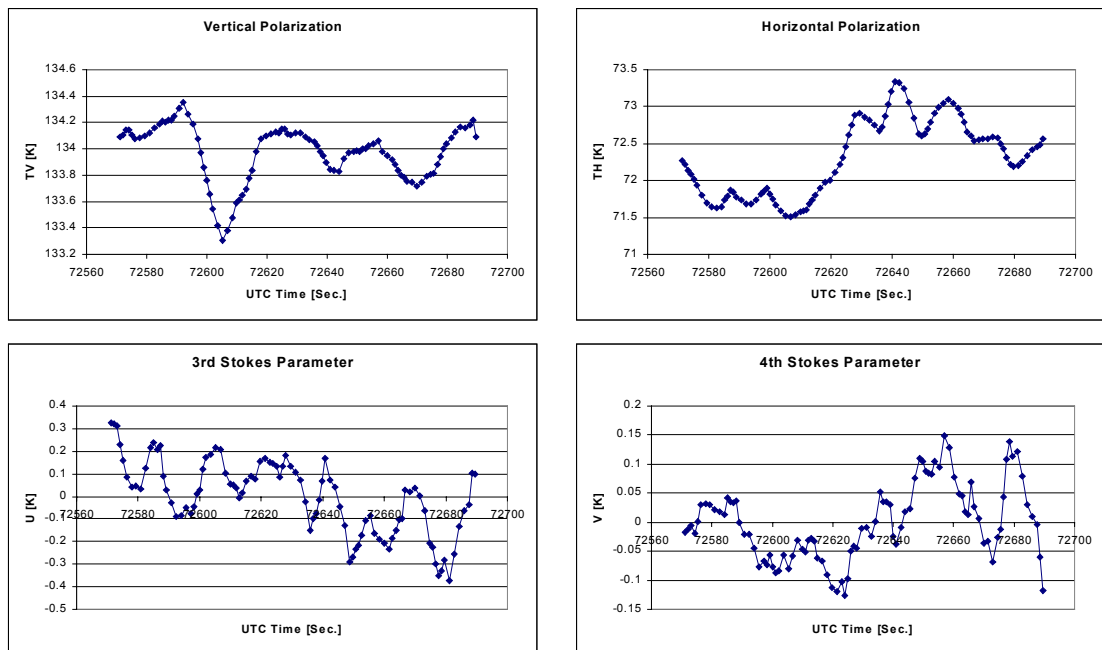
Figure 9.62. The modified Stokes parameters from the level flight track from October 20th 2003, Target A, 50° incidence angle, heading 0°.
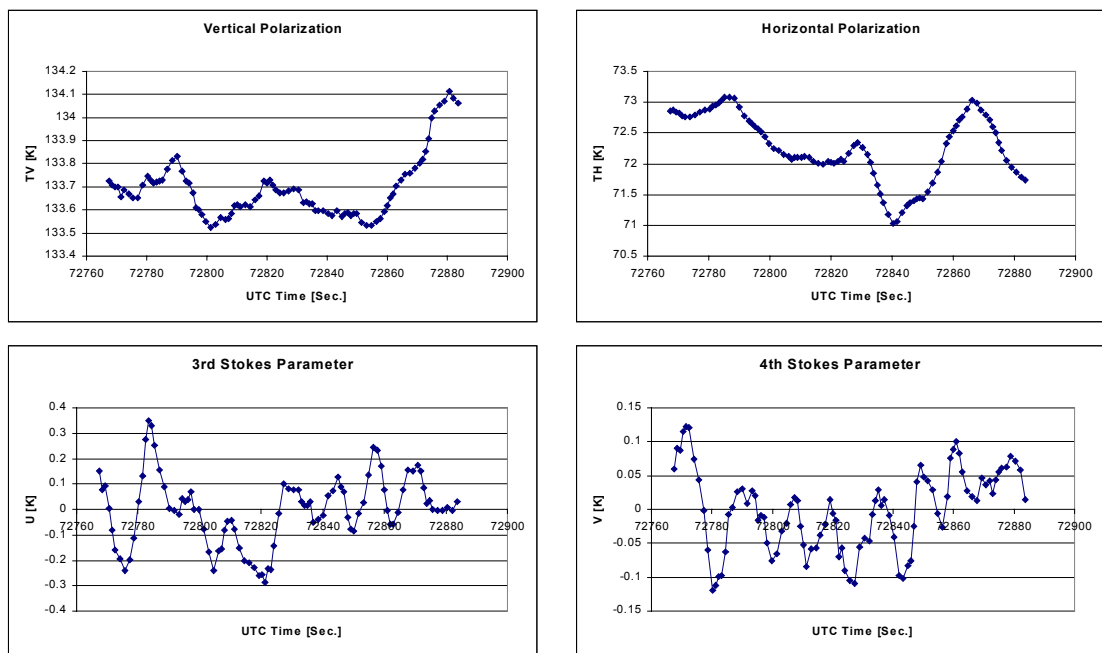
Figure 9.63. The modified Stokes parameters from the level flight track from October 20th 2003, Target A, 50° incidence angle, heading -135°.
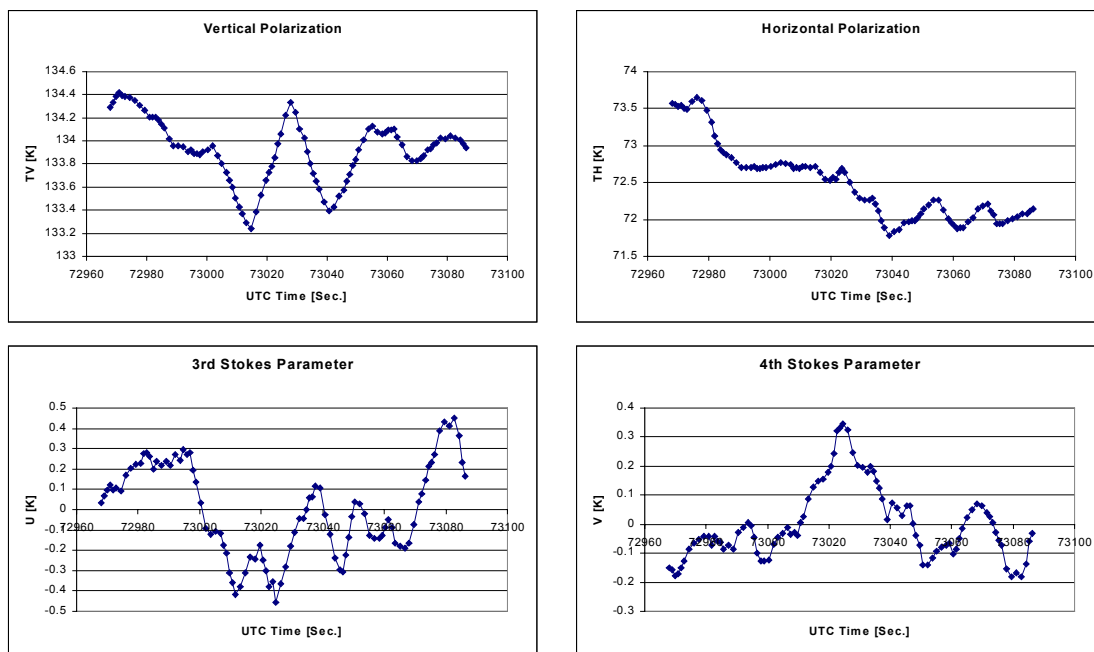
Figure 9.64. The modified Stokes parameters from the level flight track from October 20th 2003, Target A, 50° incidence angle, heading +90°.
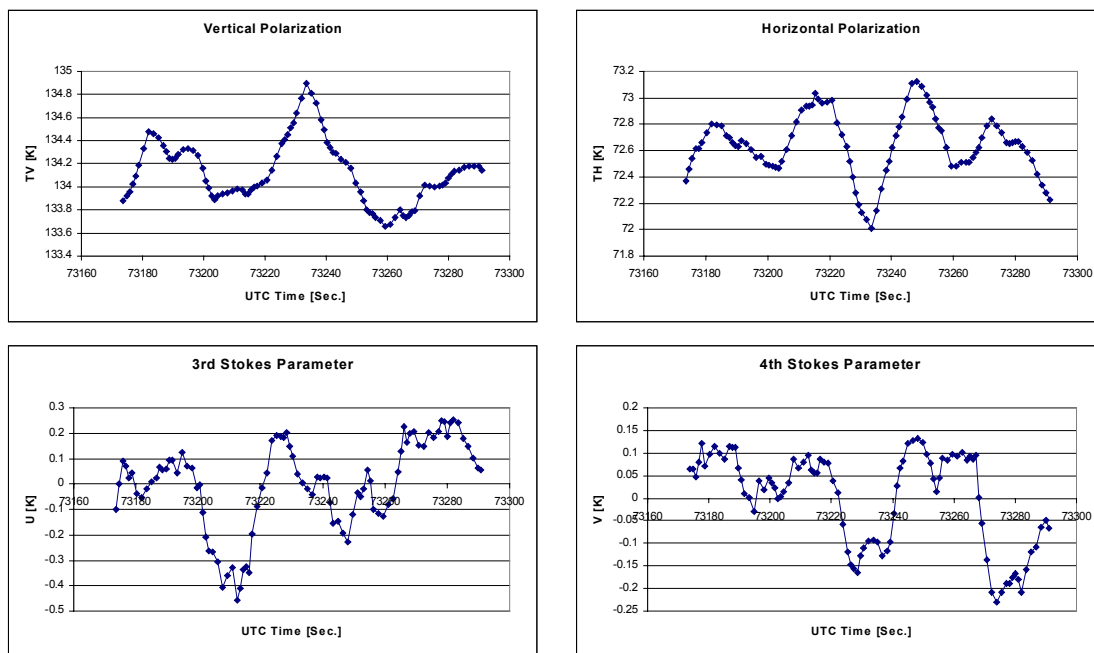
Figure 9.65. The modified Stokes parameters from the level flight track from October 20th 2003, Target A, 50° incidence angle, heading -45°.

128
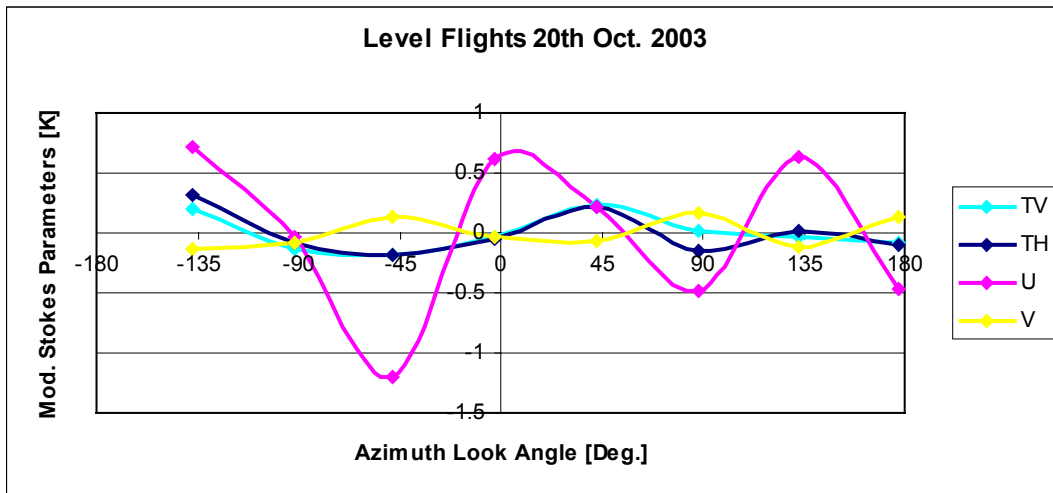
Figure 9.66. The modified Stokes parameters from the level flight tracks October 20th 2003, 50° incidence angle.
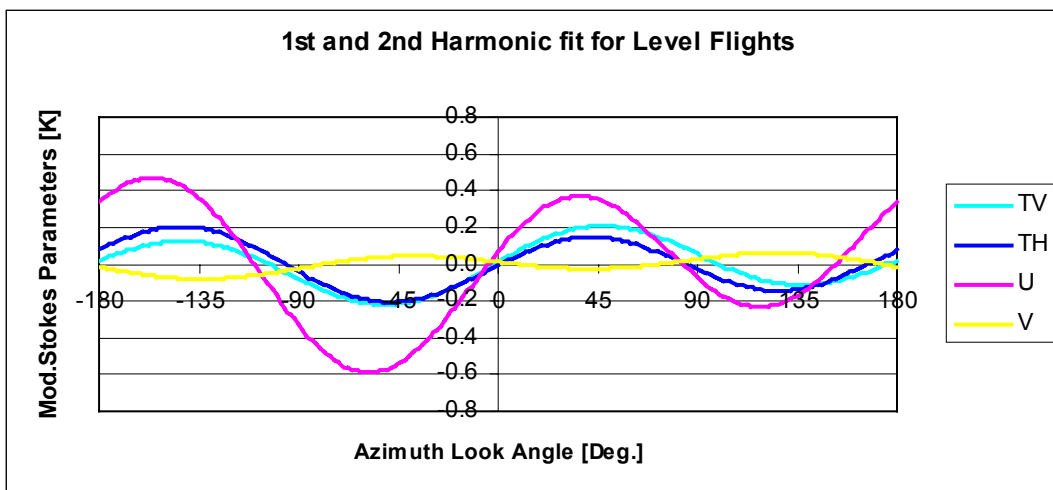
Figure 9.67. The modified Stokes parameters from the level flight tracks October 20th 2003, 50° incidence angle. Result of 1st and 2nd harmonic fit.

Inc.	Harm.	TV, M.	TV, Ph.	TH, M.	TH, Ph.	U, Mag.	U, Ph.	V, Mag.	V, Ph.
Level	1	0.07	-94.41	0.04	-172.80	0.19	-136.27	0.03	-60.97
50° inc.	2	0.16	-85.33	0.17	-78.62	0.41	-60.44	0.05	91.87

Table 9.6. The modified Stokes parameters from the level flight tracks October 20th 2003, 50° incidence angle. Result of 1st and 2nd harmonic fit.

10. Influence from the Galactic background

All the LOSAC data show large peal-to-peak variations, and from the statistical analysis it is obvious, that the signals are not fully random. Typically signals of several hundreds of mK seem to be present, and it is obvious to try to identify the origin of these contributions. Large point targets at far distances (typical RF-sources) reaching an antenna side lobe could be likely sources, as they would be expected to cover a constant angular range, repeating from circle to circle. Typically manmade sources are polarized, however, and the effect would thus appear not only in the two linear polarizations and in the 1st Stokes parameter, but in at least one of the other stokes parameters. Moreover flights were carried out over many different areas, and it is unlikely, that all target areas provide the same type of interference signals.

Natural targets will typically be unpolarized and location independent, and one possible source of errors, the sun, was already included in the experiment planing. The sun occupies a mean angle of 0.5337° by 0.5337°, equal to a size of 6.81e-5 sr. With a 15° by 15° antenna beam, the sun with an L-band brightness temperature of the order of $T = 10^5$ K will provide a downwelling radiation equal to about 100 K. The reflection from the sea surface will thus result in a signal larger than 50 K. As the flights take place after sunset, however, the sun is not a possible source of noise, but other objects on the sky could eventually cause similar effects. The moon occupies an angular space equal to the sun, but as the moon is a cold object, below 300 K, the downwelling radiation will be below 300 mK. The reflected power will thus be in the order of 150 mK, causing a visible effect in the polarimetric signature, but smaller than the observed signal in the vertical and horizontal polarizations, and thus also in the 1st Stokes parameter.

Warm objects on the sky at larger distances will typically occupy a very small angular space, but at high concentration, they may contribute to the total background. With specific help from Dr. David M. LeVine, Goddard Space Flight Center, NASA, the background radiation from the total sky was evaluated for one of the 45° incidence angle flights from October 25th 2001, the 2nd circle in the first data set, illustrated in figure 7.9. The curve is presented in figure 10.1a.
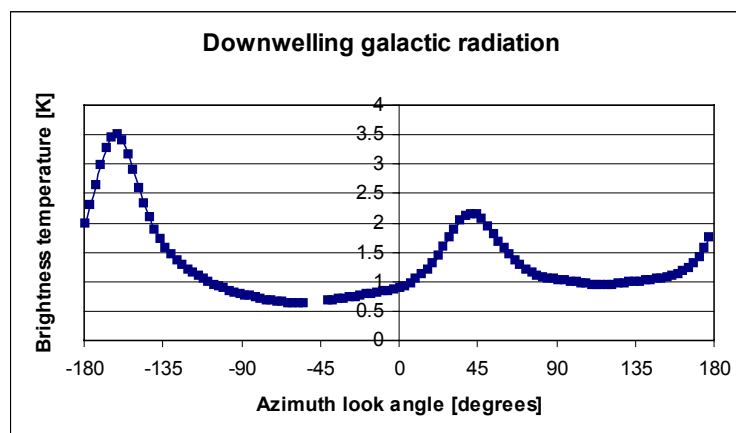
Figure 10.1a. Downwelling radiation from the galactic background as a function of the azimuth look angle. The curve corresponds to the galactic constellation at 5:25pm UTC on October 25th 2001, observed from the target area with a 45° incidence angle.

As the radiation is unpolarized, it is assumed equal in the horizontal and the vertical polarizations. Corrected for the reflection coefficient at the sea surface, evaluated using the Klein-Swift model, the incident signal to the radiometer resulting from the galactic background can be calculated, and it can be subtracted from the measured horizontal and vertical signals. This is done in figure 10.1b, illustrating the signal before (blue curves) and after (purple curves) the correction.
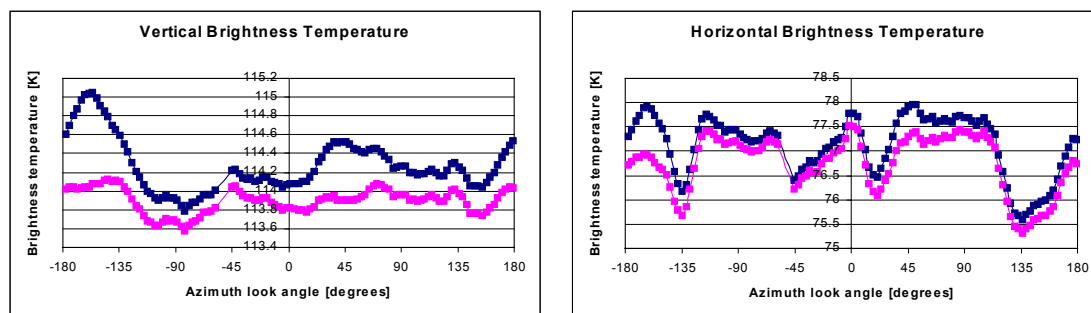
Figure 10.1b. Vertical and horizontal brightness temperatures from the 2nd circle track with 45° incidence angle from October 25th 2001. The blue curve shows the measured brightness temperatures, and the purple curve is the result after correction for the downwelling galactic background radiation.

It is observed, that the vertical polarized signal has a very high correlation with the calculated galactic background radiation, and hence a good effect of the correction. The horizontal polarization is noisier and less correlated, but still an effect of the correction is noticed. For comparison it was tried to evaluate the galactic background radiation at an incidence angle of ±0.5° equal to the effect of roll variations over the track. It was seen, however, that the resulting changes were less than 10 mK for the downwelling signal, and thus of the order of 5 mK for the signal incident to the antenna.

The results from the evaluation of the galactic background influence show, that a signal with a magnitude about 500 mK will result in the vertical and the horizontal channels for the 45° incidence angle. Likewise the results from the other incidence angles may be influenced, and to be able to conclude the LOSAC, a correction for the galactic background signals must be carried out. Basically the inputs to the correction model are the flight-time, attitude, look-direction etc. The algorithm must contain a map of the sky, and an estimate of the reflection coefficient at the sea surface must be available. With help from Dr. David M. LeVine, the skymap is made available, and the necessary geometric information for the sky-map look-up is directly calculated from the flight data. The unknown is the sea surface reflection, however, which is a bistatic reflection problem. For a perfect mirror, the reflection is easily calculated from the Klein-Swift model [4], providing information about the surface dielectric constant, and thus directly yielding the scalar reflection constant, when the antenna beam is reflected in the sea surface.

For a realistic sea surface, however, the reflected antenna beam is smeared, and the scalar reflection coefficient will overestimate the effect of the galactic background in the central part of the galaxy, and it will underestimate the effect near the edges. As the galactic map is already smeared, however, due to the relatively wide antenna beam, 15°, the effect may be relatively small for small wind speeds, and a first order approximation could be obtained by

calculation of the regression between the measured brightness temperatures and the incident galactic background. For perfect reflection, this regression is expected equal to the Fresnel reflection coefficient, found from the Klein-Swift model [4], and for more rough surfaces, the number is expected to reduce. A typical result is shown in figure 10.2a, illustrating the regression between the measured vertical brightness temperature at target A on October 20th 2003, and the incident galactic radiation, taken as the average over all 16 circles.
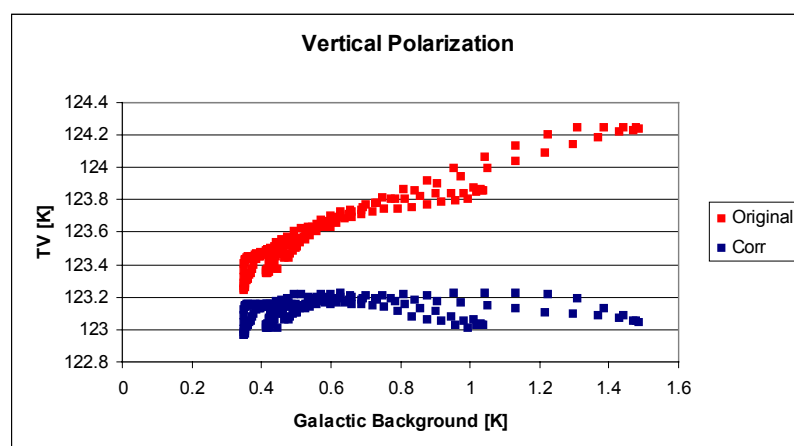
Figure 10.2a. Regression between the measured vertical brightness temperature from the October 20th 2003, Target A, 45° incidence angle flight, and the incident galactic radiation. The red points show the regression before correction, and the blue points represent the corrected data.

A multiplication factor is now introduced, being the regression coefficient divided by the expected Fresnel reflection coefficient. This factor will provide information on the surface with respect to the smearing of the galactic background signal, and it will be used for the final corrections. The multiplication factor estimation is carried out for the October 25th 2001 flight, the March 6th 2003 flight, and for the two targets of the October 20th 2003 flight. The wind speeds covered are zero, two times 10 m/sec. and 20 m/sec., and for two of the flights, both 45° and 35° incidence angles are covered.

The results turn out to provide some consistence, and for the low wind case, i.e. the October 20th 2003, target B, the multiplication factors turn out to be 0.91 and 1.13 for the vertical and horizontal polarizations, respectively. For the two cases of 10 m/sec. wind speed, the results for 45° incidence angle turn out to be 0.71 for both polarizations, within a few percent of deviation. For the 45° incidence angle at 20 m/sec., the regression decreases as expected, and 0.6 is obtained for vertical polarization, while 0.31 is found for horizontal. Almost same results are obtained for 35° incidence angle at 20 m/sec. Only the result for 35° incidence angle at 10 m/sec. turns out to deviate from the pattern, as only multiplication factors of 0.43 and 0.57 are found for vertical and horizontal polarization, respectively.

It is obvious, that additional modeling work has to be done for the correction of SMOS data, but for the correction of the LOSAC flight tracks, the estimated multiplication factors will be used for proper scaling of the galactic background signal to be subtracted from the measured data. An example is shown in figure 10.2b, illustrating the 45° incidence signature from target A of the October 20th 2003 flight, before and after correction. It is obvious, that a high

correlation exists between the downwelling signal and the measured data, especially at vertical polarization, and it is also seen, that some smearing has occurred. As expected it results in a slight over-correction in the central part of the galaxy, and small shoulders to the side. The sizes of these deformations are very small, however, and the correction method, based on the multiplication factors found from regression analysis of the data, is finally applied to all the LOSAC data sets.
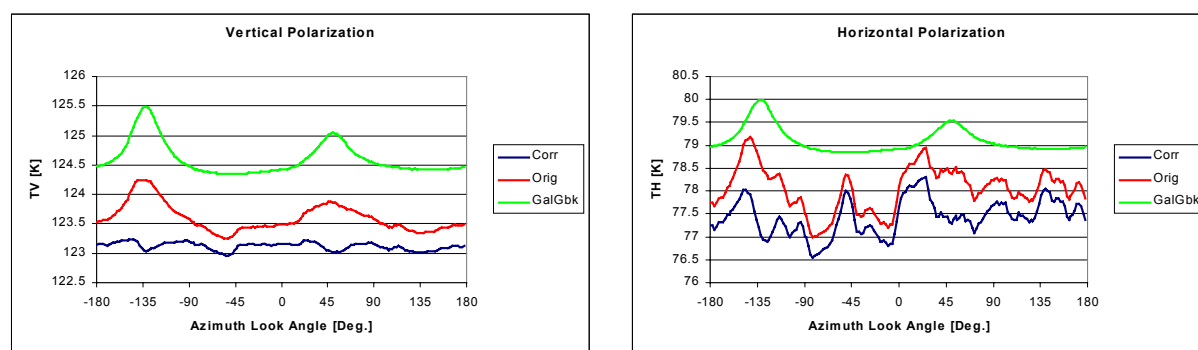
Figure 10.2b. Vertical and horizontal brightness signatures from the October 20th 2003, Target A, 45° incidence angle flight. The downwelling galactic background signal is illustrated in the green plot, which is offset properly to fit into the scale. The red plots are the originally measured data, and the blue curved show the final data after correction.

The corrected LOSAC data set is not presented fully due to the large amount of data, but averaged tracks, as well as tables are fully presented on the following pages. The March 15th 2001 flight is covered by the figures 10.3 to 10.6, and the harmonic analysis is presented in table 10.1. Likewise the figures 10.7 to 10.11 present the March 23rd 2001 flight, while table 10.2 contains the harmonic data. Data from the October 25th 2001 flight is presented in two groups according to the original data. The main data set is introduced in the figures 10.12 to 10.15 along with table 10.3, while the results of the tracks, varying the flight altitude, are shown in figures 10.16 to 10.18. A Table, estimating the effect of the larger antenna footprint, i.e. the larger spatial integration is shown in table 10.4, and the effect of integration of several tracks is shown in table 10.5. Finally table 10.6 holds the harmonic analysis of all data, taken at 45° incidence angle during that flight.

The March 6th 2003 flight is covered by the figures 10.19 to 10.21, regarding the 45° incidence angle measurements, and by the figures 10.22 to 10.24 for 35° incidence angle. Finally the measured level flight signature and the result from the 1st and 2nd harmonic estimation of the level flight data are shown in the figures 10.25 and 10.26. Tables for this flight are table 10.7 and 10.8, which illustrate the effect of integration after galactic correction, table 10.9, which is the harmonic analysis of the circle flights, and table 10.10, which contains the harmonic fit of the level flights.

Target A for the October 20th 2003 flight is presented in the figures 10.27 to 10.32, covering both incidence angles. Corresponding tables are 10.11 and 10.12, illustrating the integration gain, and table 10.13, which is the harmonic analysis. Target B is covered by the figures 10.33 to 10.35, and by the tables 10.14 and 10.15, illustrating integration gain and harmonic analysis, respectively. Finally the results from the level flights are plotted in figure 10.36 and 10.37, the latter based on the harmonic fit, presented in table 10.16.

Figure 10.3. The averaged Stokes parameters from the 1st and 3rd circle flight tracks with 20° incidence angle from the March 15th 2001 flight, after correction for the galactic background. The 2nd track is left out due to heavy interference.

Figure 10.4. The averaged Stokes parameters from the three circle flight tracks with 35° incidence angle from the March 15th 2001 flight, after correction for the galactic background.

Figure 10.5. The averaged Stokes parameters from the three circle flight tracks with 42° incidence angle from the March 15th 2001 flight, after correction for the galactic background.

Figure 10.6. The averaged Stokes parameters from the three circle flight tracks with 52° incidence angle from the March 15th 2001 flight, after correction for the galactic background.

Figure 10.7. The averaged Stokes parameters from the 1st and 2nd circle flight tracks with 20° incidence angle from the March 23rd 2001 flight, after correction for the galactic background. The 3rd track is left out due to heavy interference.

Figure 10.8. The averaged Stokes parameters from the three circle flight tracks with 35° incidence angle from the March 23rd 2001 flight, after correction for the galactic background.

Figure 10.9. The averaged Stokes parameters from the three circle flight tracks with 47° incidence angle from the March 23rd 2001 flight, after correction for the galactic background.

Figure 10.10. The averaged Stokes parameters from the three circle flight tracks with 57° incidence angle from the March 23rd 2001 flight, after correction for the galactic background.

Figure 10.11. The averaged Stokes parameters from the two circle flight tracks with 62° incidence angle from the March 23rd 2001 flight, after correction for the galactic background.

Figure 10.12. The averaged Stokes parameters from the three circle flight tracks with 29° incidence angle from the October 25th 2001 flight, after correction for the galactic background.

Inc.	Harm.	TV, M.	TV, Ph.	TH, M.	TH, Ph.	U, Mag.	U, Ph.	V, Mag.	V, Ph.
20°	1	0.02	164.08	0.17	-170.61	0.04	-86.65	0.07	150.71
	2	0.05	64.29	0.19	-76.92	0.01	-169.43	0.06	-85.83
	3	0.05	-47.40	0.18	120.23	0.03	179.33	0.03	-140.22
	4	0.04	117.37	0.09	122.61	0.01	-85.41	0.03	-42.99
35°	1	0.14	-119.35	0.21	-88.10	0.14	-6.13	0.07	50.18
	2	0.16	49.24	0.13	8.18	0.09	12.02	0.08	-44.41
	3	0.06	-48.01	0.07	-17.51	0.06	146.44	0.03	-77.35
	4	0.05	172.86	0.02	58.45	0.04	140.81	0.05	-166.46
42°	1	0.14	-130.99	0.28	-116.63	0.17	-41.21	0.07	56.83
	2	0.09	68.80	0.17	-16.80	0.10	50.60	0.22	124.05
	3	0.07	-73.10	0.12	176.94	0.03	163.63	0.11	-16.07
	4	0.01	152.47	0.05	11.51	0.01	167.06	0.07	-44.22
52°	1	0.13	-47.82	0.17	-28.41	0.11	139.78	0.13	169.70
	2	0.18	171.39	0.11	-158.32	0.08	107.95	0.07	-33.80
	3	0.09	-138.98	0.11	-174.68	0.06	108.59	0.06	10.00
	4	0.03	-60.37	0.10	-103.45	0.02	157.46	0.05	-166.06
35°, 45° and 52°	1	0.12	-101.92	0.18	-86.24	0.06	-17.25	0.05	107.25
	2	0.08	101.00	0.07	-21.79	0.07	51.94	0.03	96.63
	3	0.06	-91.28	0.05	-169.93	0.05	135.36	0.06	-14.80
	4	0.02	-166.92	0.03	-61.30	0.03	150.14	0.03	-124.90

Table 10.1. 1st, 2nd, 3rd, and 4th harmonic components in the averaged modified Stokes parameters from the circle flights from March 15th 2001, after correction for the galactic background.

Inc.	Harm.	TV, M.	TV, Ph.	TH, M.	TH, Ph.	U, Mag.	U, Ph.	V, Mag.	V, Ph.
20°	1	0.12	-88.90	0.31	-57.28	0.20	-117.97	0.19	-62.26
	2	0.13	8.72	0.27	50.11	0.09	-91.01	0.05	-151.59
	3	0.14	59.05	0.18	168.89	0.14	-100.34	0.07	121.32
	4	0.07	-58.22	0.12	109.81	0.08	60.50	0.05	-25.51
35°	1	0.09	166.46	0.55	-95.94	0.14	-10.24	0.26	-105.83
	2	0.01	-131.94	0.34	-74.82	0.15	149.02	0.04	-142.99
	3	0.11	-44.65	0.18	-159.98	0.10	-19.41	0.05	4.95
	4	0.14	-24.04	0.26	-48.17	0.02	-117.14	0.12	-48.35
47°	1	0.05	-76.67	0.22	-17.62	0.13	-104.62	0.29	-14.75
	2	0.02	-40.12	0.05	-175.80	0.12	-147.71	0.06	145.06
	3	0.07	-119.49	0.03	-148.37	0.09	-118.75	0.09	118.04
	4	0.03	-9.66	0.06	57.67	0.03	-127.07	0.04	48.62
57°	1	0.03	1.17	0.56	-91.10	0.16	121.24	0.16	178.79
	2	0.16	-164.76	0.56	4.01	0.11	-126.00	0.28	-26.48
	3	0.07	147.14	0.12	-169.12	0.08	80.25	0.23	53.61
	4	0.06	-120.40	0.12	-33.68	0.10	115.65	0.02	-123.23
62°	1	0.20	110.46	0.38	-8.59	0.39	165.14	0.27	-1.99
	2	0.24	-164.43	0.12	-165.81	0.33	74.61	0.50	-116.17
	3	0.13	166.16	0.36	57.95	0.07	-119.42	0.12	94.61
	4	0.15	173.63	0.07	136.92	0.10	109.06	0.16	-60.34
35° to 62°	1	0.05	129.89	0.34	-67.85	0.09	165.27	0.11	-45.68
	2	0.10	-160.99	0.14	-34.04	0.08	128.89	0.14	-95.95
	3	0.04	-147.80	0.06	122.47	0.02	-71.69	0.10	71.39
	4	0.03	-97.09	0.08	-33.52	0.04	125.59	0.07	-50.55

Table 10.2. 1st, 2nd, 3rd, and 4th harmonic components in the averaged modified Stokes parameters from the circle flights from March 23rd 2001, after correction for the galactic background.
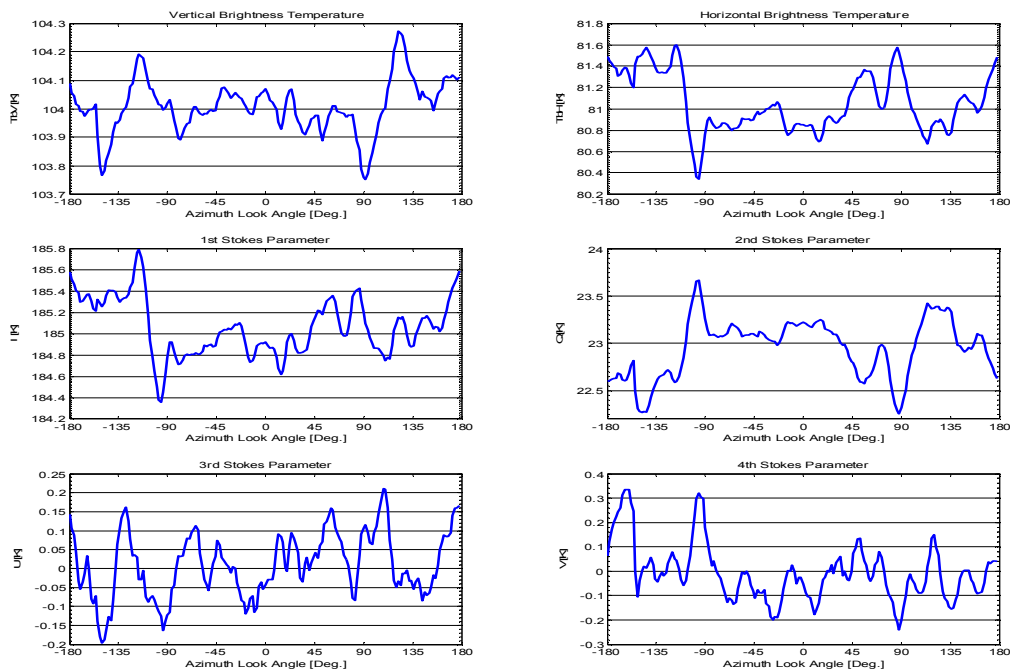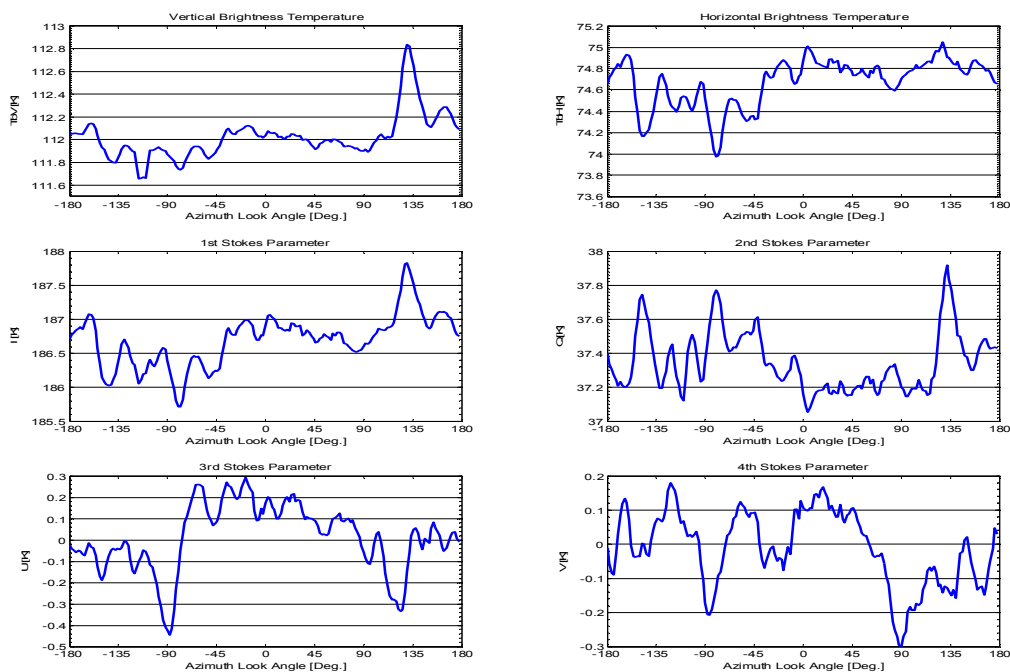
Figure 10.13. The averaged Stokes parameters from the three circle flight tracks with 35° incidence angle from the October 25th 2001 flight, after correction for the galactic background.

Figure 10.14. The averaged Stokes parameters from the three circle flight tracks with 45° incidence angle from the October 25th 2001 flight, after correction for the galactic background.

Figure 10.15. The averaged Stokes parameters from the three circle flight tracks with 55° incidence angle from the October 25th 2001 flight, after correction for the galactic background.
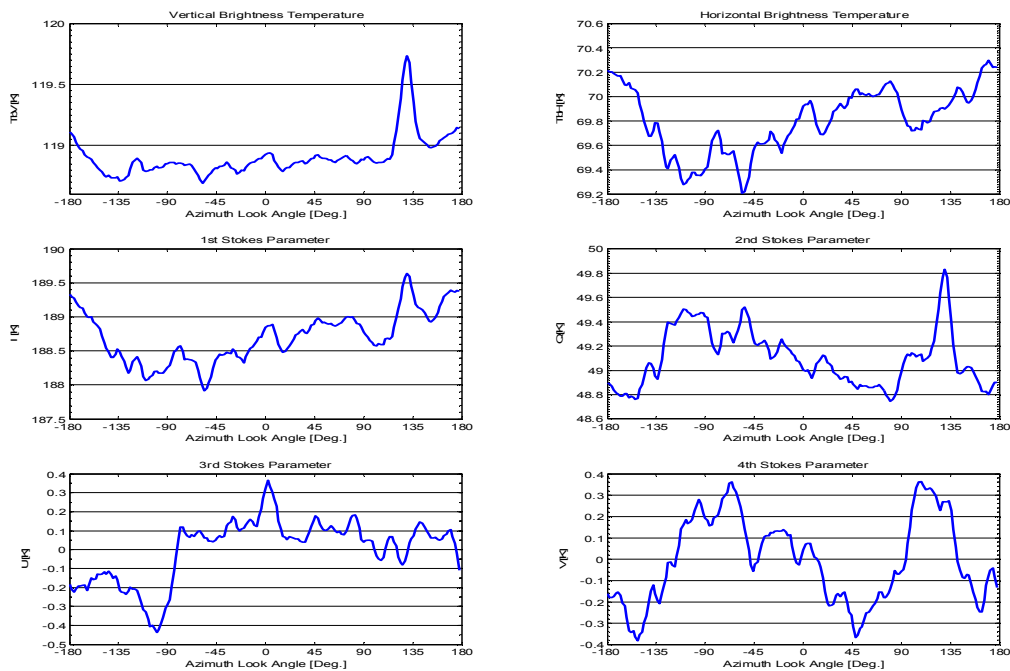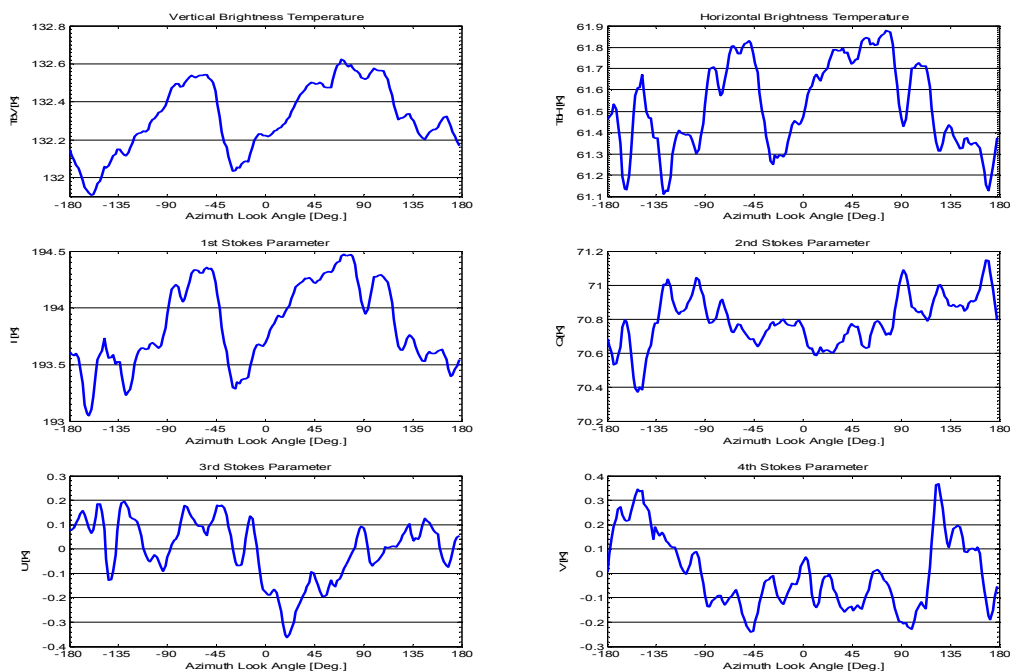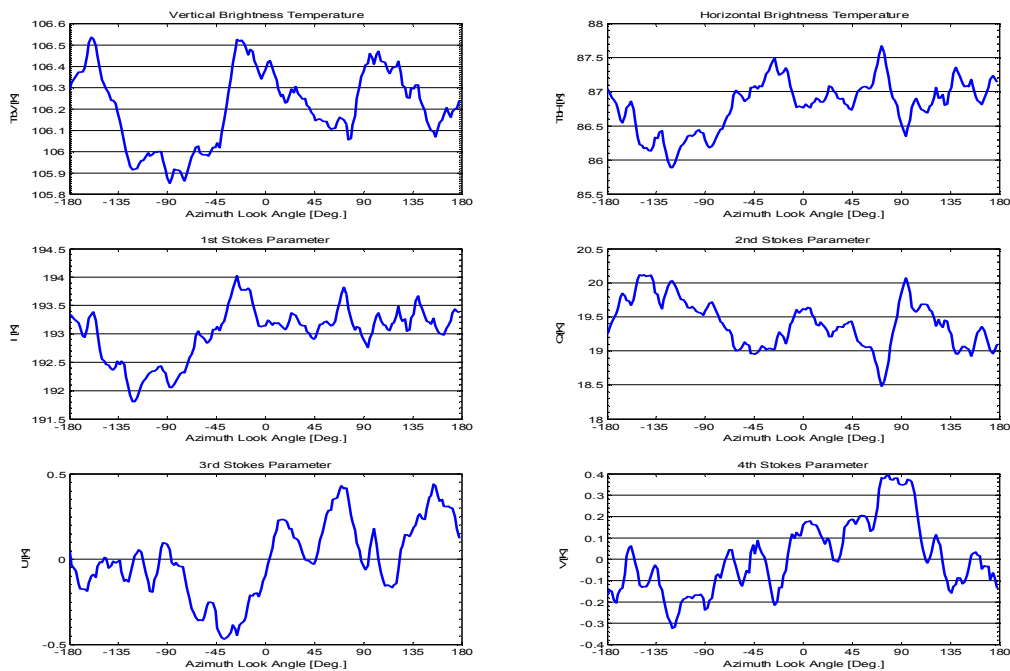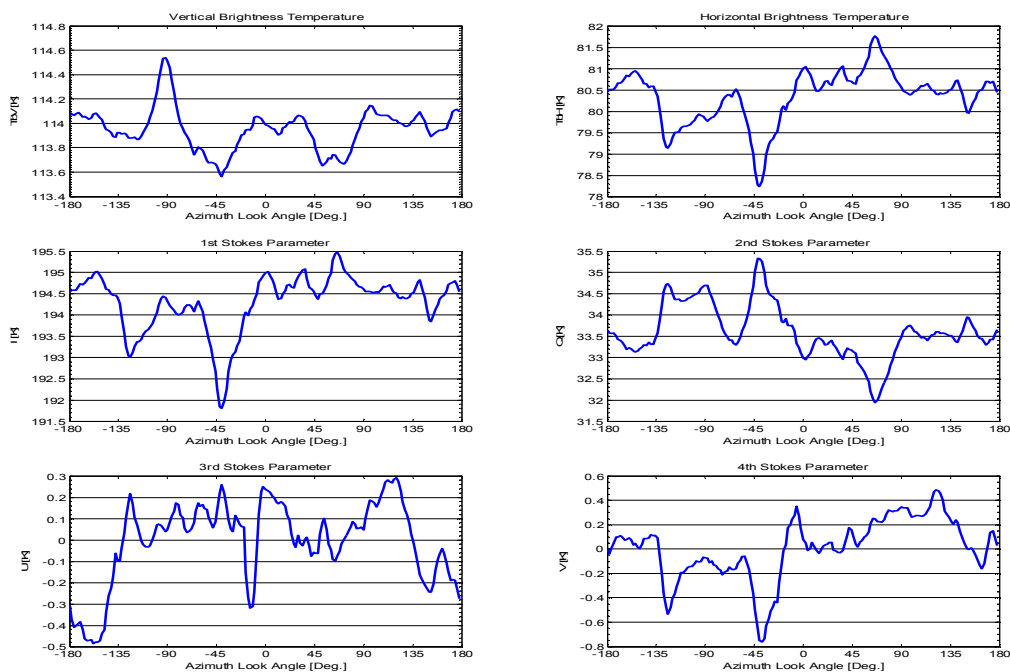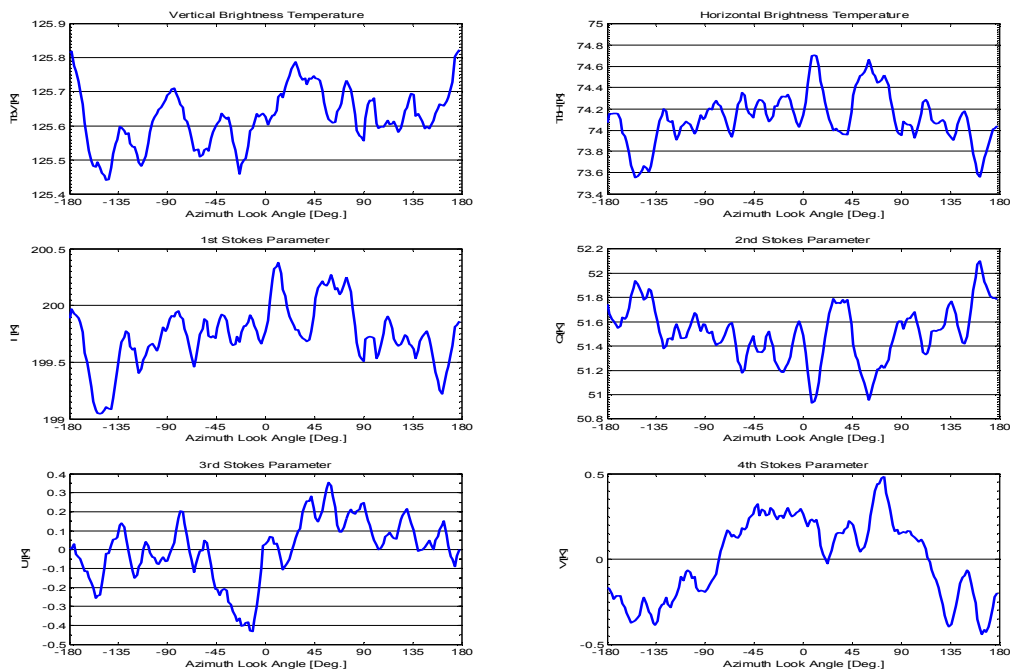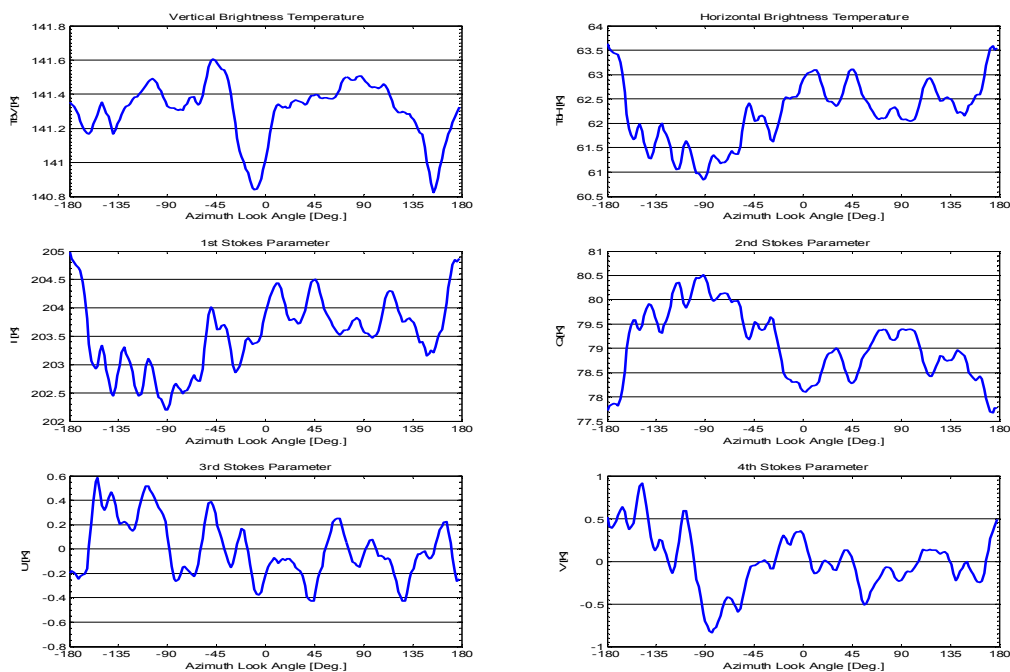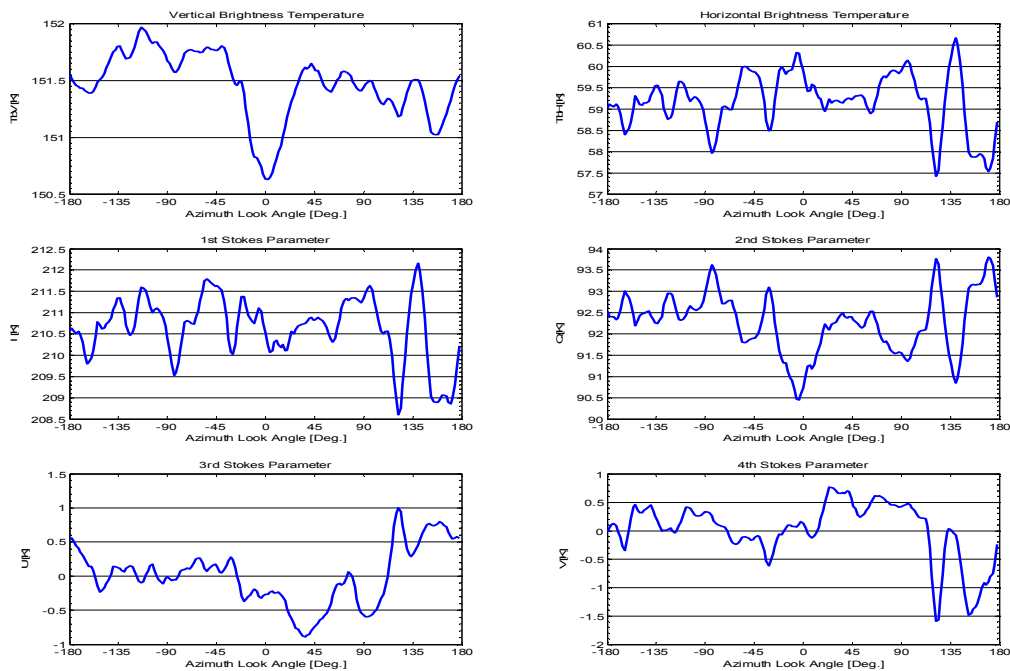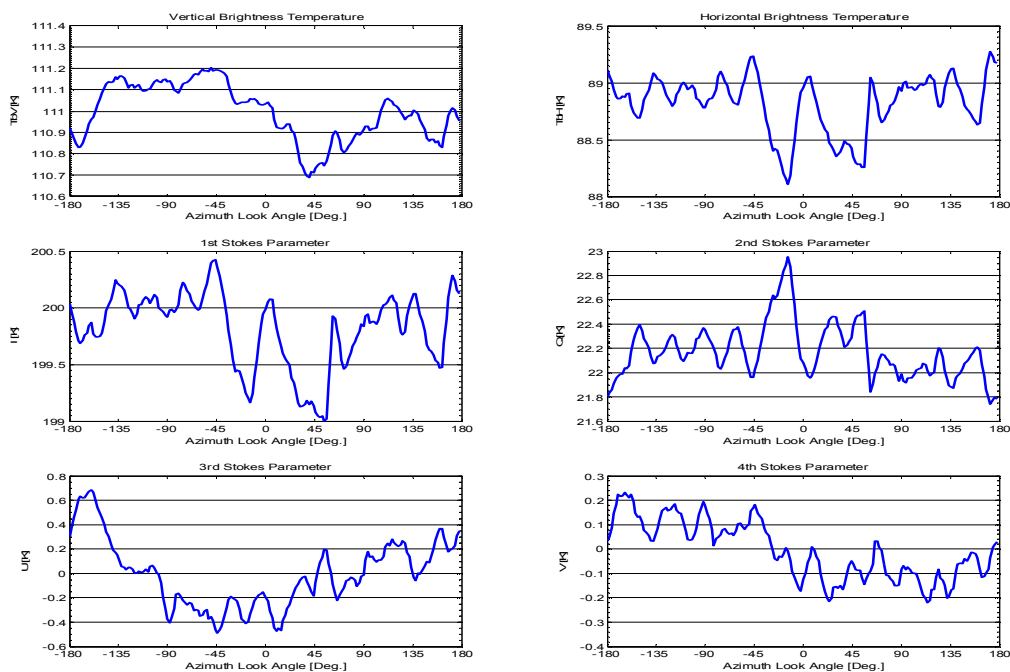

Figure 10.16. The averaged Stokes parameters from the three circle flight tracks with 45° incidence angle and 1000 m flight altitude from the October 25th 2001 flight, after correction for the galactic background.

Inc.	Harm.	TV, M.	TV, Ph.	TH, M.	TH, Ph.	U, Mag.	U, Ph.	V, Mag.	V, Ph.
29°	1	0.14	91.51	0.18	161.38	0.33	-165.07	0.14	108.72
	2	0.07	123.45	0.12	133.20	0.11	-53.59	0.02	-99.96
	3	0.06	37.76	0.02	86.63	0.07	116.46	0.05	136.74
	4	0.02	-126.00	0.08	-53.66	0.05	-81.85	0.00	122.67
35°	1	0.19	-171.07	0.11	142.74	0.05	66.74	0.01	-84.65
	2	0.04	167.01	0.10	80.40	0.12	-170.22	0.08	27.61
	3	0.06	3.11	0.14	5.92	0.06	-4.88	0.02	-178.06
	4	0.03	103.17	0.16	76.37	0.08	-41.16	0.00	-38.60
45°	1	0.06	-75.09	0.39	-50.76	0.12	101.24	0.09	-147.87
	2	0.07	-155.23	0.33	-139.00	0.11	-65.03	0.09	122.45
	3	0.01	17.37	0.26	157.24	0.06	83.13	0.05	5.28
	4	0.09	103.14	0.27	50.80	0.09	43.88	0.07	-114.76
55°	1	0.19	167.07	0.45	-34.67	0.19	98.10	0.11	161.63
	2	0.13	112.40	0.04	12.71	0.09	-43.77	0.06	75.10
	3	0.06	-1.23	0.27	73.34	0.02	-32.63	0.06	-140.61
	4	0.11	175.27	0.28	133.86	0.16	-169.32	0.12	-55.07
35°, 45° and 55°	1	0.11	-172.23	0.24	-42.40	0.12	94.91	0.06	-172.80
	2	0.07	144.43	0.08	-153.50	0.06	-90.69	0.06	76.58
	3	0.04	-0.62	0.13	92.97	0.03	28.65	0.01	-113.44
	4	0.06	135.82	0.19	88.15	0.01	-147.94	0.06	-75.14

Table 10.3. 1st, 2nd, 3rd, and 4th harmonic components in the averaged modified Stokes parameters from the circle flights from October 25th 2001, after correction for the galactic background.

Circles	TV, std.dev. [K]	TH, std.dev. [K]	U, std.dev. [K]	V, std.dev. [K]
1000m altitude 3 single circles	0.132	0.688	0.385	0.243
	0.216	0.547	0.343	0.118
	0.163	0.742	0.598	0.427
1000 m alt., average	0.170	0.659	0.442	0.263
1000 m alt., integrated	0.110	0.332	0.263	0.141
2000m altitude 3 single circles	0.211	0.675	0.423	0.220
	0.214	0.642	0.383	0.235
	0.137	0.659	0.219	0.283
2000 m alt., average	0.187	0.659	0.342	0.246
2000 m alt., integrated	0.114	0.347	0.242	0.139
3000m altitude 3 single circles	0.176	0.648	0.351	0.260
	0.204	0.684	0.532	0.606
	0.302	0.583	0.484	0.270
3000 m alt., average	0.228	0.638	0.456	0.379
3000 m alt., integrated	0.144	0.421	0.251	0.227
All integrated	0.085	0.243	0.156	0.079

Table 10.4. Square root of the total power (except DC) for the full signal in the modified Stokes parameters from the nine circle flights with 45° incidence angle from October 25th 2001, after correction for the galactic background. The power is presented for single tracks, an average of three values, and the power of the integrated track.
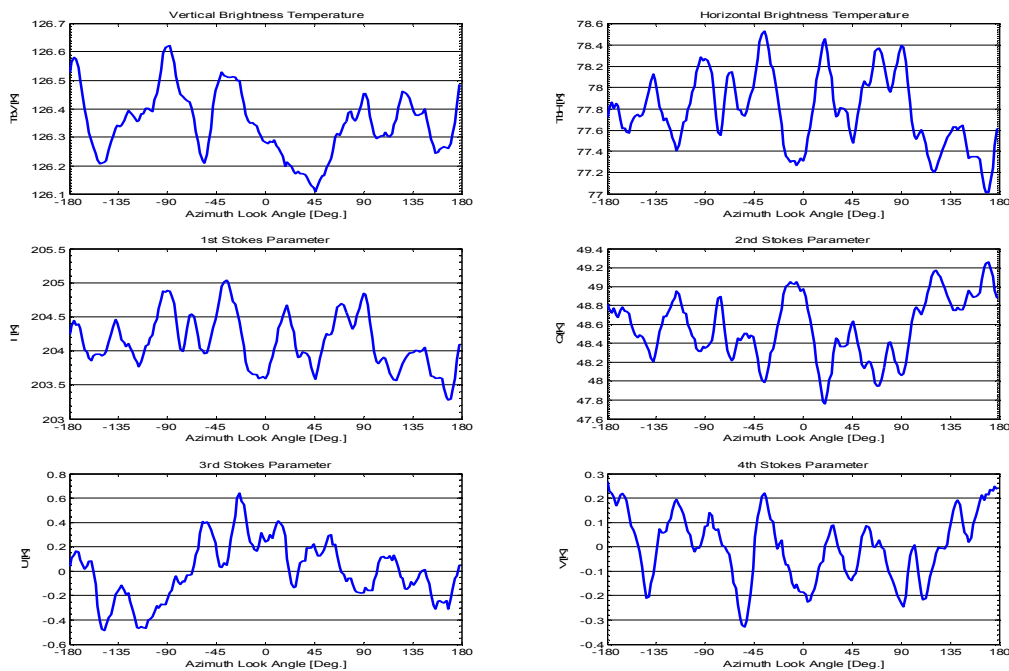
Figure 10.17. The averaged Stokes parameters from the three circle flight tracks with 45° incidence angle and 2000 m flight altitude from the October 25th 2001 flight, after correction for the galactic background.
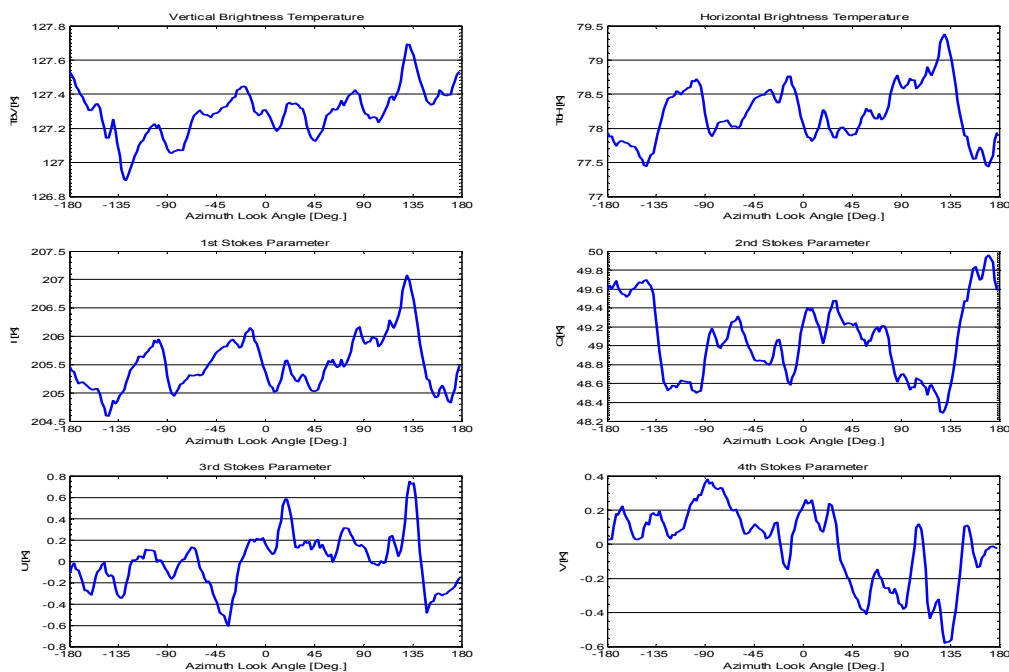
Figure 10.18. The averaged Stokes parameters from the three circle flight tracks with 45° incidence angle and 3000 m flight altitude from the October 25th 2001 flight, after correction for the galactic background.

Circles		TV, std.dev. [K]	TH, std.dev. [K]	U, std.dev. [K]	V, std.dev. [K]
1000m altitude 3 single circles		0.132	0.688	0.385	0.243
		0.216	0.547	0.343	0.118
		0.163	0.742	0.598	0.427
2000m altitude 6 single circles		0.164	0.814	0.343	0.218
		0.145	0.648	0.266	0.228
		0.284	0.696	0.258	0.170
		0.211	0.675	0.423	0.220
		0.214	0.642	0.383	0.235
		0.137	0.659	0.219	0.283
3000m altitude 3 single circles		0.176	0.648	0.351	0.260
		0.204	0.684	0.532	0.606
		0.302	0.583	0.484	0.270
Average, single		0.196	0.669	0.382	0.273
3 circles integrated	1000 m	0.110	0.332	0.263	0.141
	2000 m	0.121	0.483	0.170	0.121
		0.114	0.347	0.242	0.139
	3000 m	0.144	0.421	0.251	0.227
Average, 3 integrated		0.122	0.396	0.232	0.157
All 12 integrated		0.074	0.244	0.127	0.063

Table 10.5. Total rms. noise for the full signal in the modified Stokes parameters from the 12 circle flights with 45° incidence angle from October 25th 2001, after correction for the galactic background. The circles are processed as single tracks, averaged as 4 times three circles and averaged totally.

Altitude	Har.	I, Mag.	I, Phase	Q, Mag.	Q, Ph.	U, Mag.	U, Ph.	V, Mag.	V, Ph.
1000 m	1	0.03	-17.71	0.17	22.91	0.16	32.57	0.10	-112.59
	2	0.12	139.01	0.07	140.69	0.20	-74.53	0.07	-134.89
	3	0.02	-51.27	0.13	-82.65	0.16	132.89	0.05	116.44
	4	0.04	8.32	0.14	74.77	0.09	21.94	0.07	-177.96
2000 m 1st group	1	0.06	-75.09	0.39	-50.76	0.12	101.24	0.09	-147.87
	2	0.07	-155.23	0.33	-139.00	0.11	-65.03	0.09	122.45
	3	0.01	17.37	0.26	157.24	0.06	83.13	0.05	5.28
	4	0.09	103.14	0.27	50.80	0.09	43.88	0.07	-114.76
2000 m 2nd group	1	0.07	115.32	0.19	18.44	0.23	-14.02	0.10	160.65
	2	0.08	119.31	0.19	-148.56	0.14	39.81	0.05	-6.34
	3	0.02	71.86	0.15	142.52	0.08	131.80	0.06	-132.11
	4	0.06	30.18	0.02	-109.51	0.04	-109.39	0.06	85.88
2000 m All 6 circ.	1	0.01	179.94	0.25	-29.30	0.10	16.97	0.08	-174.21
	2	0.05	160.04	0.26	-142.49	0.08	-3.76	0.03	90.38
	3	0.01	58.89	0.21	151.82	0.06	110.58	0.02	-70.18
	4	0.06	74.56	0.13	49.45	0.03	21.15	0.01	172.80
3000 m	1	0.11	-106.84	0.16	-48.81	0.18	-55.84	0.25	81.57
	2	0.12	54.03	0.36	140.97	0.08	-133.75	0.05	-34.84
	3	0.03	151.05	0.30	15.11	0.14	-39.40	0.03	-89.91
	4	0.01	53.22	0.08	112.89	0.07	-63.11	0.11	-32.90
All 45° inc. circles	1	0.03	-99.99	0.19	-22.79	0.11	-0.37	0.05	142.31
	2	0.06	118.67	0.19	-176.14	0.07	-58.96	0.00	-106.66
	3	0.01	91.02	0.04	112.44	0.04	105.76	0.01	-102.76
	4	0.04	60.22	0.11	66.86	0.04	-4.39	0.02	-90.24

Table 10.6. 1st, 2nd, 3rd, and 4th harmonic components in the averaged modified Stokes parameters from the circle flights from Oc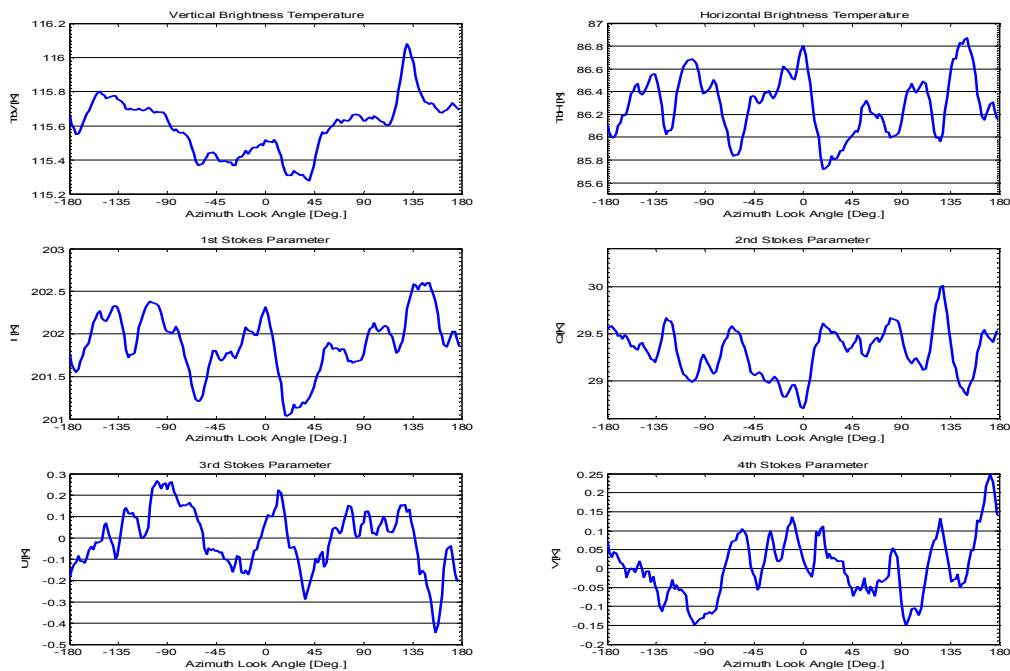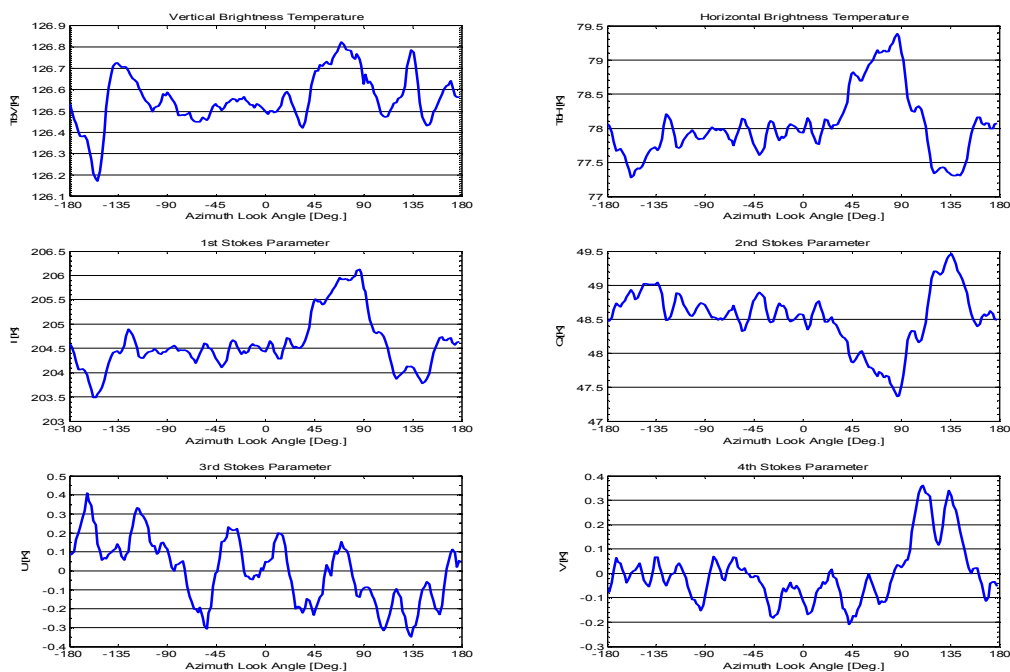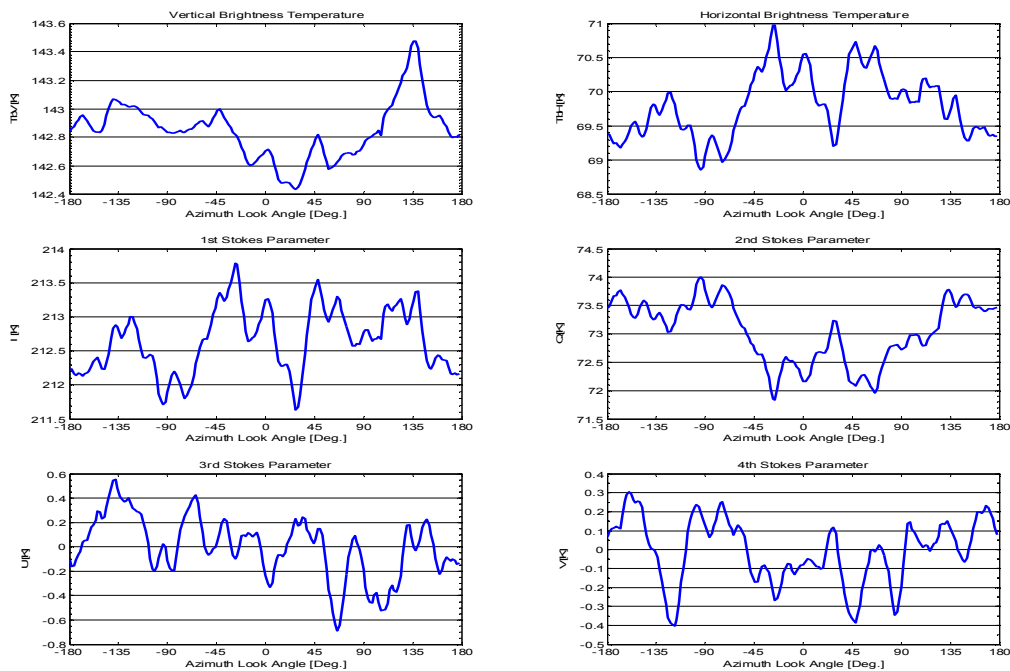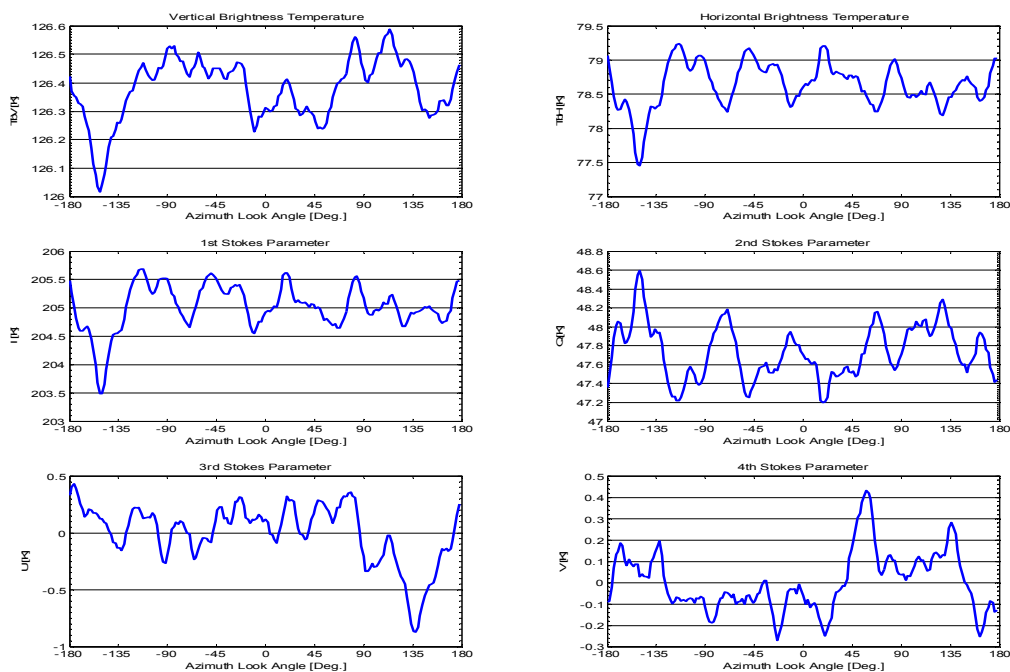tober 25th 2001, after correction for the galactic background. The incidence angle is kept constant at 45°, and the flight altitude is varied.
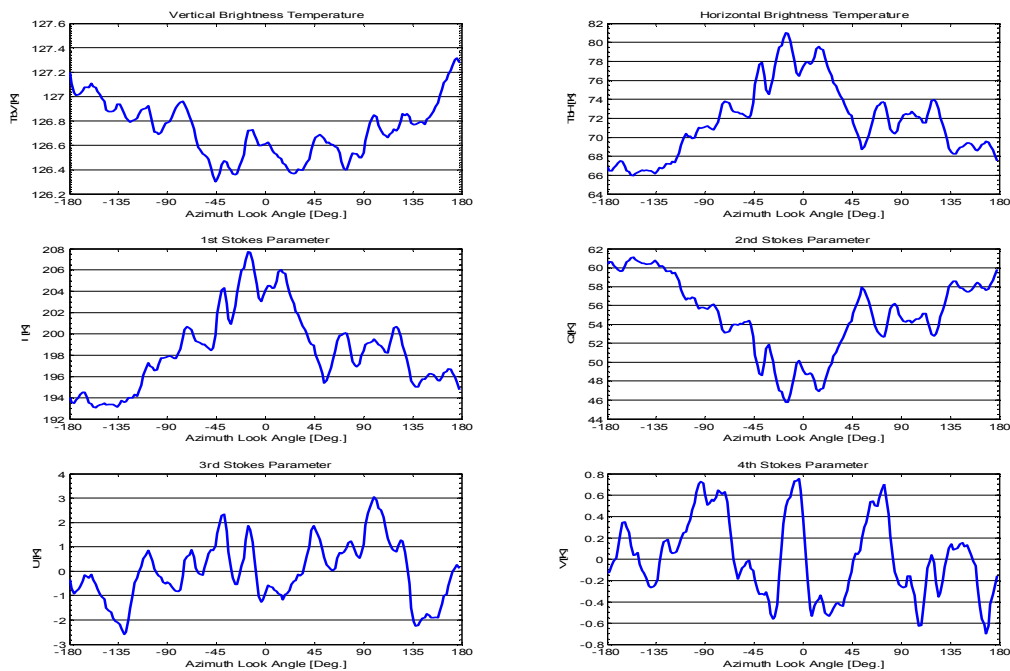
Figure 10.19. The averaged Stokes parameters from the 1st to the 6th circle flight tracks with 45° incidence angle from the March 6th 2003 flight, after correction for the galactic background.
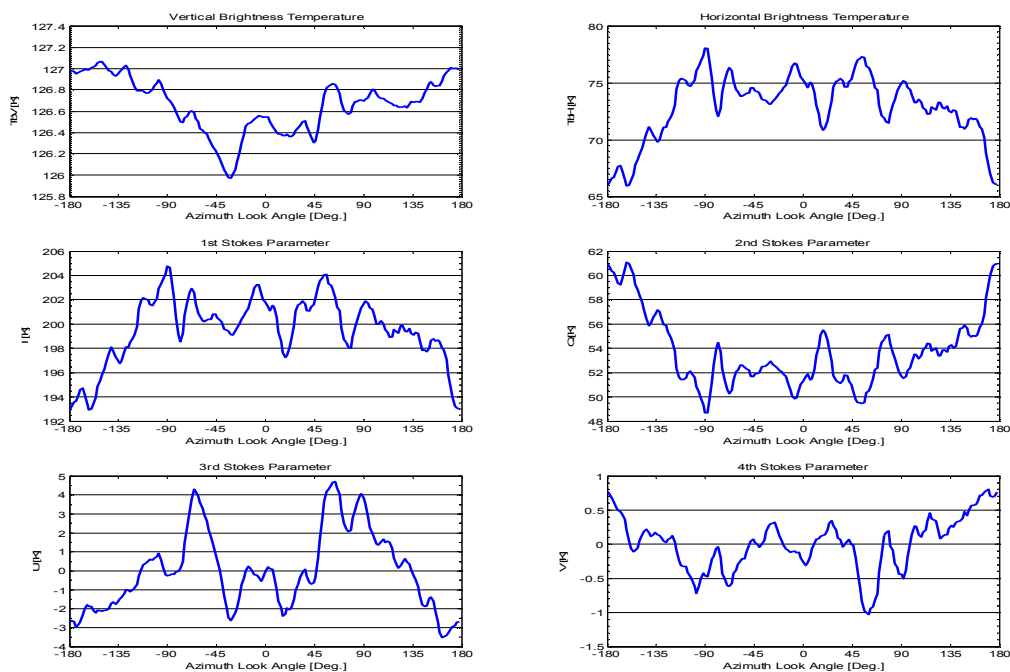
Figure 10.20. The averaged Stokes parameters from the 7th to the 13th circle flight tracks with 45° incidence angle from the March 6th 2003 flight, after correction for the galactic background.

Figure 10.21. The averaged Stokes parameters from all 13 circle flight tracks with 45° incidence angle from the March 6th 2003 flight, after correction for the galactic background.

Figure 10.22. The averaged Stokes parameters from the 1st to the 8th circle flight tracks with 35° incidence angle from the March 6th 2003 flight, after correction for the galactic background.

Figure 10.23. The averaged Stokes parameters from the 9st to the 16th circle flight tracks with 35° incidence angle from the March 6th 2003 flight, after correction for the galactic background.

Figure 10.24. The averaged Stokes parameters from all 16 circle flight tracks with 35° incidence angle from the March 6th 2003 flight, after correction for the galactic background.

| Circles	TV, std.dev. [K]	TH, std.dev. [K]	U, std.dev. [K]	V, std.dev. [K]
Single circles	0.357	3.452	2.725	0.815
45° incidence angle	0.388	10.420	1.958	1.533
	0.343	8.576	4.214	0.856
	0.476	6.012	4.027	0.819
	0.529	6.534	2.812	0.733
	0.463	5.323	2.605	0.598
	0.342	4.009	3.381	0.778
	0.331	4.341	2.748	0.731
	0.328	7.770	4.976	1.166
	0.410	7.389	4.485	0.845
	0.754	6.258	3.731	1.424
	0.612	7.013	3.737	0.894
	0.377	5.205	4.222	1.472
Average, single	0.439	6.331	3.509	0.974
3 circles	0.219	5.645	1.711	0.649
integrated	0.294	3.626	2.176	0.448
	0.298	2.765	1.928	0.508
	0.259	4.716	3.043	0.472
	0.447	3.677	2.323	0.624
Average, 3 integrated	0.303	4.086	2.236	0.540
7 integrated	0.230	3.870	1.226	0.370
	0.256	2.864	2.084	0.390
Average, 7 integrated	0.243	3.367	1.655	0.380
All 13 integrated	0.230	2.941	1.457	0.188

Table 10.7. Total rms. noise for the full signal in the modified Stokes parameters from the 13 circle flights with 45° incidence angle from March 6th 2003, after correction for the galactic background. The circles are processed as single tracks, averaged as three circles, seven circles, and averaged totally.

Generally it appears, that the variations in the circle signatures are reduced. Obviously the reduction is most visible in the signatures, containing the least geophysical noise, and it is easily noticed, that the typical two peaks, originating from the galactic background, disappear. This fact is also reflected by the tables 10.1 to 10.3, 10.6, 10.9, 10.13, and 10.15, which describe the harmonic contents in the signatures. Two observations are made, when these tables are compared to the tables 5.1, 6.1, 7.1, 7.4, 8.3, 9.3, and 9.5, which present the same signatures before correction: Firstly it is seen, that many magnitudes, especially regarding the 1st and the 2nd harmonics, are reduced, thus also reducing the total signal power. Secondly it is seen, that phases have changed dramatically through the correction, supporting the assumption, that the reflected galactic background radiation was the main contributor to the total signal.

From the harmonic analysis it is also noticed, however, that the phases in the tables do still not reflect the expected values, based on [5]. This may be due to the fact, that some amount of random noise is still present, masking out the wind driven signals, if they are present. This is supported by the tables 10.1. to 10.3, where it is seen, that the different groups of circles present no trend for their phases, although they are taken subsequently and with an incidence angle spacing of only 10°. Table 10.6 is another example, illustrating 12 circles, taken at equal incidence angle, and subdivided into 4 groups. Anyway the phases obviously appear to be random, and the magnitudes reduce as a result of averaging.

Circles	TV, std.dev. [K]	TH, std.dev. [K]	U, std.dev. [K]	V, std.dev. [K]
Single circles	0.437	7.479	1.862	2.172
35° incidence angle	0.434	6.978	4.106	2.395
	0.667	4.114	1.910	1.089
	0.381	4.140	2.322	1.011
	0.388	5.720	2.923	1.255
	0.517	4.629	2.295	1.617
	0.695	5.694	2.431	1.727
	0.347	4.289	1.646	1.037
	0.558	4.381	1.779	2.675
	0.469	3.686	1.651	1.014
	0.725	10.078	5.896	2.185
	0.462	7.590	3.091	1.157
	0.378	3.831	2.290	0.990
	0.379	6.259	2.918	1.484
	0.493	4.417	1.954	1.054
	0.509	4.586	1.785	1.152
Average, single	0.490	5.492	2.554	1.501
4 circles	0.323	2.810	1.572	0.747
integrated	0.336	3.351	0.971	0.613
	0.394	3.207	1.822	0.911
	0.367	2.958	1.450	0.495
Average, 4 integrated	0.355	3.082	1.454	0.691
8 integrated	0.277	1.413	1.005	0.447
	0.342	2.250	1.409	0.460
Average, 8 integrated	0.310	1.832	1.207	0.454
All 16 integrated	0.300	1.587	0.852	0.286

Table 10.8. Total rms. noise for the full signal in the modified Stokes parameters from the 16 circle flights with 35° incidence angle from March 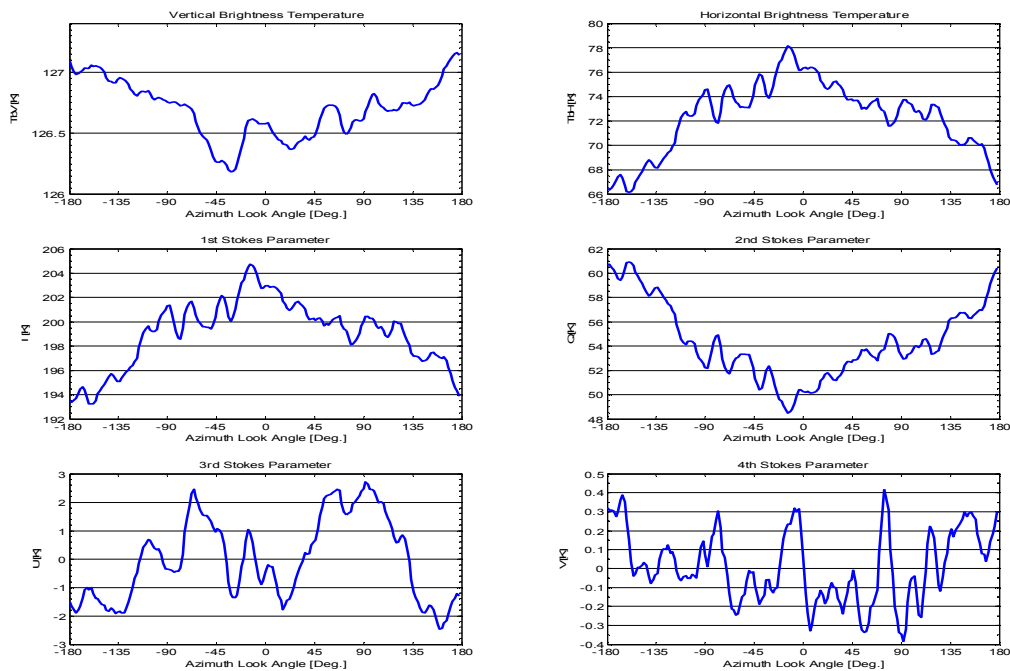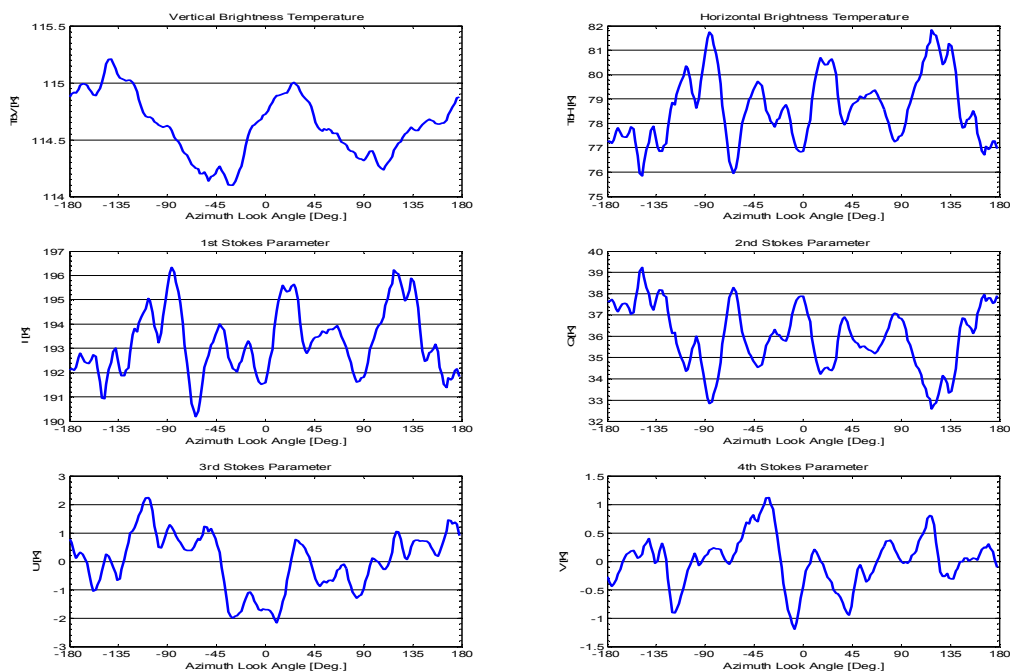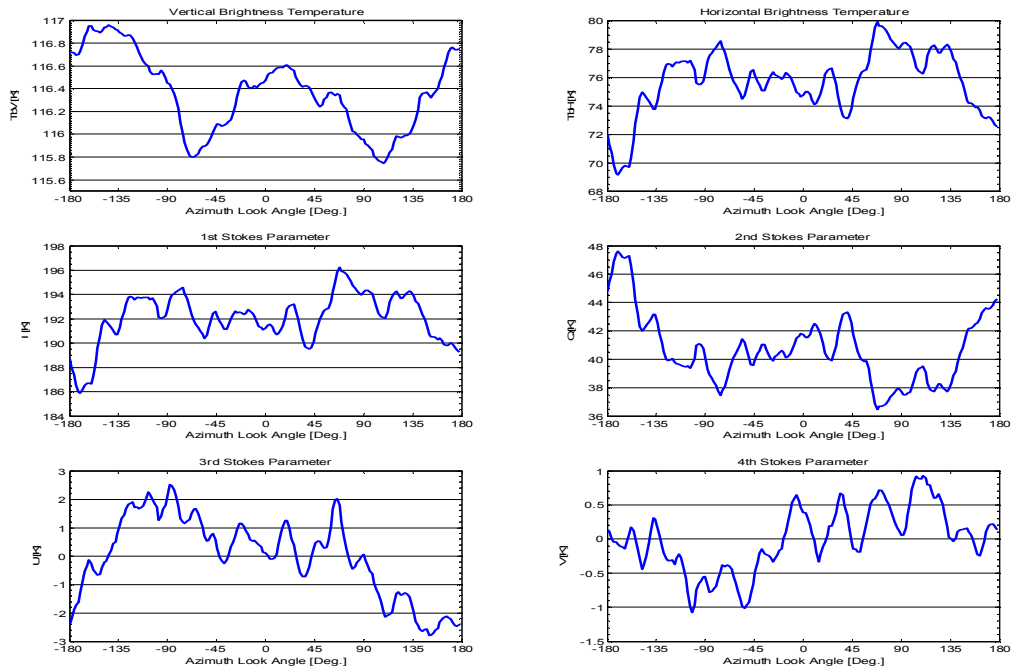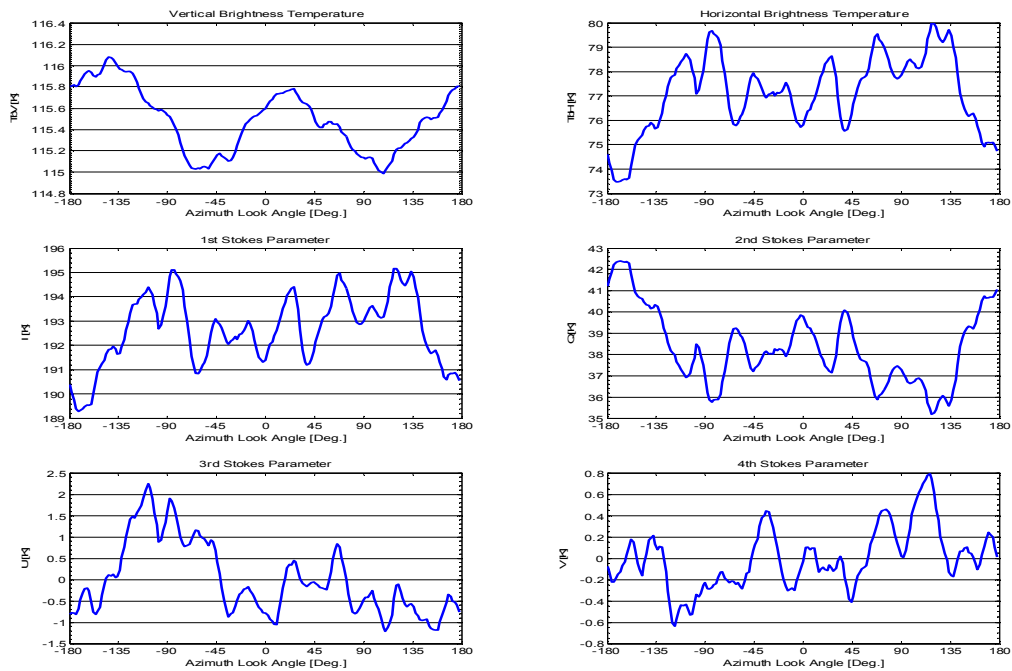6th 2003, after correction for the galactic background. The circles are processed as single tracks, averaged as 4 times four circles, 2 times eight, and averaged totally.

Inc.	Harm.	TV, M.	TV, Ph.	TH, M.	TH, Ph.	U, Mag.	U, Ph.	V, Mag.	V, Ph.
45°	1	0.28	174.92	3.72	-4.35	1.04	-34.80	0.13	165.67
	2	0.08	-75.96	1.07	119.18	1.43	171.72	0.09	32.21
	3	0.02	-131.36	1.05	-26.73	0.60	128.11	0.02	-95.80
	4	0.08	-0.16	0.46	38.50	0.16	-41.47	0.07	39.90
35°	1	0.18	145.82	0.82	-39.55	0.77	79.43	0.22	-99.21
	2	0.36	-53.64	1.55	163.49	0.72	-154.03	0.11	99.15
	3	0.08	-38.69	0.85	-29.01	0.29	-97.27	0.18	85.64
	4	0.02	59.38	0.28	132.32	0.10	129.73	0.06	-106.35

Table 10.9. 1st, 2nd, 3rd, and 4th harmonic components in the averaged modified Stokes parameters from the circle flights from March 6th 2003, after correction for the galactic background.
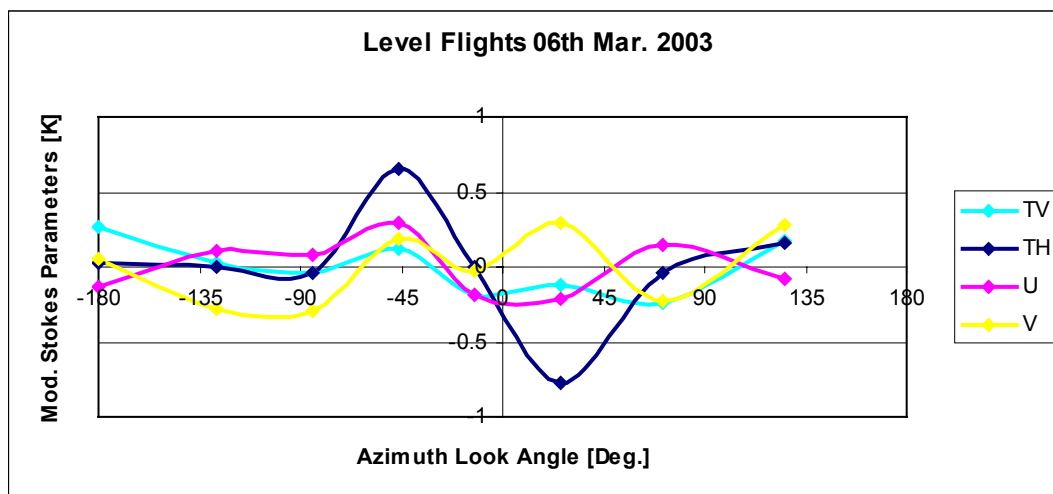
Figure 10.25. The modified Stokes parameters from the level flight tracks March 6th 2003, 50° incidence angle2003, after correction for the galactic background.
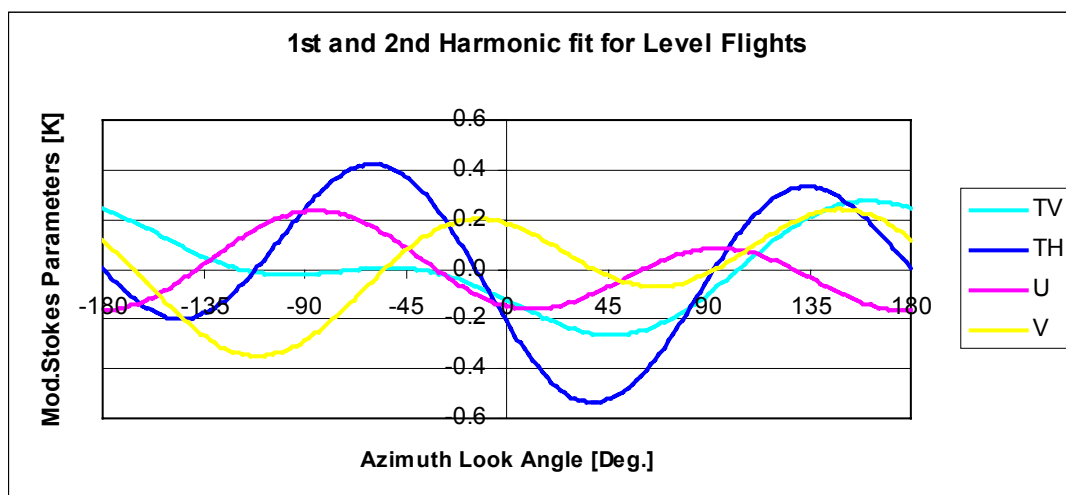
Figure 10.26. The modified Stokes parameters from the level flight tracks March 6th 2003, 50° incidence angle2003, after correction for the galactic background. Result of 1st and 2nd harmonic fit.

Inc.	Harm.	TV, M.	TV, Ph.	TH, M.	TH, Ph.	U, Mag.	U, Ph.	V, Mag.	V, Ph.
Level	1	0.21	-177.03	0.15	152.28	0.08	82.24	0.14	-76.22
50° inc.	2	0.11	65.81	0.37	110.66	0.16	170.06	0.21	43.96

Table 10.10. The modified Stokes parameters from the level flight tracks March 6th 2003, 50° incidence angle2003, after correction for the galactic background. Result of 1st and 2nd harmonic fit.

Figure 10.27. The averaged Stokes parameters from the 1st to the 8th circle flight tracks with 45° incidence angle from the October 20th 2003, Target A, flight, after correction for the galactic background.

Figure 10.28. The averaged Stokes parameters from the 9th to the 16th circle flight tracks with 45° incidence angle from the October 20th 2003, Target A, flight, after correction for the galactic background.

Figure 10.29. The averaged Stokes parameters from the 1st to the 8th circle flight tracks with 35° incidence angle from the October 20th 2003, Target A, flight, after correction for the galactic background.

Figure 10.30. The averaged Stokes parameters from the 9st to the 16th circle flight tracks with 35° incidence angle from the October 20th 2003, Target A, flight, after correction for the galactic background.

Figure 10.31. The averaged Stokes parameters from all 16 circle flight tracks with 45° incidence angle from the October 20th 2003, Target A, flight, after correction for the galactic background.

Figure 10.32. The averaged Stokes parameters from all 16 circle flight tracks with 35° incidence angle from the October 20th 2003, Target A, flight, after correction for the galactic background.

Circles	TV, std.dev. [K]	TH, std.dev. [K]	U, std.dev. [K]	V, std.dev. [K]
Single circles 45° incidence angle	0.245	1.441	1.510	0.354
	0.283	1.067	1.245	0.553
	0.357	1.356	1.335	0.912
	0.196	1.081	1.195	0.400
	0.367	1.372	1.391	0.432
	0.292	1.279	0.656	0.384
	0.152	1.348	0.924	0.360
	0.130	1.876	0.834	0.285
	0.246	1.440	1.372	0.366
	0.305	1.454	1.125	0.484
	0.256	2.331	1.877	0.558
	0.267	1.427	1.071	0.590
	0.159	0.891	1.020	0.283
	0.237	1.575	1.340	0.500
	0.236	1.508	1.021	0.482
	0.405	3.360	1.247	0.512
Average, single	0.258	1.550	1.198	0.466
4 circles integrated	0.160	0.682	0.653	0.352
	0.101	0.579	0.335	0.179
	0.120	0.888	0.698	0.181
	0.127	1.202	0.655	0.228
Average, 4 integrated	0.127	0.838	0.585	0.235
8 integrated	0.110	0.504	0.348	0.218
	0.097	0.870	0.423	0.144
Average, 8 integrated	0.103	0.687	0.386	0.181
All 16 integrated	0.064	0.389	0.285	0.090

Table 10.11. Total rms. noise for the full signal in the modified Stokes parameters from the 16 circle flights with 45° incidence angle from Octobe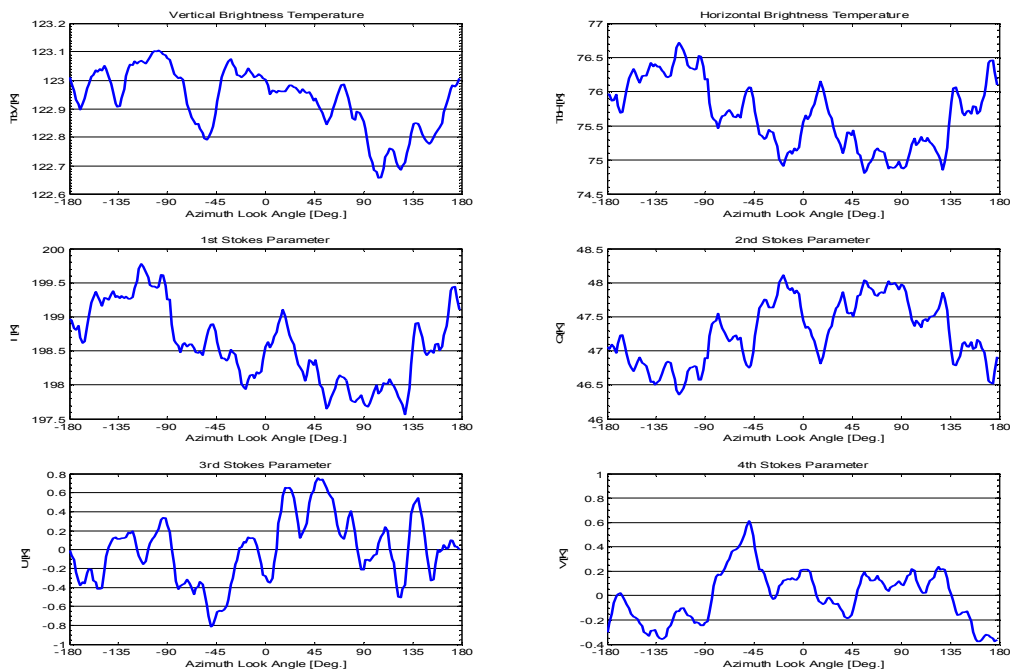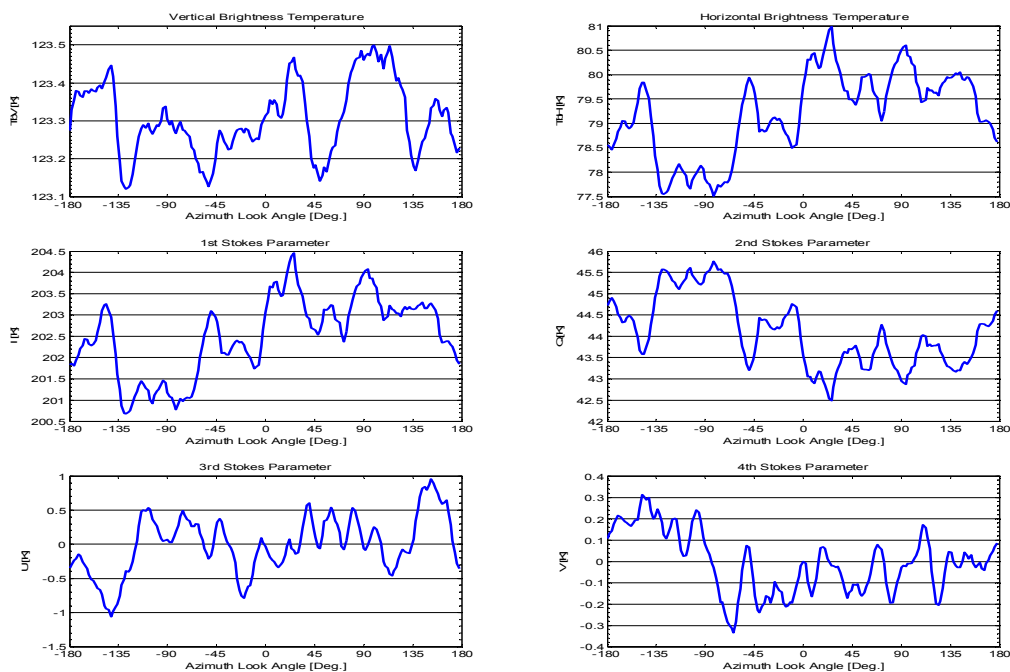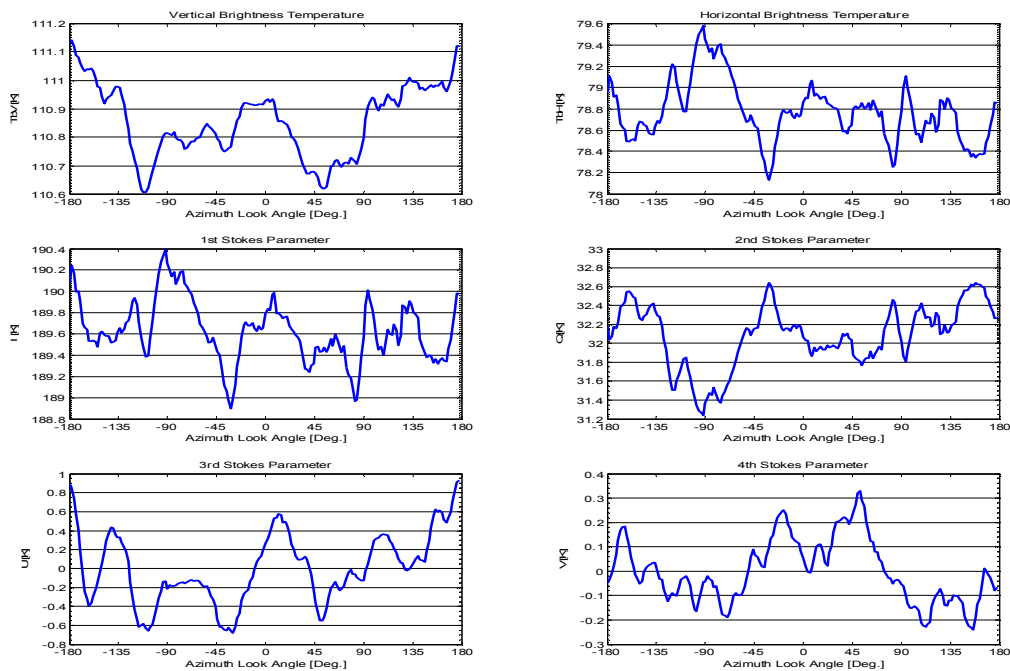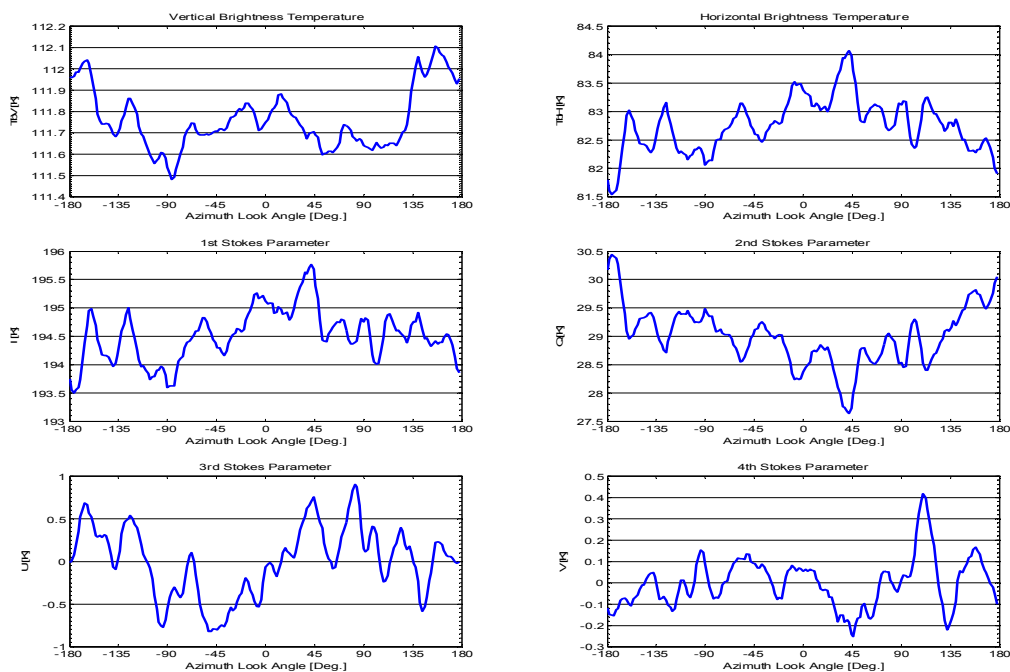r 20th 2003, Target A, after correction for the galactic background. The circles are processed as single tracks, averaged as 4 times four circles, 2 times eight, and totally.

The effect of averaging is another interesting aspect to analyze, and for a first analysis the October 25th 2001 flight is selected, as is represents a moderate wind speed, around 10 m/sec. In section 7, it was concluded, that the change of flight altitude, i.e. the change of spatial averaging was without effect on the data. Table 10.4 repeats the analysis after correction, but it must still be concluded, that no obvious gain (or loss) is identified. For temporal integration, i.e. an integration of subsequent circles, however, a clear effect is seen, and in table 10.5 an integration gain of 2.65 is achieved for vertical polarization, when 12 circles are integrated. Before correction this number was only 1.30, and it should be compared to an expected gain of 3.46 for pure Gaussian signals. The non-Gaussian component is thus estimated to provide a power of 24 mK, if assumed overlaid on top of the Gaussian signal. Likewise for the horizontal polarization, where the integration gain improved from 2.26 to 2.99, leaving only 72 mK of non-Gaussian signal.

On the October 20th 2003 flight a similar wind speed was measured, and the integration gains for 45° incidence angle after correction, corresponding to table 10.11, appear to be 4.03 and 3.98 for vertical and horizontal polarization, respectively. This obviously leaves very small room for non-Gussian components in the signal. For 35° incidence angle the results are 2.08

Circles	TV, std.dev. [K]	TH, std.dev. [K]	U, std.dev. [K]	V, std.dev. [K]
Single circles	0.126	0.768	0.475	0.262
35° incidence angle	0.185	0.920	0.846	0.241
	0.202	0.727	0.793	0.279
	0.240	0.737	0.610	0.276
	0.243	0.894	1.247	0.585
	0.415	0.714	1.733	0.451
	0.226	0.824	1.060	0.271
	0.176	1.127	1.005	0.386
	0.239	1.656	0.838	0.300
	0.177	0.874	0.827	0.336
	0.241	1.549	1.085	0.450
	0.432	0.999	1.037	0.351
	0.277	1.059	1.222	0.378
	0.257	1.850	0.984	0.559
	0.448	0.994	0.934	0.456
	0.176	1.223	1.035	0.301
Average, single	0.254	1.057	0.983	0.368
4 circles	0.117	0.481	0.312	0.126
integrated	0.154	0.400	0.634	0.195
	0.181	0.804	0.490	0.214
	0.200	0.558	0.511	0.182
Average, 4 integrated	0.163	0.561	0.487	0.179
8 integrated	0.127	0.283	0.376	0.131
	0.142	0.470	0.411	0.118
Average, 8 integrated	0.134	0.377	0.393	0.124
All 16 integrated	0.122	0.256	0.304	0.062

Table 10.12. Total rms. noise for the full signal in the modified Stokes parameters from the 16 circle flights with 35° incidence angle from October 20th 2003, Target A, after correction for the galactic background. The circles are processed as single tracks, averaged as 4 times four circles, 2 times eight, and totally.

Inc.	Harm.	TV, M.	TV, Ph.	TH, M.	TH, Ph.	U, Mag.	U, Ph.	V, Mag.	V, Ph.
45°	1	0.02	79.69	0.24	-99.52	0.17	-77.95	0.03	15.16
	2	0.04	-71.80	0.19	-16.80	0.11	-148.83	0.04	143.52
	3	0.02	38.24	0.07	-34.57	0.26	-103.94	0.05	92.61
	4	0.04	-4.38	0.17	-124.79	0.15	88.71	0.05	-95.74
35°	1	0.09	-170.78	0.23	-10.91	0.29	-129.11	0.05	-6.25
	2	0.13	20.22	0.10	-126.72	0.19	-56.06	0.02	5.02
	3	0.00	98.74	0.11	-51.34	0.03	-66.93	0.03	92.66
	4	0.02	-30.84	0.10	-104.81	0.13	-55.44	0.00	28.52

Table 10.13. 1st, 2nd, 3rd, and 4th harmonic components in the averaged modified Stokes parameters from the circle flights from October 20th 2003, target A, after correction for the galactic background.

Figure 10.33. The averaged Stokes parameters from the 1st to the 8th circle flight tracks with 45° incidence angle from the October 20th 2003, Target B, flight, after correction for the galactic background.
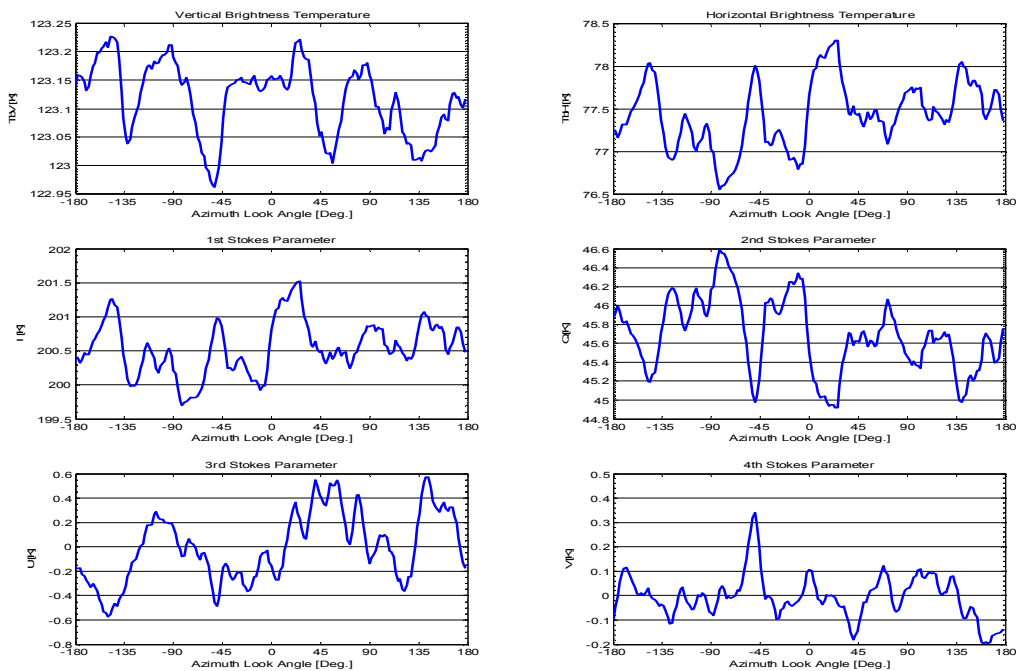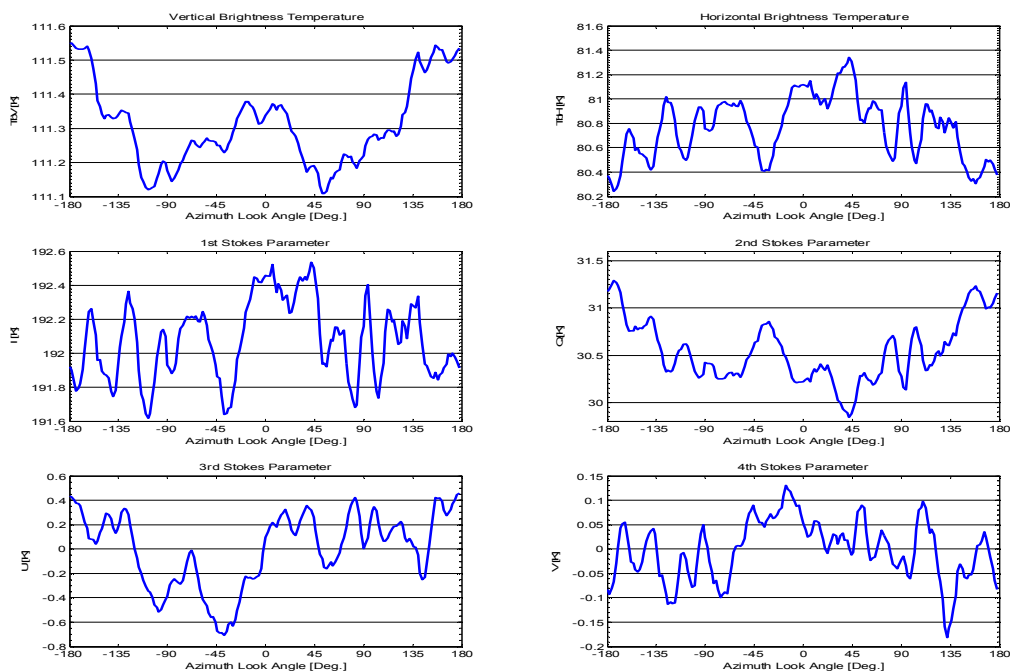

Figure 10.34. The averaged Stokes parameters from the 9th to the 16th circle flight tracks with 45° incidence angle from the October 20th 2003, Target B, flight, after correction for the galactic background.

Figure 10.35. The averaged Stokes parameters from all 16 circle flight tracks with 45° incidence angle from the October 20th 2003, Target B, flight, after correction for the galactic background.

and 4.13, actually indicating the presence of 78 mK of effective deterministic noise power. If a sinusoidal would cause the full reduction of the integration gain, its magnitude will be the square-root of two multiplied by the effective noise power, yielding a 110 mK magnitude.

For the higher wind speed, 20 m/sec. measured on the March 6th 2003 flight, larger signals were measured. For 35° incidence angle, shown in table 10.8, the power of non-Gaussian components is found to be 236 mK and 285 mK in vertical and horizontal polarizations, respectively. Likewise the components for 45° incidence are found to be 150 mK and 1.6 K, the latter probably being the result of interference, however. Ruling out this number, the largest value for the high-wind case, 285 mK, represents a magnitude of about 400 mK.

The low-wind case, taken as target B on the October 20th 2003 flight, and described in table 10.14, is expected to provide very good integration improvement, but it turns out, that the results are very much like the results from target A, taken the same day at 10 m/sec. 163 mK of power is found to be present at vertical polarization, and this number proves, that the immediate absence of wind does not cause all signals to disappear. The opposite effect is seen in the October 25th 2001 data, mentioned above, where only 24 mK was found at a higher wind speed. These numbers are taken as a strong indication, that the signatures, observed from the surface, are more likely to be the result of swell than the result of wind driven capillary waves, as it might be expected at higher frequencies.

Circles	TV, std.dev. [K]	TH, std.dev. [K]	U, std.dev. [K]	V, std.dev. [K]
Single circles	0.255	0.671	0.856	0.244
45° incidence angle	0.415	1.173	1.193	0.304
	0.229	0.737	0.908	0.219
	0.397	0.906	0.862	0.346
	0.292	1.250	1.360	0.308
	0.319	1.390	1.960	0.514
	0.350	1.526	1.196	0.414
	0.380	0.525	0.920	0.353
	0.252	0.831	0.752	0.369
	1.742	2.039	0.825	0.404
	0.355	1.160	1.248	0.290
	0.354	1.864	1.191	0.402
	0.347	0.625	1.122	0.474
	0.208	0.646	0.872	0.290
	0.228	0.798	0.981	0.357
	0.247	0.732	0.632	0.475
Average, single	0.398	1.054	1.055	0.360
4 circles	0.237	0.602	0.477	0.137
integrated	0.216	0.444	0.819	0.225
	0.506	0.693	0.356	0.156
	0.197	0.373	0.513	0.147
Average, 4 integrated	0.289	0.528	0.541	0.166
8 integrated	0.184	0.284	0.394	0.104
	0.299	0.327	0.323	0.086
Average, 8 integrated	0.241	0.305	0.359	0.095
All 16 integrated	0.222	0.240	0.284	0.060

Table 10.14. Total rms. noise for the full signal in the modified Stokes parameters from the 16 circle flights with 45° incidence angle from October 20th 2003, Target B, after correction for the galactic background. The circles are processed as single tracks, averaged as 4 times four circles, 2 times eight, and totally.

Inc.	Harm.	TV, M.	TV, Ph.	TH, M.	TH, Ph.	U, Mag.	U, Ph.	V, Mag.	V, Ph.
45°	1	0.12	-92.73	0.22	-71.47	0.35	-72.96	0.02	92.65
	2	0.25	45.39	0.10	6.75	0.11	-62.21	0.01	6.70
	3	0.06	169.22	0.05	149.21	0.08	-179.36	0.04	151.00
	4	0.08	81.34	0.04	60.63	0.03	-55.62	0.03	149.28

Table 10.15. 1st, 2nd, 3rd, and 4th harmonic components in the averaged modified Stokes parameters from the circle flights from October 20th 2003, Target B, after correction for the galactic background.
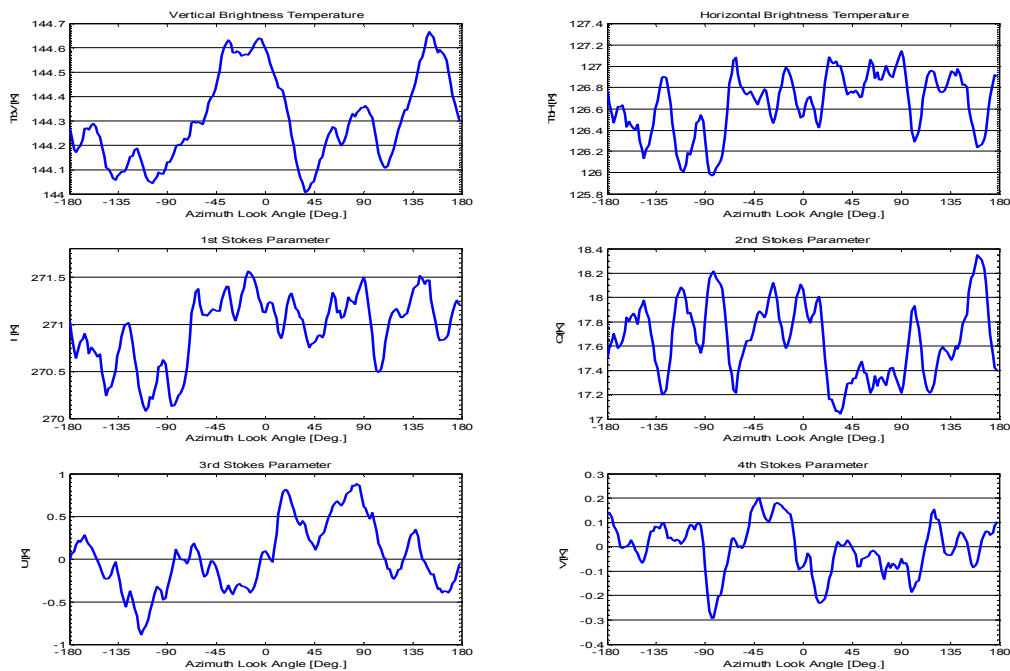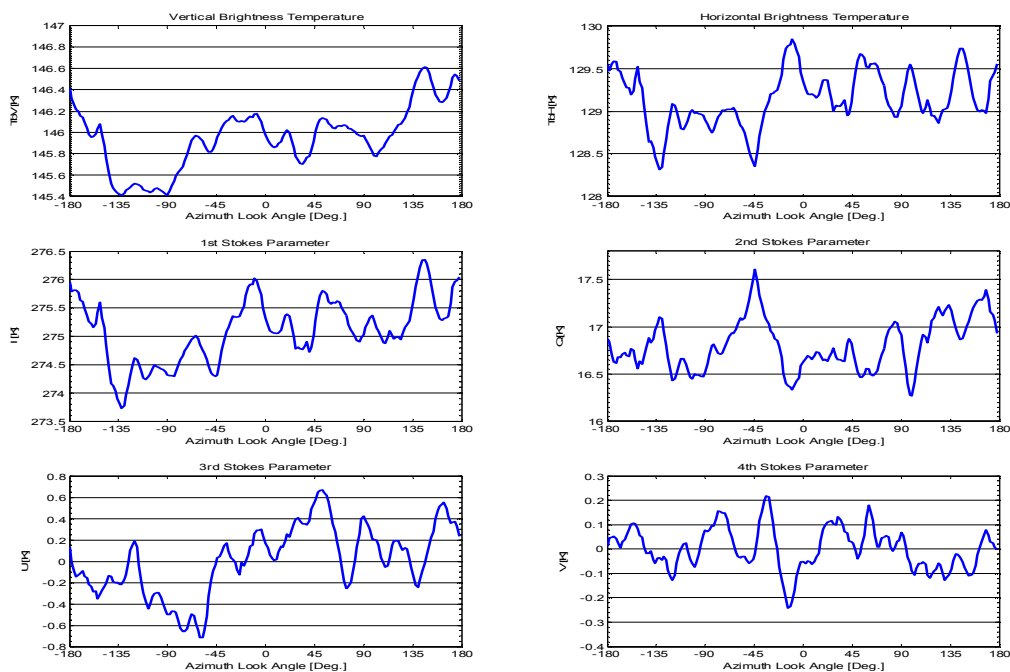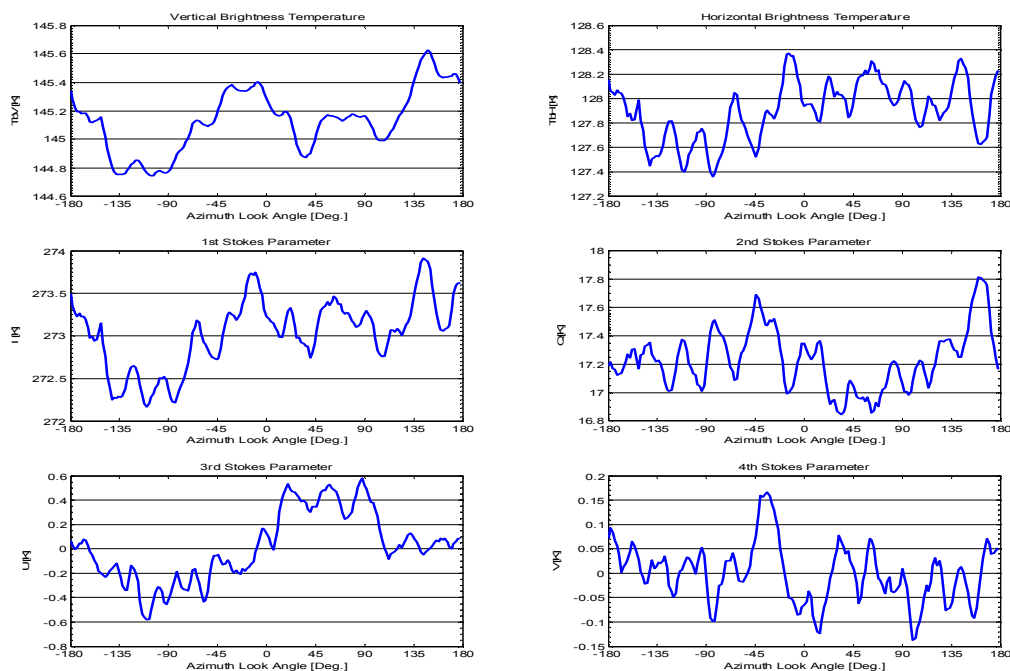
Figure 10.36. The modified Stokes parameters from the level flight tracks October 20th 2003, 50° incidence angle.

Figure 10.37. The modified Stokes parameters from the level flight tracks October 20th 2003, 50° incidence angle. Result of 1st and 2nd harmonic fit.

Inc.	Harm.	TV, M.	TV, Ph.	TH, M.	TH, Ph.	U, Mag.	U, Ph.	V, Mag.	V, Ph.
Level	1	0.06	-78.52	0.02	167.43	0.19	-136.27	0.03	-60.97
50° inc.	2	0.08	-12.45	0.13	16.95	0.41	-60.44	0.05	91.87

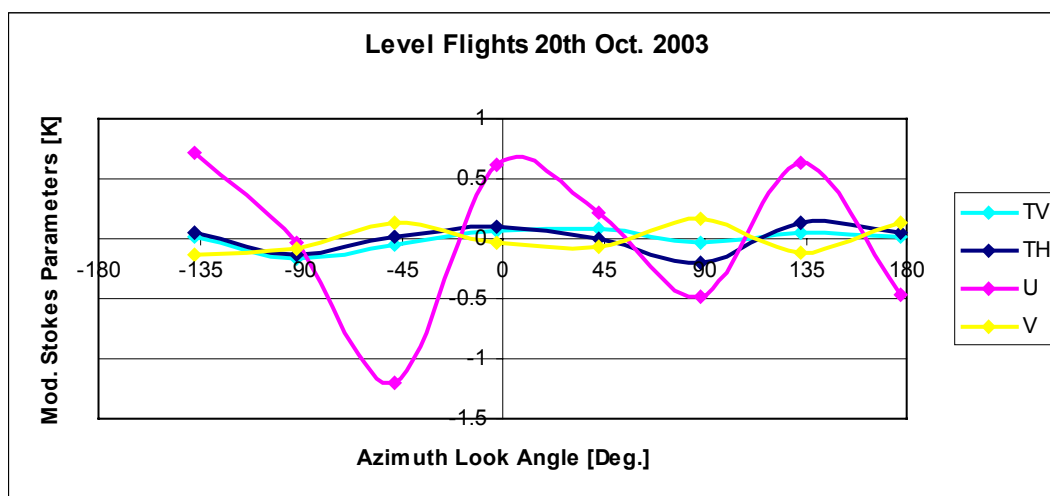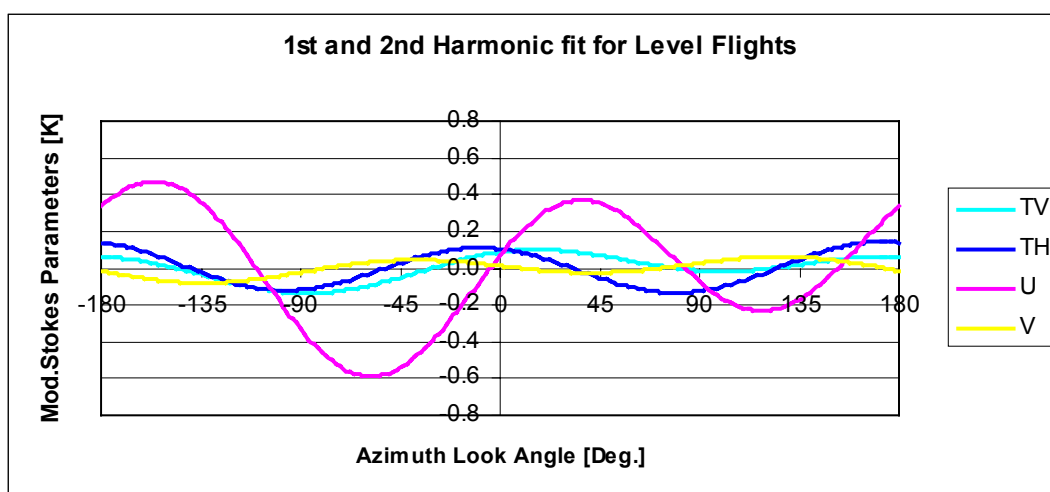*Table 10.16. The modified Stokes parameters from the level flight tracks October 20th 2003, 50° incidence angle. Result of 1st and 2nd harmonic fit.*

The two level flights, presented as 1st and 2nd order harmonic fits in figure 10.26 and figure 10.37 seem to support the quantitative estimates of eventual wind driven signatures. Their harmonic components, presented in table 10.10 and 10.16 indicate maximum magnitudes for each components in the order of 200 mK and 100 mK for the 1st and 2nd order harmonic of the vertical brightness temperature, respectively. If appearing in-phase, as it might be expected from [5], typical peak-to-peak variations would be in the order of 400 mK, which is about 50% of the value estimated from the circle flights. For the 10 m/sec. measurement approximately half magnitudes are observed, this scaling being consistent with the circle flights. Generally, however, it is also in the level flights observed, that no correlation between the measured phases and the expected phases can be proven.

11. Conclusions

The LOSAC campaign was planed to identify eventual azimuth dependence over a full circle signature, carried out over the ocean. This has been done in six flights, providing six different wind conditions. At first sight all data show large peak-to-peak variations, typically in the order of many Kelvin. From a single circle, the identification of polarimetric signatures in the order of 100 mK is hence difficult or impossible.

In all circles, narrow peaks are visible, and in some cases the peaks are narrower for larger circles. Point targets at the sea surface are shown to be a possible origin, as the antenna footprint will fly by the target, giving an almost constant fly by time. As the roll angle will determine the angular velocity, a constant fly by time will thus provide objects of varying angular size in the final signature, as observed. Point targets of the described kind can origin from different sources. As a basic for the selected flight pattern, it is assumed, that the ocean surface is homogeneous, and that the antenna footprint can move over the surface without influencing the measured data. If a ship or another manmade object is present, however, a point target will appear, and data of the received kind will result. As point targets are present in all signatures, however, and as several are observed during a single signature, a large number of targets should be present on the sea surface. As no objects were visually identified in the clear weather conditions October 25th, however, it is unlikely, that all noise peaks origin from manmade objects.

Noise will also be observed, however, if the sea surface is not completely homogeneous. This may result from local changes in the wind field, causing the wind speed and thus the surface signal to fluctuate. The effect was investigated directly in the level flights, where a number of straight tracks of 2 minutes were flown, resulting in the signatures as seen in e.g. figure 8.37. As it is seen in the track, some variation in the Stokes parameters is noticed, and the variations have a length of approximately 10 sec. to 20 sec., which is similar to the duration of the small peaks in the circular signatures. The length also might be similar to the time constant of the larger waves on the sea surface.

The noise is investigated through integration of several circles, and it is assumed, that an eventual random (Gaussian) signal, added to the real surface signature, being searched for, would reduce, leaving out eventual deterministic (sinusoidal) components. The integration gain is used as an indicator, and estimates of the approximate size of an eventual deterministic component are made from the different measurements. At first it appears, that a

clear deterministic signal is present, but after identification and correction for the downwelling galactic background signal, the results are blurrier. Integration gains vary around the expected values, determined as the square-root of the number of independent circles integrated, but variations of approximately +20 % / -50 % are typical. It is thus difficult to make a clear conclusion regarding the exact magnitude of eventual deterministic signals, but some trends are clear. The highest deterministic signal was found for the highest wind speed, i.e. 20 m/sec., and magnitudes up to 300 mK were found. The value was supported by combination of level flight legs, but it must be emphasized, that the values are expected to be worst case examples, as it is assumed, that all non-Gaussian noise power originates from a single sinusoidal. The magnitude of non-Gaussian signals reduces with the wind speed, however, and for 10 m/sec., approximate half magnitudes, i.e. less than 200 mK is observed, and again the trend is confirmed by the level flight signature.

An important observation is made in two cases, where the wind speed was changing prior to the flight. Values smaller than expected, less than 75 mK, were found at 10 m/sec., during a flight, where the wind increased from 5 m/sec. to 10 m/sec., only hours before data acquisition. The opposite effect was observed during measurements of an area with no immediate wind, where values corresponding to the wind field of 10 m/sec., which actually left the target area a few hours before data takes, were observed. This leads to the direct conclusion, that sea surface signatures at L-band are primarily results of swell, and that no direct connection between the immediate wind and the sea surface brightness temperature can be presented.

Apart from the temporal integration of data circles, another integration approach was made. Since the sea surface is not fully homogeneous over space and time, a larger antenna footprint could be expected to provide results with less noise. As a wider beam width is not desired, it was instead decided to increase the flight altitude. Selecting a range from 1000 m to 3000 m, a factor of 9 was gained on the surface, providing a maximum pixel size of approximately 1200 m by 1200 m. Analysis of the results proved no improvement, however, and probably this is due to the fact, that variations on the ground still have larger spacing than the pixel size. The result may be supported by the level flights, where it is observed, that typical variations have a period of 10 sec. to 20 sec. With an aircraft speed of 150 m/sec. this corresponds to at least 1500 m, and it still exceeds the size of the largest pixel. To confirm, that this effect will not cause disturbance for the SMOS measurements, a new experiment must thus be set up, preferably providing a footprint of several km.

A direct benefit from the LOSAC is the availability of circle signatures, and through those a unique information on the influence from external disturbances, such as the moon and the galactic background. The moon has not been searched for, as its expected contribution is in the order of 150 mK, but a further work might take advantage of the LOSAC data set in order to verify this expectation. A strong effect, however, is the influence from the galactic background, and some work has been carried out in this field. An unpolarized sky-map was used, and some estimates were made regarding the bistatic scattering at the sea surface. It was shown, that some smearing occurred, compared to simple Fresnel reflection, but a first order correction could be based on a simple regression analysis, introducing a weighting coefficient, based on the linear regression between the measured signal and the downwelling radiation, into the correction algorithm. The weighting coefficient turned out to vary between 0.3 and 1.0, depending on the wind speed, and it was shown, that an obvious trend could be

identified. Some difference between 35° incidence angle and 45° incidence angle was observed, but due to the limited amount of data, it can not be concluded, weather this is a statistical coincidence.

For the correction of the SMOS data, the effect of smearing is expected to be worse by at least an order of magnitude, as the synthesized beam of SMOS of much more narrow than the beam of the EMIRAD real aperture radiometer. The contrasts of the skymap are thus much larger, 20 K instead of 2 K), over a few beam widths, and the reflection mechanism has to be subject for further investigation, which is far beyond the scope of LOSAC. Another aspect is the estimation of weighting coefficients, which is only possible in LOSAC due to the presence of full azimuth signatures. For SMOS only a single pixel is available, and the determination of reflection parameters as a function of wind speed, swell, etc. must be fully understood. Finally the assumption, that the galactic background map is fully unpolarized has to be proven and eventually further investigated. It was clearly demonstrated, that the vertical and horizontal brightness temperatures could be corrected, thus improving their integration gain and reducing their total noise, but especially the circle signature in figure 10.37 could indicate, that the 3rd Stokes parameter also contains some external signal.

Concluding the LOSAC campaign, it must be emphasized, that all results are related to some uncertainty due to the relative limited amount of data, covering a large range of parameters. During the first flights, several incidence angles were covered, and as a result, too little statistic material was sampled for averaging. Four cases were studied thoroughly with respect to the presence of eventual deterministic signals. Being conservative, it would be assumed, that all non-Gaussian signal, present in the data set, is related to a single sinusoidal, and with this assumption, 300 mK, +20 %/-50 %, of magnitude is identified as an upper boundary, covering wind speeds up to 20 m/sec. Another limitation is the distance to target areas, making it difficult to operate in real ocean conditions. Only one flight took place at water depth higher than 25 m, and as swell has been identified as an important issue, this may be regarded as a limitation to LOSAC.

Future experiments over the sea surface are strongly desired, and the availability of an aircraft over a longer time period is an important parameter, which should be considered. The temporal sampling, and the ability to cover different weather situations is directly related to the flexibility of the carrier, and for a more precise estimation of the magnitude of sea surface signals, this has to be improved. Furthermore the amount of data collected at each site has to be increased, and it is obvious, that the sampling of at least 16 individual circles for each case is essential. In the case of level cloverleaf patterns, the legs should preferably be longer, as it is easily seen from the LOSAC level flight signatures, that only a few periods of ripples are covered, still making the sampling vulnerable to variations. This may explain, why the estimated signatures from circle flights and level flights do not provide the same harmonics after all the processing, and it may thus indicate, that the magnitudes of the sea surface signatures are overestimated. Finally it is desired to make a future installation in a type of aircraft, which can fly at higher altitude, providing the evidence, that ripples can be removed through temporal averaging, as it is expected to be done in SMOS.

12. References

[1]   Jesper Rotbøll, Sten Schmidl Søbjærg and Niels Skou: "A novel L-Band Polarimetric Radiometer featuring Subharmonic Sampling", Radio Science, vol. 38, issue 3, pp MAR11/1-MAR11/7, March 2003.

[2]   Sten Schmidl Søbjærg: "Polarimetric Radiometers and their Applications", Ph.D. Thesis, ISBN 87-91184-17-17, Technical University of Denmark, 2002.

[3]   "Prime item development specification for the embedded GPS/INS (EGI) H-764", DS34200300 Rev. F, Part I, Honeywell Inc. Military avionics division, 1995.

[4]   L. A. Klein and C. T. Swift, "An improved model for the dielectric constant of sea water at microwave frequencies", IEEE Transactions on Antennas and propagation, vol. AP-25, no. 1, January 1977, pp. 104-111.

[5]   S. Yueh, "Modeling of wind direction signals in polarimetric sea surface brightness temperatures", IEEE Transactions on Geoscience and Remote Sensing", vol. 35, no. 6, pp. 1400-1418, 1997.